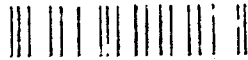
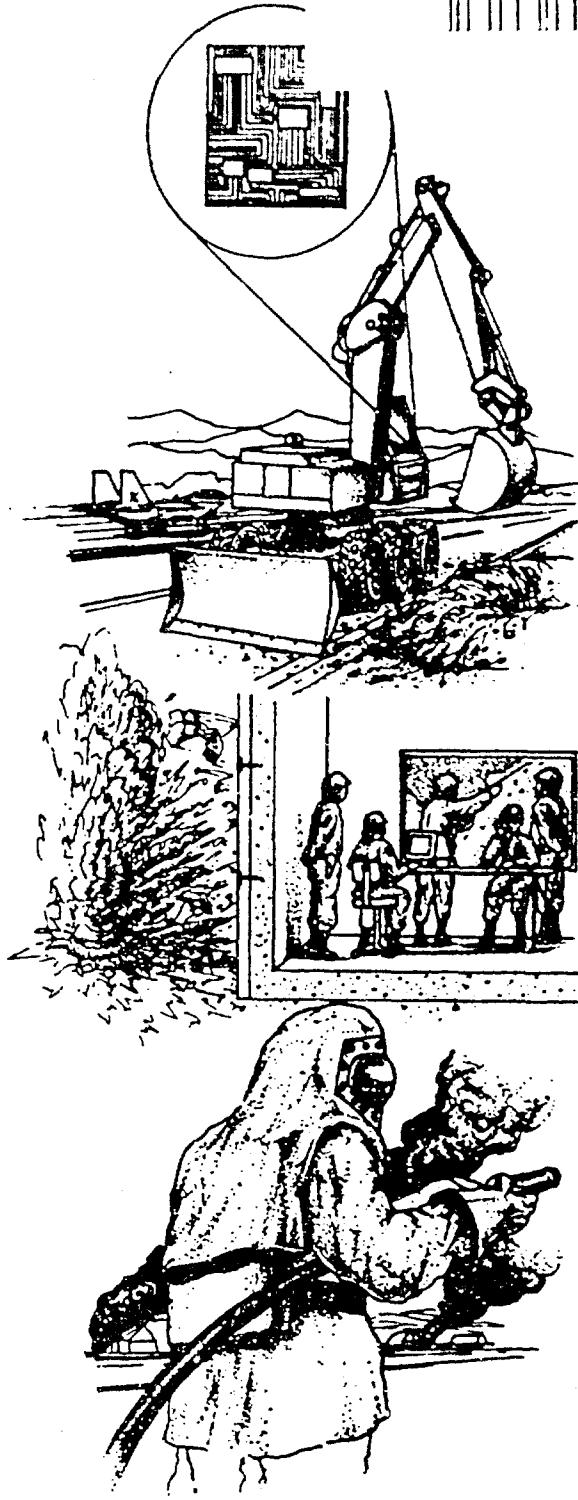


AD-A272 985



ESL-TR-92-47



DYNAMIC RESPONSE OF REINFORCED SOIL SYSTEMS VOLUME I: REPORT

R.C. BACHUS, R.J. FRAGASZY, M. JABER, K.L. OLEN, Z. YUAN, R. JEWELL

GEOSYNTEC CONSULTANTS
5775 PEACHTREE DUNWOODY ROAD
SUITE 200F
ATLANTA GA 30342

MARCH 1993

FINAL REPORT

JUNE 1990 - JUNE 1992

APPROVED FOR PUBLIC RELEASE:
DISTRIBUTION UNLIMITED

S DTIC
ELECTE
NOV 22 1993
A

93-28358



ENGINEERING RESEARCH DIVISION
Air Force Civil Engineering Support Agency
Civil Engineering Laboratory
Tyndall Air Force Base, Florida 32403



93 11 19 024

NOTICE

The following commercial products (requiring Trademark®) are mentioned in this report. Because of the frequency of usage, the Trademark was not indicated. If it becomes necessary to reproduce any segment of this document containing any of these names, this notice must be included as part of that reproduction.

Matrex
Miragrid
Reinforced Earth
Tensar

Mention of the products listed above does not constitute Air Force endorsement or rejection of this product, and use of information contained herein for advertising purposes without obtaining clearance according to existing contractual agreement is prohibited.

NOTICE

PLEASE DO NOT REQUEST COPIES OF THIS REPORT FROM
HQ AFCEA/RA (CIVIL ENGINEERING LABORATORY).

ADDITIONAL COPIES MAY BE PURCHASED FROM:

DEFENSE TECHNICAL INFORMATION CENTER
CAMERON STATION
ALEXANDRIA, VIRGINIA 22314

REPORT DOCUMENTATION PAGE

1a. REPORT SECURITY CLASSIFICATION UNCLASSIFIED			1b. RESTRICTIVE MARKINGS		
2a. SECURITY CLASSIFICATION AUTHORITY			3. DISTRIBUTION/AVAILABILITY OF REPORT UNLIMITED		
2b. DECLASSIFICATION/DOWNGRADING SCHEDULE			4. PERFORMING ORGANIZATION REPORT NUMBER(S)		
4. PERFORMING ORGANIZATION REPORT NUMBER(S)			5. MONITORING ORGANIZATION REPORT NUMBER(S) CEL-TR-92-47		
6a. NAME OF PERFORMING ORGANIZATION GEOSYNTEC CONSULTANTS		6b. OFFICE SYMBOL (if applicable)	7a. NAME OF MONITORING ORGANIZATION AIR FORCE CIVIL ENGINEERING SUPPORT AGENCY		
6c. ADDRESS (City, State, and ZIP Code) 5775 Peachtree Dunwoody Road, Suite 200 F Atlanta, Georgia 30342			7b. ADDRESS (City, State, and ZIP Code) Civil Engineering Laboratory 139 Barnes Drive Tyndall Air Force Base, Florida 32403		
8a. NAME OF FUNDING/SPONSORING ORGANIZATION AF CIVIL ENGRG SPT AGENCY		8b. OFFICE SYMBOL (if applicable) RACS	9. PROCUREMENT INSTRUMENT IDENTIFICATION NUMBER FO 8635-90-C-0198		
8c. ADDRESS (City, State, and ZIP Code) Civil Engineering Laboratory 139 Barnes Drive Tyndall Air Force Base, Florida 32403			10. SOURCE OF FUNDING NUMBERS		
	PROGRAM ELEMENT NO. 2673	PROJECT NO. 1024	TASK NO.	WORK UNIT ACCESSION NO.	
11. TITLE (Include Security Classification) DYNAMIC RESPONSE OF REINFORCED SOIL SYSTEMS, VOLUME I OF II: REPORT					
12. PERSONAL AUTHOR(S) BACHUS, R.C.; FRAGASZY, R.J.; JABER, M.; OLEN, K.L.; YUAN, Z. AND JEWELL R.					
13a. TYPE OF REPORT FINAL		13b. TIME COVERED FROM JUN 90 TO JUN 92		14. DATE OF REPORT (Year, Month, Day) March 1993	15. PAGE COUNT
16. SUPPLEMENTARY NOTATION					
17. COSATI CODES			18. SUBJECT TERMS (Continue on reverse if necessary and identify by block number)		
FIELD	GROUP	SUB-GROUP	Blast resistant structures; Blast loading; Reinforced soil; Geosynthetics; Centrifuge modeling; Finite Element analysis; Pullout test.		
19. ABSTRACT (Continue on reverse if necessary and identify by block number)					
<p>This report describes the results of a comprehensive laboratory, numerical and physical modeling investigation of the response of reinforced soil structures to blast loading. Dynamic laboratory pullout testing of geogrid and metal strip reinforcement embedded in cohesionless soil shows negligible rate effects with rise times to peak pullout load ranging from several minutes to less than 50 ms. Triaxial tests on fiber-reinforced soil show</p> <p style="text-align: right;">(continued on back of page)</p>					
20. DISTRIBUTION/AVAILABILITY OF ABSTRACT <input type="checkbox"/> UNCLASSIFIED/UNLIMITED <input checked="" type="checkbox"/> SAME AS RPT <input type="checkbox"/> DTIC USERS			21. ABSTRACT SECURITY CLASSIFICATION UNCLASSIFIED		
22a. NAME OF RESPONSIBLE INDIVIDUAL CAPT. RICHARD A. REID			22b. TELEPHONE (include Area Code) (904) 238-4912		22c. OFFICE SYMBOL RACS

significant increases in peak strength, axial strain at peak strength and volume reduction with increasing fiber content.

A numerical model was developed using the DYNA3D finite-element code. A numerical parametric study shows the importance of reinforcement stiffness, soil compaction and roof support on the response of a reinforced soil wall to blast loading.

Centrifuge model tests were conducted on 1:30 scale models of reinforced soil walls. Centrifuge results compare well to numerical predictions and full scale tests. Geogrid reinforced walls (modeled with nylon mesh) performed better than steel strip reinforced walls.

This technical report is divided into two volumes. Volume I contains the main body of the report and Volume II contains the Appendices.

Accession For	
NTIS CRA&I	<input checked="" type="checkbox"/>
DTIC TAB	<input type="checkbox"/>
Unannounced	<input type="checkbox"/>
Justification	
By	
Distribution/	
Availability Codes	
Dist	Avail and/or Special
A-1	

DTIC QUALITY INSPECTED 1

EXECUTIVE SUMMARY

A. OBJECTIVE

The objective of this study was to investigate the response of reinforced soil systems subjected to blast loading and to assess the feasibility of using reinforced soil to provide blast resistance. To meet this objective, a testing program was developed and executed to accomplish the following: (i) to establish the properties of reinforced soil subjected to blast loading, (ii) to develop numerical and physical modeling techniques which are appropriate for evaluating the response of reinforced soil systems subjected to blast loading, and (iii) to establish preliminary analysis methods which can be used for the design of reinforced soil systems subjected to blast loading.

B. BACKGROUND

Blast-protective structures are commonly used by the United States Air Force (USAF) and other branches of the armed forces to protect equipment, explosives, and personnel from conventional weapons effects. These effects include high-pressure impulse loading, projectile/fragment impact and penetration, and cratering. Currently, these structures are constructed either as heavily-reinforced concrete structures or as buried structures protected by a burster slab. These protection measures are costly, time consuming to construct, and sensitive to multiple strikes.

Soil has been used to increase the survivability of these structures by providing a cover or barrier to reduce the shock, pressure, and impact on the structures. However, soil berms must be built at relatively flat slopes (about 2.5 horizontal:1 vertical (2.5H:1V)) for adequate stability. Because of this, the use of a soil cover or berm is restricted by the amount of land available for construction and the logistics of moving large quantities of soil to the site.

The USAF has recently expressed interest in using reinforced soil in the development of blast-protective structures. Reinforced soil is a composite material made up of soil and high-tensile-strength materials such as steel or

geogrid. Soil alone has no tensile strength, and the reinforcement strengthens the soil by confining it and restricting movement parallel to the reinforcement. Incorporating reinforced soil structures in the development of blast-protective structures can accomplish the following: (1) eliminate the use of heavily reinforced concrete, (2) reduce volume of soil required for construction, (3) reduce the amount of land space required, (4) reduce the construction time, (5) simplify structural repair due to bomb damage as compared to reinforced concrete structures, and (6) reduce initial cost of construction compared to other types of structures.

To design blast-protective structures using reinforced soil, the dynamic response characteristics and analytical theory of reinforced soil subjected to blast loading must be established. Although a substantial amount of research has been performed in the past decade to determine the properties of reinforced soil under static loading condition, little work has been carried out to determine reinforced soil properties or theory under blast loading conditions. Research is therefore required to develop a better understanding of the response of reinforced soil to blast loading. This report represents the first comprehensive research effort conducted to understand the response of reinforced soil wall systems subjected to blast loading.

C. SCOPE

A scope of work was developed to achieve the objectives outlined in Section

A. This scope of work includes the following:

- an extensive literature review for evaluation of soil and reinforced soil response to blast loading and availability of soil constitutive models and finite element numerical codes for analyzing reinforced soil systems;
- development of laboratory dynamic soil testing equipment and a laboratory testing program to evaluate dynamic response of a reinforced soil system subjected to blast (i.e.: impulse) loading;

- development and utilization of a numerical simulation for analysis of reinforced soil wall systems subjected to blast loading; and
- physical modeling of reinforced soil systems subjected to blast loading using centrifuge modeling.

Using this technical approach makes it possible to compare the different analysis techniques and results, provide a quantitative assessment of the properties of reinforced soil and reinforced soil systems subjected to blast loading, and provide preliminary guidelines for selecting appropriate analysis techniques for the design of reinforced soil systems for blast protection.

D. TEST DESCRIPTION

Laboratory testing, numerical modeling and physical modeling was conducted to study the response of reinforced soil structures subjected to blast loading. A brief description of each test is presented below.

Laboratory Tests: Laboratory strength tests were conducted on three types of reinforcing systems: fiber-reinforced sands, geogrid-reinforced sands and steel-reinforced sands. Triaxial tests were conducted on fiber-reinforced sand to estimate the sand's strength properties. Static pullout tests were conducted with both steel and geogrid reinforcement and sands under various confining pressures to characterize the static load-deflection behavior of the reinforced soil. Dynamic pullout tests were then performed using the same parameters as the static tests. A standard static pullout test box was modified to a dynamic load system by installing an impact beam, hydraulic cylinders, springs, and a trigger system. The system was capable of loading the sample in just a few micro-seconds to simulate a blast load. Dynamic load-deflection behavior was characterized and compared to that obtained from static testing.

Numerical Modeling: A numerical model was developed based on the computer code DYNA3D, a non-linear, three-dimensional finite-element code developed by the Lawrence Livermore National Laboratory for use in the analysis of dynamic solid and structural mechanics problems. A parametric study was conducted to

observe the influence of several critical factors on the behavior of the reinforced soil wall subjected to blast loading. These factors included reinforcement strength, reinforcement length, weapon size, and weapon location.

Physical Modeling: Nine 1/30th scale model reinforced soil walls were tested in the Air Force Civil Engineering Support Agency (AFCESA) centrifuge at Tyndall Air Force Base, Florida. A parametric study was conducted to observe the influence of several critical factors on the behavior of the model reinforced soil walls subjected to blast loading. These factors included reinforcement length, reinforcement type, reinforcement width, weapon location, and influence of a roof slab on the structure.

E. CONCLUSIONS

A brief summary of results obtained from the laboratory testing, numerical modeling, and physical modeling portions of the study are presented below.

Laboratory Testing Results: Results of triaxial testing on fiber-reinforced sand indicate that soil strength, strain at failure and compressibility increase and stiffness decreases as fiber content increases. Results of the pullout testing indicate that dynamic pullout behavior of geogrid in sand, when measured in terms of load vs. displacement, is very similar under constant normal stress to that observed with standard pullout rates used for static design. The dynamic pullout tests subjected the geogrid to a stress path similar to that caused by blast loading.

Numerical Modeling Results: Results of the numerical modeling program indicate that soil stiffness and friction angle significantly affect was performance, as does reinforcement stiffness. Reinforcement length and soil/reinforcement interface friction coefficient are relatively less important parameters, provided they are kept within normal ranges for static stability.

Physical Modeling: Results of the physical modeling tests indicate that reinforcement type and width play a significant role in wall behavior. The importance of a horizontal constraint along the top of the wall (i.e., a roof

slab) has also been demonstrated. Reproducibility of test results and similarity to numerical predictions provide evidence of the appropriateness of the centrifuge modeling technique for this problem.

F. RECOMMENDATIONS

The results of limited laboratory, centrifuge modeling, and numerical modeling tests conducted in this study indicate that statically designed reinforced soil structures perform favorably as blast-protective structures. It is recommended that the Air Force pursue a more comprehensive study of the use of reinforced soil structures for blast protection with the ultimate goal of developing design procedures and design drawings for reinforced soil structures. This study should include full-scale testing, a comprehensive series of centrifuge tests, modifications to the numerical model, and comprehensive numerical modeling of the centrifuge tests. Ultimately, studies should be developed that investigate other weapons effects on reinforced soil structures such as airblasts and projectile penetrations.


PREFACE

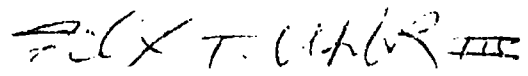
This report was prepared by GeoSyntec Consultants, 5775 Peachtree Dunwoody Road, Suite 200F, Atlanta, Georgia 30342 under Contractor Number F08635-90-C-0198 for the Air Force Civil Engineering Support Agency (AFCESA), Civil Engineering Laboratory, 139 Barnes Drive, Tyndall Air Force Base, Florida 32403-6001.

This report summarizes work accomplished between 8 June 1990 and 30 June 1992. Captain Richard A. Reid, USAF, was the AFCESA/RACS technical program manager.

This report has been reviewed by the Public Affairs Office and is releasable to the National Technical Information Service (NTIS). At NTIS, it will be available to the general public, including foreign nationals.

This technical report has been reviewed and is approved for publication.


RICHARD A. REID, Capt, USAF
Project Officer


FELIX T. UHLIK III, Lt Col, USAF
Chief, Engineering Research
Division

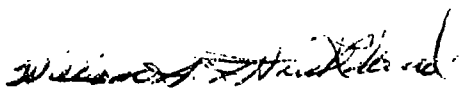

WILLIAM S. STRICKLAND, GM-14
Chief, Air Base Survivability
Branch

TABLE OF CONTENTS

Section	Title	Page
I	INTRODUCTION	1
	A. OBJECTIVE	1
	B. BACKGROUND	1
	C. SCOPE OF WORK	3
II	LITERATURE REVIEW	5
	A. GOALS AND ORGANIZATION	5
	B. USE OF EARTH BERMS FOR PROTECTION OF STRUCTURES	5
	1. Typical Protective Berm Construction	6
	2. Dynamic Performance	6
	3. Reinforced Soil Berm As Structure Protection	9
	C. DYNAMIC RESPONSE OF COHESIONLESS SOIL	11
	1. Introduction	11
	2. Dynamic Uniaxial Behavior	12
	a. Description of Equipment	12
	b. Laboratory Testing Methods and Results	15
	(1) Compressed Nitrogen	15
	(2) Piston-Driven Compressed Gas	15
	(3) Split-Hopkinson Pressure Bar	16
	(4) Exploding Bridgewire	16
	3. Dynamic Shear Behavior	19
	a. Direct Shear Tests	19
	b. Triaxial Tests	22
	c. Fast Triaxial Shear Device	22
	4. Load Rate Effects	24

TABLE OF CONTENTS
(Continued)

Section	Title	Page
D.	REINFORCED SOIL SYSTEMS	26
1.	Concept and Description	26
2.	Response of Geosynthetic Reinforcement	29
3.	Response of Microreinforced Soil	33
a.	Fiber Reinforcement	33
b.	Microgrid Reinforcement	36
c.	Summary of Microreinforced Soil	38
E.	CONSTITUTIVE MODELS OF SOIL BEHAVIOR	40
1.	Introduction to Types of Models	40
2.	Deformation Theories	41
3.	Incremental Theories	42
4.	Endochronic Theories	42
5.	Elastoplastic Theories	42
6.	Brief Outline of a Cap Model	43
7.	Two-Invariant Cap Model	43
F.	NUMERICAL MODELING OF REINFORCED SOIL AND DYNAMIC LOADING	45
1.	ANSYS	45
2.	ABAQUS	46
3.	ADINA	47
4.	DYNA3D	47
III	DESIGN CRITERIA FOR REINFORCED SOIL STRUCTURES	48
A.	GOALS AND ORGANIZATION	48
B.	CURRENT DESIGN PROCESS	48
C.	DESIGN PARAMETERS	51

TABLE OF CONTENTS
(Continued)

Section	Title	Page
	1. Introduction	51
	2. Reinforced Soil Wall Characteristics	51
	3. Soil	52
	4. Blast Loading Characteristics	52
	D. RECOMMENDATIONS FOR PERFORMANCE CRITERIA	52
IV	LABORATORY TESTING PROGRAM	53
	A. INTRODUCTION	53
	1. Overview	53
	2. Organization	56
	B. SOILS AND REINFORCEMENT	57
	1. Soils	57
	2. Microreinforcements	57
	3. Polymer Geogrid Reinforcement	57
	4. Reinforced Earth Company Steel Strips	60
	C. DESCRIPTION OF TEST AND TEST EQUIPMENT	62
	1. Triaxial Tests	62
	2. Static Pullout Tests	62
	3. Dynamic Pullout Tests	62
	D. RESULTS OF DIRECT SHEAR TESTS ON SOILS	63
	E. RESULTS OF TRIAXIAL TESTS ON MICROREINFORCED SAND	65
	1. Test Procedures	65
	2. Test Results	66

TABLE OF CONTENTS
(Continued)

Section	Title	Page
F.	RESULTS OF TESTS ON GEOGRID	74
1.	Procedure	74
2.	Static Tensile Tests	77
3.	Impact Tensile Tests	77
G.	PULLOUT TEST RESULTS	79
1.	Test Procedures	79
2.	Static	80
a.	Preliminary Tests	80
b.	Pullout Resistance of Clamp Plate	82
c.	Geogrids in SP and SW-SM Sand	82
d.	Reinforced Earth Bar in SP and SW-SM Sand	90
e.	Rate Dependence	96
	(1) Rate-Dependent Behavior of Reinforcement in Soil	96
	(2) Rate-Dependent Pullout Behavior of Geogrids in SP Sand	97
3.	Impact	97
a.	Interpretation of Impact Pullout Tests	99
b.	Comparison Between Impact and Static Pullout Resistance	106
V	NUMERICAL MODELING AND PARAMETRIC STUDY RESULTS	111
A.	GOALS AND ORGANIZATION	111
B.	DESCRIPTION OF THE NUMERICAL MODEL	111

TABLE OF CONTENTS
(Continued)

Section	Title	Page
	1. Background	112
	2. Finite-Element Mesh	112
	3. Material Properties	116
	4. Loading Conditions	118
	a. Gravity	118
	b. Blast	119
	5. Discussion	121
C.	PARAMETRIC STUDY	122
	1. Test Matrix	123
	2. Basis for Comparisons	125
	3. Behavior of the Standard Wall	127
	4. Effect of Reinforcement Stiffness	139
	5. Effect of Reinforcement Length	142
	6. Effect of the Roof	143
	7. Effect of Weapon Size	144
	8. Effect of Weapon Location	145
	9. Effect of Soil-Reinforcement Interface Friction	146
	10. Effect of Soil Stiffness	147
	11. Effect of Soil Strength	148
	12. Effect of Gravity Initialization	149
D.	CONCLUSIONS OF PARAMETRIC STUDY	151
E.	RECOMMENDATIONS FOR FURTHER MODEL DEVELOPMENT	152
VI	PHYSICAL MODELING OF REINFORCED SOIL WALL SYSTEMS	155
	A. GOALS AND ORGANIZATION	155
	F. TYPES OF PHYSICAL MODELS	156

TABLE OF CONTENTS
(Continued)

Section	Title	Page
C.	CENTRIFUGE MODELING	157
	1. Similitude and Centrifuge Scaling Relations	157
	2. Centrifuge Description	158
	3. Model Description	159
D.	MODEL MATERIALS	159
	1. Wall Components	161
	2. Soil	164
	3. Instrumentation	169
	4. Detonator Assembly	169
	5. Containment Bucket and Bracing Block	173
E.	TEST PROCEDURE	175
	1. Model Construction	175
	2. Centrifugation	177
	3. Data Collection and Model Disassembly	177
	4. Data Reduction	179
F.	PRELIMINARY TESTS	183
G.	PRODUCTION TESTS	184
	1. Presentation of Data	185
	2. Comparative Studies	190
	a. Comparison 1: Centrifuge Model Results to Expected Values	190
	b. Comparison 2: Centrifuge Model Results to Each Other	193
	c. Comparison 3: Centrifuge Model Results to Numerical Model Results	206

TABLE OF CONTENTS
(Continued)

Section	Title	Page
	d. Comparison 4: Centrifuge Model Results to Full Scale Model Results	212
	H. CONCLUSIONS AND RECOMMENDATIONS	213
VII	SUMMARY AND CONCLUSIONS	215
	A. SUMMARY	215
	B. CONCLUSIONS	216
VIII	RECOMMENDATIONS	219
	A. GOALS AND ORGANIZATION	219
	B. RECOMMENDATIONS	219
REFERENCES	222

LIST OF FIGURES

Figure	Title	Page
1	Example of Protective Soil Berm	7
2	Reinforced Soil Bunker Used in Field Tests	10
3	Schematic Diagram of High Strain-Rate Uniaxial Strain Device	13
4	Schematic Diagram of Split-Hopkinson Pressure Bar	14
5	Typical Stress-Strain Response from SHPB Test	17
6	Uniaxial Strain Test Results for Enewetak Beach Sand	18
7	Comparison of Rate Effects in Enewetak Beach Sand and Flume Sand	20
8	Comparison of Dynamic and Static Direct Shear Test Results	21
9	WES Fast Triaxial Shear Device (FTRXD)	23
10	Effects of Loading Rate of Behavior of CARES-Dry Soil	25
11	Mechanisms of Stress Transfer in Reinforced Soil	27
12	Strength Representation of Reinforced Soil	28
13	Schematic Diagram of a Reinforced Soil Wall Using Geotextile Shear Reinforcements	30
14	Schematic Diagram of Reinforced Soil Embankment Using Geogrid Reinforcement	31
15	Effects of Fiber Content and Fiber Aspect Ratio on Strength of Fiber Reinforced Soil	35
16	Influence of Glass Fiber Content on Shear Modulus Ratio-Confining Pressure = 43 kPa	37
17	Triaxial Test Results for Sand and Sand Containing 0.19 Percent Miniature Geogrids	39
18	Typical Yield Surfaces in CAP Model	44
19	Protective Structure Design Process	49
20	Schematic Diagram of Direct Shear Test for Measuring Soil-Reinforcement Interface Properties	54
21	Schematic Diagram of Pullout Test for Measuring Soil-Reinforcement Interface Properties	55
22	Grain Size Distribution Curves for SP and SW-SM Sands	58
23	Moisture-Density Relationship for SW-SM Sand	59
24	Geometric Characteristics of Ribbed Strips	61

LIST OF FIGURES
(Continued)

Figure	Title	Page
25	Schematic Diagram of the Dynamic Loading System	64
26	Stress-Strain Curves for Fibrillated Fiber - Reinforced Sand (F_{360} Fiber)	67
27	Stress-Strain Curves for Fibrillated Reinforced Sand (F_r Fiber)	68
28	Stress-Strain Curves for Monofilament Reinforced Sand	70
29	Effect of Fiber Content on Volumetric Strain	71
30	Effect of Fiber Content on Volumetric Strain at 10 Percent Axial Strain for Low Compactive Effort	72
31	Effect of Fiber Content on Volumetric Strain at 10 Percent Axial Strain for High Compactive Effort	73
32	Effect of Fiber Content on Tangent Modulus for Low Compactive Effort	75
33	Effect of Fiber Content on Tangent Modulus for High Compactive Effort	76
34	Static and Dynamic Tensile Test Results for UX1500, Miragrid 10T and Matrex 120 Geogrids	78
35	Series P1 Pullout Test Results	81
36	Series P2 Pullout Test Results	83
37	Results of Clamp1 Pullout Tests	84
38	Results of Clamp2 Pullout Tests	85
39	Pullout Response of UX1500 Geogrid in SP Sand	88
40	Pullout Response of UX1500 Geogrid in SW-SM Sand	89
41	Sand-Geogrid Interface Shear Strength Curves	91
42	Variation of Apparent Friction Coefficient with Normal Stress for Geogrids	92
43	Pullout Response of Reinforced Earth Bar in SW-SM Sand	93
44	Variation of Apparent Friction Coefficient with Normal Stress for Reinforced Earth Bar	94
45	Pullout Rate Effect on Sand-Geogrid Interface Shear Strength	98

LIST OF FIGURES
(Continued)

Figure	Title	Page
46	Acceleration-Time History for Miragrid 10T in SP Sand	101
47	Force-Time History for Miragrid 10T in SP Sand	102
48	Calculated Velocity-Time History for Miragrid 10T in SP Sand	103
49	Effect of Initial Velocity on Displacement-Time History	104
50	Effect of Initial Velocity on Calculated Pullout Response	105
51	Comparison of Impact and Static Pullout Resistances in SP Sand	107
52	Comparison of Impact and Static Pullout Resistances in SW-SM Sand	108
53	Impact Pullout Response of Matrex 120 Geogrid in SW-SM Sand at High Confining Pressure	110
54	Standard Finite-Element Mesh	113
55	Standard Finite-Element Mesh Showing Boundary Conditions and Interface	115
56	Input Time Histories	120
57	Nodes and Elements Selected for Time History Data Dumps	126
58	Deformed Shape of Wall at $t = 410$ ms - Analysis PS1	128
59	Time Histories of Velocity for Nodes 3330 and 3378 - Analysis PS1	131
60	Time Histories of Acceleration for Nodes 3330 and 3378 - Analysis PS1	133
61	Time Histories of σ_x for Elements 330 and 885 - Analysis PS1	140
62	Wall Geometry (Model and Prototype)	160
63	Interlocking Panel Structure	163
64	Geogrid Reinforced Panels	165
65	Steel Reinforced Panels	166
66	Top Restraint	167

LIST OF FIGURES
(Continued)

Figure	Title	Page
67	Grain Size Distribution, Tyndall AFB Sand	168
68	Resistor Placement	170
69	Accelerometer Placement	171
70	Bracing Block	174
71	Berm	178
72	Acceleration-Time History	180
73	Voltage-Time History	181
74	Pressure-Voltage Calibration Curve	182
75	Peak Pressure vs. Distance (Prototype)	191
76	Peak Acceleration vs. Distance (Prototype)	192
77	Deformed Wall Geometry: Test 1	195
78	Deformed Wall Geometry: Test 2	196
79	Deformed Wall Geometry: Test 3	197
80	Deformed Wall Geometry: Test 4	198
81	Deformed Wall Geometry: Test 5	199
82	Deformed Wall Geometry: Test 6	200
83	Deformed Wall Geometry: Test 7	201
84	Deformed Wall Geometry: Test 8	202
85	Deformed Wall Geometry: Test 9	203

LIST OF TABLES

Table	Title	Page
1	SUMMARY OF NUMERICAL CODES CONSIDERED	46
2	DESIGN PARAMETERS	50
3	PROPERTIES OF MICROREINFORCEMENT	60
4	PROPERTIES OF GEOGRID REINFORCEMENT	60
5	TEST MATRIX FOR TRIAXIAL TESTS ON MICROREINFORCED SOIL	55
6	SUMMARY OF IMPACT TENSILE TEST RESULTS FOR GEOGRIDS	79
7	SUMMARY OF STATIC PULLOUT TEST RESULTS FOR GEOGRIDS IN SP AND SW-SM SANDS	87
8	SUMMARY OF STATIC PULLOUT TEST RESULTS FOR GALVANIZED REINFORCED EARTH BAR IN SP AND SW-SM SANDS	95
9	SUMMARY OF IMPACT PULLOUT TEST RESULTS FOR GEOGRIDS IN SP AND SW-SM SANDS	100
10	STANDARD MATERIAL PROPERTIES	117
11	TEST MATRIX FOR PARAMETRIC STUDY	124
12	MAXIMUM DISPLACEMENT OF FACING PANELS	129
13	MAXIMUM VELOCITY OF FACING PANELS	130
14	MAXIMUM ACCELERATION OF FACING PANELS	132
15	PEAK HORIZONTAL STRESSES IN ELEMENTS ADJACENT TO FACING PANEL NO. 3	135
16	PEAK REINFORCEMENT STRESSES	136
17	PEAK HORIZONTAL STRESS VS. DISTANCE FROM EXPLOSIVE	138
18	SCALING RELATIONS	158
19	MODEL/PROTOTYPE DIMENSIONS	161
20	STRENGTH PROPERTIES OF REINFORCED SOIL WALL COMPONENTS	162
21	GAGE PLACEMENT	172
22	PRELIMINARY TEST PARAMETERS	183
23	PRODUCTION RUN TEST MATRIX	185
24	PEAK PANEL ACCELERATIONS	186
25	PEAK WAVE PRESSURES	187
26	WAVE VELOCITIES	187
27	MEASURED PANEL DISPLACEMENTS	188
28	COMPARISON OF CENTRIFUGE AND NUMERICAL PREDICTIONS OF PROTOTYPE PANEL DISPLACEMENTS AND ACCELERATIONS	210

SECTION I

INTRODUCTION

A. OBJECTIVE

The objective of this project was to evaluate the response of reinforced soil systems subjected to blast loading and to assess the feasibility of using reinforced soil systems to provide blast resistance. To meet this objective, a research program was developed: (1) to establish the properties of reinforced soil or reinforced soil systems subjected to blast loading; (2) to develop numerical and physical modeling techniques which are appropriate for evaluating the response of reinforced soil systems subjected to blast loading; and (3) to establish preliminary analysis methods which can be used for the design of reinforced soil systems subjected to blast loading.

B. BACKGROUND

The United States Air Force (USAF), as well as other branches of the armed services, often requires various structures, such as aircraft shelters, to be designed to resist the blast effects from conventional weapons. Blast effects include high-pressure impulse loading, projectile/fragment impact and penetration, and cratering. Blast protection is currently provided by either: (1) heavily reinforcing concrete structures; (2) burying structures in unreinforced soil and using a burster slab; or (3) various combinations of (1) and (2). These protection methods are, however, expensive and these types of structures may be sensitive to multiple strikes.

Soil has been used to increase the survivability of structures by providing a cover or barrier to reduce the shock, pressure, and impact on the structure. However, the use of a soil cover or berm is often restricted by the amount of land available for construction and by the logistics of moving large volumes of soil. Unreinforced soil berms require significant land area and soil volume for construction, largely because the berm slopes must be built at an inclination of about 2.5H:1V (horizontal:vertical) for adequate stability. If berm slopes could be made steeper, less land area and soil volume would be required.

Reinforced soil slopes can be constructed at steep inclinations. In many cases, the reinforced soil may be constructed vertically, either with or without facing panels. The concept of soil reinforcement, therefore, promises an economical technique for construction of blast protection structures. Reinforced soil is a composite material made of soil and high-tensile-strength materials such as steel strips or geosynthetics. Reinforcement increases the strength of the soil by confining the soil and suppressing soil strains in the direction parallel to the reinforcement. Incorporating reinforced soil into the design of blast protection structures: (1) reduces the land area and quantity of soil required for construction compared to unreinforced soil structures; (2) simplifies repair of bomb damage compared to reinforced concrete structures; (3) reduces the initial cost of construction compared to other types of structures; (4) reduces construction time compared to reinforced concrete structures; and (5) provides flexibility for design of blast protection structures. In addition, by confining the soil and minimizing crater ejecta, it may be possible to maintain a reinforced soil cover and, thereby, minimize damage from successive strikes. As a result, reinforced soil berms and covers may allow for less expensive construction while providing increased survivability. Reinforced soil may be used to "retrofit" existing structures as a means of providing enhanced blast protection. Geosynthetic reinforcement may be used to construct new structures, retrofit existing structures, or repair damaged structures using a relatively unskilled labor force in an expedited construction.

To design blast protection structures using reinforced soil, the dynamic response characteristics and analytical theory of reinforced soil subject to "blast type" loading must be established. Although soil reinforcement has been practiced for many years, it is still a relatively young technology in scientific terms. A substantial amount of research has been performed in the past decade to determine the properties of reinforced soil under static loading conditions. However, little work has been carried out to determine reinforced soil properties or theory under "blast-type" loading conditions. In fact, the use of reinforced soil in blast protection structures has been previously considered by the Royal Air Force (RAF) in Great Britain and the U.S. Navy. In both of these cases, however, the design of the reinforced soil berms was based on static loading conditions and did not account for the dynamic or impact load induced by the blast. This design approach is believed to be inadequate for the design of blast protective structures. A better fundamental understanding is required for reinforced soil material under blast-loading conditions.

In summary, there are several reasons why reinforced soil should be considered for use as an integral component in the design of blast protective structures. These include:

- reinforced soil structures can be constructed in stages with standard equipment and relatively unskilled labor forces;
- reinforced soil structures can be constructed faster than reinforced concrete structures and with the use of precast facing panels, no concrete curing time is needed;
- reinforced soil is less expensive than reinforced concrete;
- reinforced soil structures require much less steel and concrete than reinforced concrete structures;
- reinforced soil can withstand more deformation prior to failure than reinforced concrete;
- reinforced soil structures are flexible and have significant energy absorbing potential; and
- reinforced soil may increase survivability of structures and reduce susceptibility to multiple strikes.

If reinforced soil is used as an integral component of a blast protection structure design, the design of the structure must account for blast loading conditions. In this regard, the properties of reinforced soil used in the design must be appropriate for blast conditions. Establishing reinforced soil properties and analysis methods applicable to blast conditions are needed.

C. SCOPE OF WORK

A scope of work was developed to achieve the previously summarized objective of evaluating the response of reinforced soil systems subjected to blast loading. This scope of work includes the following four-phased technical approach:

- extensive review of technical literature for: (1) evaluation of information on the response of soils and the response of reinforced soil

systems to blast loading, and (2) availability and characteristics of soil constitutive models and finite element numerical codes for analyzing reinforced soil systems;

- development of laboratory testing facilities and a laboratory testing program to evaluate dynamic response of a reinforced soil system subjected to impulse loading;
- development of a numerical simulation and analysis of reinforced soil wall systems subjected to blast loading; and
- physical modeling of reinforced soil systems subjected to blast loading using centrifuge modeling techniques.

Using this four-phased technical approach, it was possible: (1) to compare the different analysis/modeling techniques for suitability to evaluate the response of reinforced soil systems subjected to blast loading; (2) to provide a quantitative assessment of the properties of reinforced soil and the performance of reinforced soil systems subjected to blast loading; and (3) to provide preliminary guidelines for selecting analysis methods which are appropriate for the design of reinforced soil systems which will be used for blast protection.

This study addressed only the impulse loading effects on the reinforced soil system due to: (1) high pressure incident shock waves; and (2) crater-induced ground motions. Projectile penetration of geosynthetic-reinforced soil structures was not addressed in this study. Finally, the scope of work for this investigation specifically did not include the development of standard structure geometries, design details, design manuals, and construction manuals.

SECTION II

LITERATURE REVIEW

A. GOALS AND ORGANIZATION

This section presents the results of the literature review. A summary of the current state of the art in each of five areas related to the dynamic response of reinforced soil structures is described.

Section II is organized as follows:

- The use of earth berms for the protection of structures from blast loading is described in Section II-B;
- The response of cohesionless soil to dynamic loading and the effort to determine possible strain-rate effects on soil properties is described in Section II-C;
- A review of reinforced soil systems, including both geogrid/geotextile (or macro-) reinforced soils and microreinforced soils, with emphasis on current knowledge of the response of reinforced soil to impulse loading is presented in Section II-D;
- Constitutive modeling of soils under dynamic loading is described in Section II-E; and
- The implementation of constitutive models for dynamic loading of soils into numerical models is described in Section II-F.

B. USE OF EARTH BERMS FOR PROTECTION OF STRUCTURES

The belief that reinforced soil structures might provide cost-effective protection from blast loading stems from the demonstrated ability of unreinforced earth berms to provide such protection. Earth berms are frequently used for the expedient hardening of existing structures (i.e., being placed against existing walls or used as free-standing structures). The berms provide protection against near-misses of general-purpose bombs, high explosive rounds, and ballistic penetration (Reference 1).

Earth berms provide significant advantages over other forms of expedient hardening such as concrete revetments, spill plates and sacrificial panels. Earth berms are easy to construct, usually with local materials, and require minimal time, equipment and labor. This form of protection usually can survive to provide a second strike capability.

The main disadvantage of berms is the large space requirements for side-slopes, especially in the case of free standing berms (Reference 1). Earth berms are also difficult to build in rocky terrain, and in locations where grading equipment is not available. Berms sited adjacent to taxiways and runways may contribute to problems from blowing dust and debris and encroach on safety clearances.

1. Typical Protective Berm Construction

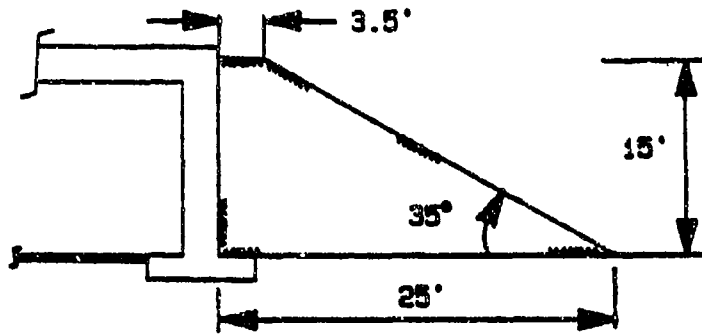
Free-draining granular soil is the preferred material for the construction of earth berms for blast protection. Typically the berm will be maintained at full height to a distance of several feet from the structure, before sloping down to ground level at an inclination of the order 1.5H:1V to 2.5H:1V. The dimensions of the earth berm are chosen depending on the design threat and the required hardness of the structure.

For example, the Air Force design manual (Reference 2) presents a berm design for protection of a 300 mm (12 inches) thick, 4.9 meters (16 feet) high, reinforced concrete wall subjected to the explosion of a 227 kg (500 pound) bomb at a 1.8 meters (6 feet) stand-off distance. The recommended berm, shown in Figure 1, has a thickness at full height of 1.1 meters (3.5 feet), a slope of 35 degrees (1.43H:1V), and extends around three sides of the structure. The construction of such a berm can be accomplished very quickly without the need for skilled labor, form work, or prefabricated materials. The density of the soil in the berm affects its performance; however, in emergency situations it may be more efficient simply to build a larger berm to compensate for lack of thorough compaction.

2. Dynamic Performance

Several studies have been published on the performance of protective earth berms in comparison with other types of expedient hardening (References 1, 3, 4, 5). Coltharp et al., (Reference 3) report the comparative performance of

SECTION



PLAN

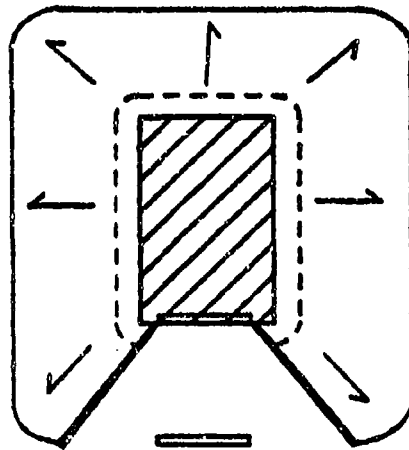


Figure 1. Example of Protective Soil Berm (Reference 2).

earth berms, spall plates and increased wall thickness as alternative means of reducing or eliminating spall caused by blast loading on reinforced concrete box structures with an interior height of 1.65 meters (5.4 feet) and a wall thickness varying between 325 mm (12.8 inches) and 550 mm (21.7 inches). Measured peak pressure against the wall averaged approximately 65 MPa (9,400 psi) in six tests without berms and approximately 8 MPa (1,200 psi) in two tests with berms. Maximum midspan deflections were similarly reduced by the presence of a berm from averages of approximately 30 mm (1.2 inches) and 16 mm (0.6 inch) in tests with spall plates and increased wall thickness, respectively, to only 5 mm (0.2 inch) with the use of berm protection. Peak accelerations were reduced by at least 50 percent, and in some cases by over 90 percent, by protective berms. While fragment penetrations into the concrete wall of between 40 mm (1.6 inches) and 50 mm (2 inches) and spalling occurred in tests without berms, no wall damage occurred in tests with berms. Coltharp et al. (Reference 3) conclude that "berming permits the use of lower steel ratios, produces a more flexural-type response, and is the most cost effective solution."

Reference 4 presents the results of full-scale tests conducted on a hardened reinforced concrete structure built above ground. The effects of a sand berm, precast concrete panels, sand grids and Bitburg revetments on peak pressure, acceleration and wall deflection were compared. Peak accelerations and pressures were reduced by more than an order of magnitude by each method, with smaller reductions in deflection. All four methods were effective in eliminating spall. Although the sand berm did not produce the largest reduction in pressure, acceleration or deflection, it remained largely intact after the test. By contrast, neither the revetments nor the precast panels survived the test blast sufficiently to provide any second strike protection. Hyde (Reference 4) concluded that a sand berm is the most cost effective solution.

Sues et al. (Reference 1) summarize the available test data on a wider range of hardening methods than in the previous two studies. In addition to sacrificial panels and concrete modular revetments, the studies examined four types of protective structure which could be considered earth structures: earth berms, sand grids, sandbagging and bin revetments. The conclusion was that the most effective protection is provided by the earth structures. While the sand grids, sandbagging and bin revetments have the advantage of generally occupying less space (for a given height) and being less susceptible to erosion than earth berms, they generally do not provide multiple hit protection because their

stability comes mainly from materials (plastic forms, bags, and bins, respectively) which are damaged or destroyed by the first strike.

3. Reinforced Soil Berms As Structure Protection

The second-strike protection of earth berms would seem to be directly related to the mass of earth used. A highly efficient reinforced berm of low mass may not give the same protection as the unreinforced berm of greater mass. However, a reinforced soil structure can be designed to function as the shelter itself, offering potential economies. Because of the ease and speed of construction, the relatively small amount of reinforcing and facing materials required, and the simple equipment used to build reinforced soil structures, this form of construction could provide the best expedient protective structures, particularly in remote regions.

The concept of a protective structure constructed from reinforced soil has been verified by Reid (Reference 6), in a test carried out jointly by Terre Armee LTD, the Israeli Air Force and the United States Air Force Engineering and Services Center (AFESC). A bunker with internal dimensions approximately 14.3 meters (47 feet) by 6.6 meters (22 feet), and 3.5 meters (11 feet) high, was constructed from reinforced soil with concrete facing panels, and a reinforced concrete floor and roof. The reinforced soil mass extended at uniform height for a distance 4.0 meters (13 feet) from the facing panels (which formed the interior wall of the bunker). A cross-section and plan view of the bunker is given in Figure 2.

To simulate the loading caused by the destruction of an adjacent ammunition storage bunker, forty 454 kg (1,000 pounds) bombs, each with an equivalent explosive weight of 189 kg (416 pounds), were simultaneously detonated at a distance of 26.5 meters (87 feet) from a side wall of the structure. No noticeable effect on the structure was observed. Detonations of 227 kg (500 pounds) bombs, each with an equivalent explosive weight of 89.4 kg (197 pounds), just outside the reinforced soil mass produced small displacements of individual facing panels, generally less than 100 mm (3.9 inches). Detonations of 227 kg (500 pounds) bombs within the reinforced mass, as close as 3 meters (10 feet) from the facing, produced some localized failures, which were categorized as being amenable to rapid repair. Based on this test, Reid (Reference 6) concluded that "reinforced soil is a very effective construction technique."

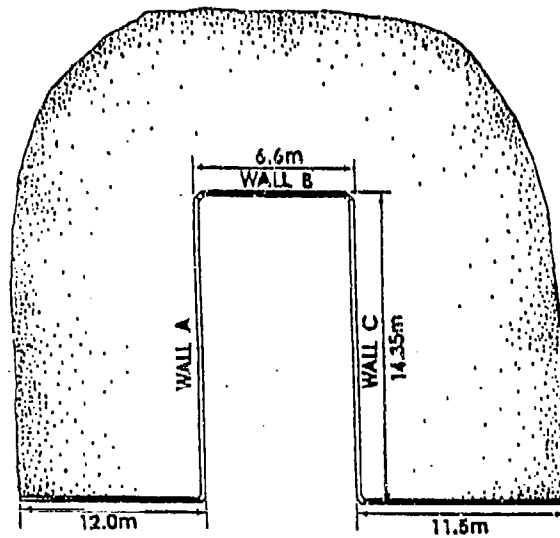
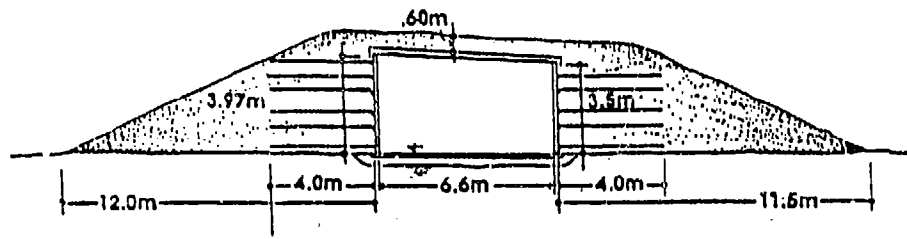


Figure 2. Reinforced Soil Bunker Used in Field Tests (Reference 6):

The reinforced soil structure tested by Reid was designed by conventional static analysis using the patented Reinforced Earth wall system of metal reinforcement strips and concrete facing panels. Because many other types of reinforcement and wall panels are available, research is needed to determine the optimal type of reinforced soil system to employ, bearing in mind the desirable features of convenience and ease of construction and resistance to dynamic loading.

A thorough design for reinforced soil shelters will require knowledge of the behavior of reinforced soil under dynamic loading, knowledge of dynamic reinforcement-soil and panel-soil interaction, as well as knowledge of the dynamic failure modes and mechanisms for reinforced soil structures. The following sections summarize the current state of knowledge of the dynamic response of granular soils and the dynamic behavior of reinforced soil.

C. DYNAMIC RESPONSE OF COHESIONLESS SOILS

1. Introduction

The description of blast-effects on earth berms points to the need to understand the behavior of soils subjected to high strain rate (impulse) loading. Rise times for blast waves are a function of explosive type and distance and typically range from a few milliseconds (ms) to less than 1 ms. The corresponding strain rates in soil can exceed several percent per ms. Since the late 1940s, researchers have been developing techniques for the accurate testing of geologic materials at increasingly greater strain-rates. However, only recently has it been possible to apply submillisecond rise times in controlled laboratory tests and to record accurately the response of the soil. Using these techniques, the response of soils to impulse loading has been investigated by several researchers.

The methods of dynamic testing of soils relevant to this research include uniaxial compression, direct shear, and triaxial compression. A review of the literature for each test is given below, followed by an assessment of the current state of knowledge.

2. Dynamic Uniaxial Behavior

A major reason for research into the response of soil subject to high strain-rate loading has been the desire to characterize soil response to air blast loading from a nuclear detonation. Because of the large areal extent of a nuclear blast compared to a typical soil strata thickness, the loading on the ground surface is essentially one-dimensional. Consequently, 1-D (uniaxial) loading tests have been used most extensively for the research. There are primarily two types of 1-D testing equipment used for most of the past studies; the uniaxial strain device and the Split-Hopkinson Pressure Bar (SHPB). Both devices can provide strain rates needed to model blast loading.

a. Description of Equipment

The uniaxial strain device is similar to an oedometer, as used in conventional soil mechanics to evaluate soil compressibility. A cylindrical soil specimen with a typical height to diameter ratio of approximately 1:4 is placed in a rigid ring on a rigid base. A schematic diagram of a uniaxial strain device is shown in Figure 3. A transient vertical pressure is applied to the specimen and the time histories of pressure and axial deformation are recorded. From these data, dynamic bulk modulus versus axial strain is obtained for both loading and unloading. The uniaxial strain device has been used extensively to measure dynamic response of soils since Whitman's pioneering work (References 7, 8). According to Farr and Woods (Reference 9), the popularity of this method is due to its relative simplicity and the direct measurement of the stress-strain response.

In the SHPB, a cylindrical soil specimen with a typical length to diameter ratio of approximately 1:2 to 1:5 is placed between solid steel incident and transmitter bars. A confining cylinder around the specimen is typically used to minimize radial expansion. A schematic diagram of a SHPB is shown in Figure 4. To load the specimen, a striker bar is launched by a gas gun and impacts the incident bar causing a P-wave to propagate down the incident bar. The amplitude of this P-wave is proportional to the velocity of the striker bar and its duration is a function of the length of the striker bar. When the P-wave reaches the soil specimen, a portion of the energy is transmitted through the specimen and a portion is reflected as a tension wave. When the P-wave reaches the interface with the transmitter bar, it is again split into transmitted and reflected waves. Strain gauges mounted on the incident and transmitter bars

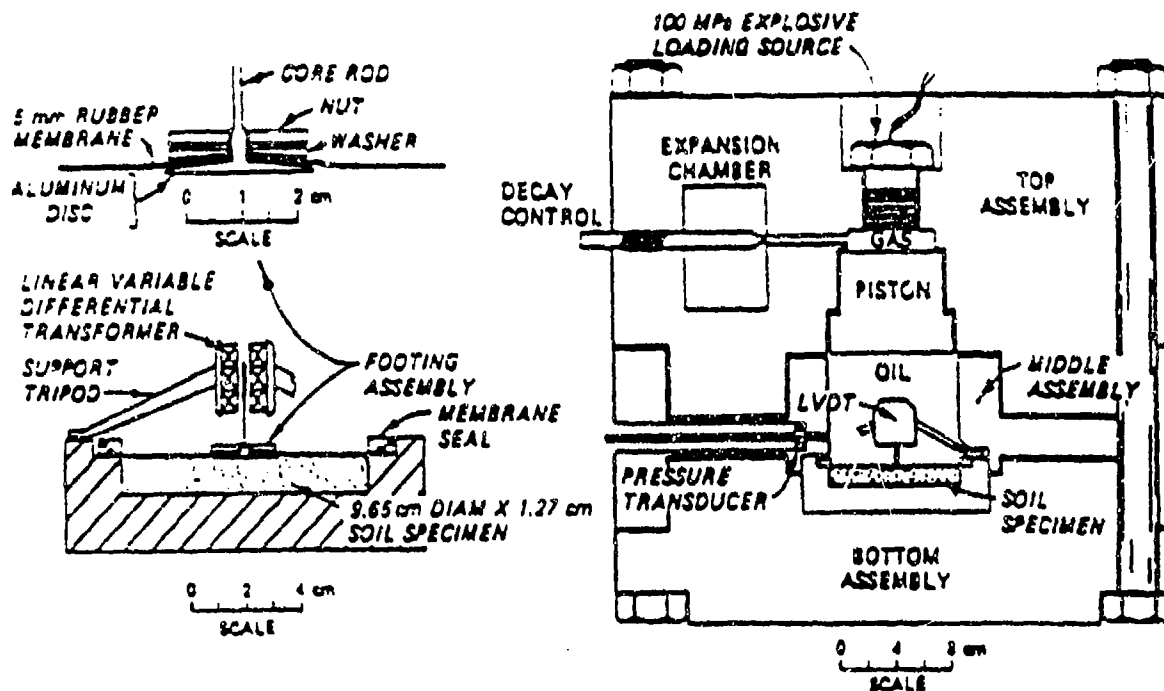
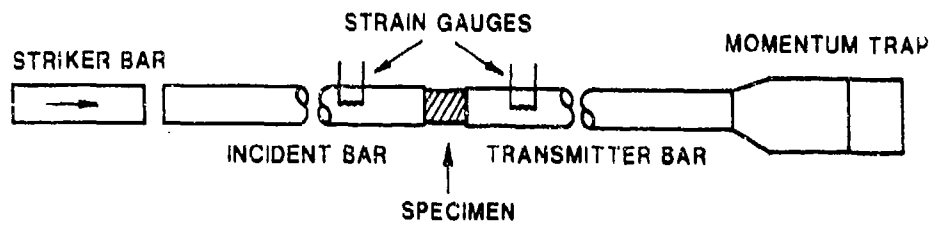
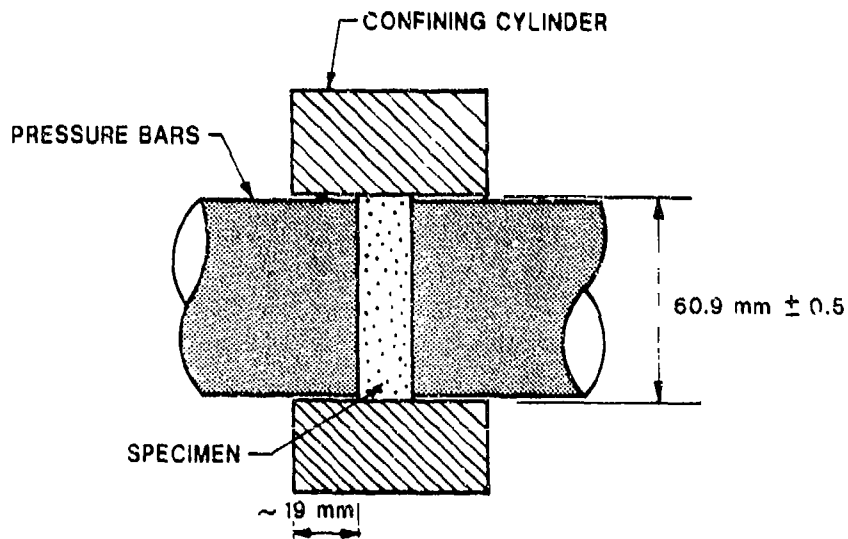


Figure 3. Schematic Diagram of High Strain-Rate Uniaxial Strain Device (Reference 16).



a) main components of SHPB



b) expanded view showing confining cylinder for tests on soil

Figure 4. Schematic Diagram of Split-Hopkinson Pressure Bar (Reference 10).

monitor the stresses which pass them, and the data are recorded. Using 1-D wave propagation theory together with the data from the strain gauges and a correction procedure detailed by Felice et al. (Reference 10) allows the stress-time and stress-strain curves for the soil to be calculated.

b. Laboratory Testing Methods and Results

(1) Compressed Nitrogen

Since the first use of dynamic uniaxial strain devices, researchers have continually strived for faster loading rates and more accurate data acquisition. Early researchers in the groups at the Massachusetts Institute of Technology (MIT) (Reference 7, 8), Stanford Research Institute (Reference 11), and the Eric H. Wang Civil Engineering Research Facility (Reference 12) used high pressure bottled nitrogen to apply the compressive load. Compressive load rise times of several ms were achieved but there was lack of uniformity and control of the load as well as time lags caused by the instrumentation (Reference 13). Whitman (Reference 14) speculated that a significant increase in stiffness, of the order 10 times or more, could occur when the loading rate drops below 1 ms.

(2) Piston-Driven Compressed Gas

A series of uniaxial strain devices were developed at the U.S. Army Engineer Waterways Experiment Station (WES), beginning in the late 1960s, to achieve the desired submillisecond loading rates. Schindler (Reference 13) describes the first device that used a piston driven by compressed gas to load the specimen through a confined liquid. The apparatus produced a more uniform stress distribution within the specimen, compared with previous devices, and rise times as fast as 1 ms were achieved.

This apparatus was modified further to produce submillisecond rise times using an explosively driven piston, linked to an improved data acquisition system (Reference 15). Tests using this system indicate that the ratio of dynamic to static modulus for a partially saturated quartz sand increases approximately ten fold as the loading time to peak pressure approaches the submillisecond range.

(3) Split-Hopkinson Pressure Bar

The above finding was contradicted by the results obtained using the SHPB apparatus by Felice et al. (Reference 10). They presented data from tests on partially saturated, compacted, clayey silty sand specimens (classified SC). The peak applied pressures were in the range 130 to 160 MPa (19 to 23 ksi) and the peak rate of strain between 50 and 500 percent per ms. A typical stress-strain response from such a test is shown in Figure 5.

Over 200 tests were conducted by Felice et al. (Reference 10), and these were highly repeatable. No significant strain-rate effects were observed for rise times below 1 ms. However, a significant increase in stiffness was reported as the pore air in the soil dissolved in the pore water. The initial gas porosity of the specimens ranged between approximately 5 and 10 percent. Therefore, volumetric strain during a test frequently reached the specimen's initial gas porosity, causing saturation in the specimen. Significant stiffening of the response then occurred due to the high bulk modulus of water. This effect is seen beginning at Point A in Figure 5.

(4) Exploding Bridgewire

Perhaps prompted by the apparent discrepancies between the data of Jackson et al. (Reference 15) and Felice et al. (Reference 10), Farr and Woods (Reference 9) developed a new generation of submillisecond, uniaxial strain devices at WES (the 0.1 ms uniaxial strain device). This apparatus uses an exploding bridgewire to produce the submillisecond rise time. Static (slow rise time) loading tests can also be carried out in the same apparatus to allow direct comparison.

They reported the results of a series of tests using the 0.1 ms device on a carbonate sand from Enewetak Island prepared at a water content of 5 percent, a relative density of approximately 40 percent, and initial gas porosity of approximately 30 percent. To determine the effect of loading rate on constrained modulus ratio (dynamic modulus divided by static modulus), loading time to 36 MPa (5 ksi) varied from over 150 seconds to 0.2 ms. Stress-strain curves for typical tests are shown in Figure 6. Clearly, there is a rate effect on modulus found from the data in Figure 6; however, the dramatic increase reported by Jackson et al. (Reference 15) at a rise time of 1 ms was not observed.

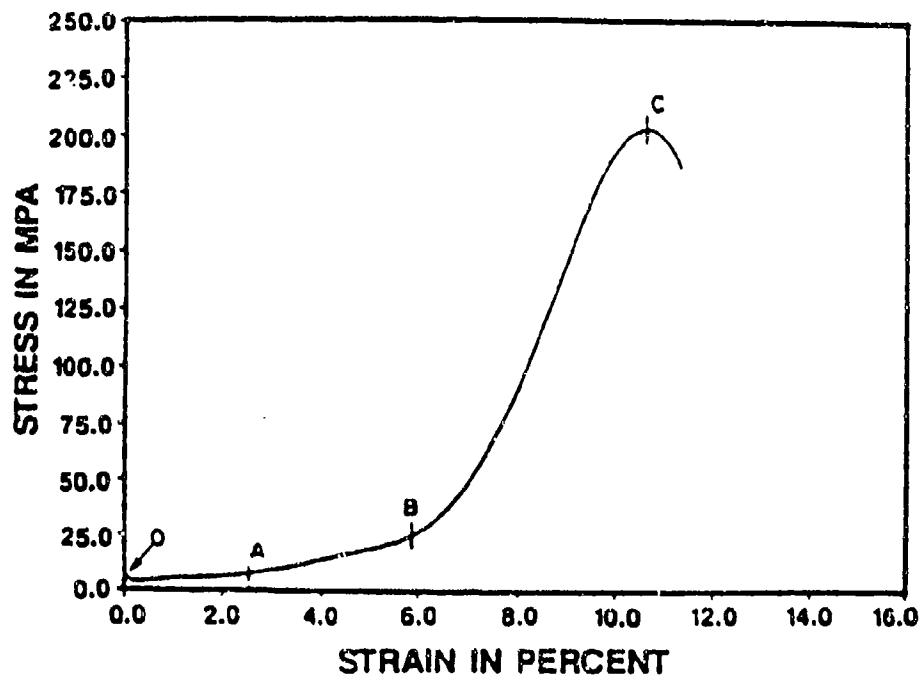


Figure 5. Typical Stress-Strain Response from SHPB Test (Reference 10).

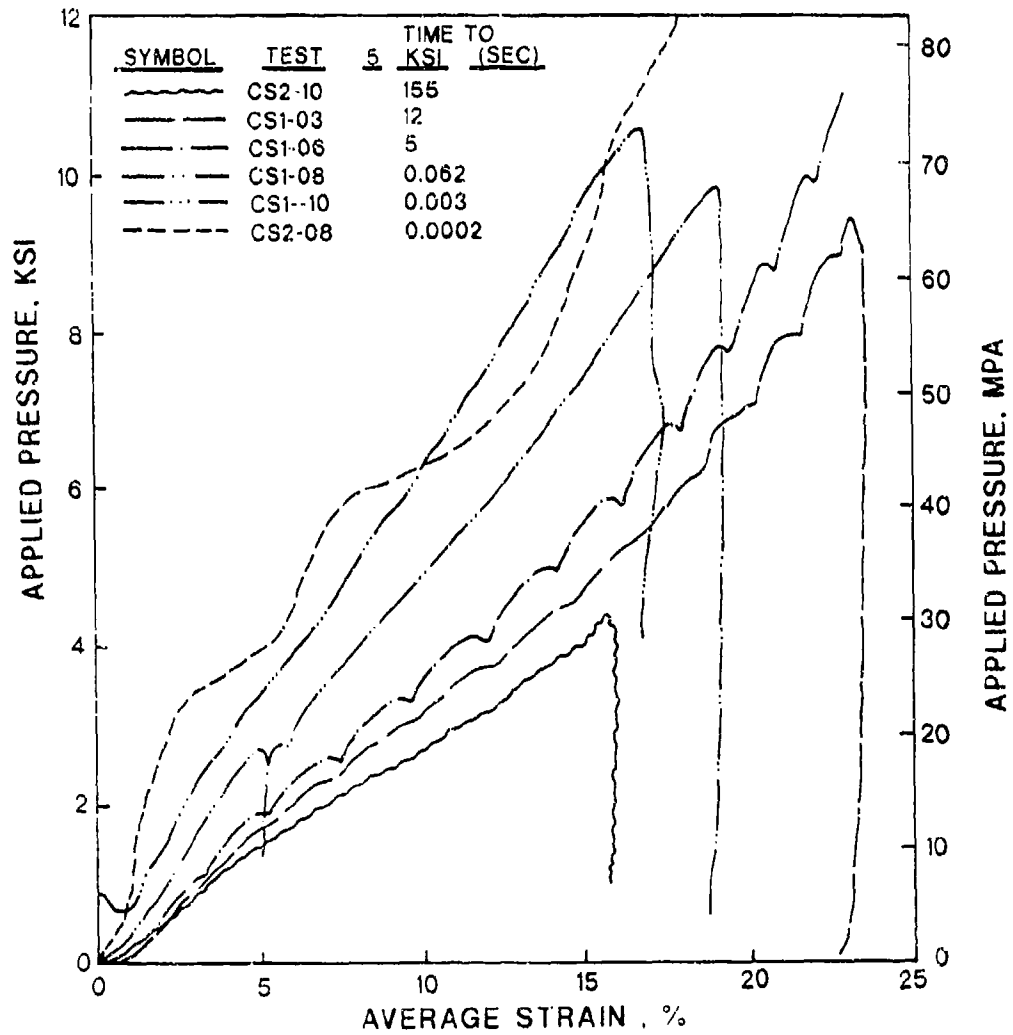


Figure 6. Uniaxial Strain Test Results for Enewetak Beach Sand (Reference 9).

Additional tests on a clean quartz sand (flume sand) were carried out by Farr (Reference 16). The flume sand and the Enewetak sand both show a stiffening as strain rate increases, however this rate effect occurs at a much lower strain rate for Enewetak sand than for the flume sand, as seen in Figure 7. The results indicate a gradual increase in the modulus ratio for Enewetak sand above quasi-static rates of loading (10^{-4} percent per ms), until a plateau is reached at a stiffness ratio of approximately 2.2, at a strain rate of about 10 percent per ms and above. In contrast, no strain rate effect is observed for the flume sand until the strain rate exceeds about 0.1 percent per ms, after which the modulus ratio increases with strain rate before reaching a limiting value. For the flume sand, the maximum stiffness ratio is limited to about 1.4, for soil strain in the range 0-7 percent, or 1.1 when a larger range of strain, 0-10 percent, is considered, as shown in Figure 7. The limits apply above a strain rate of the order 10 percent per ms.

3. Dynamic Shear Behavior

The conventional uniaxial strain device and the SHBP apparatus can provide data on soil stiffness under 1-D compressive loading, but cannot provide information on the influence of strain rate on the shear strength of soil. Both stiffness and strength data are required to model the behavior of soil structures subjected to loading from conventional weapons detonated in or near the structure. Direct shear and triaxial shear tests have been used to investigate the dynamic shear strength of soils, although triaxial testing is used most frequently.

a. Direct Shear Tests

Schimming and Saxe (Reference 17) used a direct shear device to test Ottawa sand under both static and dynamic conditions. Specimens 102 mm (4 inches) in diameter and 19 mm (3/4 inch) thick were sheared to failure in either 40 seconds or 3-4 ms. The vertical and horizontal loads and the displacements in both vertical and horizontal directions were measured. In some tests a pneumatic piston was used to provide 165 to 275 kPa (24 to 40 psi) vertical stress to the specimens, and in this case, no difference in shear strength was observed between the static and dynamic tests, as seen in Figure 8.

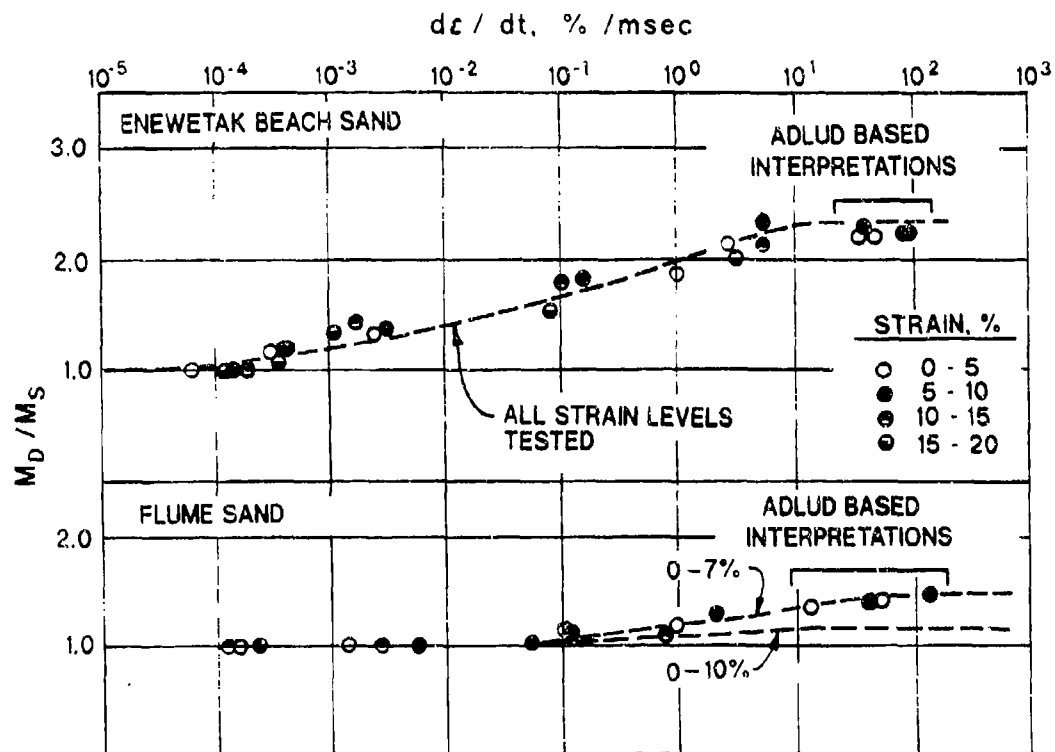


Figure 7. Comparison of Rate Effects in Enewetak Beach Sand and Flume Sand (Reference 16).

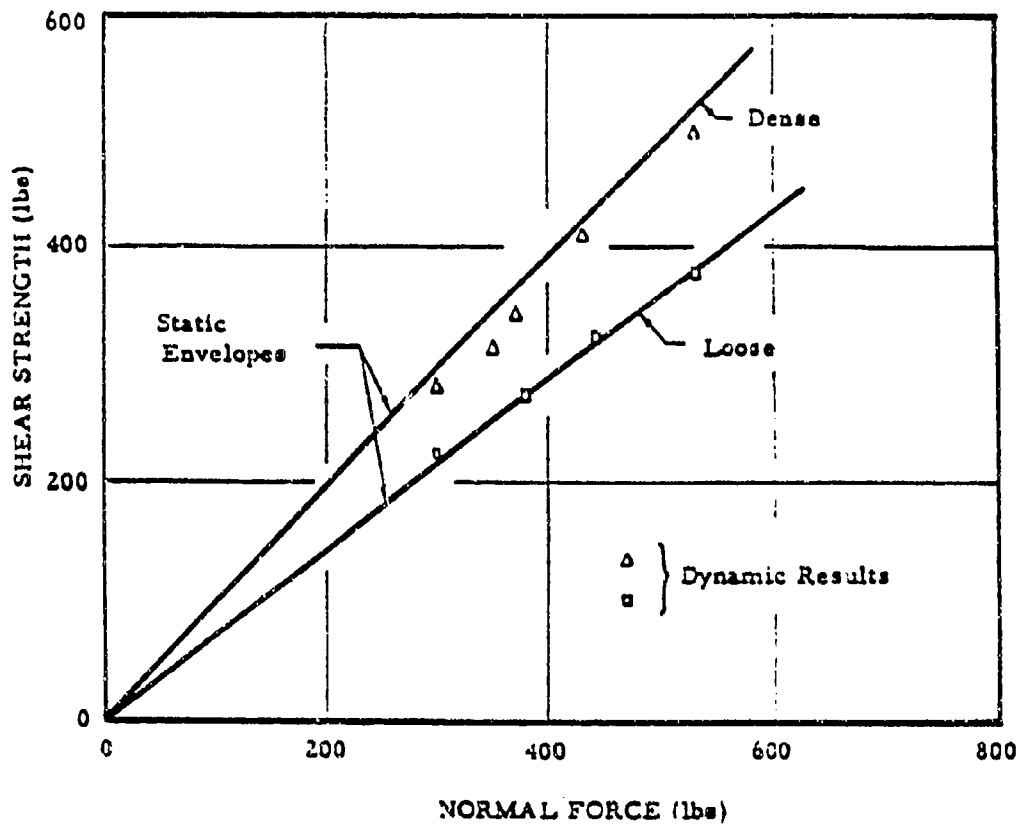


Figure 8. Comparison of Dynamic and Static Direct Shear Test Results (Reference 17).

Additional tests were carried out to investigate the effects of inertia across the shear plane for dense specimens that dilate when sheared. A dead weight was used to apply a vertical stress between 17 and 80 kPa (2.4 and 12 psi). The dynamic friction angle for these tests was 61 degrees, compared to the static friction angle of 43 degrees, showing a clear influence of the inertia of the loading system. The loading rate at which these inertia effects became critical could not be determined, as only one loading rate was tested.

b. Triaxial Tests

The effect of loading rate on the response of soils to triaxial shear loading has been investigated for over 40 years (References 18, 19, 20, 21). This work indicates that soil type, degree of saturation and drainage conditions are the major influences on strength ratio (peak dynamic strength divided by peak static strength) of soils (Reference 8).

For example, dry cohesionless soils exhibit very low strength ratios, typically 1.05, or at most 1.2, for times to failure down to about 10 ms. Saturated cohesionless soils in which drainage is allowed exhibit a wide variety of strength ratios. The permeability of the soil, and any tendency for volume change during shear, influence significantly the dynamic strength. A large strength ratio would be expected in a dilative soil with relatively low permeability, due to the negative pore pressure caused by the loading. Undrained shear of compacted cohesionless soil gives typical strength ratios of the order 1.2 to 2.5 as an upper bound, the particular value depending greatly on the volume change characteristics of the soil. Clays exhibit the largest strength ratios, when subjected to undrained shear, varying typically from about 1.6 to 4 or more, in extreme cases.

c. Fast Triaxial Shear Device

To investigate the loading regime, 1 ms or less, a fast triaxial shear device (FTRXD) was developed at WES. This apparatus is capable of loading to failure in less than 1 ms, specimens with dimensions 1.9 cm (3/4 inch) in diameter by 3.8 cm (1.5 inches) high (Reference 22).

The loading is applied by a ram-piston assembly driven by compressed nitrogen as shown schematically in Figure 9. Slow loading (>20 ms to failure) is accomplished by filling the lower chamber with oil and pressurizing the upper

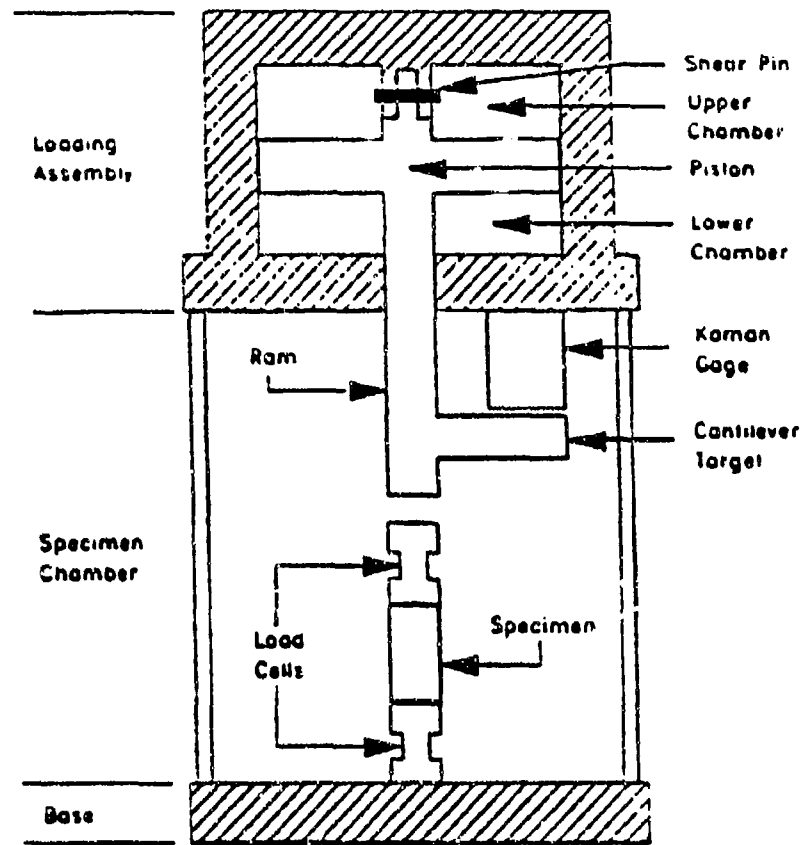


Figure 9. WES Fast Triaxial Shear Device (FTRXD) (Reference 23).

chamber with nitrogen. Opening a valve in the lower chamber allows the oil to escape at a constant rate, regulating the strain rate of the test. For faster loading of the specimen, the lower chamber is open to the atmosphere. The test is initiated when the nitrogen pressure in the upper chamber is sufficient to shear a pin connecting the ram-piston to the top of the cylinder. Different strength pins allow a range of loading rates. Carrol (Reference 23) reports that the fastest constant velocity achieved to date is 85 cm/s (33 inches/s) using the oil filled chamber, and the fastest constant acceleration achieved is 400 g, using the shear pin connection.

Load and deformation measurement in the FTRXD is complicated by the fast displacement rates. Two load cells are used, one immediately above and one immediately below the specimen, and displacement is measured by a noncontact sensor (Kamen gauge) and target attached to the ram. While problems were experienced with the development of the top load cell (as described in Reference 23) the lower load cell gave relatively stable readings at all loading rates. However, these difficulties in data acquisition at high loading rates serve to illustrate the need to examine carefully the mechanical and electrical interaction between components in dynamic test equipment. The requirement for high natural frequency components in such equipment is especially important.

In a series of tests reported by Carrol (Reference 24), the time to failure had relatively little measurable effect on the peak deviator stress, as seen in Figure 10. An increase of approximately 10 percent is seen between 120 seconds and 2 ms loading time. The tangent modulus at low strain (<1 percent) is nearly identical in all four tests. Except for the slowest test, the stress-strain curves vary little. Random variation among specimens could easily account for the different shape of the curve for the slowest test.

4. Load Rate Effects

The review of the literature points to the conclusion that loading rate does not significantly affect the shear strength of relatively dry, cohesionless soils. As the time to failure varies from hundreds of seconds to less than 1 ms, the peak shear strength increases by only 10 percent or less in the cohesionless soils tested to date. A broadly similar conclusion is reached for constrained modulus. However, tests on Enewetak sand have indicated that the dynamic constrained modulus could be of the order twice the static constrained modulus for sand materials with more crushable and/or softer grains than quartz.

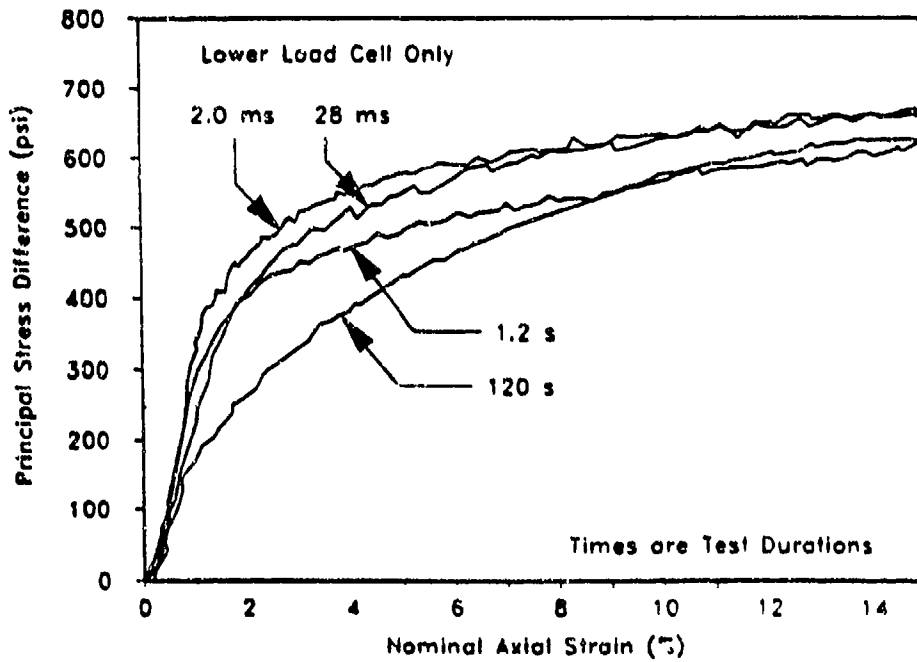


Figure 10. Effects of Loading Rate on Behavior of CARES-Dry Soil (Reference 23).

Saturated or nearly saturated soils can exhibit significant rate effects both for the compressive modulus and peak shear strength. A significant increase (50 percent or more) in stiffness and strength has been observed in saturated cohesionless soils and clays, and 20 percent to 50 percent in nearly saturated soils. The effect on shear strength is observed in soils which dilate on shear, which causes a reduction in pore pressure in the soil. The increase in compressive stiffness at higher rates of loading is due mainly to the water phase in saturated soils, and the high bulk modulus of water.

Clean sands composed of quartz, or similarly hard minerals, are used most frequently for reinforced soil structures. These materials are free-draining and, provided they are placed above the water table, are unlikely to be near saturation. Rate effects on the compressive modulus and shear strength of such soil should be unimportant for the purposes of the present research. The inherent simplifications in the available constitutive models for granular soil are likely to have a more significant influence on the results of numerical analysis than any rate effects on the soil modulus or shear strength.

D. REINFORCED SOIL SYSTEMS

1. Concept and Description

The reinforcement of soil is defined by Mitchell and Villet (Reference 25) as the "inclusion of resistant elements in a soil mass to improve mechanical properties." The basic concept behind reinforced soil has similarities with that for reinforced concrete; soil, which has little tensile capacity, but which is strong in compression and shear, is reinforced with inclusions that are strong in tension thus forming a composite material benefiting from the best load carrying features of each material. Stress is transferred between the soil and the reinforcement by means of interface friction or passive resistance, or a combination of both (Figure 11).

The presence of high tensile modulus reinforcement in soil serves to restrain the deformation of the soil in a direction parallel to the reinforcement. In simple terms, the resulting increase in strength has been viewed as reinforcement imparting an anisotropic cohesion in the soil (Reference 26) or an increased confining pressure (Reference 27), as illustrated in Figure 12.

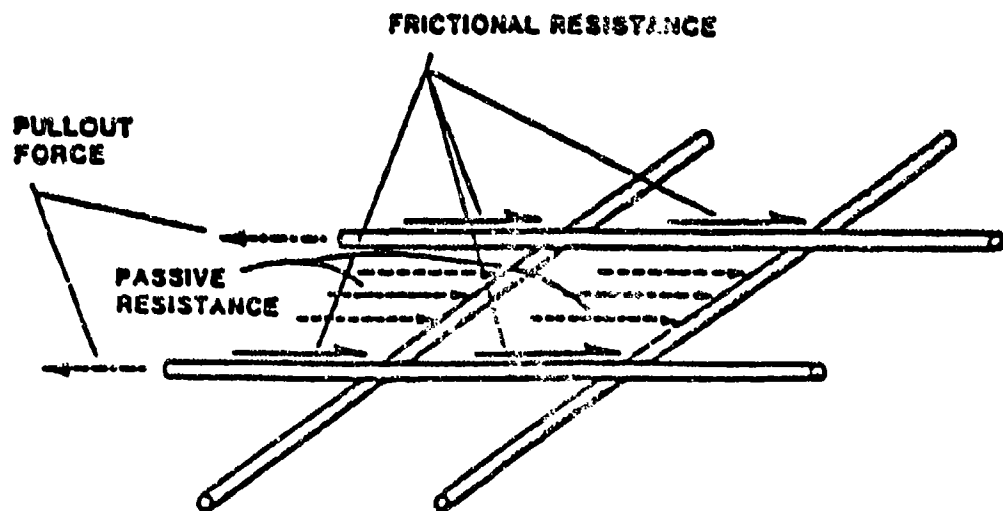
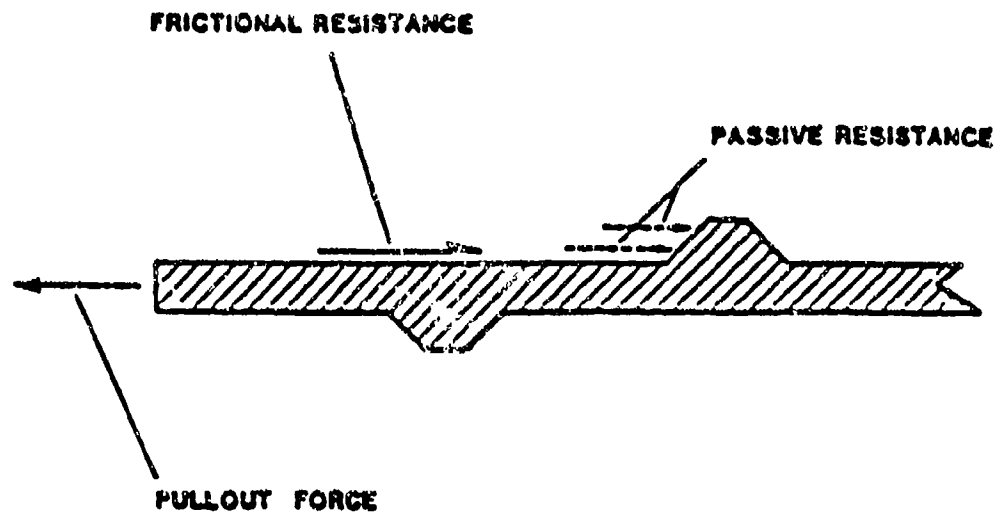
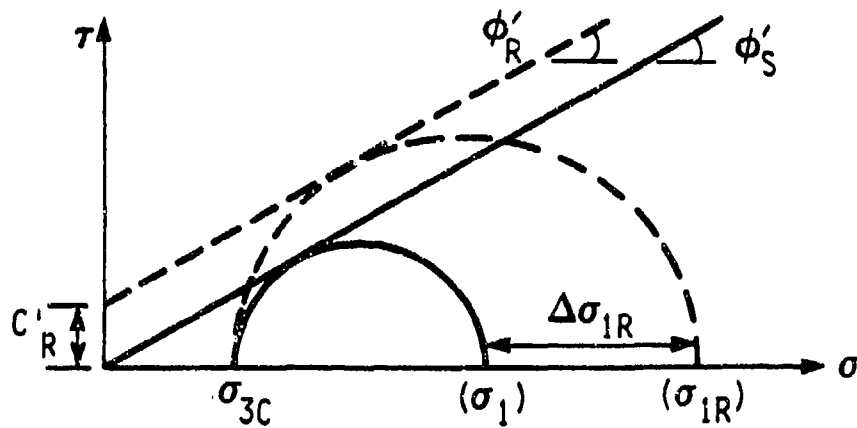
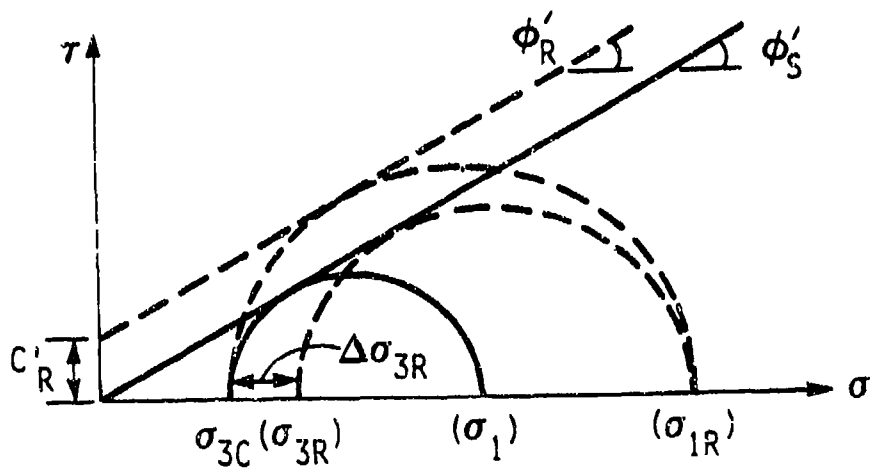


Figure 11. Mechanisms of Stress Transfer in Reinforced Soil (Reference 25).



a) Apparent Cohesion Interpretation
(Reference 26)



b) Increased Confinement Interpretation
(Reference 27)

Figure 12. Strength Representation of Reinforced Soil.

The concept of soil reinforcement is rather old (e.g., the use of straw in clay brick), but it was first introduced into modern engineering with the use of metal or geosynthetic inclusions in the late 1960s. The earliest, and still the most common application of reinforced soil is for the construction of retaining structures, which have been built to a height as great as 45 meters (150 feet).

Geosynthetic reinforcement is typically in the form of a sheet structure manufactured from polyethylene, polyester, or polypropylene (or a mixture of these). The most commonly used types of geosynthetic reinforcements are geotextiles and geogrids (Figures 13 and 14). While not as stiff as steel reinforcement, certain geosynthetics present the advantage of better durability than steel and a more ductile stress-strain behavior. The latter property may be particularly beneficial if the reinforced soil structure is subject to conventional weapons effects where the load is very high but of short duration.

Recently, a new form of geosynthetic reinforcement, termed "micro-reinforcement," has been introduced. Microreinforcement comprises small size inclusions that are mechanically mixed into the soil matrix. Both one-dimensional (monofilament) and two-dimensional (fibrillated fiber) elements have been used, as well as miniature geogrids (Reference 28). Test data suggest that rather small quantities of reinforcement, as low as a few tenths of one percent (by mass), can result in significant improvement in strength. An advantage of micro-reinforcement in comparison to traditional geosynthetics is that it causes a more uniform or isotropic improvement of soil properties, compared to the highly structured or orthotropic improvement of soils reinforced with sheets of geosynthetics.

2. Response of Geosynthetic Reinforcement

The design of structures utilizing geosynthetic reinforcement requires knowledge of the geosynthetic's strength and load-deformation behavior, as well as the interface friction coefficient between the reinforcement and the soil. In-air and confined extension tests are used to determine strength and load-deformation behavior and direct shear and pullout tests are used to determine interface friction coefficient (Reference 29).

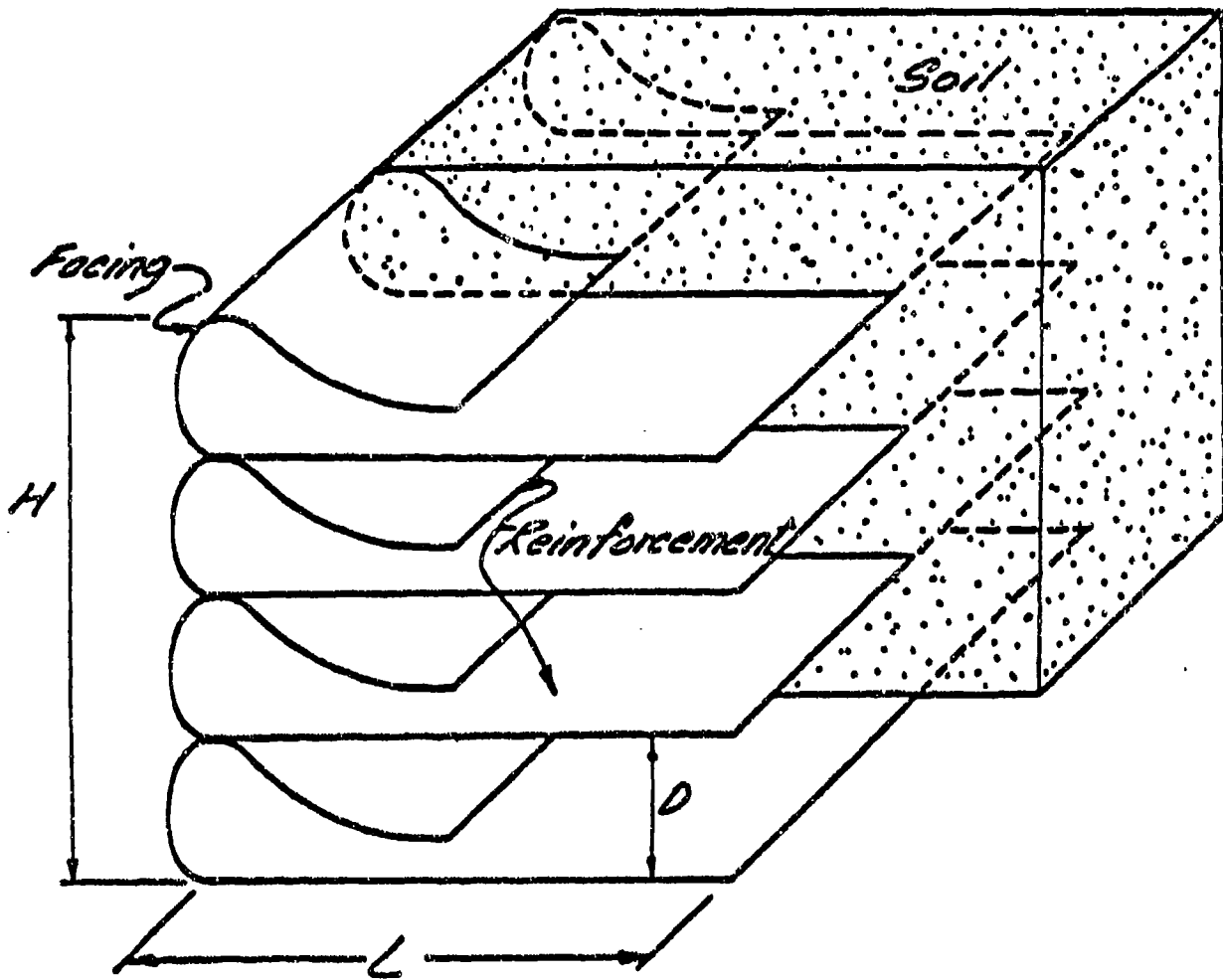


Figure 13. Schematic Diagram of a Reinforced Soil Wall Using Geotextile Shear Reinforcements (Reference 25).

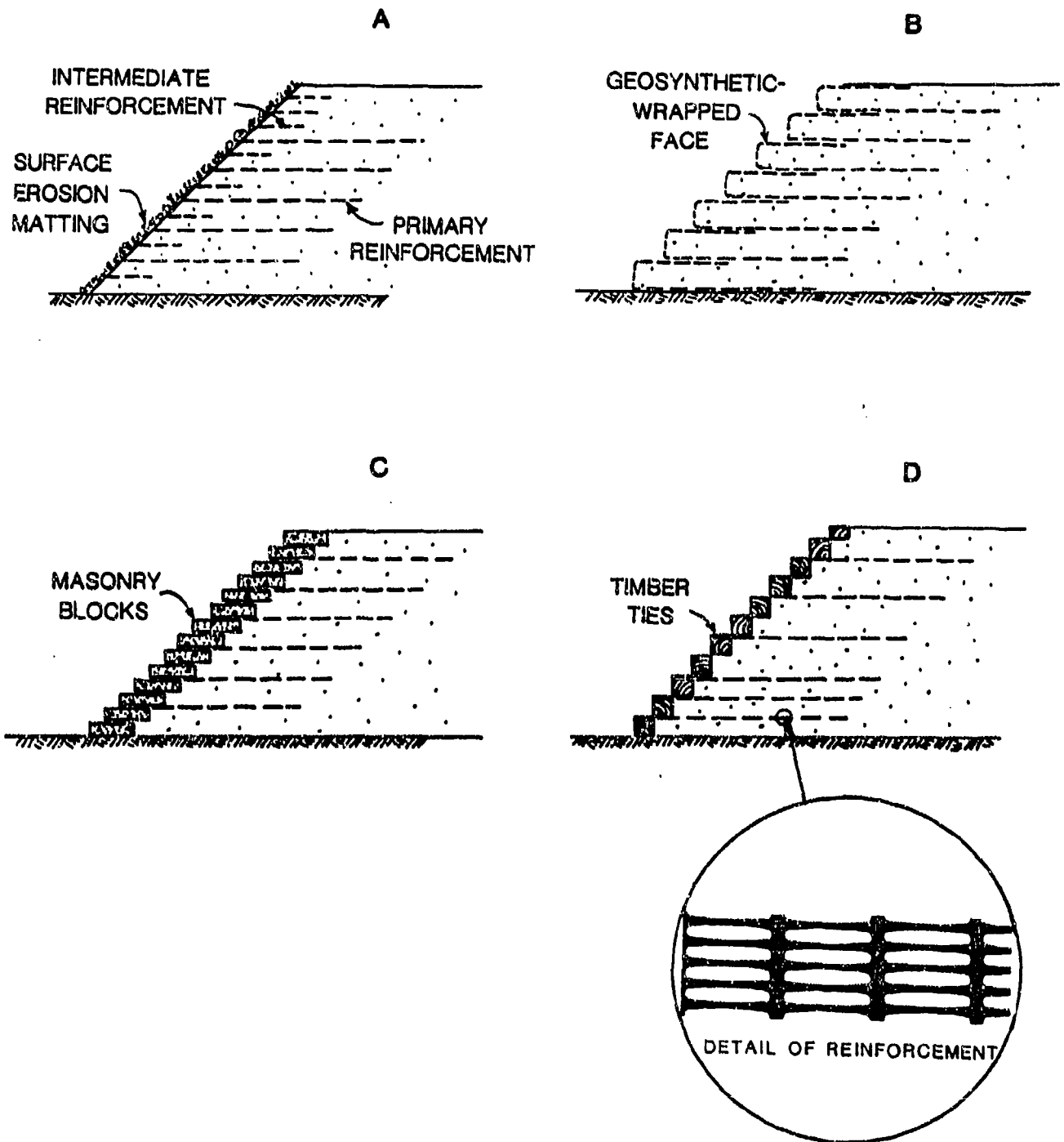


Figure 14. Schematic Diagram of Reinforced Soil Embankment Using Geogrid Reinforcement.

Although in-air extension tests are relatively easy to perform, confined extension tests in which the geosynthetic is in contact with soil better simulate in-situ behavior. McGown et al. (Reference 30) and Siel et al. (Reference 31) have shown that both the geosynthetic strength and deformation modulus increase with increasing confining pressure. The effect of confining pressure is greater for geogrid compared to geotextile because of the passive resistance on transverse elements of the geogrid (Reference 29).

The effect of high strain rates on strength and deformation of geosynthetics is an important consideration in the investigation of blast response of reinforced soil systems; however, very little information on this topic was found in the literature. Rowe and Ho (Reference 32) performed a series of unconfined extension tests on four woven geotextiles and one geogrid to investigate the effects of strain rate on strength and deformation modulus. Strain rates from 0.2 percent per minute to 10 percent per minute were used. Test results showed a linear relationship between tensile strength and log of the strain rate. All materials exhibited an increase in strength with increasing strain rate. The geogrid (Tensar SR2) was the most sensitive to strain rate with an increase in strength of approximately 33 percent from .2 percent to 10 percent strain per minute. The geotextiles ranged from 15-20 percent increase in strength over the approximately two log cycles of testing. All materials exhibited similar increases in tangent modulus (measured from 5-10 percent strain) with increasing log of strain rate. The increase for geogrid was approximately 80 percent and for geotextiles the increase ranged from 25-55 percent.

The highest strain rate tested (10 percent per minute) is significantly lower (approximately 3-4 orders of magnitude) than what might be expected with blast loading conditions. Therefore, interpolation of these results to the blast loading regime is not advisable. It is clear, however, that strain rate effects do have some influence on strength and modulus of geosynthetics.

Soil-geosynthetic interface behavior is typically expressed in terms of an efficiency factor, which is the ratio between the soil-reinforcement interface friction angle ($\tan \delta$) and the soil friction angle ($\tan \phi$) (Reference 29). Although both direct shear and pullout tests are used to evaluate interface behavior, the two tests differ significantly in loading path and boundary conditions. The fundamental difference between the two tests is the distribution of mobilized shear strain. In the direct shear test, the mobilized shear strain

is uniform along the reinforcement, while in the pullout test the mobilized shear strain is a combination of interface shear strain and reinforcement extension. Therefore, in the pullout test, the shear stress-shear strain distribution is nonuniform, as it is in most field applications of reinforced soil.

Less information is available on rate effects in direct shear and pullout tests than on extension tests. Myles (Reference 33) conducted a limited number of direct shear tests on four geotextiles in which the deformation rate ranged from 10 mm/minute (0.39 inch/minute) to 75 mm/minute (2.95 inches/minute). The soil used was a uniform sand. No rate effects were observed in any of the tests.

Farrag (Reference 29) reported the results of nine pullout tests on Tensor SR-2 geogrid in which the pullout rate ranged from 4 mm/minutes to 20 mm/minute. A slight decrease in peak pullout resistance was observed in tests with a pullout rate over 6 mm/minute (0.23 inch/minute). However, due to the small number of tests and the variation in soil density [1.66 Mg/m^3 to 1.70 Mg/m^3 (103.4 pcf to 106 pcf)] from one test to another, the results are of questionable value. Also, the pullout rates are very low compared to that expected under blast loading conditions.

3. Response of Microreinforced Soil

a. Fiber reinforcement

The investigation of the behavior of micro-reinforced soil had its origins in work conducted in the 1960s on soil reinforced with plant roots (References 34, 35). This work and later investigations indicate that plant roots increase the shear strength of soil. Most investigations have shown that the increase in strength can be accounted for by a change in apparent cohesion, as shown in Figure 12 (Reference 36).

Work on microreinforcement of soils with discrete artificial materials dates back to the mid-1970s and can be divided into studies of soil reinforced with fibers oriented in specific directions and studies of randomly oriented fibers. The work on randomly distributed, fiber-reinforced sand (RDFS) is more applicable to this research project and the following review concentrates on this portion of the literature.

Almost all the testing of RDFS reported in the literature has had the aim of determining the static stress-strain properties of the material. Hoare (Reference 37) investigated the static stress-strain and compaction properties of a crushed sandy gravel reinforced with two types of inclusion, a polypropylene/nylon fabric sheet cut into 66 x 7 mm (2.6 x 0.3 inches) strips and a 52 mm (2 inches) chopped polypropylene staple fiber. The fiber content was found to have a significant effect on the compacted density, and the triaxial tests showed that the effect of the lower soil density dominates the reinforcing effect for fiber strip reinforced specimens.

Gray and Al-Refeai (Reference 38) reported on an extensive series of static triaxial tests on RDFS. They used common basket reed and glass fiber to reinforce a clean, uniform, medium-grained sand. Factors which were varied in the tests were confining stress, fiber weight fraction, fiber aspect ratio, compactive effort, and fiber modulus and surface friction characteristics. In addition, the authors note that the reed fibers have rougher surfaces, and hence a higher friction coefficient compared to the glass; however, no data are provided on actual friction coefficients. The majority of tests were conducted at fiber weight fractions between 0.21 and 2 percent; however, weight fractions up to 6 percent were used for tests on 25 mm (1 inch) glass fibers.

The results of Gray and Al-Refeai's tests show that the inclusion of randomly oriented fibers can significantly increase the maximum deviator stress, reduce the post-peak strength loss and increase the axial strain at failure compared to the unreinforced sand at the same porosity. Based on a limited number of tests on glass fiber, it appears that the strength enhancement continues to increase with increasing fiber content until a limiting value is reached (Figure 15).

A recent comprehensive study by Maher (Reference 36) has reported on the static and dynamic behavior of RDFS. Eight different sands were used, as well as a "sand" made from glass beads. Maher confirmed the observation of Gray and Al-Refeai (Reference 38) that a planar failure surface develops in RDFS, and showed that the orientation accords with Coulomb's theory. Maher also confirmed the existence of a critical confining stress, σ_{crit} , above which the failure envelope for RDFS is parallel to that of the unreinforced sand. Below this critical confining stress the failure envelope tends to be curved for the more uniform soils and linear for the well-graded sands. No satisfactory explanation was given for either the existence of a critical confining pressure or the

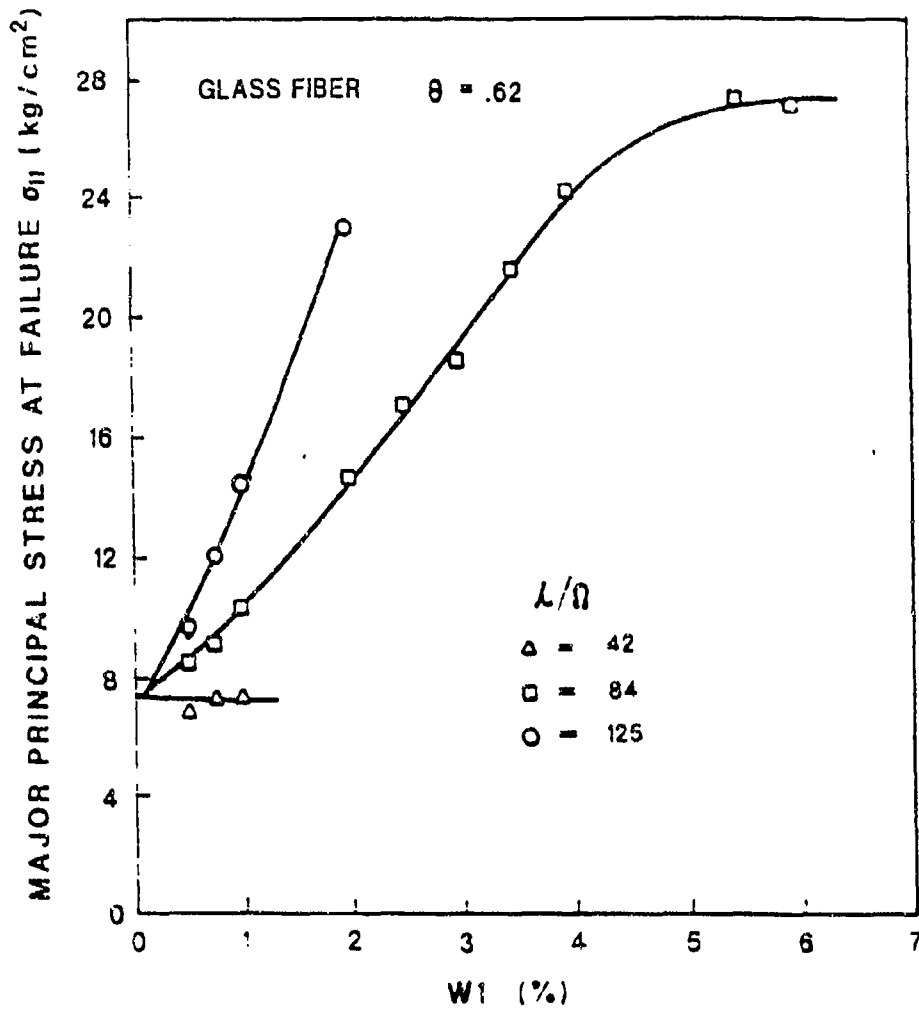


Figure 15. Effects of Fiber Content and Fiber Aspect Ratio on Strength of Fiber Reinforced Soil (Reference 38).

apparent effect of soil gradation on the slope of the failure envelope. Maher did note, however, that there was no evidence of fiber rupture in any of the tests, apparently eliminating the possibility that a change in failure mode from fiber slippage to fiber rupture occurs at the critical confining stress.

Resonant-column and torsional shear tests on RDFS have also been reported by Maher (Reference 36) and Maher and Woods (Reference 39). These tests were carried out to determine the influence of testing parameters (strain amplitude, confining pressure and cyclic prestraining) and material parameters (fiber content, aspect ratio, modulus and orientation) on the shear modulus (G) and damping ratio (D) of RDFS. The same fibers used for the static tests described above were used in the dynamic testing.

The addition of glass fiber with an aspect ratio, (length to diameter ratio) of 80 caused an increase in shear modulus compared to the unreinforced soil. The ratio of reinforced to unreinforced modulus varies from 1.1 to 1.4 (Figure 16). The shear modulus ratio increases both with increasing fiber and shear strain amplitude. For this particular combination of fiber and soil, increasing fiber content above 5 percent by weight does not lead to increased modulus ratio. However, the increase in modulus ratio with shear strain amplitude continues at approximately a constant slope through 3 percent strain. Damping ratio is also affected by fiber content at very low (<0.1 percent) strain where the damping ratio factor (reinforced D divided by unreinforced D) varies from approximately 3 to 7 at a strain of 10^{-4} percent to 1.5 to 2.0 at a strain of 10^{-2} percent. The upper end of these ranges is obtained with 5 percent fiber, the lower with 1 percent fiber. In the range between 10^{-1} and 3 percent strain, however, where damping ratio factors are 1 to 1.3, fiber content is not directly correlated with damping ratio.

b. Microgrid Reinforcement

A different type of microreinforcement, miniature geogrids, has been proposed by Mercer et al (Reference 28) who report the behavior of a clean poorly graded subangular sand [$D_{60} = 0.5\text{mm}$ (0.02 inch)] reinforced with up to 0.6 percent weight fraction of 40 mm (1.6 inches) square elements of Netlon Mesh Type 7. The geogrid elements have openings 6 - 7 mm (0.24 - 0.27 inch) wide, approximately equal to the maximum grain size of the soil. This type of microreinforcement is thought to be more efficient than fibers because strengthening of the soil could stem from interlocking of soil particles within

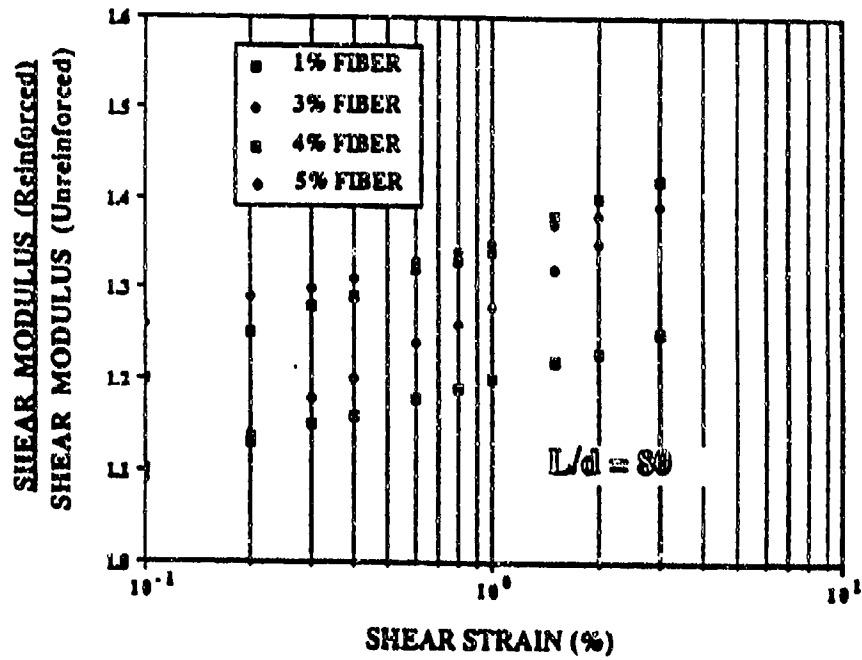


Figure 16. Influence of Glass Fiber Content on Shear Modulus Ratio - Confining Pressure = 43 kPa (Reference 39).

the mesh rather than simply from interface friction between a fiber and the soil. The authors conducted CBR, triaxial and bearing capacity tests on reinforced and unreinforced specimens. CBR test results showed a roughly proportional increase in CBR value with percentage of reinforcement until the percentage reached approximately 0.5 percent where it appeared to level off at approximately 3.5 and 5 times the unreinforced value for 2.5 mm (0.1 inch) and 5 mm (0.2 inch) penetration, respectively.

The effect of 0.19 percent reinforcement on triaxial test results is qualitatively similar to that seen with RDFS. Peak strength increases and post-peak softening decreases, as seen in Figure 17.

As with RDFS, the percentage increase in peak strength decreases with increasing confining pressure. For these test results the increase is 60 percent and 25 percent for confining pressures of 50 kPa (7.3 psi) and 150 kPa (21.8 psi), respectively. Although post-peak softening is reduced compared to the unreinforced soil, the effect does not seem to be as great as with RDFS. The initial tangent modulus appears to be unaffected by the reinforcement.

No data on dynamic properties of soil reinforced with miniature geogrids have been found in the literature. Based on the limited data available on static behavior, it may be reasonable to assume that qualitatively this type of reinforcement may behave like RDFS under dynamic loading conditions. However, a comparison of test results is needed to verify this assumption and to determine if either reinforcement method offers significant advantages over the other. Triaxial testing of miniature geogrid-reinforced sand specimens may require specimens 150 mm (6 inches) or more in diameter if the size of the granular particles dictates a geogrid element too large for testing with 72 mm (2.8 inches) specimens.

c. Summary of Microreinforced Soil

Overall, the literature review has shown that microreinforcement of granular soils with synthetic fibers can significantly increase both the static strength and the ductility of the soil. This enhancement comes at the cost of increased difficulty in compacting RDFS compared to unreinforced soil. No work to date has clearly separated the positive effect of reinforcement from the negative effect of lower soil dry density inherent in the use of the same compactive effort for both materials. Also, the influence of the physical

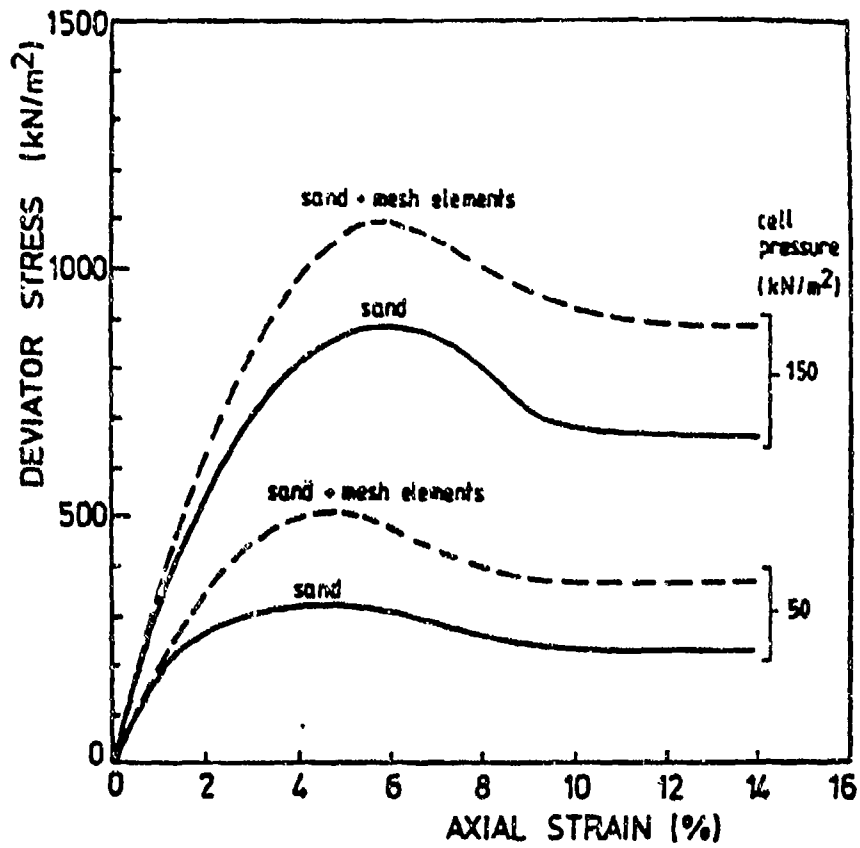


Figure 17. Triaxial Test Results for Sand and Sand Containing 0.19 Percent Miniature Geogrids (Reference 28).

properties and geometry of the reinforcement on strength, deformation and compaction of RDFS has not been thoroughly investigated. Clearly, data in the literature cannot be confidently used to predict the effect of any specific fiber on static behavior.

The effects of fiber reinforcement on dynamic behavior are less well understood. The increase in shear modulus of granular soils appear to be greatest at low confining pressures [< 100 kPa (< 7 psi)] and high shear strain amplitudes (> 1 percent). However, even in these ranges the increase in shear modulus is limited to approximately 50 percent or less, compared to the unreinforced soil. The effects on damping ratio are much more significant at low shear strain amplitudes (< 1 percent) where damping is much higher (100 - 700 percent) in the reinforced soil compared with the unreinforced soil. However, at higher shear strain amplitudes, the presence of fiber reinforcement appears to have little to no effect on damping.

Unfortunately, it does not appear that any dynamic compressive or triaxial loading tests on RDFS specimens have been described in the literature. For the conditions which are expected in a fiber-reinforced soil wall subjected to blast loading (high strains at relatively low confining pressures), one might expect an increase in shear modulus of 50 percent or more, with little effect on damping, compared to an unreinforced berm. If RDFS responds to dynamic shear and compressive loading in a manner similar to that of unreinforced sand, one might expect little to no increase in shear strength, but significant increase in bulk modulus with increasing strain rate. However, the lack of compressive and triaxial test results in this loading regime makes any estimate of dynamic strength or compressibility speculative.

E. CONSTITUTIVE MODELS OF SOIL BEHAVIOR

1. Introduction to Types of Models

For the purpose of conventional stability analysis or settlement analysis, it is generally sufficient to idealize only one aspect of the soil behavior. For example, the strength and self weight of the soil are important for stability analysis, while "elastic" bulk properties for the soil might be used for the analysis of immediate settlement. Where consolidation under a foundation is important, attention is often focussed on the relation between

applied stress and volume compression when the soil is loaded under one dimensional conditions (in an oedometer).

Where a more complete analysis is required for the equilibrium and deformation in a soil structure, it is necessary to model numerically the complete behavior of the structure. This is most widely accomplished numerically with finite element analysis, in which it is necessary to describe mathematically the complete behavior of the soil, and other constituent materials. This mathematical description of material behavior is called the constitutive relations.

A large number of constitutive relations have been formulated to describe the behavior of soils. Such models have formed the subject matter of several symposia and workshops, the most recent of which was held in 1987, at Case Western Reserve University, Cleveland, Ohio. Saada (Reference 40) presented in this workshop an overview of constitutive models for soils and classified them as follows:

- Deformation Theories
- Incremental Theories
- Endochronic Theory
- Elastoplastic Theories

These theories together with the "cap" outgrowth of the elastoplastic theory are briefly discussed next.

2. Deformation Theories

The family of hyperbolic models (References 41, 42) are an example of deformation based models. Despite certain known limitations, the model has been used extensively for the numerical analysis of geotechnical problems. For example, the hyperbolic model has been incorporated in a finite element code that has been used for the analysis of reinforced soil walls under working stress conditions (References 43, 44, 45). However, because of the limitations, hyperbolic models are not suited for dynamic analysis.

A model similar to the hyperbolic model (in its initial stages) but extended to allow for non-linear, hysteretic behavior of soil under seismic loading has been developed and used by Finn (Reference 46). This is unlikely to be suited to analysis involving weapons effects in which the levels of stress are much higher than those in seismic problems, and where the deformation is frequently much larger.

3. Incremental Theories

Incremental theories allow one to follow the path of the state of stress or the state of strain (Reference 40). Hypoelasticity, first proposed by Truesdell (Reference 47), is a theory that falls under this category. Hypoelasticity describes a class of material in which the stress and strain increments are related by coefficients which, in their simplest form, are often functions of the stress or the strain or of both. The behavior is infinitesimally reversible. Comparisons between the hypoelastic and plastic approaches have been made by Mroz (Reference 48) and Desai (Reference 49).

4. Endochronic Theory

In this theory, the thermodynamics of irreversible phenomena are used to formulate stress-strain relations for systems exhibiting viscoplastic and relaxation properties. First proposed by Biot (Reference 50), the endochronic theory was applied to modeling soil behavior by Bazant and his coworkers (References 51, 52, 53) and Lanier (Reference 54). The endochronic theory does not require identification of a yield surface or the definition of loading and unloading, which makes it particularly attractive for soils which develop plastic strain from the onset of loading (Reference 40).

5. Elastoplastic Theories

Elastoplastic theories have been used extensively in geotechnical engineering. Most of the models are based on the work of Drucker, et al., (Reference 55) in which soils are treated as work hardening materials. The yield surface then consists of a Mohr-Coulomb surface and a cap which passes through the isotropic compression axis.

The cam-clay model, first proposed by Roscoe et al. (Reference 56), and then modified by Roscoe and Burland (Reference 57), introduced the concept of a

critical state, and has been used extensively for the modeling of clays. For cohesionless soils, constitutive relationships based on elastoplastic theories have been proposed by Lade and Duncan (Reference 58), and Prevost (Reference 59), among others.

6. Brief Outline of a Cap Model

Perhaps the most commonly used constitutive equations for granular soil are those of the cap model proposed by DiMaggio and Sandler (Reference 60). This model is also referred to as the "Weidlinger Cap Model," or the "Inviscid Two-Invariant Cap Model." In addition to a generalized Mohr-Coulomb failure envelope, the yield surface of this elasti-plastic model has a moving cap (intersecting the hydrostatic loading line) whose position is a function of the plastic volumetric strain. This type of model has been used to represent both the low and high pressure behavior of many geologic materials and has been used for computational studies of ground shock and the complicated effects of explosions (e.g., References 61, 62, 63).

The cap model, a formulation of classical plasticity, is a mathematical model that is properly described for both static and dynamic boundary value problems. This means that the model can be expressed in terms of a computational algorithm which produces reasonable answers for all possible boundary value problems.

In general terms, the cap model is a plasticity model defined by a nonsoftening convex yield surface, and a plastic strain rate vector that is normal to the yield surface in stress space. This normality condition is necessary for uniqueness in dynamic problems whenever a rate-independent plasticity model is employed. The yield surface is composed of two parts, a fixed, or perfectly plastic, failure envelope together with a hardening cap, as shown in Figure 18. The cap model was originally developed, and was used extensively, for computational studies of ground shock and structure-medium interaction effects arising from explosion.

7. Two-Invariant Cap Model

The cap model was generalized by Sandler et al. (Reference 62) to describe the behavior of a wide variety of geological materials, and they show how the parameters in the equations of the model can be manipulated to describe

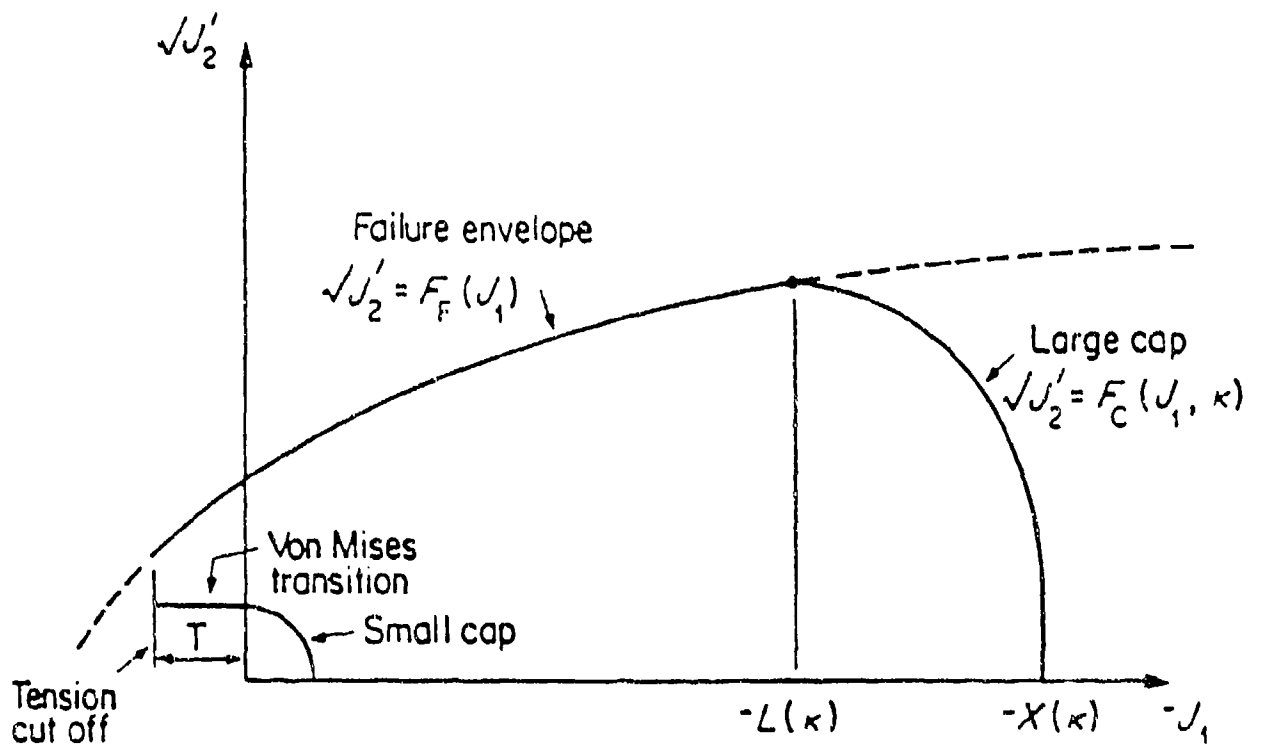


Figure 18. Typical Yield Surfaces in CAP Model (Reference 64).

granular soils as well as rock. It is also possible to include other features of behavior in cap models, such as anisotropy, rate dependence and hardening of the modified Drucker-Prager portion of the yield surface (isotropic or kinematic hardening, or both). Indeed, kinematic hardening was introduced in the cap model by Sandler and Baron (Reference 65) to model cyclic hysteresis in soils subjected to seismic loading. Katona (Reference 66) and Simo et al. (Reference 67), both introduced rate dependence of the Perzyna (Reference 68) type to the cap model.

Based on the above discussion, it appears that the Weidlinger Cap model is well suited for the present study. It has been used extensively for ground shock problems, and it is versatile enough to incorporate various effects that may prove important during the study, such as rate effects. An algorithm and a modular subroutine for the generalized rate independent cap model is listed by Sandler and Rubin (Reference 64).

F. NUMERICAL MODELING OF REINFORCED SOIL AND DYNAMIC LOADING

A large number of numerical codes for nonlinear finite-element/difference analysis is available. These codes have been used for the dynamic analysis of protective structures subjected to weapons effects. However, while most of these codes incorporate a large library of material behavior and elements, very few offer soil models of the type appropriate for sophisticated non-linear dynamic analyses, such as the cap model described in the previous section.

The main numerical codes available for the current research are summarized in Table 1. These codes all have large element libraries that include 3-D solid elements, beam elements, and slide lines or interface elements. In an analysis of reinforced soil structures, solid elements are used to represent the soil, beam or truss elements are used to represent the reinforcements, and slide lines or interface elements are essential to correctly model the interaction between the soil and the reinforcements. A brief description of each code follows:

1. ANSYS

ANSYS is a general-purpose finite-element analysis code developed by Swanson Analysis Systems, Inc., Houston, Pennsylvania. It is available for a wide array of computing platforms, from mainframes to IBM PCs. It has a library of more than 70 element types and an extensive material library. ANSYS offers two nonlinear models for soils: a classic bilinear kinematic hardening model and

TABLE 1. SUMMARY OF NUMERICAL CODES CONSIDERED.

CODE	SOIL MATERIAL MODELS	AVAILABILITY	COMMENTS
ANSYS	<ul style="list-style-type: none"> • Bilinear Kinematic hardening • Drucker-Prager 	Swanson Analysis, Inc.	<ul style="list-style-type: none"> • Need to implement defined soil cap model • Relatively expensive
ABAQUS	<ul style="list-style-type: none"> • Cam-Clay • Drucker-Prager 	HKS, Inc.	<ul style="list-style-type: none"> • Need to implement user-defined soil cap model • Relatively expensive
ADINA	<ul style="list-style-type: none"> • Vm-Mises • Drucker-Prager with vertical cap 	ADINA R&D	<ul style="list-style-type: none"> • Need to implement user-defined soil cap model • Relatively expensive if obtained from ADINA R&D • Can be obtained from Air Force
DYNA3D	<ul style="list-style-type: none"> • Inviscid two-invariant cap 	LLNL	<ul style="list-style-type: none"> • Best soil model • Public domain software

the Drucker-Prager Model. If the cap model is to be used for this study, it would have to be incorporated in the program through the use of a user-defined material model option.

2. ABAQUS

ABAQUS is a general-purpose finite-element code developed by Hibbit, Karlsson and Sorensen, Inc. (HKS), Providence, Rhode Island. As is the case for ANSYS, it is mainly geared toward structural analysis. ABAQUS also has extensive element and material libraries. Among the non-linear material models offered, ABAQUS has implemented the modified cam-clay model, and an elastoplastic model based on Drucker-Prager. A user-defined constitutive model can be incorporated. ABAQUS is available for mainframes and engineering workstations (e.g., SUN, VAX...).

3. ADINA

ADINA is a general-purpose finite-element code developed by ADINA R&D, Inc., Watertown, Massachusetts. ADINA has large material and element libraries and is available for mainframes, workstations, and PCs. A Drucker-Prager material model with a vertical cap and tension cut-off is available in ADINA. An elliptical cap model such as described in the previous section would have to be incorporated as a user-defined material model.

4. DYNA3D

DYNA3D is a public domain software developed at the Lawrence Livermore National Laboratory, (LLNL) Livermore, California. DYNA3D is an explicit finite element code for analyzing the large deformation dynamic response of inelastic solids and structures. It has large element and material libraries, and is available for mainframes and workstations.

Recently, the algorithm developed for the inviscid two-invariant cap model by Simo et al. (Reference 67) was implemented in DYNA3D. Unfortunately, its viscoplastic extension was not. A user-defined material model option is also offered in DYNA3D.

The fact that it was developed specifically for the analysis of blast problems, incorporates the preferred cap model for soil behavior, and has a public domain status, makes DYNA3D was the most suitable choice for the present research. Furthermore, the anticipated level of support and collaboration offered through the LLNL was considered a significant factor in the implementation of the analysis to as complex a boundary value problem as that for reinforced soil under explosive loading.

SECTION III DESIGN CRITERIA FOR REINFORCED SOIL STRUCTURES

A. GOALS AND ORGANIZATION

The purpose of this section is to review the current process used to design reinforced concrete blast protective structures and to recommend the introduction of reinforced soil structures into this process. The section is organized as follows:

- Section B presents a review of the current protective structure design process as described in Section I of the Protective Construction Design Manual [Reference 2] and introduces the design considerations for this study of the response of reinforced soil structures to blast loading.
- Section C presents a discussion of the parameters for reinforced soil structures considered in this study, including structural components, backfill soil, and blast characteristics.
- Section D presents a recommendation for incorporating design calculations and design drawings for reinforced soil structures into the Protective Construction Design Manual.

B. CURRENT DESIGN PROCESS

The design process currently in use for protective structures is presented in flowchart form in Figure 19. The steps in this process include: (1) identification of the threat to the structure; (2) preliminary design of the protective structure; (3) performance of necessary analyses to calculate the blast loads on the structure and the structure's response to this loading; and, (4) comparison of the structure's response to the design criteria. If the response of the structure meets the design criteria, the process is complete; if not, a new design must be proposed for analysis.

Equations and calculations for a variety of weapons effects, protective/protected elements, and failure criteria modes are included in Reference 2, as shown in Table 2. However, most of the calculations presented in the Protective Construction Design Manual are related to reinforced concrete, which is used in

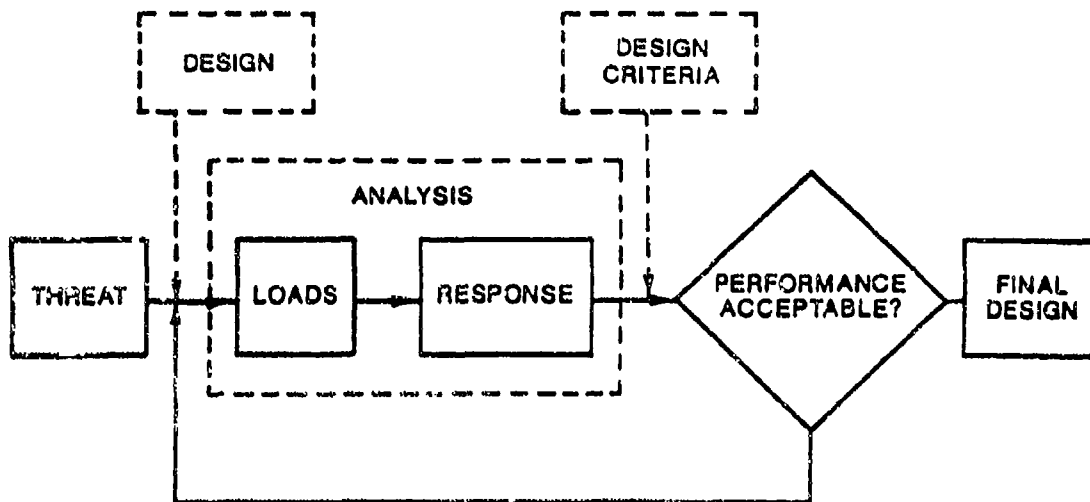


Figure 19. Protective Structure Design Process (Reference 2).

TABLE 2. DESIGN PARAMETERS (REFERENCE 2).

Weapons Effects	Protective/Protected Elements	Failure Modes
Airblast	Exposed walls, roof, arch	Breaching
Airblast/fragment impulse	Floor	Flexure
Fragment penetration	Buried walls, floor, roof, arch	Shear
Projectile penetration	Doors	Compression
Ground shock	Soil berm	Perforation
Cratering	Revetment	Spall
Ejecta	Tunnels	Shock tolerance
In-structure shock	Taxiway, driveway	
Spall	Burster slab	
	Rock rubble	
	Blast valves	
	Piping	
	Air ducting	
	Cable	
	Personnel	
	Equipment	

the design of most protective structures. Calculations for reinforced soil structures are not currently addressed in the Protective Construction Design Manual.

The research and testing conducted for this study of the response of reinforced soil structures to blast loading provide an investigation of one set of design parameters included in Table 2: the effects of ground shock using side wall breaching as the failure criteria. The design parameters for this study are discussed below.

C. DESIGN PARAMETERS

1. Introduction

In this study, the response of an above-ground bermed reinforced soil structure was investigated by means of centrifuge modeling and numerical modeling. Design parameters selected for the models were influenced by those used in full-scale tests conducted in 1990 (Reference 6). The design parameters considered in the study are presented below.

2. Reinforced Soil Wall Characteristics

The three-sided, full-scale model was 3.5 meters (11.5 feet) high. Due to size and space limitations of the centrifuge models, and numerical complexities in the numerical modeling, a 4.6 meters (15 feet) high wall (i.e., one side only) with a top restraint (to simulate a roof) was studied in the centrifuge and numerical modeling portions of this study.

The concrete facing panels used in the full-scale tests were of cruciform shape with overall dimensions of 1.5 meters (4.9 feet) high by 1.7 meters (5.6 feet) wide by 180 mm (7.1 inches) thick and panel edges cut so that interlocking of the panels during construction was possible. Similar panels were constructed out of gypsum for the centrifuge tests. The interlocking structure was the same; however, to minimize construction difficulties, square shapes were used instead of cruciform shapes. For the numerical models, panel strength characteristics for concrete were defined. Panel interfaces were specified as "sliding" to model the ability of the panels to move independently of one another.

Reinforcing materials for the full-scale testing consisted of steel strips 41 mm (1.6 inches) wide by 5 mm (0.2 inch) thick by 4 meters (13.1 feet) long. Four strips were connected to each panel, two along the top half of the panel and two along the bottom half of the panel. Reinforcing for the centrifuge models consisted of 4 mm (0.16 inch) wide steel strips (to model the full-scale reinforcing) and 51 mm (2.0 inches) wide geogrid strips, both of varying lengths. The strength properties of geogrid were used in the numerical modeling study and the length of reinforcement was 4.5 meters (15 feet).

Test parameters for the full-scale tests consisted only of variation of weapon location. Boundary conditions for the centrifuge models included weapon proximity, the use of a top restraint (to investigate wall response both with and without a roof), and the implementation of a berm (to investigate wall response of buried structures (i.e., fully coupled events) vs. bermed above ground structures).

3. Soil

The backfill soil for full-scale models consisted of well graded gravel. Due to the effects of gravity scaling in the centrifuge, a fine-grained quartz sand [$D_{50} = 0.02 \text{ mm}$ (7.9×10^{-4} inches)] was used as backfill material for the centrifuge tests. Fine grained sand was also modeled in the numerical analyses

4. Blast Loading Characteristics

General purpose bombs, 227 kg and 454 kg (500 pounds and 1000 pounds) in mass, were used in the full-scale testing. The smaller bombs were WW II era weapons with a net explosive mass of 89.4 kg (197 pounds) of TNT. The larger ones contained H6 explosive with a net explosive mass of 188.9 kg (416 pounds). The bombs were detonated within the soil berm surrounding the structure, with decreasing proximity to the wall for each subsequent test. Security restrictions prohibit publication of the exact locations of the weapons. In general, four were within the soil berm behind the structure and three were outside the berm. The explosives used in both the centrifuge models and the numerical models simulated 227 kg (500 pounds) general purpose bombs. All weapons modeled in the centrifuge and numerically were located within the soil berm behind the reinforced soil mass.

D. RECOMMENDATIONS FOR PERFORMANCE CRITERIA

The design parameters considered in this study represent only one of many parameters presented in Table 2. The study of reinforced soil for blast protective structures can be broadened to include the study of other weapon effects (i.e., airblast, cratering), and other failure modes (i.e., flexure, spall). It is recommended that design calculations for reinforced soil structures for various weapons effects and failure mode criteria be developed and integrated into the current Protective Construction Design Manual¹.

SECTION IV LABORATORY TESTING PROGRAM

A. INTRODUCTION

1. Overview

The most common method of analyzing reinforced soil structures in current design practice concentrates on ultimate behavior (the limit equilibrium state), characterized by the formation of slip planes in the soil mass, rupture and pullout of reinforcement. This approach considers stresses in the soil, in the reinforcement, and on the soil-reinforcement interface separately. Localized failures can be directly analyzed to evaluate the internal stability of reinforced soil structures. For this approach soil-reinforcement interaction properties are fundamental design parameters. These parameters can be obtained from large scale direct shear or pullout box tests. Figures 20 and 21 show schematic diagrams of the direct shear and pullout tests, respectively.

In the direct shear test, a reinforcement is usually fixed on a plane face, usually onto a wooden block, with a soil mass sliding over it. This type of test simulates the soil mass sliding along the reinforcement, the direct shear failure mode. The pullout test is more elaborate. A reinforcement is placed at the middle depth in a rectangular container full of soil and pulled out through a sleeve in the front of the box. This type of test simulates the pullout failure and rupture mode. These two types of tests are associated with different testing procedures and boundary conditions, and simulate different failure modes of soil-reinforcement systems. Therefore, soil-reinforcement interface parameters obtained from these two types of tests may vary. Choice of the testing method depends on potential or anticipated failure modes.

The pullout testing method was selected for determining soil-reinforcement interface properties for this project. Eight series of static pullout tests with a constant pullout displacement rate of 1.0 mm/minute (0.04 inch/minute) were first conducted in a uniform sand and a well graded silty sand. Three commercially available geogrids, (i.e., Tensar UX1500, Miragrid 10T and Matrex 120) and one steel strip, (i.e., galvanized Reinforced Earth Bar) were tested in both soils. Effects of the pullout displacement rate were investigated by conducting three series of pullout tests on the geogrids in the uniform sand.

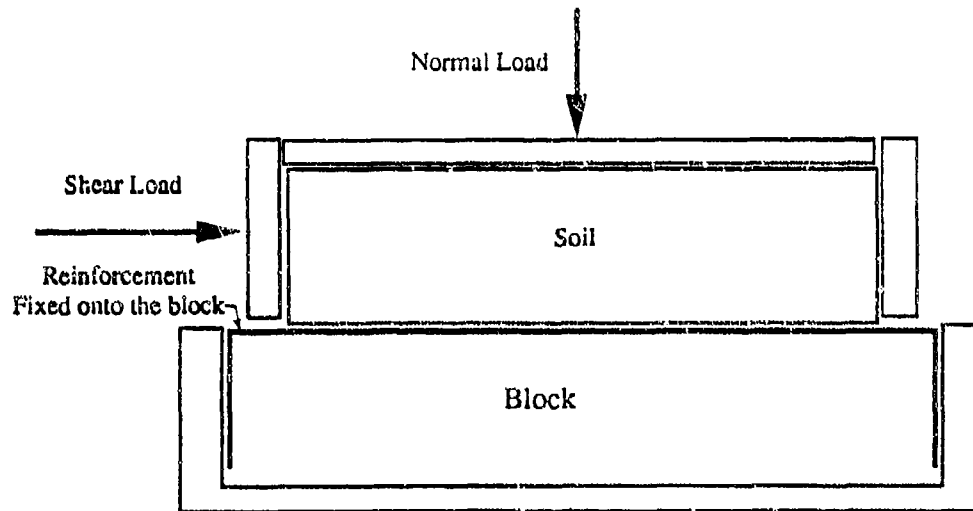


Figure 20. Schematic Diagram of Direct Shear Test for Measuring Soil-Reinforcement Interface Properties.

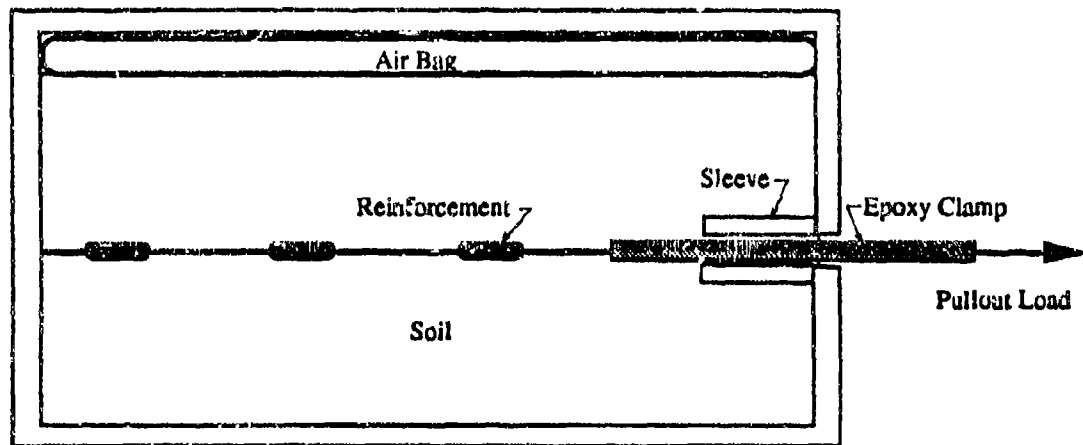


Figure 21. Schematic Diagram of Pullout Test for Measuring Soil-Reinforcement Interface Properties.

A constant pullout rate of 152 mm/minute (6.0 inches/minute) were used in these three series of tests. Six series of impact pullout tests on the three geogrids in both soils were conducted to evaluate impact pullout resistance. Static and impact tensile tests were also conducted on the three geogrids. The impact tensile strength and pullout resistance of the geogrids were determined and compared with the static tensile strength and pullout resistance.

The testing of microreinforced soil differs from that described above because of the small size and random orientation of the reinforcement. Triaxial compression tests are more commonly used to evaluate the properties of a micro-reinforced soil and Mohr-Coulomb ($c-\phi$) strength parameters are obtained. For this study, 33 triaxial tests were performed on microreinforced soil. Three types of commercially available microreinforcement were used, one monofilament (M_{50}) and two fibrillated fibers (F_1 and F_{360}). The influence of fiber type and content on peak strength, axial strain at failure, stiffness, and volume change during shear were investigated.

2. Organization

The remaining portion of this section is organized as follows:

- Section B describes the soils and reinforcements used in the testing;
- Section C describes the tests and test equipment;
- Section D presents the results of direct shear tests on the soils used in the testing program;
- Section E presents results of triaxial tests on micro-reinforced soil;
- Section F presents results of tests on geogrids; and
- Section G presents results of pullout tests.

B. SOILS AND REINFORCEMENT

1. Soils

Two soils were used in the pullout testing program, a uniform medium sand and a well-graded coarse-to-fine silty sand. The uniform medium sand is classified as SP according to the Unified Soil Classification System (USCS). Maximum and minimum dry unit weights of the sand are 15.42 kN/m^3 (98.1 pcf) and 12.97 kN/m^3 (82.5 pcf), respectively. The well graded coarse to fine silty sand is a Vulcan material No. 810 with particles ranging from silt to fine gravel. It is classified as a SW-SM, well graded silty sand with gravel, according to the USCS. It has maximum and minimum dry unit weights of 20.88 kN/m^3 (132.8 pcf) and 16.77 kN/m^3 (106.7 pcf), respectively. Grain size distribution curves for both soils are shown in Figure 22. A Modified Proctor test [American Society for Testing and Materials (ASTM) test procedure D-1557] was performed on the SW-SM soil and the maximum dry unit weight was found to be 20.61 kN/m^3 (131.3 pcf) at an optimum moisture content of 8 percent. The moisture-density curve for the SW-SM sand is shown in Figure 23. The uniform sand and the well graded silty sand will hereafter be referred to as the SP sand and the SW-SM sand, respectively in the remainder of Section IV.

2. Microreinforcements

Three types of fiber reinforcement, supplied by Synthetic Industries in Chattanooga, Tennessee, were used. Two are fibrillated fibers, F_{360} and F_x , and one is a monofilament, M_{60} . The geometric and mechanical properties of these fibers are presented in Table 3.

3. Polymer Geogrid Reinforcement

Three commercially available geogrids were selected for the laboratory pullout testing. These included Tensar UX1500, Miragrid 10T, and Matrex 120. Their polymer composition and mechanical properties are presented in Table 4. Geometric properties of geogrids are commonly characterized by their aperture size in both machine and cross-machine direction. Tensar UX1500, Miragrid 10T and Matrex 120 have aperture sizes of 145×15 , 23×22 and 81×8 mm (5.71×0.59 , 0.91×0.87 , 3.19×0.31 inch) in the machine and cross-machine directions, respectively.

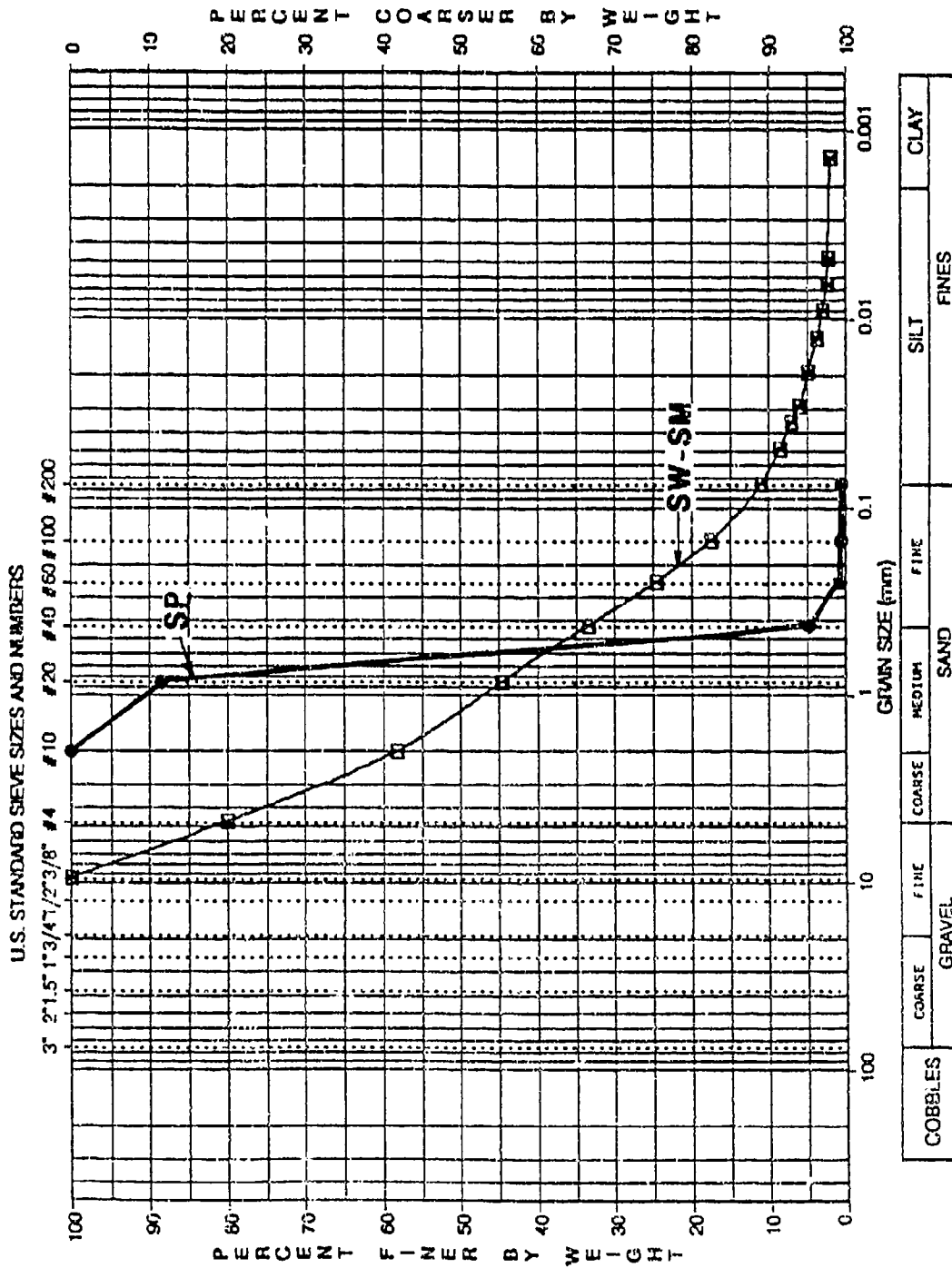


Figure 22. Grain Size Distribution Curves for SP and SW-SM Sands.

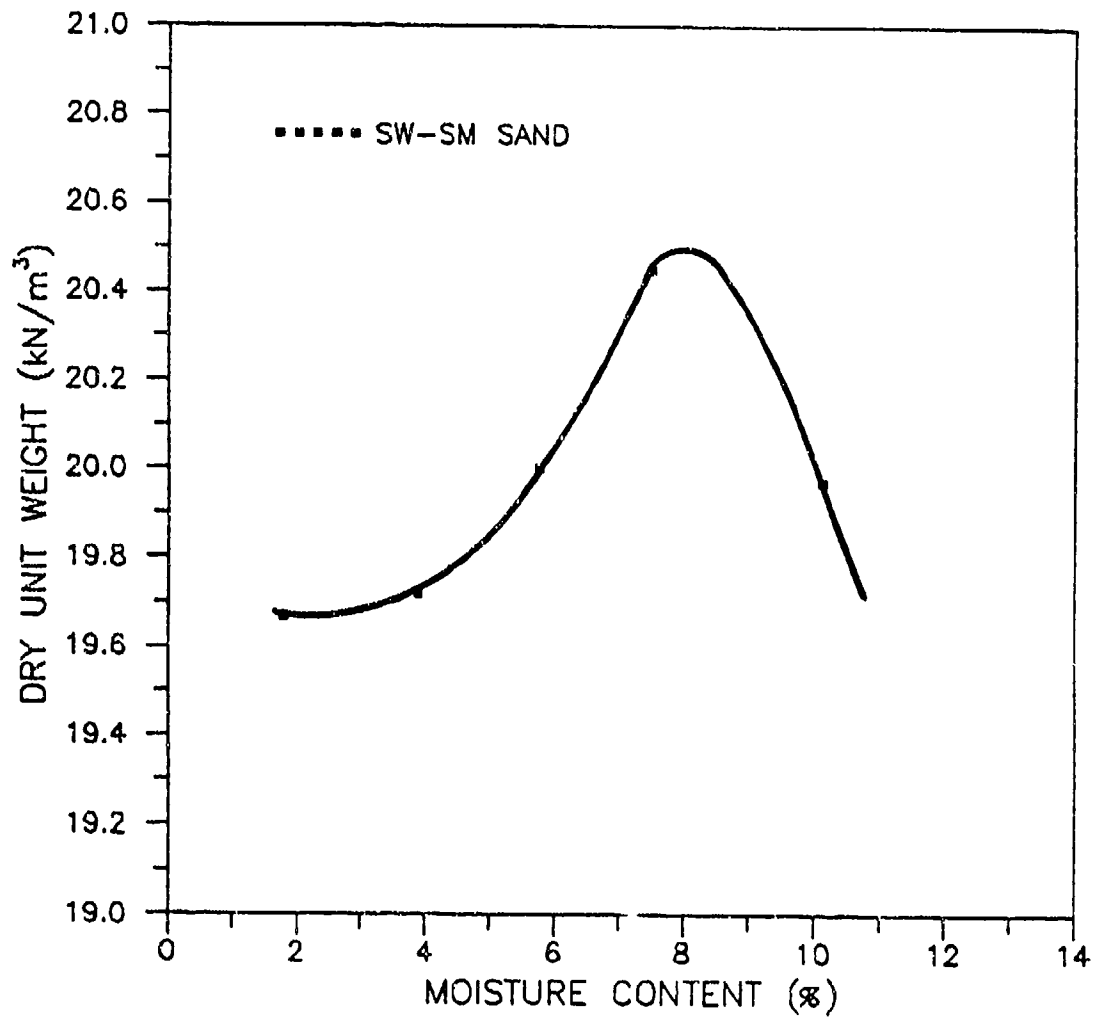


Figure 23. Moisture-Density Relationship for SW-SM Sand.

TABLE 3. PROPERTIES OF MICROREINFORCEMENT.

	Product		
	F ₃₆₀	F _r	M ₅₀
Material	polypropylene	polypropylene	polypropylene
Structure	fibrillated	fibrillated	monofilament
Length(mm)	41	2.5	19
Thickness	360 denier	150-1000 denier	50 denier
Density(Mg/m ³)	0.91	0.91	0.91
Strength(MPa)	124.2	124.2	124.2

TABLE 4. PROPERTIES OF GEOGRID REINFORCEMENT (REFERENCE 69).

Product Name	Manufacture	Structure	Polymer Composition	Ultimate Tensile Strength (kN/m)
UX1500	The Tensar Corporation	Punched Sheet-Drawn	Polyethylene	86.0
Miragrid 10T	Mirafi, Inc.	Woven	Polyester	93.6
Matrex120	The Reinforced Earth Company	Woven	Polyester	181.3

4. Reinforced Earth Company Steel Strips

Galvanized metal strips with ribs on both sides from the Reinforced Earth Company were selected for evaluation of their pullout resistances in both the SP sand and the SW-SP sand. The strip was made of A572 steel with ultimate tensile strength of 552 MPa (80 ksi). A transverse cross section of the strip was 50 mm (2.0 inches) wide by 4 mm (0.16 inch) thick. Other geometric characteristics of ribbed strips are shown in Figure 24.

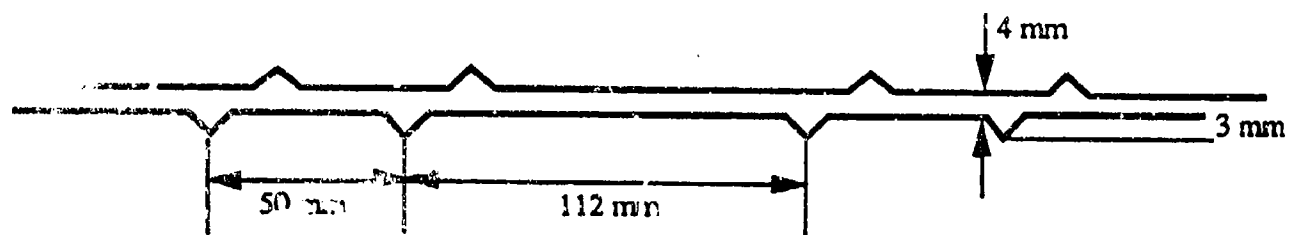


Figure 24. Geometric Characteristics of Ribbed Strips.

C. DESCRIPTION OF TEST AND TEST EQUIPMENT

1. Triaxial Tests

Triaxial testing was conducted using a Karo? Warner triaxial loading frame with a capacity of 17.8 kN (4,000 pounds). During shearing, a commercially available data acquisition system was used to record the output from a load cell and a linear variable displacement transducer (LVDT). Volume change was measured by hand with a burette connected to the triaxial specimen. All tests were conducted on cylindrical specimens with a diameter of 71 mm (2.8 inches) and a height of 152 mm (6.0 inches).

2. Static Pullout Tests

The static pullout tests were performed in a 1.52 meters (5 feet) long by 0.61 meters (2 feet) wide by 0.30 meters (1 foot) deep steel pullout box. The reinforcement specimen was placed in the middle of the box with 150 mm (6 inches) of soil above and below. A constant normal pressure was applied to the upper soil surface through an air bag. Pullout was obtained by two, 98 kN (10 ton) hydraulic jacks operated at a constant rate. Pullout force and displacement were measured by a load cell and a LVDT and collected by a data acquisition system.

To minimize boundary effects, the distance between the internal surface of the pullout box and the edge of the reinforcement specimen was 178 mm (7 inches) or greater. A sleeve was installed in the front of box for reducing the rigid front wall effect on pullout results.

3. Dynamic Pullout Tests

The static pullout resistance of the reinforcement embedded in a soil is well defined, although it is still difficult to precisely interpret soil-reinforcement interaction parameters from directly measured pullout load-displacement responses. However, there is little information regarding dynamic pullout testing and no clear definition of dynamic pullout resistance. Therefore, it is necessary to define what the dynamic pullout test and dynamic pullout resistance mean.

For the purpose of this study, a dynamic pullout test is defined as one in which a reinforcement is subjected to an impulsive pullout load with a rise time of a few tens of ms or less. Unlike the static pullout test, a peak in the load-displacement or load-time curve is not necessarily the dynamic pullout resistance for a given normal stress. To define the dynamic pullout resistance, the concept of input kinetic energy is introduced here. For the same normal stress, the peak is expected to vary with the input kinetic energy applied to the reinforcement. The maximum of all the peaks for a given normal stress hereafter is defined as the dynamic pullout resistance. This requires several dynamic pullout tests with varying kinetic energy to be conducted for a given normal stress in order to define the dynamic pullout resistance.

A dynamic load system was designed, built and installed onto an existing pullout box. It consists of four major components:

- two, 98-kN (10-ton) hydraulic cylinders;
- two springs with stiffness of 175 kN/meters (1,000 pounds/inches);
- an impact beam; and
- a trigger system.

A schematic diagram of the load system is shown in Figure 25. The springs are compressed by the two hydraulic cylinders. During compression, the springs are supported by two shear pins which are controlled by the trigger system. The total potential energy stored in the springs is converted into the kinetic energy of the impact beam when the trigger is initiated. The moving beam impacts the sample connection frame and creates an impulse load. The impulse load is transferred to the specimen through a rigid epoxy clamp. The advantage of this impact loading system is that input kinetic energy to a reinforcement can be easily and precisely controlled by varying compression of the springs.

D. RESULTS OF DIRECT SHEAR TESTS ON SOILS

Two types of soils, as described above in B-1, were selected for both static and dynamic pullout tests. The friction angle of the dry SP sand at 80 percent relative density (D_r), determined from a series of direct shear tests, is 38 degrees. A series of direct shear tests were also conducted on the well-graded silty sand compacted to 95 percent of maximum dry density ($D_r = 75$ percent) at a moisture content of 3 percent. The results of these tests indicate a friction angle of 47 degrees.

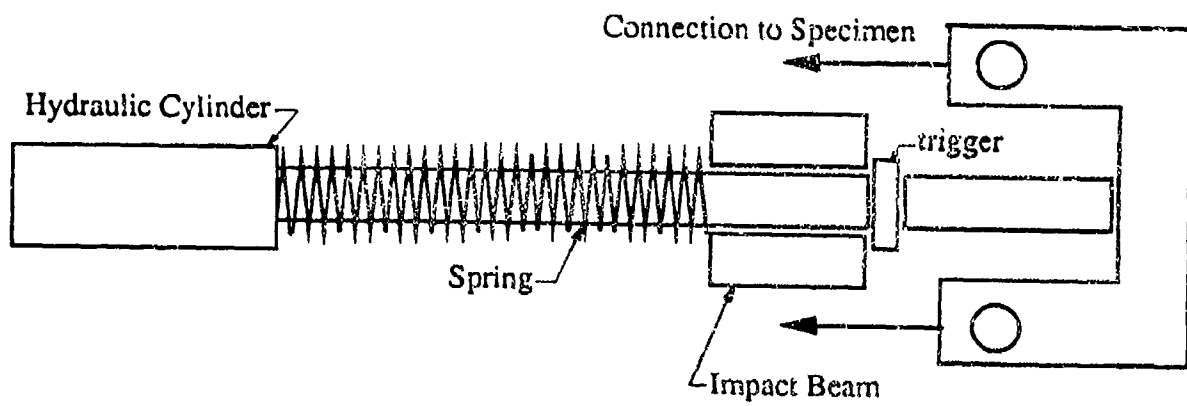


Figure 25. Schematic Diagram of the Dynamic Loading System.

E. RESULTS OF TRIAXIAL TESTS ON MICROREINFORCED SAND

1. Test Procedures

All triaxial testing of microreinforced soil utilized the SP sand described above. A total of 33 triaxial tests were performed on both microreinforced and unreinforced soils. The test matrix is shown in Table 5.

TABLE 5. TEST MATRIX FOR TRIAXIAL TESTS ON MICROREINFORCED SOIL.

Fiber Type	Percent by Dry Mass	Low Compactive Effort		High Compactive Effort	
		T ₃ = 34 kPa	T ₃ = 34 kPa	T ₃ = 34 Kpa	T ₃ = 50 psi
F ₁₈₀	0.5	•	•	•	•
F ₃₈₀	1.0				•
F ₃₈₀	2.0	•	•	•	•
F _x	0.1				•
F _x	0.5	•	•	•	•
F _x	1.0				•
F _x	1.5				•
F _x	2.0	•	•	•	•
M ₆₀	0.5	•	•	•	•
M ₆₀	1.0				•
M ₆₀	2.0	•	•	•	•
Sand Only		•	•	•	•

Specimen preparation was accomplished by first placing a quantity of dry sand in a mixing bowl and adding the required amount of reinforcement to achieve the mass fraction (i.e., mass of reinforcement divided by mass of soil) needed for the test. Even distribution of the fiber throughout the sand required the addition of water prior to mixing. A water content of 10 percent was found to be adequate. Hand mixing resulted in a more uniform distribution of fibers than mechanical mixing.

Following mixing, the triaxial specimen was formed directly on the base of the triaxial cell using a specimen mold with a latex membrane inside. The 152 mm (6.0 inches) tall, 71 mm (2.8 inches) diameter specimen was formed in four

lifts. Each lift was compacted with a pneumatic vibrator placed against the specimen mold. Two different compactive efforts were used. Low compactive effort was achieved by vibrating each layer for one second, using an air pressure of 69 kPa (10 psi). Sixty seconds of vibration and 104 kPa (15 psi) air pressure were used to achieve high compactive effort. After compaction of the fourth lift, the top platen was placed on the specimen, a small vacuum was applied, and the specimen mold was removed. Initial dimensions of the specimen were measured at this time.

Prior to shearing, an effective confining stress of 14 kPa (2 psi) was placed on the specimen. Deaired water was allowed to flow through the specimen under a differential head of 3.5 kPa (0.5 psi). The cell pressure and the backpressure were gradually increased over several hours until the cell and back pressures reached 276 and 262 kPa (40 and 38 psi), respectively. Consolidation of the specimen to an effective confining pressure of either 34 kPa (5 psi) or 345 kPa (50 psi) was then accomplished. Volume changes recorded during this time indicated that between 10 and 100 minutes were required for complete consolidation.

Following consolidation, the specimens were sheared at a deformation rate of 1.0 mm/minute (0.05 inch/minute). A test was terminated when either the capacity of the testing machine was reached or when the radial strain in the specimen became excessive.

2. Test Results

Four test parameters were varied in the triaxial testing program: (1) reinforcement type (F_{300} , F_v , or M_{60}); (2) mass fraction of reinforcement (0.1 to 2.0 percent); (3) effective confining stress (34 kPa or 345 kPa); and, (4) compactive effort (high or low).

Figures 26 and 27 present axial stress-axial strain curves for tests performed on the specimens with fibrillated fiber reinforcement at fiber mass fractions of 0.5 and 2.0 percent. All data on those figures are for high compactive effort. For comparison, results from tests on unreinforced sand are also presented. These figures clearly show the effect of the fiber reinforcement on peak strength, axial strain at peak strength, and stiffness.

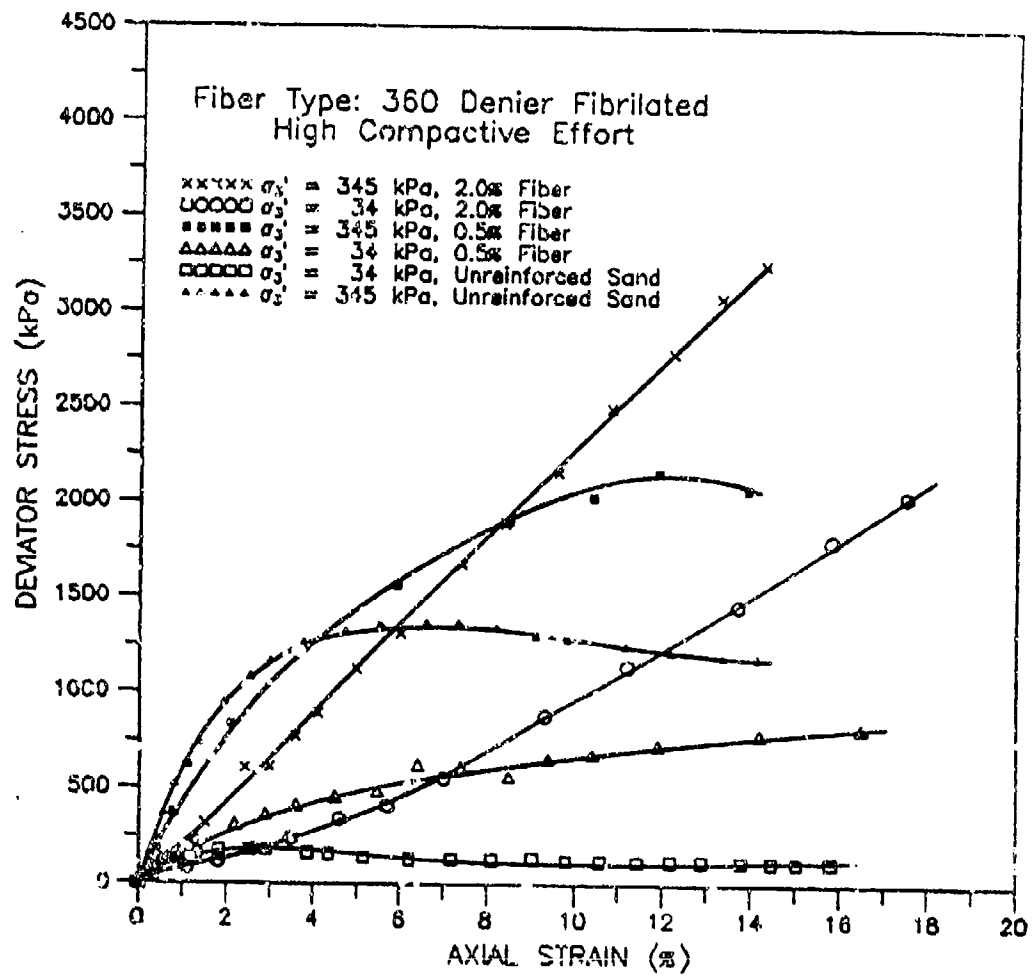


Figure 26. Stress-Strain Curves for Fibrillated Fiber Reinforced Sand (F₃₆₀ Fiber).

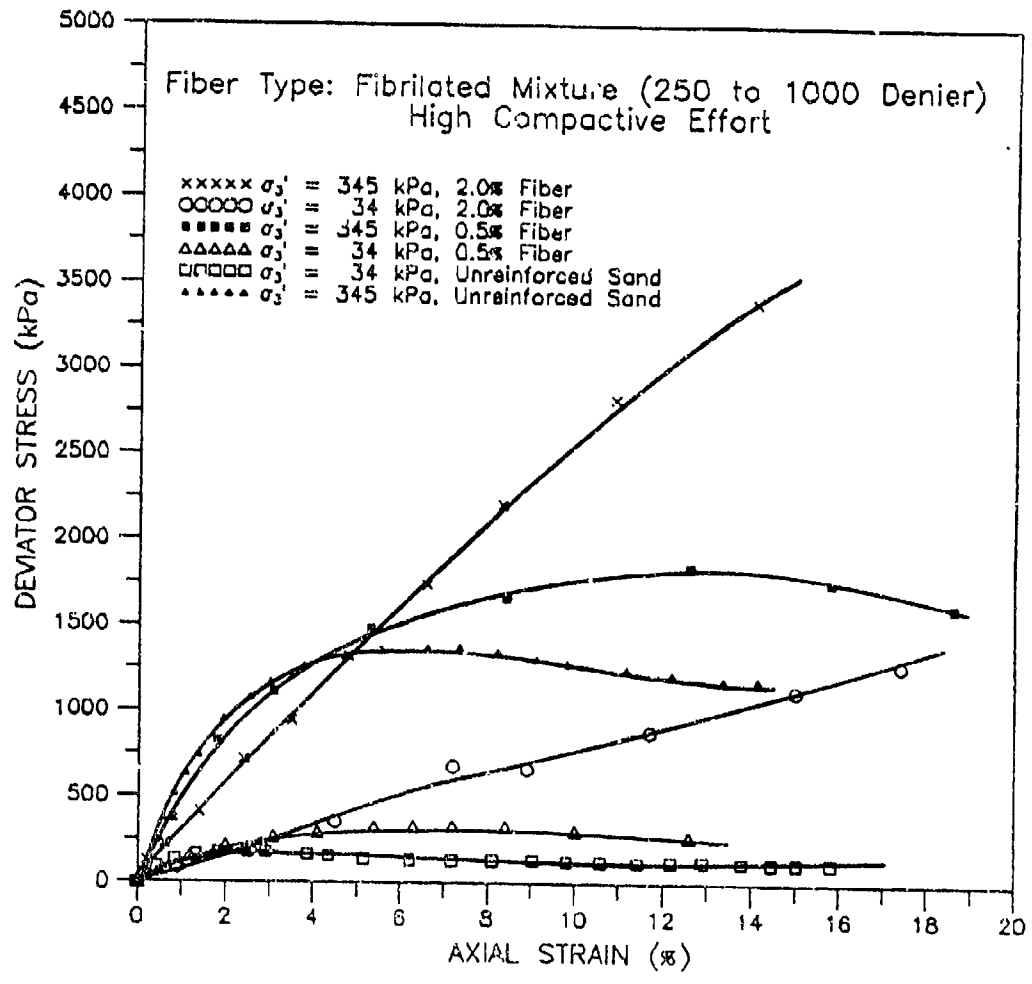


Figure 27. Stress-Strain Curves for Fibrillated Reinforced Sand (F_r Fiber).

The inclusion of either of the two fibrillated fibers greatly enhances the peak strength of the sand. The strength of both specimens with 2.0 percent fiber content, tested at 345 kPa (50 psi), exceeded the capacity of the testing machine. The difference between the effects of the two fibrillated fibers in improving the strength of the sand appears small; however, not enough tests were conducted to confirm that the differences are statistically insignificant. Even more striking than the increase in strength is the high axial strains that occur before peak strength is reached. None of the stress-strain curves peak at an axial strain lower than 8 percent. The four tests with 2 percent fiber content do not reach peak strength, despite axial strains as high as 20 percent.

Figure 28 presents the axial stress-axial strain curves for the tests performed on the monofilament reinforced soil specimens prepared with high compactive effort. The monofilament is much less efficient in improving the strength of the sand, compared to the fibrillated fibers. The effect of the reinforcement on axial strain at failure also is less pronounced with the monofilament.

The effect of fiber reinforcement on volume change during shear is illustrated in Figure 29. This figure shows volumetric strain-axial strain curves for six tests on specimens prepared with high compactive effort, all conducted at 345 kPa (50 psi) confining pressure.

The unreinforced sand dilates significantly after an initial small compaction. This behavior is typical of dense, cohesionless materials. The addition of F_1 mixed denier fibrillated fibers changes the volumetric behavior significantly. At fiber contents below 1 percent, the dilation of the soil is reduced by over 50 percent. Significant volume reduction (up to approximately 3 percent) occurs at fiber contents of 1.5 and 2 percent. Similar changes in volumetric behavior were found in tests conducted on the F_{240} and M_{60} specimens. Figures 30 and 31 present the data from all tests in the form of plots of volumetric strain at 10 percent axial strain versus fiber content for low and high compactive effort, respectively.

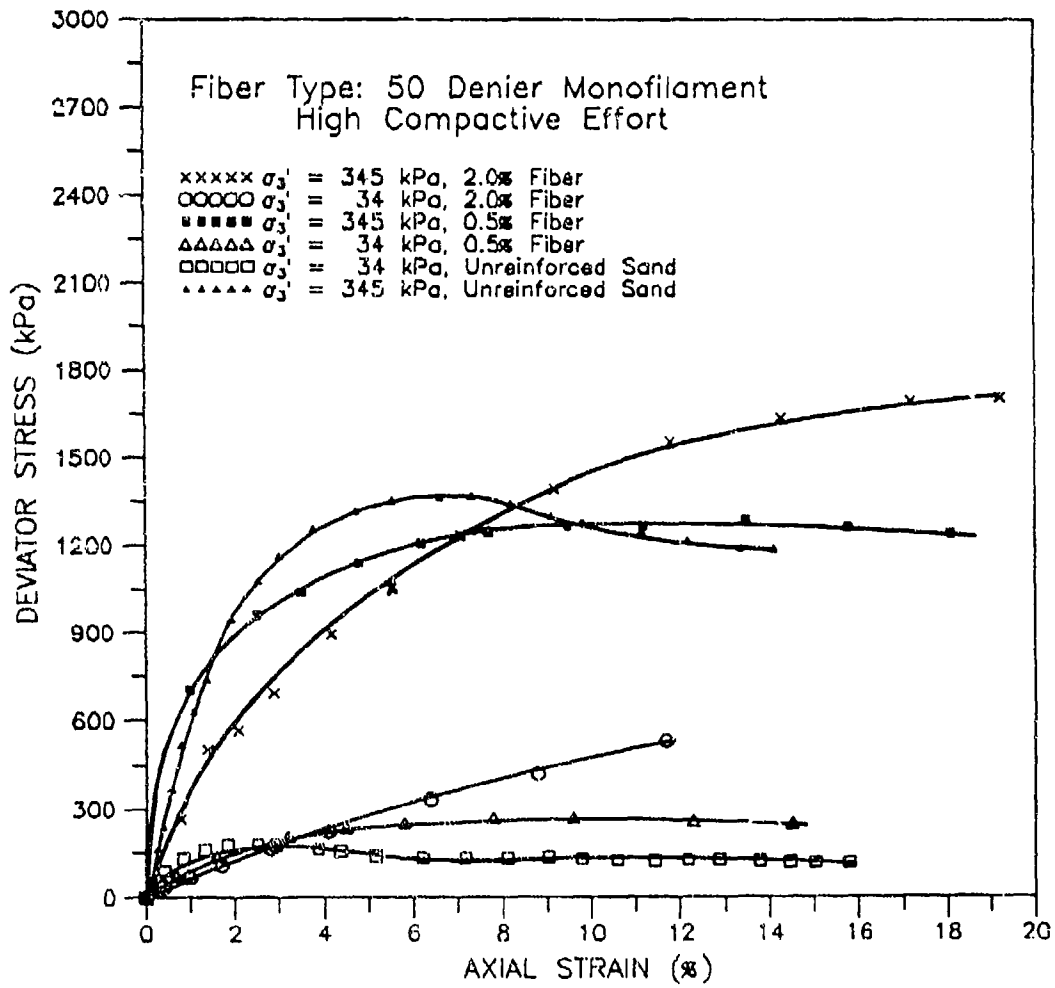


Figure 28. Stress-Strain Curves for Monofilament Reinforced Sand.

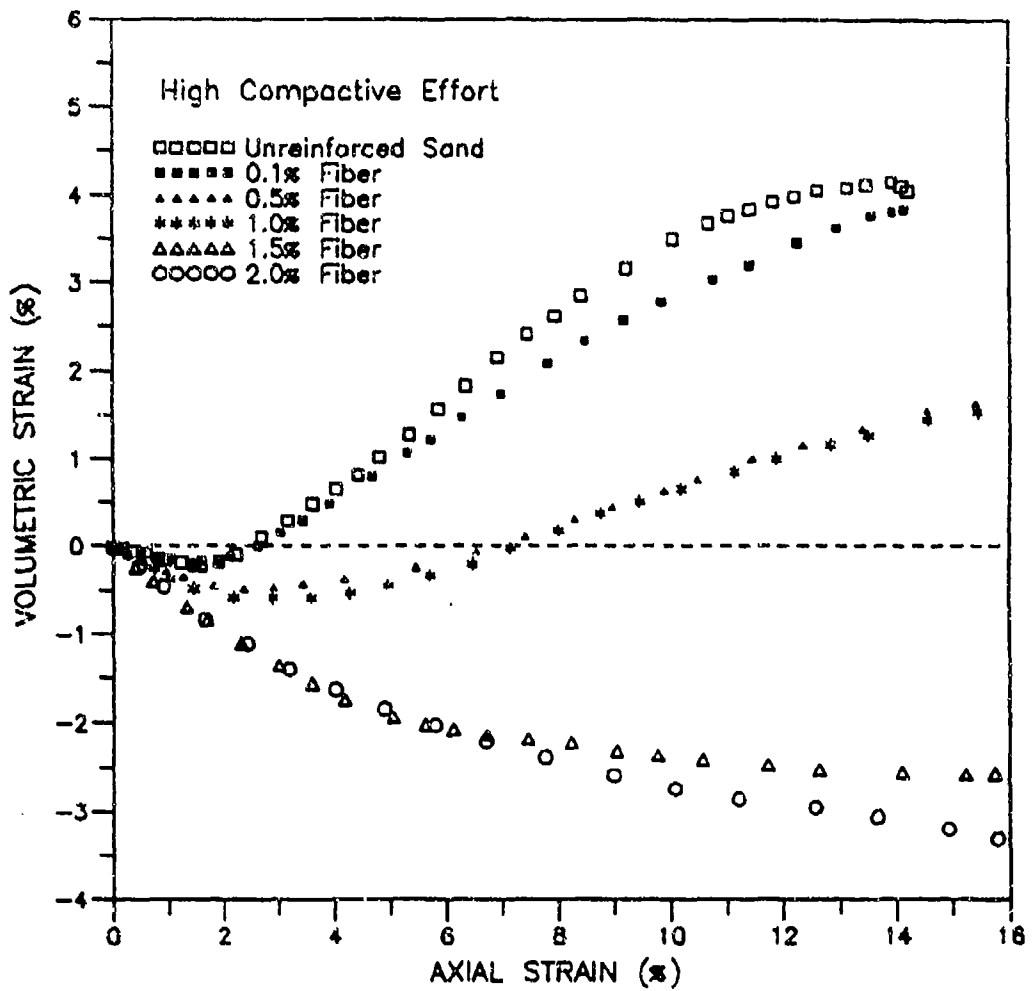


Figure 29. Effect of Fiber Content on Volumetric Strain.

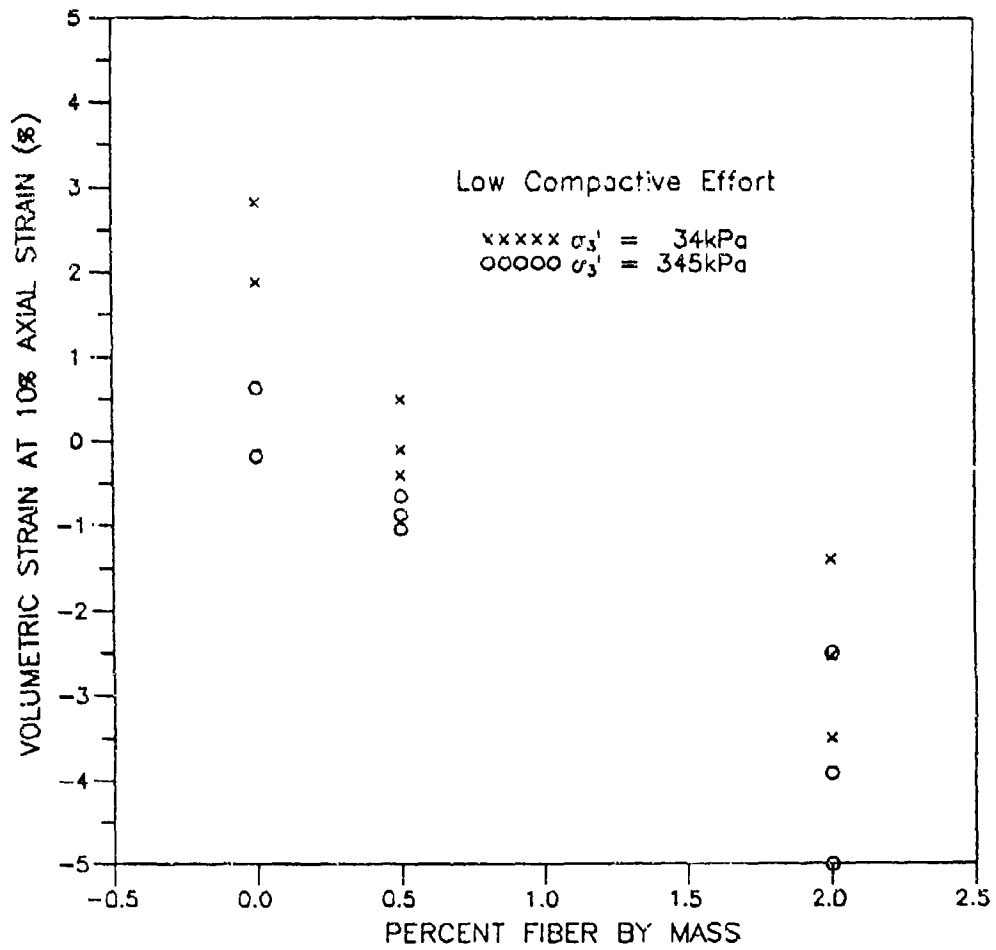


Figure 30. Effect of Fiber Content on Volumetric Strain at 10 Percent Axial Strain for Low Compactive Effort.

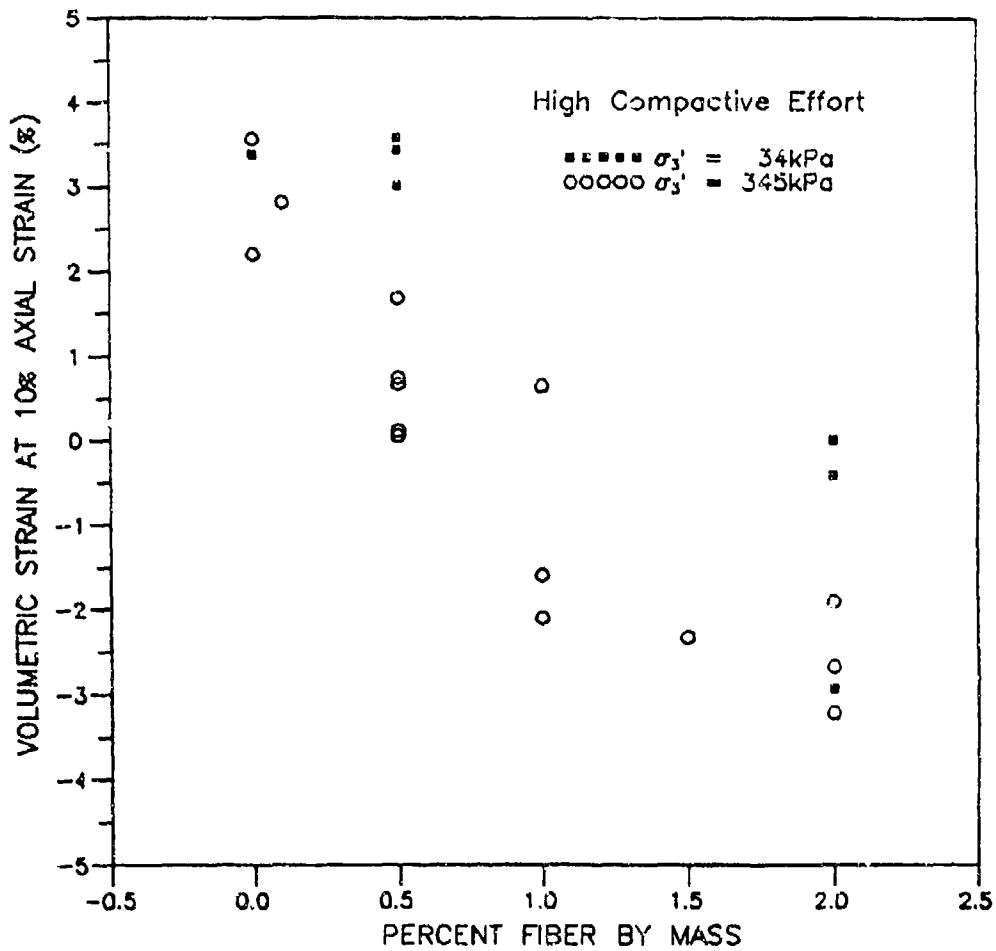


Figure 31. Effect of Fiber Content on Volumetric Strain at 10 Percent Axial Strain for High Compactive Effort.

Fiber content has a negative effect on tangent modulus measured at 1 percent axial strain. This can be observed in Figures 26 through 28 by comparing the initial slopes of the stress-strain curves. The calculated values of 1 percent tangent modulus as a function of fiber content are presented in Figures 32 and 33 for low and high compactive effort, respectively. These figures include data from all tests on fiber-reinforced and unreinforced sand. While there is considerable scatter in the data, the trend of decreasing stiffness with increasing fiber content is clear from the figures.

These test results confirm that strength and deformation characteristics change significantly when randomly-oriented fiber reinforcement is added to a clean sand. They also show the large differences in behavior between monofilament and fibrillated fiber-reinforced soil. It had been anticipated prior to testing that the fibrillated fiber reinforcement would open during mixing and compaction, thereby providing interlocking with the sand particles, and, hopefully, added strength compared to monofilaments. However, careful observations after mixing, after compaction, and after shearing revealed little evidence of opened fibers. Despite this, the fibrillated fibers produced considerably greater strength enhancement for the same mass fraction. It is not clear if this increase in strength comes from an opening of the fibers too small to see; the longer length of the fibrillated fibers compared to the monofilament; or, perhaps, the difference in surface area to volume ratio.

F. RESULTS OF TESTS ON GEOGRID

1. Procedure

The wide-width tensile test has been widely used to determine stress-strain behavior and tensile strength of geogrids. This type of test is performed in general accordance with ASTM Standard Test Method D4595-86. The specimen should be tested under a constant strain rate of 10 percent per minute, at 21 degrees Celcius and 65 percent relative humidity. Changes in these test conditions may result in variation of measured stress-strain response and tensile strength. The tensile strength for a given geosynthetic determined by using the standard method may not be the same as the break strength measured from pullout tests. This will be discussed in the following section.

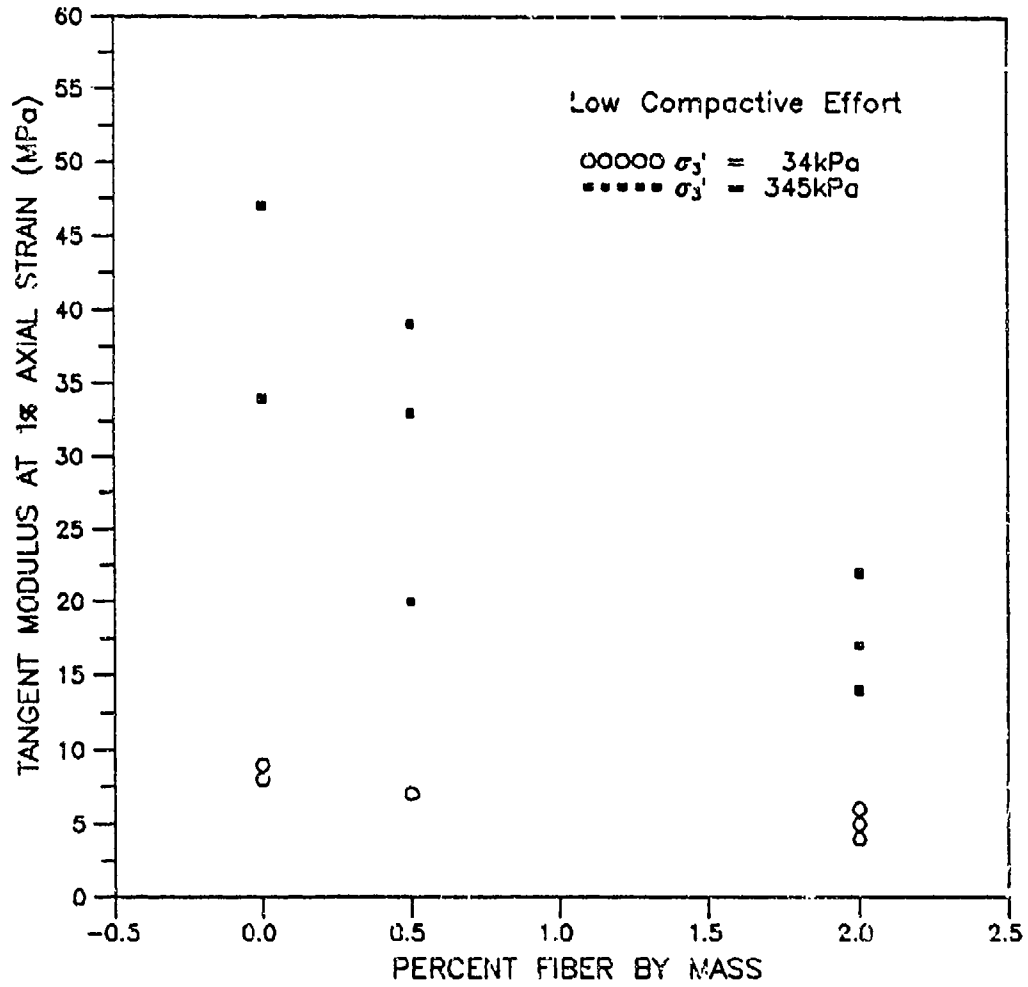


Figure 32. Effect of Fiber Content on Tangent Modulus for Low Compactive Effort.

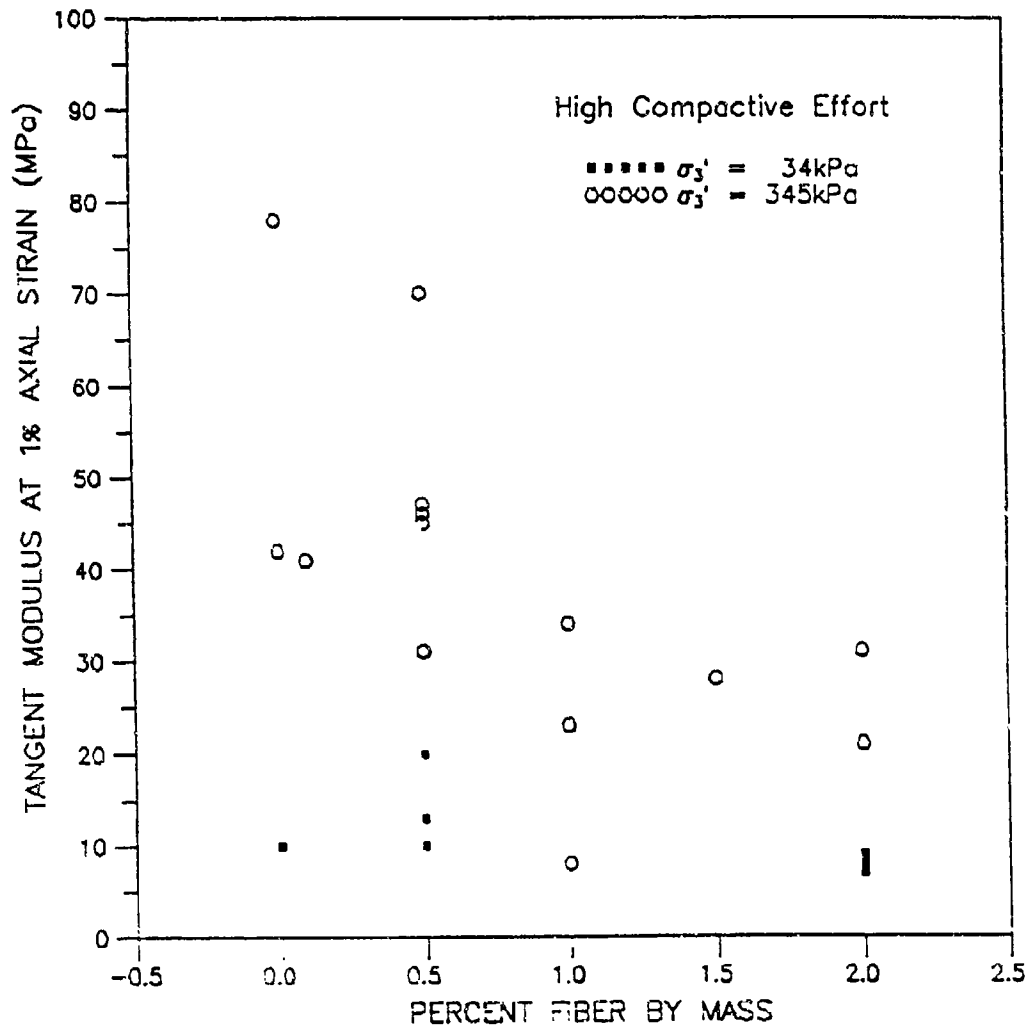


Figure 33. Effect of Fiber Content on Tangent Modulus for High Compactive Effort.

2. Static Tensile Tests

Three static tensile tests were performed on Tensar UX1500, Miragrid 10T and Matrex 120 geogrids at a constant rate of approximately 10 percent per minute. Geogrid specimens approximately 0.33 meters (13 inches) in length were used. Specimen widths varied in order to keep the maximum load within the load cell capacity. Both ends of the specimens were cast in epoxy to form the test specimen clamp. One end was connected to the hydraulic loading system and the other fixed at the front of the pullout box. Static tensile stress-strain responses of the three geogrids are shown in Figure 34. This figure clearly indicates that the tensile strength of Matrex 120 is the highest of the three. Tensar UX1500 and Miragrid 10T have approximately the same ultimate tensile strength but significant differences exist between tensile moduli of these two geogrids. All of these three geogrids exhibit non-linear stress-strain behavior, even at stresses less than 50 percent of ultimate tensile strength. It is noted that the measured static tensile strengths for the three geogrids differ from those in Table 4 as reported by the manufacturer. The difference is likely due to effects of the rigid epoxy clamp and different specimen widths.

3. Impact Tensile Tests

The dynamic tensile tests of the three geogrids were conducted using the dynamic loading system. The geogrid specimen was prepared by using the same method as in the static tensile tests. One end of the specimen was connected to the dynamic loading system and the other fixed at the front of the pullout box. A loading impulse was generated by the dynamic loading system, producing a tensile stress wave which traveled along the specimen. For each impact tensile test, input kinetic energy was high enough so that the geogrid broke in a few tens of ms.

The results of three dynamic tensile tests on UX1500, Miragrid 10T, and Matrex 120 geogrids are presented in Table 6 and shown in Figure 34. Force, acceleration, velocity and displacement traces for these three dynamic tensile tests are presented in Volume 2, Appendix A of this report. The dynamic stress-strain responses in Figure 34 are actual test measurements, and not representative of the true material response because of nonuniform wave propagation within the specimen during testing. In other words, the material behavior is coupled with the structural response of the specimen during rapid loading rate testing. The "true" stress-strain response can be backcalculated using a numerical technique, which is not attempted here.

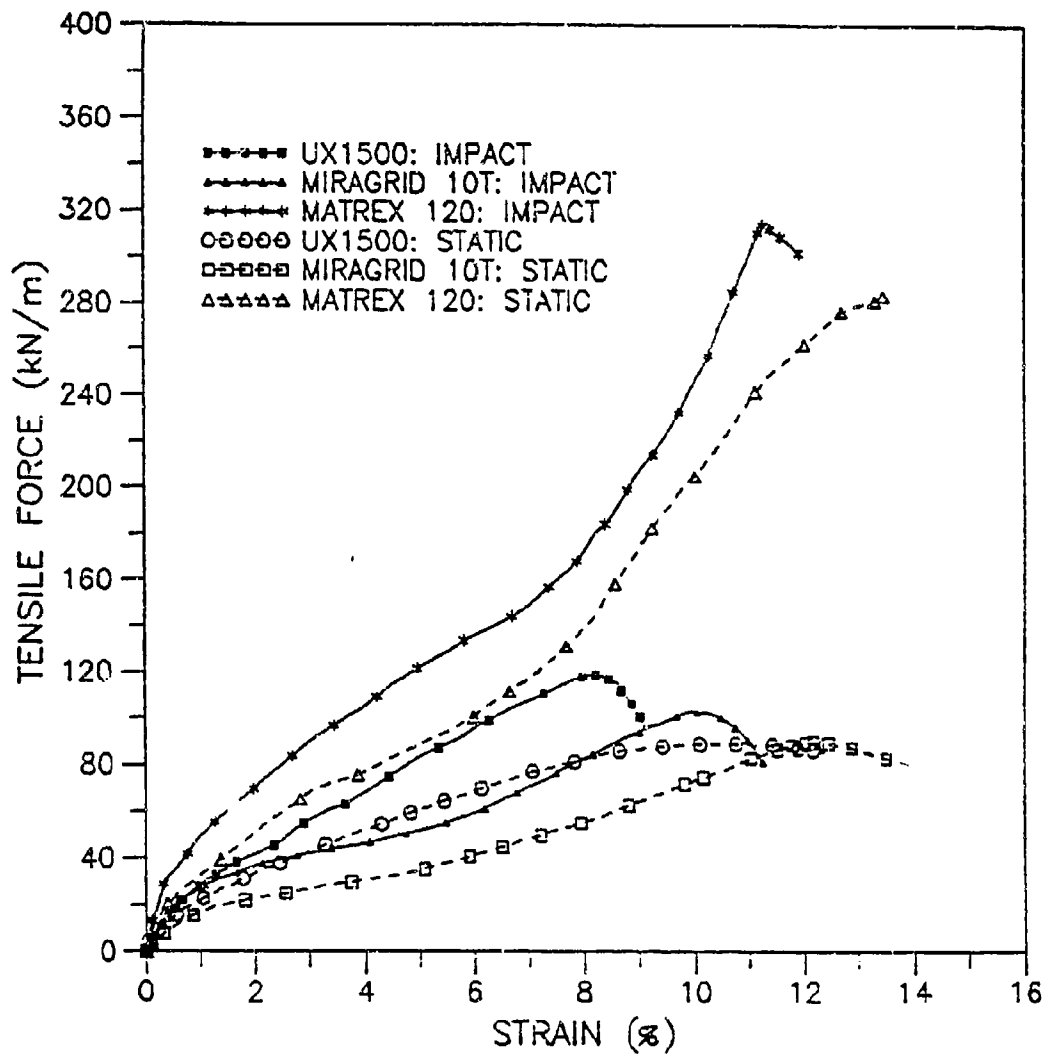


Figure 34. Static and Dynamic Tensile Test Results for UX1500, Miragrid 10T, and Matrex 120 Geogrids.

Comparison between the static and dynamic tensile test results for the three geogrids are presented in Table 6. Figure 34 shows the static and dynamic tensile stress-strain curves for the three geogrids, and that the dynamic tensile strength is higher than the static tensile strength, as is the dynamic tensile stiffness of the three geogrids. The relative increase of tensile strength, defined as ratio of net increase to static strength, is 33.8, 14.5, and 10.7 percent for UX1500, Miragrid 10T, and Matrex 120 geogrids, respectively. The three tested specimens were different in width. However, each geogrid was tested using the same width in both static and dynamic tensile tests for a direct comparison between the static and the dynamic tensile strength.

TABLE 6. SUMMARY OF IMPACT TENSILE TEST RESULTS FOR GEOGRIDS.

Test Series	Geosynthetic Type	Specimen Width (ribs)	Specimen Length (mm)	Input Kinetic Energy (kJ-m)	Measured Impact Tensile Strength (kN/m)	Measured Static Tensile Strength (kN/m)	Relative Increase (%)
DT1	UX1500	4	325	1.81	118.8	88.9	33.8
DT2	Miragrid 10T	3	325	1.81	102.8	89.8	14.5
DT3	Matrex 120	2	325	1.81	313.7	283.3	10.7

G. PULLOUT TEST RESULTS

1. Test Procedures

Pullout testing generally consists of measuring the force necessary to pull a specimen, such as geogrid or geotextile, out of a soil mass. The required force, divided by the width of the test specimen, is commonly referred to as the pullout resistance, and has units of force per unit width. The pullout resistance divided by twice the plan area of the embedded reinforcement is defined as the average or apparent shear strength. This type of test is performed in general accordance with ASTM Draft Standard Test Method D35.01.87.02, "Measuring Geosynthetic Pullout Resistance in Soil."

The following procedures were adopted in all the static and dynamic pullout tests performed:

- the rigid front plate [250 mm (10 inches) long x 200 mm (8 inches) wide x 13 mm (0.5 inch) thick] is cast using epoxy and non-woven geotextiles;
- the soil is placed in the lower half of the pullout box and compacted to the required density;
- the specimen is placed on the compacted soil surface at the middle level of the box;
- the soil is placed in the upper half of the box and compacted to the required density;
- a confining pressure is applied to the soil mass through an air bag which is confined between the rigid roof of the box and the upper soil surface; and
- the specimen is pulled out of soil at a constant displacement rate measured at the pulling end in static pullout tests. In dynamic pullout testing, the specimen is subjected to an impulse loading.

2. Static

a. Preliminary Tests

Two preliminary series of pullout tests were conducted to evaluate the precision of the equipment and to confirm the reproducibility of test results. The first series, P1, of pullout tests was conducted with UX1500 geogrid placed in the SP sand at the relative density of 95-100 percent, achieved by the raining method. The geogrid specimens were 1320 mm (52 inches) long x 165 mm (6.5 inches) wide, and pulled out at a constant displacement rate of 1 mm/minute (0.4 inch/minute) measured at the pulling end. All test conditions were identical for the three tests conducted in this series. The test results in terms of pullout force versus displacement are shown in Figure 35. Good reproducibility was achieved. A load cell and a LVDT were used to measure forces and displacements with absolute errors of +/- 11 N (2.5 pounds) and +/- 0.013 mm (0.0005 inch), respectively. Output from the load cell and LVDT were collected by a data acquisition system.

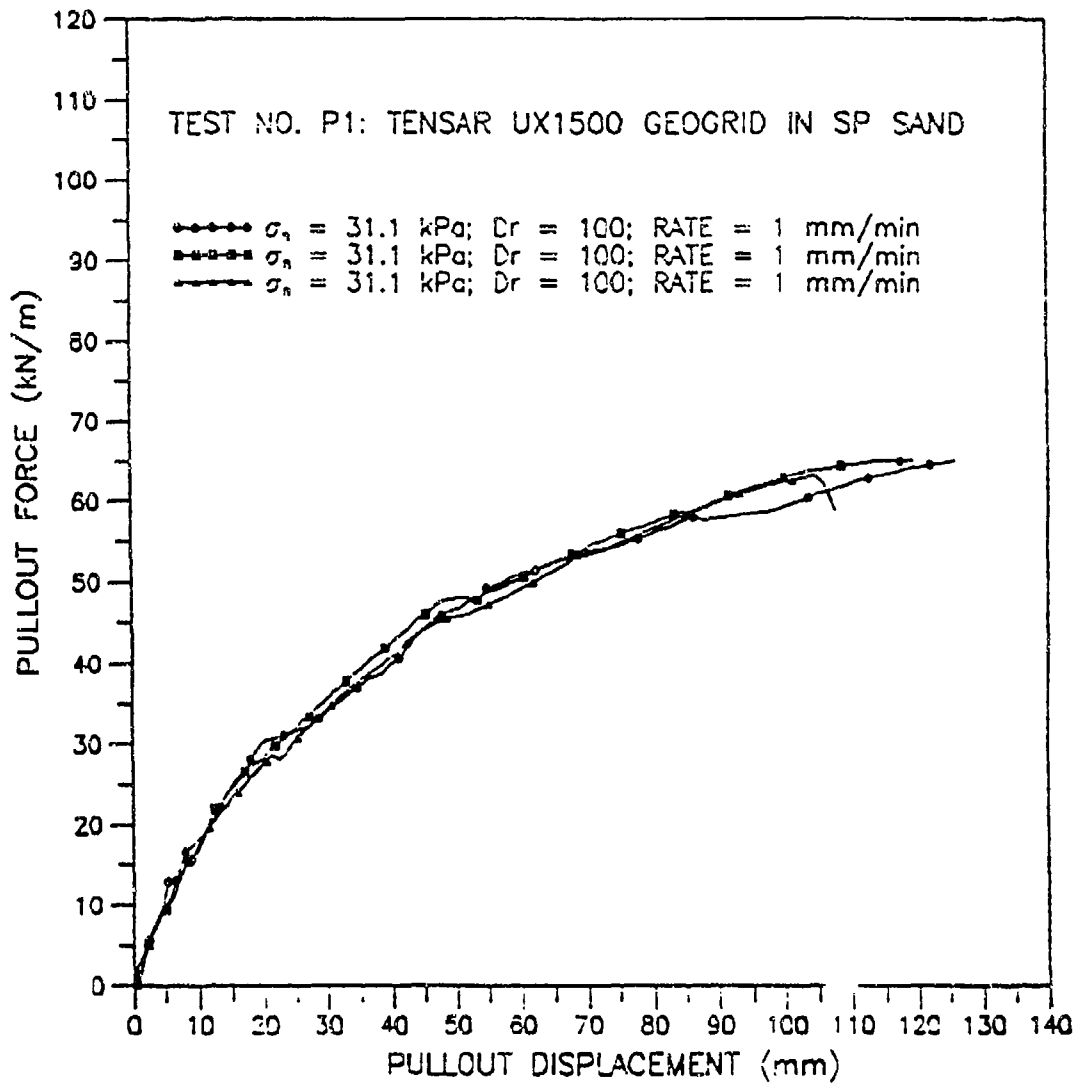


Figure 35. Series P1 Pullout Test Results.

The second series, P2, of pullout tests was conducted in the SP sand with a relative density of 80 percent achieved by hand tamping. The geogrid specimens were 991 mm (39 inches) long x 165 mm (6.5 inches) wide and subjected to 2.1 kPa (0.3 psi) overburden pressure. The reproducibility of the test results can be seen in Figure 36.

b. Pullout Resistance of Clamp Plate

For all the pullout tests conducted in this study, a portion of the epoxy clamp plate was embedded in soil, as shown in Figure 21. The embedded portion had initial dimensions of 102 mm (4 inches) long x 229 mm (9 inches) wide x 13 mm (0.5 inch) thick. Since the ultimate pullout displacement was less than 102 mm (4 inches) in all cases, the embedded geogrid area was constant during testing and an area correction was not necessary for interpreting test results. However, the embedded clamp plate contributed to the measured pullout force. This contribution was determined and subtracted from the measured pullout force in order to obtain the true geogrid pullout resistance.

Two series of pullout tests, Clamp1 and Clamp2, were conducted with a clamp plate alone in the SP sand and the SW-SM sand. Figures 37 and 38 show the clamp pullout responses in the SP and SW-SM sands, respectively. Test conditions are also described in the two figures. The results indicate a peak SP sand-plate interface friction angle of 32 degrees and a nonlinear shear strength curve for the SW-SM sand-plate interface.

In both sands, the clamp plate pullout resistance decreases sharply after peak and approaches zero when the pullout displacement is greater than 51 mm (2 inches). In the majority of the pullout tests conducted, peak pullout resistance occurred at displacements greater than 51 mm (2 inches). Therefore, the effect of the clamp plate on soil-geogrid interface shear strength was negligible, although it could affect the initial portion of a pullout force-displacement curve considerably.

c. Geogrids in SP and SW-SM Sand

To establish static pullout strength curves for UX1500, Miragrid 10T, and Matrex 120 geogrids, nine series of pullout tests were conducted on the three geogrids in the SP and SW-SM sands. Six of them were conducted in the SP sand compacted to a relative density of approximately 80 percent by hand tamping.

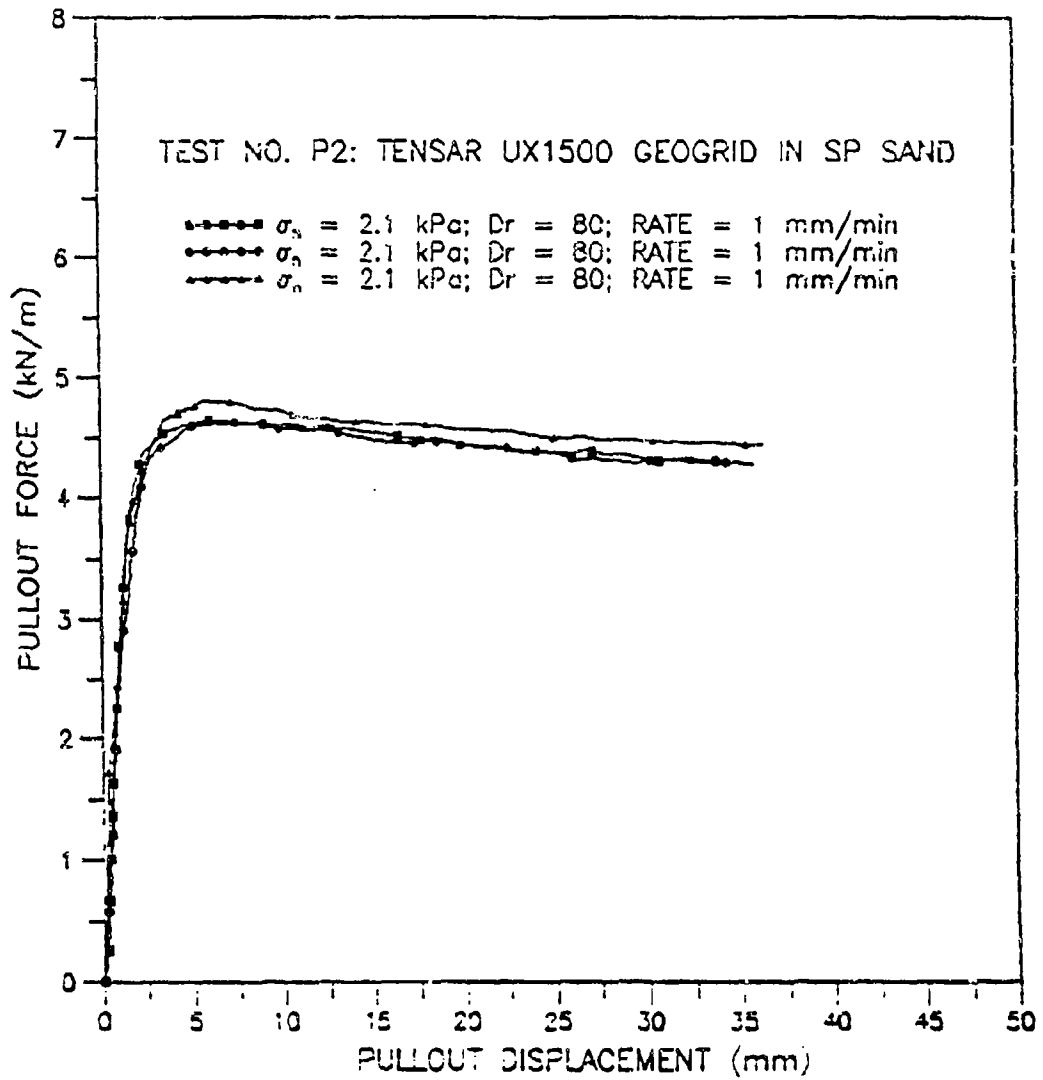


Figure 36. Series P2 Pullout Test Results.

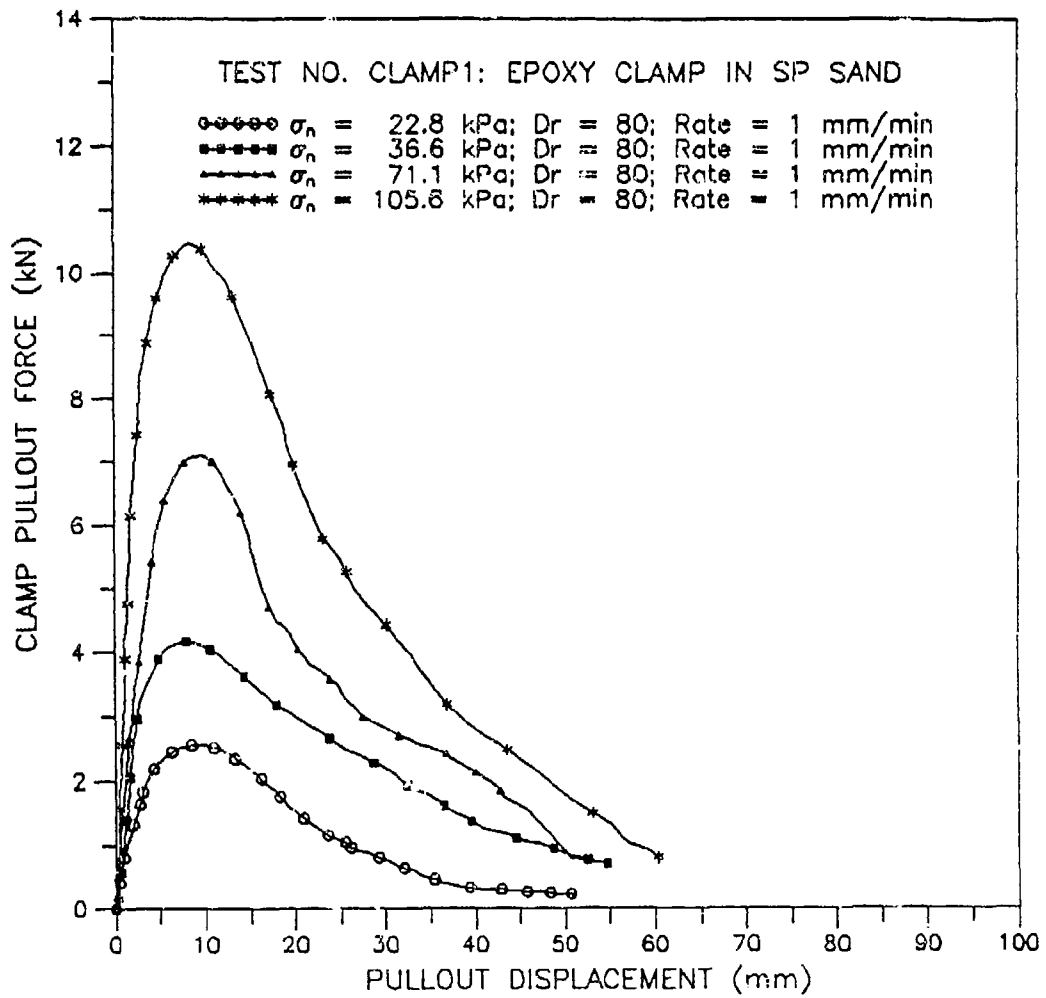


Figure 37. Results of Clamp1 Pullout Tests.

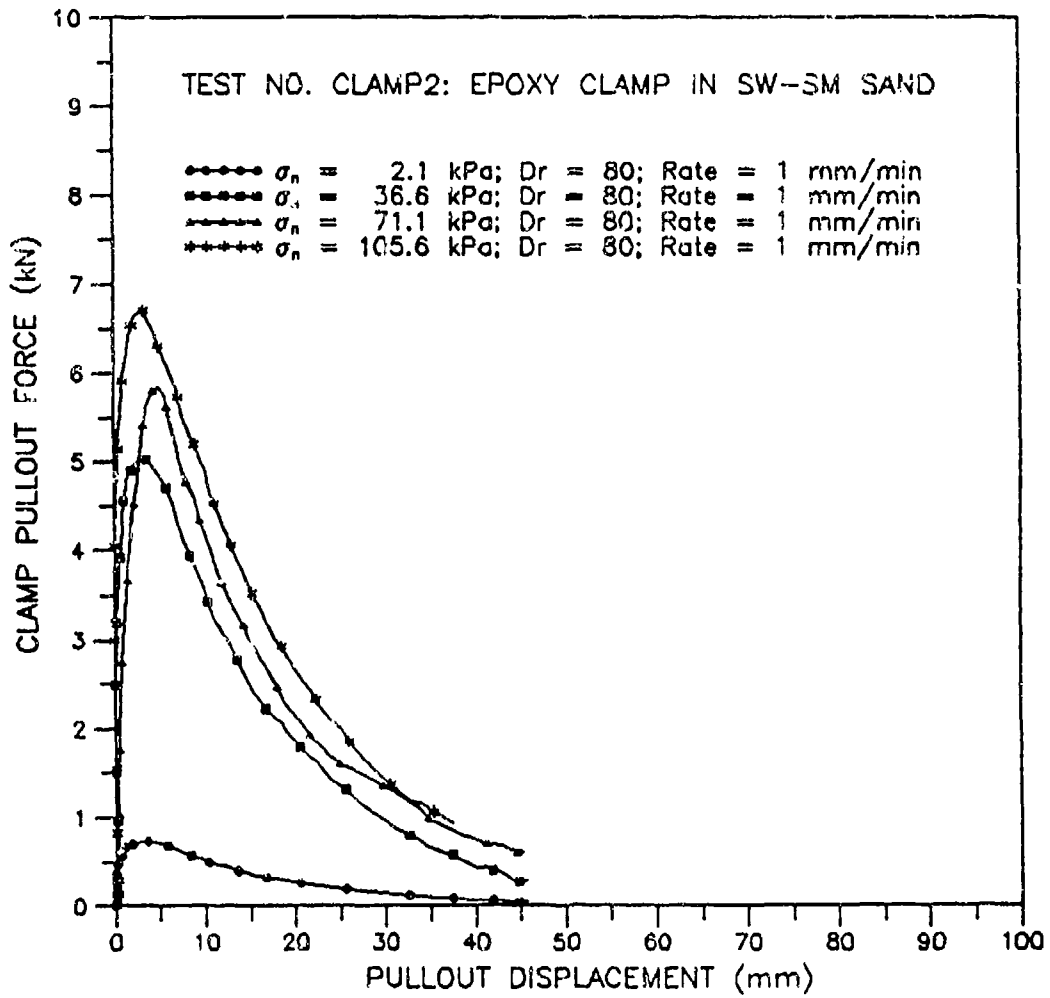


Figure 38. Results of Clamp2 Pullout Tests.

Three of the SP sand series were conducted at a pullout rate of 1 mm/minute (0.2 inch/minute) and three were conducted at a pullout rate of 152 mm/minute (6 inches/minute). Three were conducted in the SW-SM sand compacted to a relative density of approximately 75 percent at a moisture content of 3.0 percent and at a pullout rate of 1 mm/minute (0.2 inch/minute). Detailed test conditions and results for these nine series of tests are presented in Table 7. Figures 39 and 40 show two typical sets of pullout force-displacement curves for Tensar UX1500 in the SP and in the SW-SM sand, respectively. Pullout force-displacement curves for Miragrid 10T and Matrex 120 in both soils are presented in Volume 2, Appendix A of this report.

Since the three geogrids have different geometric and mechanical properties, it is not anticipated that they would have the same pullout response even under the same test conditions. However, it is generally true that load-displacement curves are concave toward the displacement axis and pullout stiffness, the slope of load-displacement curves, increases with increasing normal stresses. The maximum pullout resistance also increases with increasing normal stress, but is limited by the tensile strength of a given reinforcement. Geogrid rupture will be the failure mode instead of pullout when the normal stress is high enough. The minimum normal stress required to break UX1500 and Miragrid 10T is approximately 71 kPa (10.3 psi) in the SP sand and 37 kPa (5.3 psi) in the SW-SM sand. For Matrex 120 at a normal stress of 110 kPa (15.3 psi) in the SP sand and 71 kPa (10.3 psi) in SW-SM sand, the maximum pullout resistance was close to the tensile strength as reported by the manufacturer, although no rupture was observed during testing. The pullout displacement required to mobilize the maximum pullout resistances varies with geogrid type and confining pressure. The higher the pressure, the larger the pullout displacement required to achieve the maximum pullout resistance. For Matrex 120, the displacement required to mobilize the maximum pullout resistance is smaller than that of UX1500 and Miragrid 10T. This is likely due to the higher tensile stiffness of Matrex 120 geogrids.

The pullout response directly measured from a pullout test can be used to obtain strength parameters of the soil-reinforcement interface. There are two simple interpretation methods, the conventional and effective length methods. These methods may result in significant differences in soil-reinforcement interface strength parameters. The differences are caused by the first step of interpreting pullout response, (i.e., the shear stress determination). The conventional method calculates the average shear stress

TABLE 7. SUMMARY OF STATIC PULLOUT TEST RESULTS FOR GEOGRIDS IN SP AND SW-SM SANDS.

Test Series	Geosynthetic Type	Soil Type	Specimen Width (mm)	Specimen Length (mm)	Normal Stress (kPa)	Soil Condition ^(a)		Rate of Pullout (mm/min)	Pullout Resistance (kN/m)	Apparent Friction Coefficient
						D, (%)	w (%)			
1	UX1500	SP	165	991	2.1	80	0	1	4.6	1.12
	UX1500	Sand	165	991	22.8	80	0	1	47.6	1.05
	UX1500		165	991	36.8	80	0	1	60.7	0.94
	UX1500		165	991	71.1	80	0	1	73.8	0.52 ^(b)
2	Miragrid 10T	SP	165	991	2.1	80	0	1	5.7	1.39
	Miragrid 10T	Sand	165	991	22.8	80	0	1	49.0	1.09
	Miragrid 10T		165	991	36.8	80	0	1	68.6	0.95
	Miragrid 10T		165	991	71.1	80	0	1	94.0	0.65 ^(b)
3	Matrex 120	SP	146	991	2.1	80	0	1	4.5	1.09
	Matrex 120	Sand	146	991	22.8	80	0	1	50.8	1.13
	Matrex 120		146	991	50.4	80	0	1	90.3	0.90
	Matrex 120		146	991	71.1	80	0	1	115.1	0.82
	Matrex 120		146	991	105.6	80	0	1	166.6	
4	UX1500	SW-	165	991	2.4	75	3.0	1	13.3	2.89
	UX1500	SM	165	991	23.1	75	3.0	1	67.7	1.48
	UX1500	Sand	165	991	36.9	75	3.0	1	71.4	0.98 ^(b)
5	Miragrid 10T	SW-	165	991	2.4	75	3.0	1	14.0	2.93
	Miragrid 10T	SM	165	991	23.1	75	3.0	1	65.3	1.43
	Miragrid 10T	Sand	165	991	36.9	75	3.0	1	90.6	1.26 ^(b)
6	Matrex 120	SW-	146	991	23.1	75	3.0	1	59.3	1.30
	Matrex 120	SM	146	991	36.9	75	3.0	1	95.9	1.31
	Matrex 120	Sand	146	991	71.4	75	3.0	1	143.7	1.32
7	UX1500	SP	165	991	2.1	80	0	152	4.9	1.20
	UX1500	Sand	165	991	22.8	80	0	152	47.0	1.07
	UX1500		165	991	36.8	80	0	152	73.8	1.02
	UX1500		165	991	71.1	80	0	152	82.8	0.59 ^(b)
8	Miragrid 10T	SP	165	991	22.8	80	0	152	53.2	1.17
	Miragrid 10T	Sand	165	991	36.8	80	0	152	85.0	1.17
	Miragrid 10T		165	991	71.1	80	0	152	93.0	0.67 ^(b)
9	Matrex 120	SP	146	991	2.1	80	0	152	4.8	1.15
	Matrex 120	Sand	146	991	22.8	80	0	152	46.6	1.02
	Matrex 120		146	991	50.4	80	0	152	92.0	0.92
	Matrex 120		146	991	71.1	80	0	152	122.6	0.88
	Matrex 120		146	991	105.6	80	0	152	164.0	0.79

Notes. ^(a) D, and w are relative density and moisture content, respectively

^(b) Failure due to specimen rupture rather than pullout.

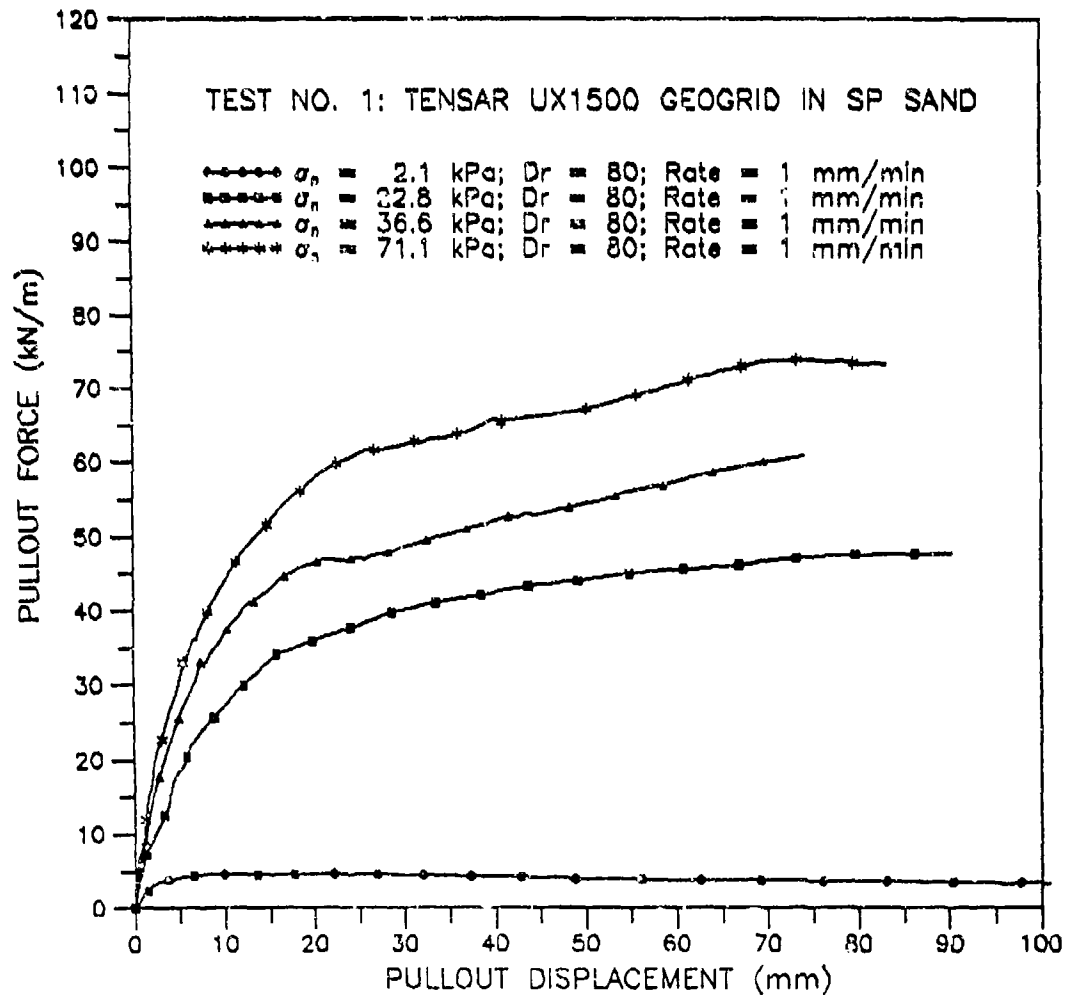


Figure 39. Pullout Response of UX1500 Geogrid in SP Sand.

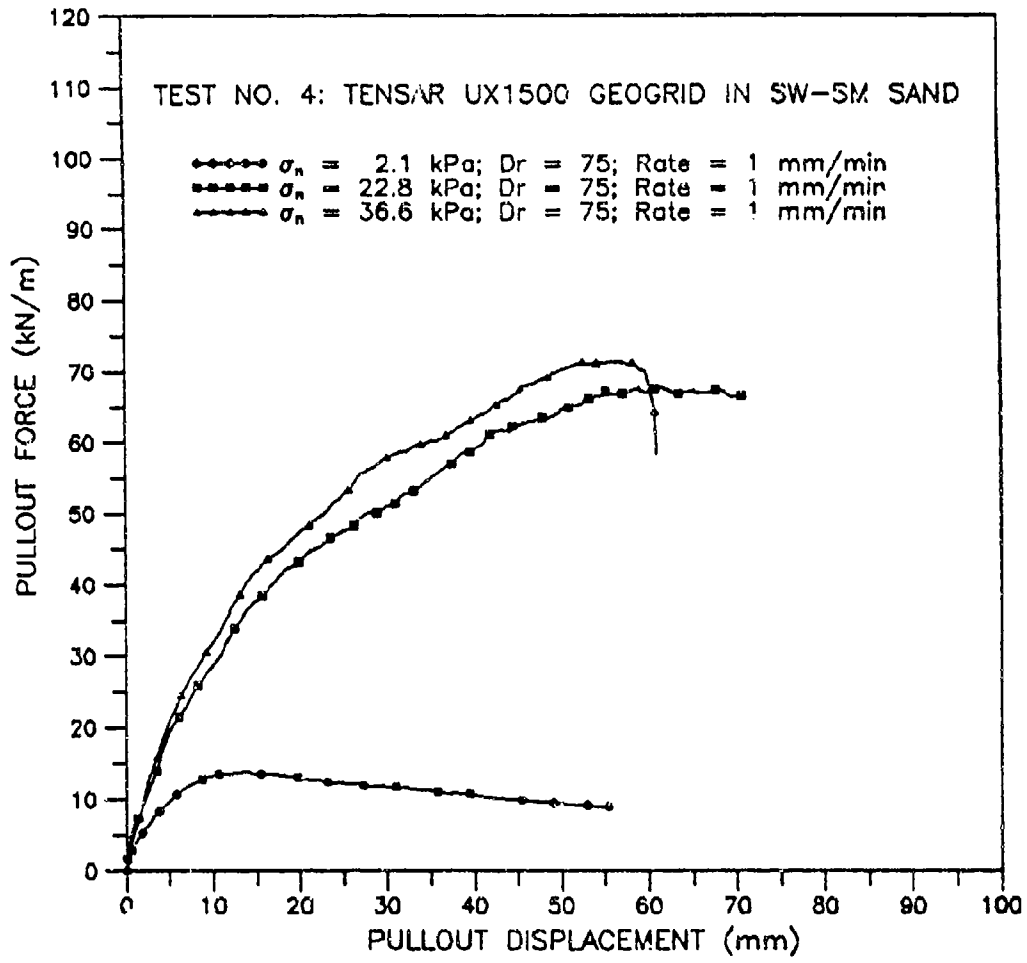


Figure 40. Pullout Response of UX1500 Geogrid in SW-SM Sand.

based on the embedded length regardless of nonuniform mobilization of shear stresses. It is possible that the back portion of a reinforcement does not move at all during testing. Consequently, using the total length potentially underestimates interface strength parameters. The mobilized or effective length method has been used by Solomone et al. (Reference 70). The effective length is defined as the length along which every point of a reinforcement moves during testing as detected from the tell-tail data. If the free end of reinforcement moves during testing, these two methods lead to identical results.

The conventional method was used to interpret the pullout test results. The maximum apparent shear stress of a soil-geogrid interface, defined as the pullout resistance divided by twice the plan area of the embedded reinforcement, was determined for each pullout test. Soil-geogrid interface shear strength envelopes and peak apparent shear stresses versus normal stresses, for all the six pullout tests, are shown in Figure 41. These envelopes clearly indicate that soil-geogrid interface shear strength is non-linearly related to normal stresses. Therefore, it can not be simply characterized by a constant soil-geogrid interface friction angle and adhesion. The apparent friction coefficient for each normal stress, defined as the maximum apparent shear stress divided by the corresponding normal stress, was used to characterize interface shear strength. Variation of apparent friction coefficient with normal stress is shown in Figure 42. These data show that the apparent friction coefficient decreases with normal stress for all three geogrids. In fact, the apparent friction coefficient obtained this way approaches zero if normal stresses are high enough.

d. Reinforced Earth Bar in SP and SW-SM Sand

Two series of pullout tests were conducted on a galvanized metal strip (Reinforced Earth Bar) with ribs on both sides from the Reinforced Earth Company, in the SP and in the SW-SM sand. The test procedures were the same as those used in the geogrid pullout test except that the rigid epoxy clamp was not used. Instead, one end of the strip was directly connected to the loading system. Detailed test conditions and results of these two series are presented in Table 8. A typical set of pullout force-displacement curves is shown in Figure 43. Variation of apparent friction coefficient with normal stress for both test series are shown in Figure 44.

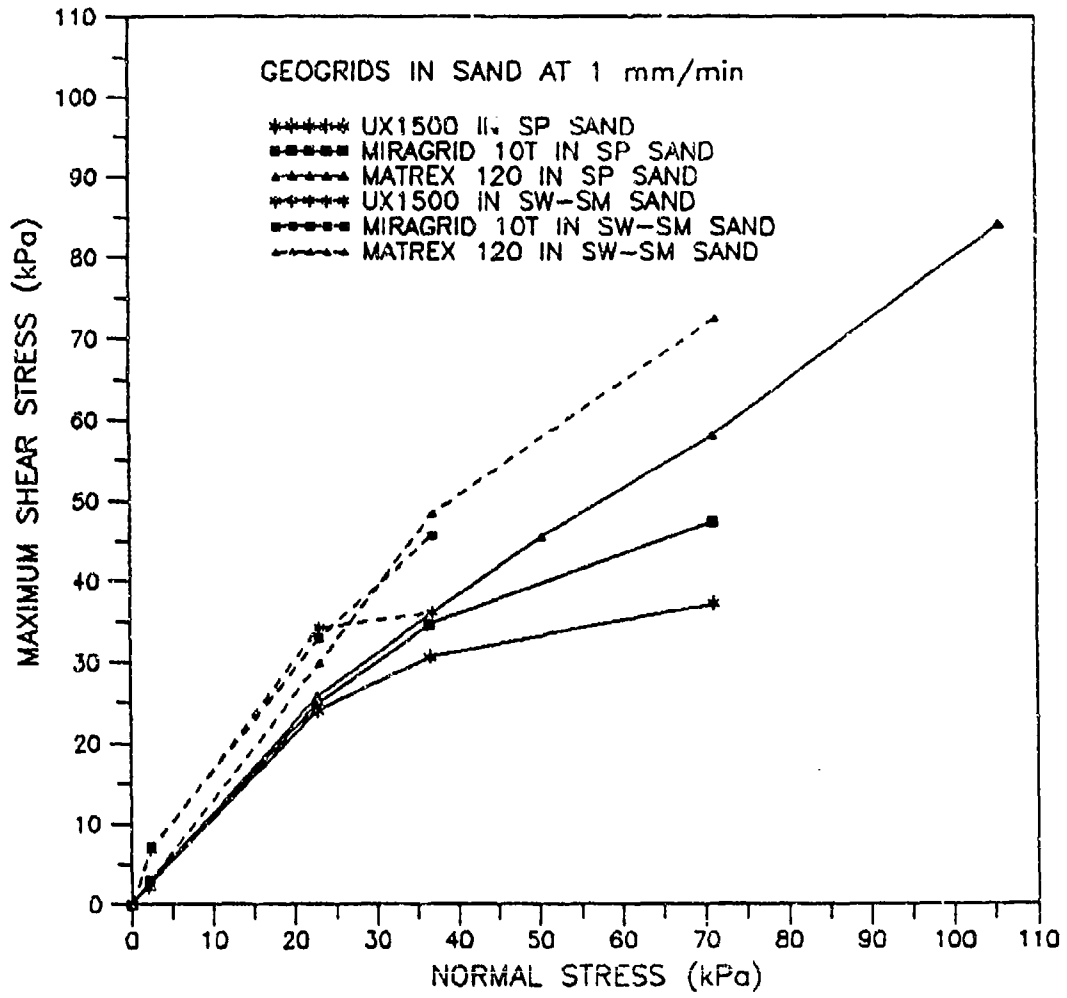


Figure 41. Sand-Geogrid Interface Shear Strength Curves.

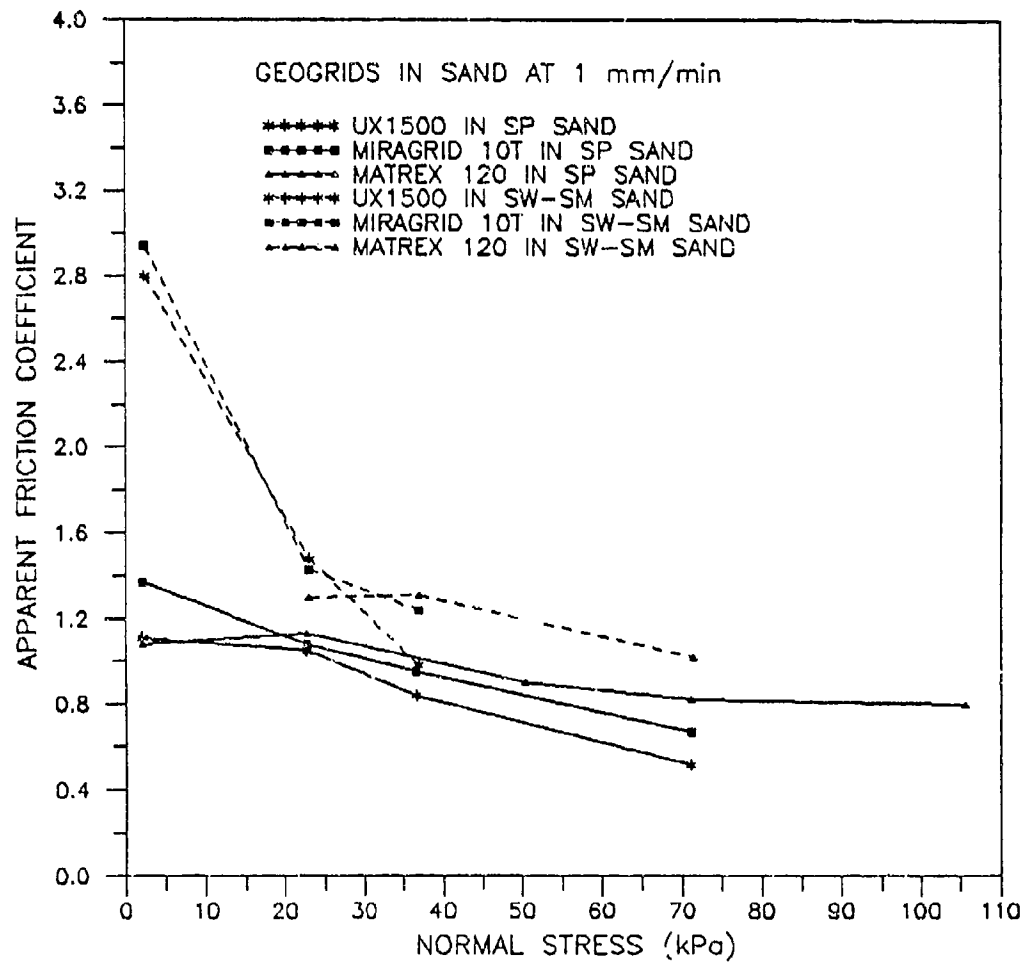


Figure 42. Variation of Apparent Friction Coefficient with Normal Stress for Geogrids.

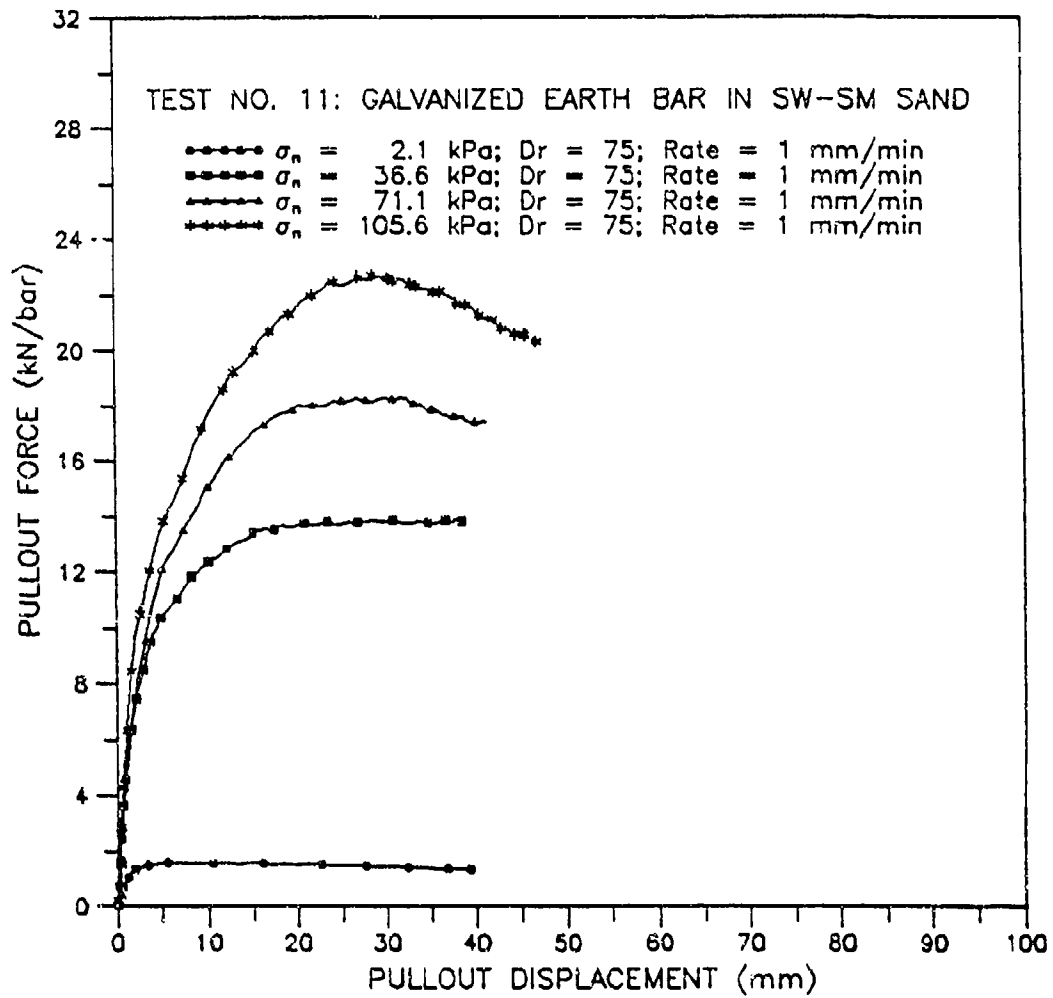


Figure 43. Pullout Response of Reinforced Earth Bar in SW-SM Sand.

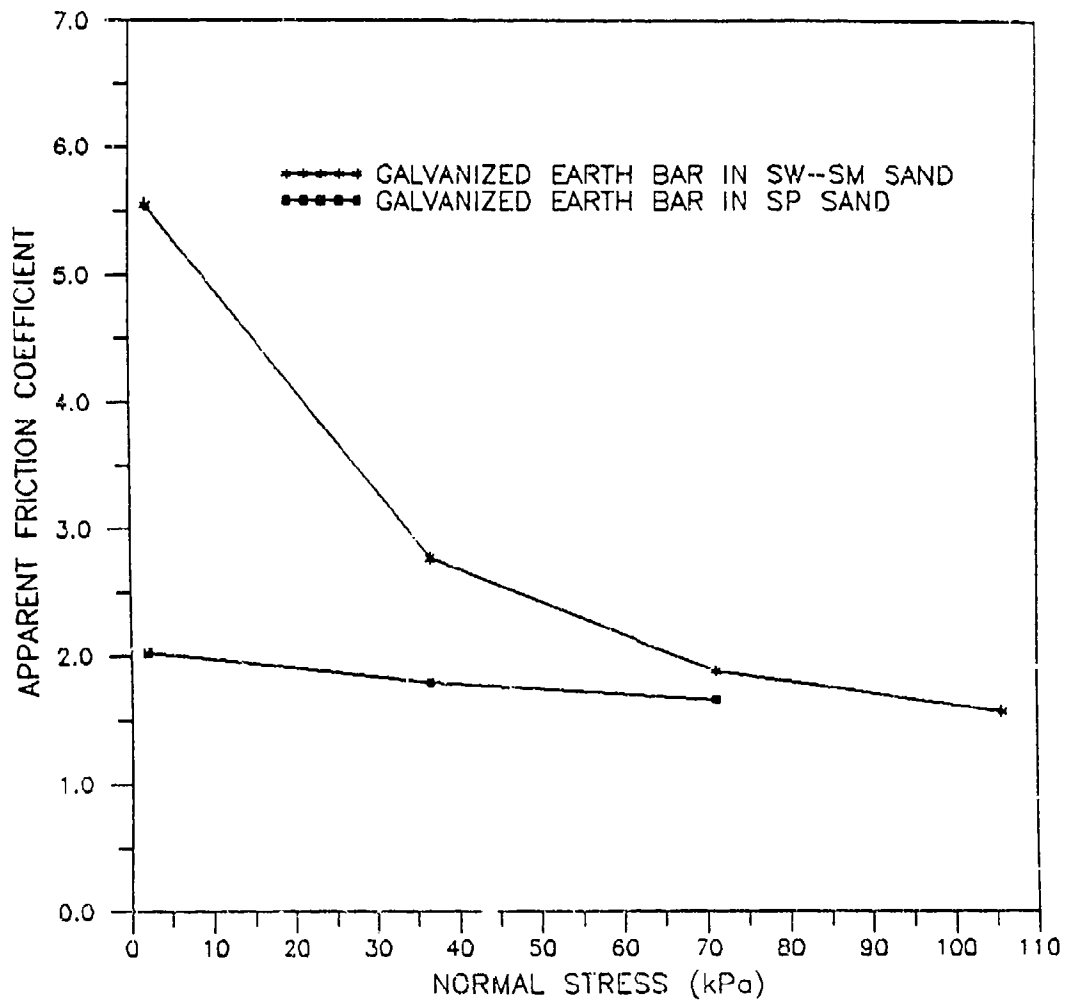


Figure 44. Variation of Apparent Friction Coefficient with Normal Stress for Reinforced Earth Bar.

TABLE 8. SUMMARY OF STATIC PULLOUT TEST RESULTS FOR GALVANIZED REINFORCED EARTH BAR IN SP AND SW-SM SANDS.

Test Series	Reinforcement Type	Soil Type	Specimen Width (mm)	Specimen Length (mm)	Normal Stress (kPa)	Soil Condition ^(a)		Pullout Rate (mm/min)	Pullout Resistance (kN/bar)	Apparent Friction Coefficient
						D, (%)	w (%)			
10	Galvanized Earth Bar	SP Sand	50	1372	2.1	80	0	1	0.6	2.08
			50	1372	38.8	80	0	1	9.2	1.83
			50	1372	71.1	80	0	1	17.2	1.76
11	Galvanized Earth Bar	SW-SM Sand	50	1372	2.1	75	3.0	1	1.6	4.81
			50	1372	38.8	75	3.0	1	13.9	2.68
			50	1372	71.1	75	3.0	1	18.3	1.97
			50	1372	105.6	75	3.0	1	22.7	1.58

Note: ^(a) D, and w are relative density and moisture content, respectively.

Comparison between Figures 42 and 44 clearly indicates that the galvanized earth bar has a higher apparent friction coefficient than the geogrids in either soil. This is likely due to edge effects. A geogrid specimen has a thickness typically much less than its width. Therefore, frictional resistance along its edge is negligible and it is reasonable to calculate strength parameters by using the plan area. However, the thickness of the earth bar is 8 percent of its width without considering the height of the ribs and thus the apparent friction coefficient based on its plan area is higher than the actual value.

Comparison between Figures 40 and 43 indicates that the earth bar mobilized the maximum pullout resistance at smaller displacement than the geogrid. This is likely due to higher tensile stiffness of the earth bar, which can also be observed in comparing pullout response of Matrex 120 with UX1500 and Miragrid 10T geogrids.

Comparison between the two curves in Figure 44 shows that the SW-SM sand-earth bar interface strength is higher than the SP sand-earth bar interface strength. The three geogrids also show higher interface shear strength in the SW-SM sand than in the SP sand. This is due to the higher friction angle of the SW-SM sand.

All the static pullout tests on the geogrids and strips in both soils have shown a general trend that the apparent friction coefficient or angle

decreases with increasing normal stress. This is partially related to soil dilation which is more pronounced at the lower confining pressure. It may also be related to nonuniform distribution of shear stresses along the reinforcement. At the higher confining pressure, the soil-reinforcement interface shear strength may not be fully mobilized along the back portion of the reinforcement and thus the maximum apparent shear stress is less than the available interface shear strength.

e. Rate Dependence

ASTM D35.01.87.02 recommends a standard pullout displacement rate of 1 mm/minutes (0.04 inch/minute) measured at the pulling end of geosynthetic specimens. Varying this rate may change the pullout resistance for a given soil-geosynthetic system because behavior of soil reinforcement and soil-reinforcement interface may be strain-rate dependent.

(1) Rate-Dependent Behavior of Reinforcement in Soil

Strain-rate dependency of Tensar UX1500 geogrids was investigated by McGown et al. (Reference 30). Their results indicate that the tensile strength of UX1500 geogrids increases with increasing strain rate based on a series of constant strain rate tests. The rate effect on stress-strain behavior for UX1500, Miragrid 10T and Matrex 120 geogrids can also be observed from the impact tensile test results as shown in Figure 34. The maximum strain rate in the three impact tensile tests was on the order of 10,000 percent/minute in contrast to 10 percent/minute used in the three static tensile tests. As can be seen from Figure 34, the directly measured impact tensile strengths for the three geogrids are higher than static tensile strengths.

Strain-rate dependency of soils is primarily related to pore pressure dissipation. If the load is applied to a soil mass rapidly, pore pressure may build up and the undrained shear strength is mobilized. This condition frequently occurs with clay. With coarse granular soils, dissipation generally occurs so quickly that no measurable additional pore pressure actually develops. For situations of partially saturated or dry granular soils, the pore phase can be highly compressible relative to the compressibility of the soil skeleton and the pore pressure parameter is very small. Therefore, the load is essentially carried by soil skeleton whether it is applied to the soil mass fast or slow. In all of the pullout tests performed, the SP and SW-SM sands were

tested dry and at 3.0 percent moisture content, respectively. Pore pressure related rate-dependency is unlikely to affect the pullout results.

(2) Rate-Dependent Pullout Behavior of Geogrids in SP Sand

Three series of pullout tests were conducted on the three geogrids in the SP sand at a displacement rate of 152 mm/minutes (6 inches/minute). Pullout force-displacement curves for the three test series are presented in Volume 2, Appendix A to this report. Figure 45 shows comparison of pullout resistance curves at 1.0 mm/minute (0.04 inch/minute) and those at 152 mm/minute (6 inches/minute). This figure shows that the pullout resistance at two different displacement rates is almost identical for the three geogrids at lower confining pressure. At higher confining pressure, the pullout resistance of Tensar UX1500 geogrid at 152 mm/minute (6 inches/minute) increased by 12 percent and no significant increase was observed for Miragrid 10T and Matrex 120 geogrids.

Based on the above analyses and limited test results, it appears that the pullout rate dependency is more likely related to reinforcing material, when tested in granular soils. For low confining pressures, the reinforcement may move through the soil like a rigid body with low strain rate and strain even though it is pulled out of soil very rapidly. Therefore, the strain-rate dependency of the reinforcement will not be reflected in the pullout test results. However, at a high confining pressure, the back portion of the reinforcement may be totally anchored during testing. If a high pullout displacement rate is imposed to the specimen, the front portion is subjected to high strain rate and strain. Therefore, rate-dependency of the reinforcement will affect the pullout results. This indicates that the pullout displacement rate does not directly affect the pullout behavior. It is the mobilized strain rate of the reinforcement that actually does.

3. Impact

An impact or dynamic pullout test is one in which a reinforcement is subjected to an impulse pullout load with a rise time of a few tens of ms. As mentioned in Section IV-B-3, the peak dynamic pullout resistance is expected to vary with input kinetic energy for a given normal stress. The maximum of all the peaks for a given normal stress is defined as the dynamic pullout resistance. This requires several dynamic pullout tests for a given normal stress in order

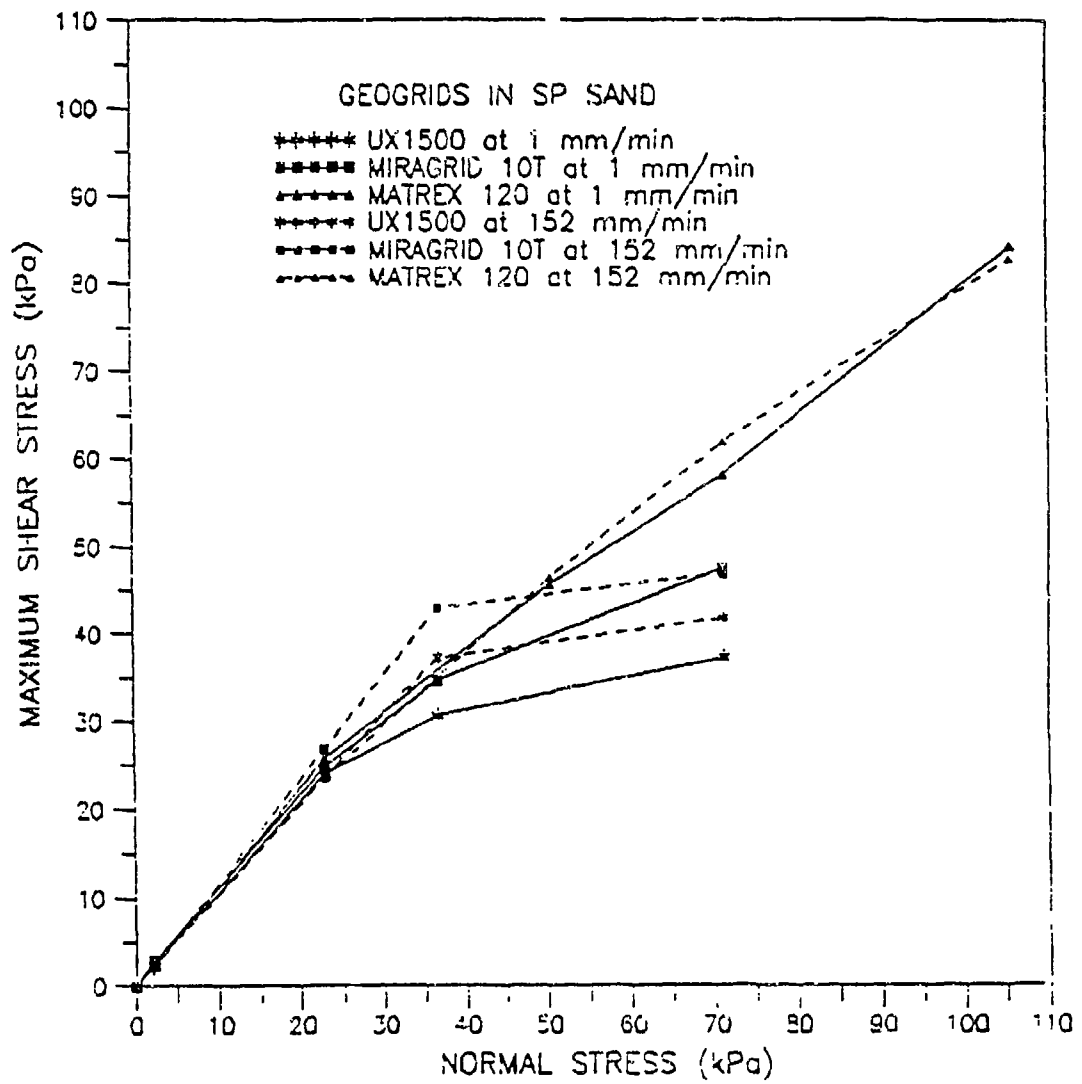


Figure 45. Pullout Rate Effect on Sand-Geogrid Interface Shear Strength.

to define a dynamic pullout resistance. However, several initial tests show that the specimen is not pulled out and the maximum dynamic pullout resistance is not fully mobilized if input kinetic energy is too low. The input kinetic energy of 1.81 kN-meters (16,000 pound-inches), high enough to break the specimen according to the impact tensile tests, was used for all the dynamic pullout tests. The maximum dynamic pullout force associated with this input kinetic energy is considered as the dynamic pullout resistance hereafter.

Six series of impact pullout tests on the three geogrids in the SP and SW-SM sands were conducted. During each test, a 100g accelerometer and 22 kN (5,000 pounds) load cell were used to measure acceleration and pullout force, respectively, at the specimen clamp. Output from the accelerometer and load cell were collected by an oscilloscope. A sampling rate of 3 points per ms was used in all the impact pullout tests. All of the dynamic pullout tests were conducted in the large steel pullout box 2,100 mm (7 feet) long x 900 mm (3 feet) wide x 600 mm (2 feet) deep. Detailed test conditions and results are presented in Table 9. Pullout force, acceleration, velocity and displacement traces, and force-displacement curves for each impact pullout test are graphically presented in Volume 2, Appendix A of this report.

a. Interpretation of Impact Pullout Tests

Typical acceleration and pullout force records of a geogrid in the SP sand are shown in Figures 46 and 47, respectively. It is observed from Figure 46 that the acceleration signal is associated with high frequency noise. This noise is likely due to vibration of the specimen connection frame and distributed randomly in time. To determine the true acceleration signal, it is necessary to eliminate the noise from the directly recorded signal. However, care must be exercised to assure that the process of noise elimination properly preserves the legitimate time variation of the acceleration signal.

Since the noise associated with the acceleration signal has high frequency and varies in a random manner, it will be automatically removed with integration. Theoretical proof of this claim can be done easily and is not presented here. Therefore, the velocity and displacement history obtained by the numerical integration are not affected by the random high frequency noise. This can also be shown from the velocity and displacement curves of the typical impact pullout test in Figures 48 and 49, respectively.

TABLE 9. SUMMARY OF IMPACT PULLOUT TEST RESULTS FOR GEOGRIDS IN SP AND SW-SM SANDS.

Test Series	Geosynthetic Type	Soil Type	Specimen Width (mm)	Specimen Length (mm)	Normal Stress (kPa)	Soil Condition ^(a)		Input Kinetic Energy (kJ-m)	Pullout Resistance (kN/m)	Apparent Friction Coefficient
						D _r (%)	w (%)			
D1	UX1500	SP	165	991	3.5	80	0	1.81	4.8	0.69
	UX1500	Sand	165	991	24.2	80	0	1.81	39.8	0.83
	UX1500		165	991	38.0	80	0	1.81	58.9	0.78
	UX1500		165	991	72.5	80	0	1.81	77.0	0.54
D2	Miragrid 10T	SP	165	991	24.2	80	0	1.81	48.3	1.05
	Miragrid 10T	Sand	165	991	38.0	80	0	1.81	69.7	0.93
	Miragrid 10T		165	991	72.5	80	0	1.81	93.0	0.65
D3	Matrex 120	SP	146	991	24.2	80	0	1.81	67.0	1.40
	Matrex 120	Sand	146	991	38.0	80	0	1.81	96.4	1.28
	Matrex 120		146	991	61.8	80	0	1.81	113.3	1.10
	Matrex 120		146	991	72.5	80	0	1.81	143.9	1.00
D4	UX1500	SW-SM Sand	165	991	24.2	75	3.0	1.81	69.6	1.45
D5	Miragrid 10T	SW-SM Sand	165	991	24.2	75	3.0	1.81	58.0	1.21
D6	Matrex 120	SW-SM Sand	146	991	24.2	75	3.0	1.81	60.3	1.26

Note: ^(a) D_r and w are relative density and moisture content, respectively.

It was found from the numerical integration that the calculated velocity may not be zero and the calculated displacement may not be equal to the measured displacement at the end of a test. It is not fully understood why at the present time. One possible cause is that the noise may not be exactly random. To satisfy the displacement boundary condition at the end of test, a small initial velocity, V_i , was added to the calculated velocity. The effect of V_i on the displacement trace is shown in Figure 49, which indicates that the peak displacement is not sensitive to V_i . The effect of imposed V_i on the dynamic pullout force-displacement curves was also investigated. It was found that the effect of V_i on the force-displacement curve is negligible as shown in Figure 50.

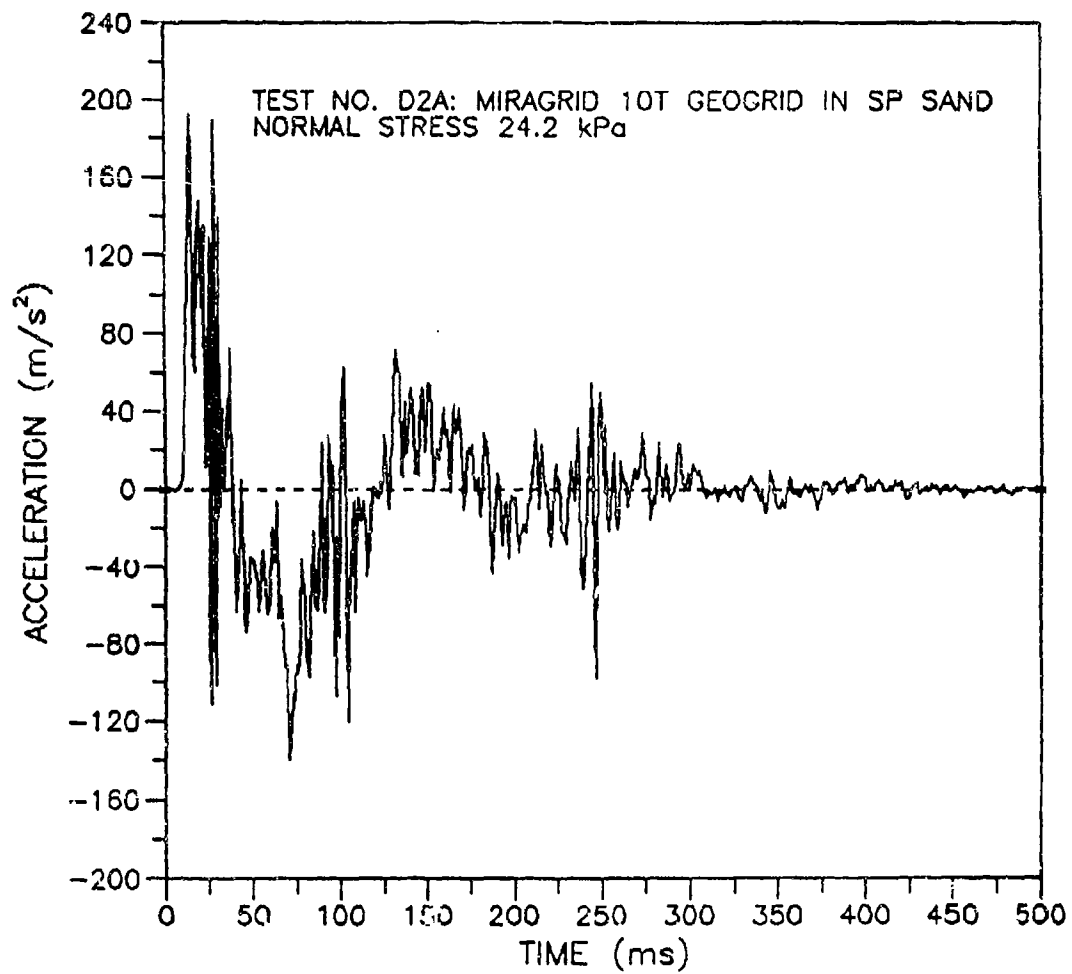


Figure 46. Acceleration-Time History for Miragrid 10T in SP Sand.

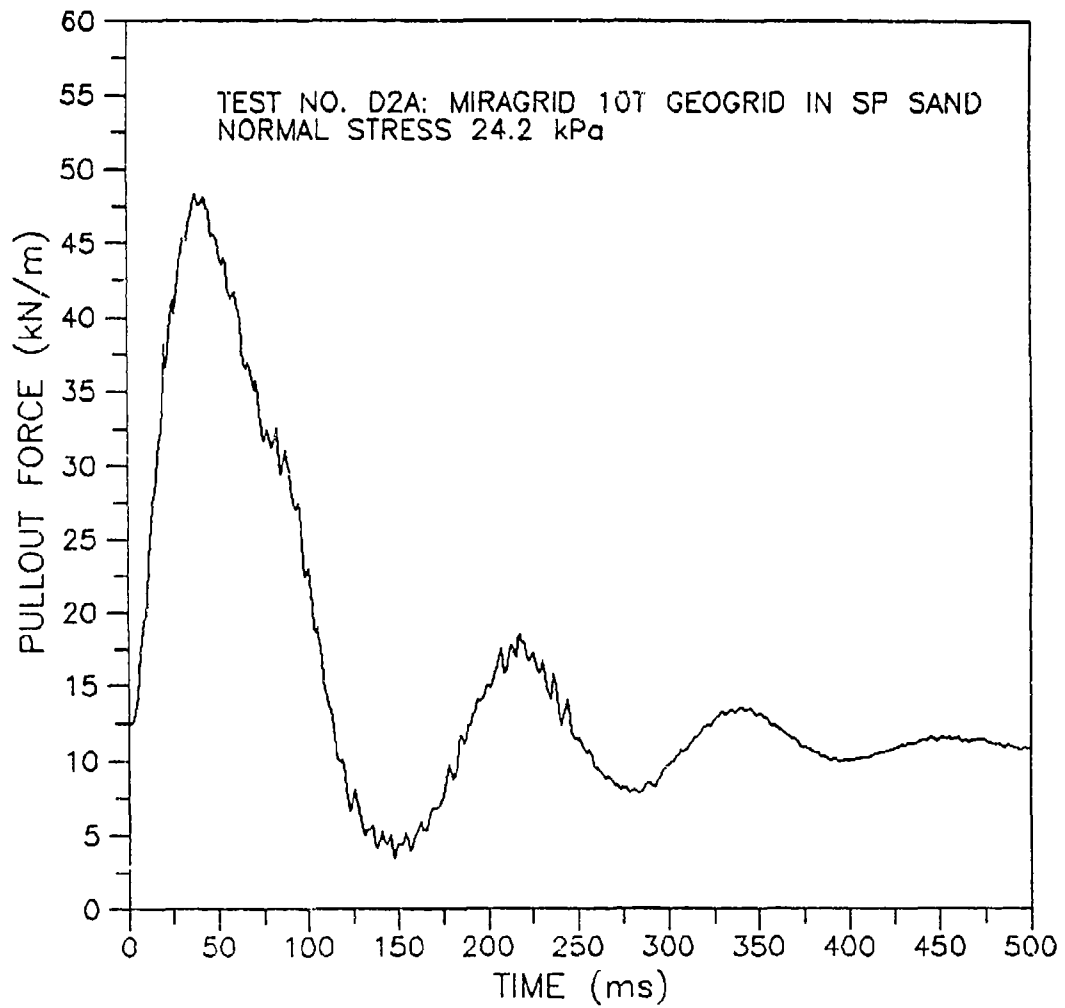


Figure 47. Force-Time History for Miragrid 10T in SP Sand.

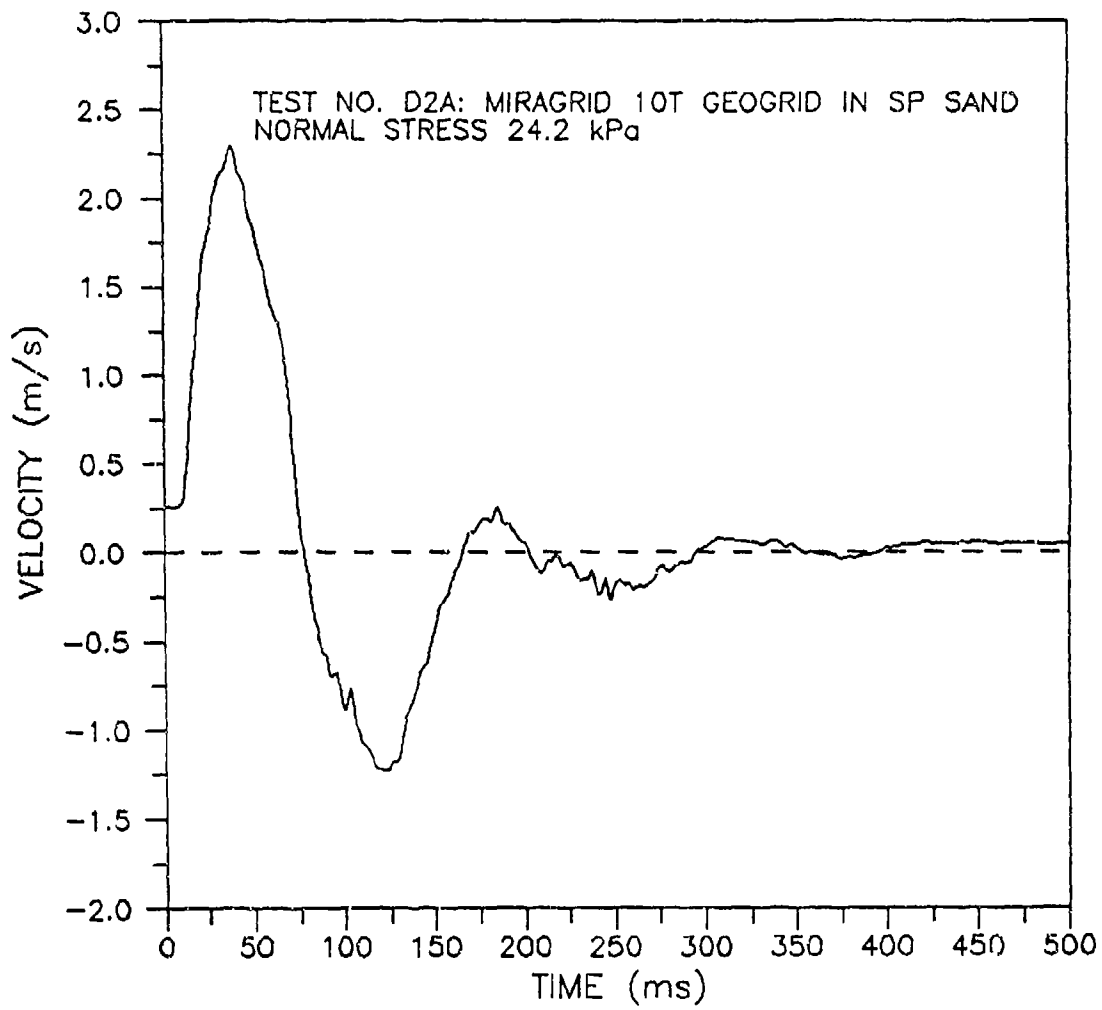


Figure 48. Calculated Velocity-Time History for Miragrid 10T in SP Sand.

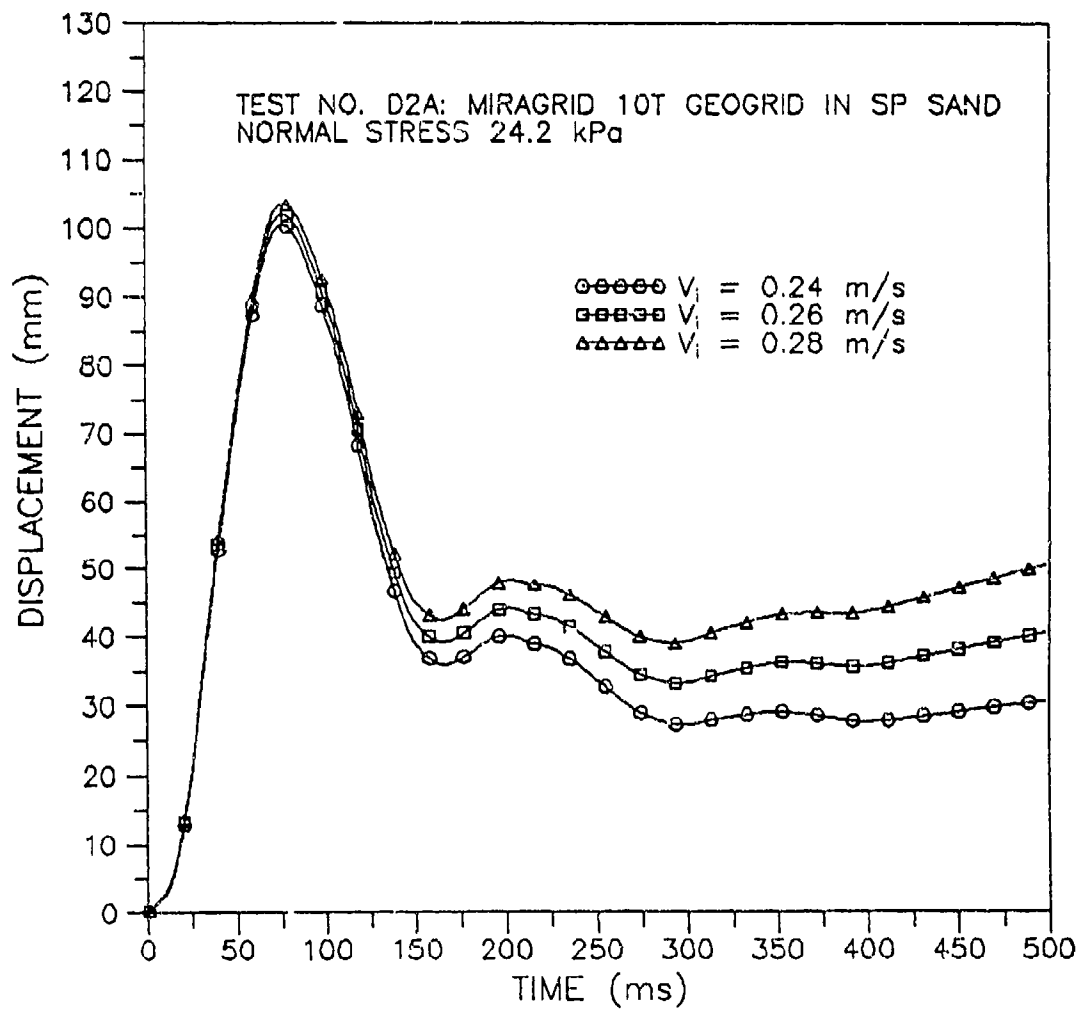


Figure 49. Effect of Initial Velocity on Displacement-Time History.

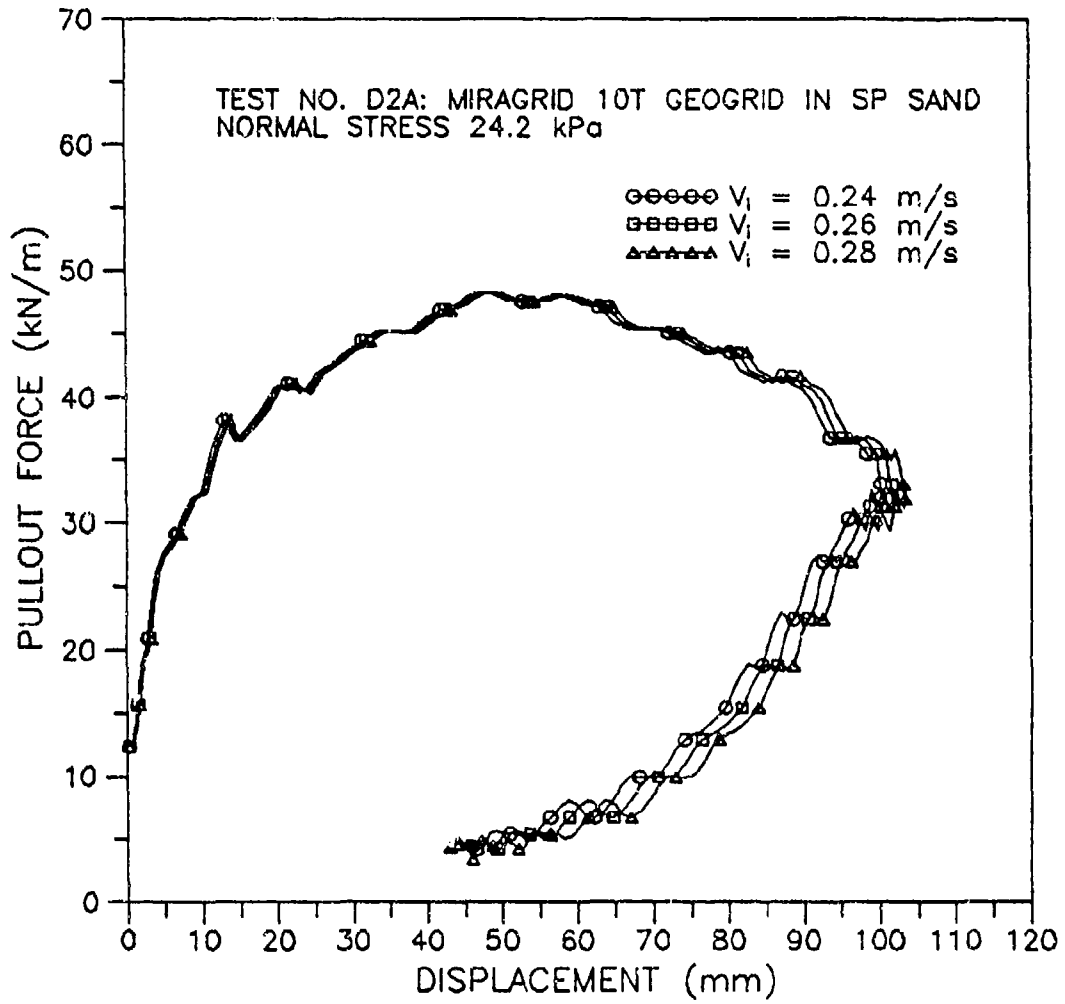


Figure 50. Effect of Initial Velocity on Calculated Pullout Response.

The developed interpretation method is summarized below:

- integration of acceleration signal to obtain velocity, this velocity is referred to as the calculated velocity;
- integration of the calculated velocity to obtain displacement, this displacement is referred to as the calculated displacement;
- check if the calculated displacement at the specimen clamp is equal to the measured one at the end of the test, if not, add an initial velocity, V_i , to the calculated velocity and repeat Step 2 until difference between the calculated and the measured displacement is less than an acceptable error; and
- use the calculated displacement and recorded impact pullout force traces to determine the pullout force-displacement curve.

The above procedures were used for interpreting all the impact pullout test results. The trapezoid rule was used for the numerical integration. Its accuracy was verified by comparing the numerical integration result with the closed-form solution for a given signal. The verification is presented in Volume 2, Appendix A of this report.

b. Comparison Between Impact and Static Pullout Resistance

Comparison is made between the impact and static pullout resistances for the three geogrids in the SP sand, as shown in Figure 51. For UX1500 and Miragrid 10T geogrids, the impact and static pullout resistance curves in the SP sand are almost identical for normal stresses from 0 to 71.1 kPa (10.3 psi). However, for Matrex 120 geogrid, the impact pullout resistance is higher than the static one. The relative increase is in the range of 0 to 15 percent. The high confining pressure results in a high relative increase. For the geogrids in SW-SM sand, impact and static pullout resistances at one normal stress are compared in Figure 52. The difference between the impact and static pullout resistance is insignificant.

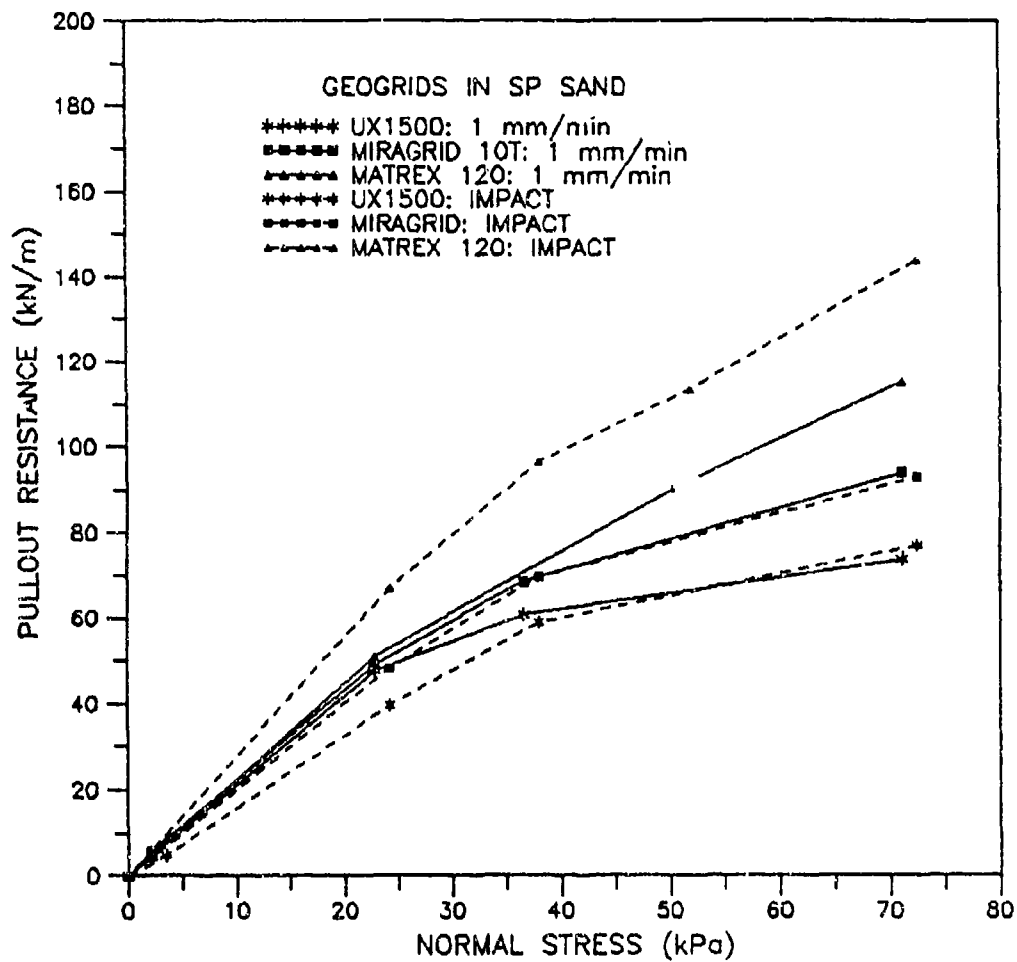


Figure 51. Comparison of Impact and Static Pullout Resistances in SP Sand.

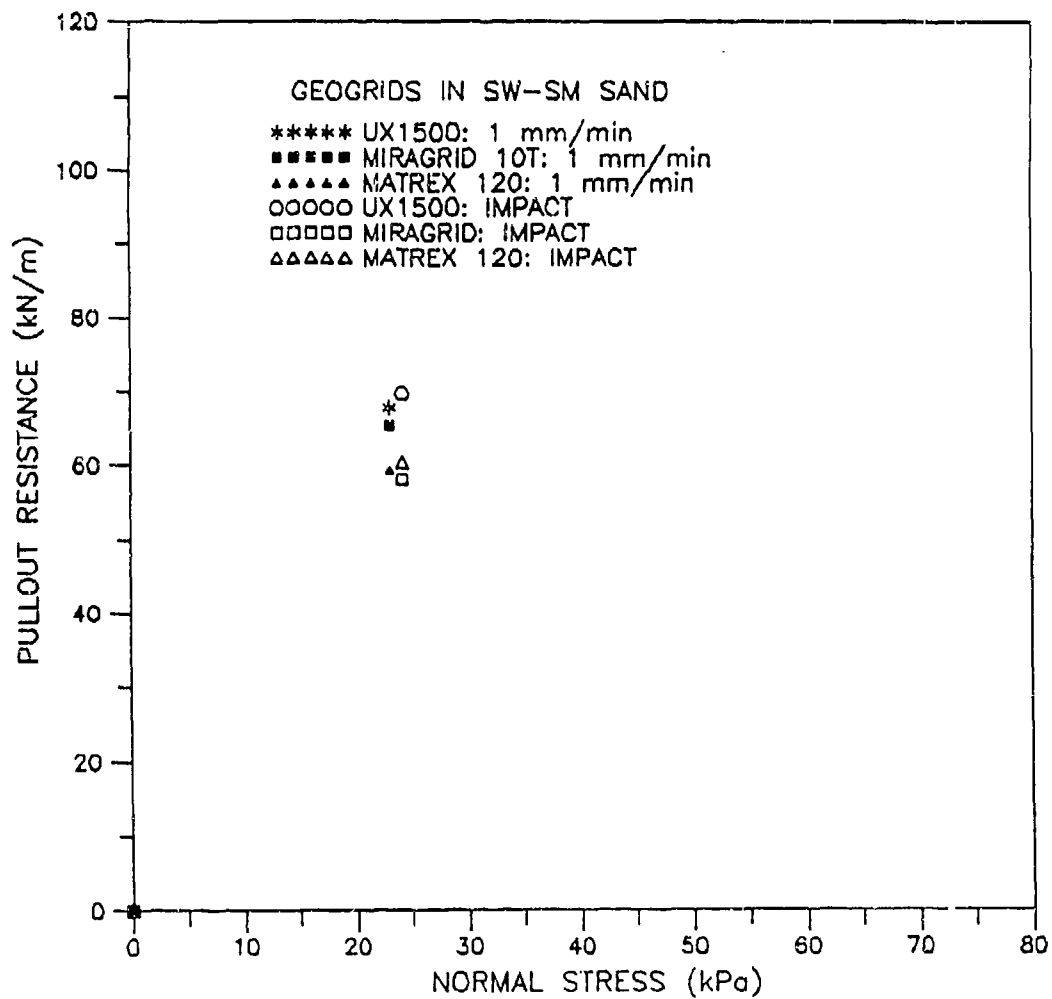


Figure 52. Comparison of Impact and Static Pullout Resistances in SW-SM Sand.

It has been shown that the static pullout resistance is limited by the static tensile strength. This static tensile strength may not be equal to the tensile strength from the wide-width test. In the impact pullout tests, the maximum impact pullout resistance is also believed to be limited by some dynamic tensile strength. To verify this, one dynamic pullout test was conducted on Matrex 120 geogrid at a normal stress of 138.0 kPa (20 psi). The measured peak pullout resistance was 295.4 kN/meters (1690 pound/inches) which is close to the dynamic tensile strength of 313.7 kN/meters (1790 pound/inches). Figure 53 shows the force-displacement curve for this test. It should be noted that the tested specimen was only two ribs wide to keep the maximum load within the load cell capacity. More impact pullout tests should be performed at very high confining pressures to understand fully the dynamic pullout behavior of reinforcements.

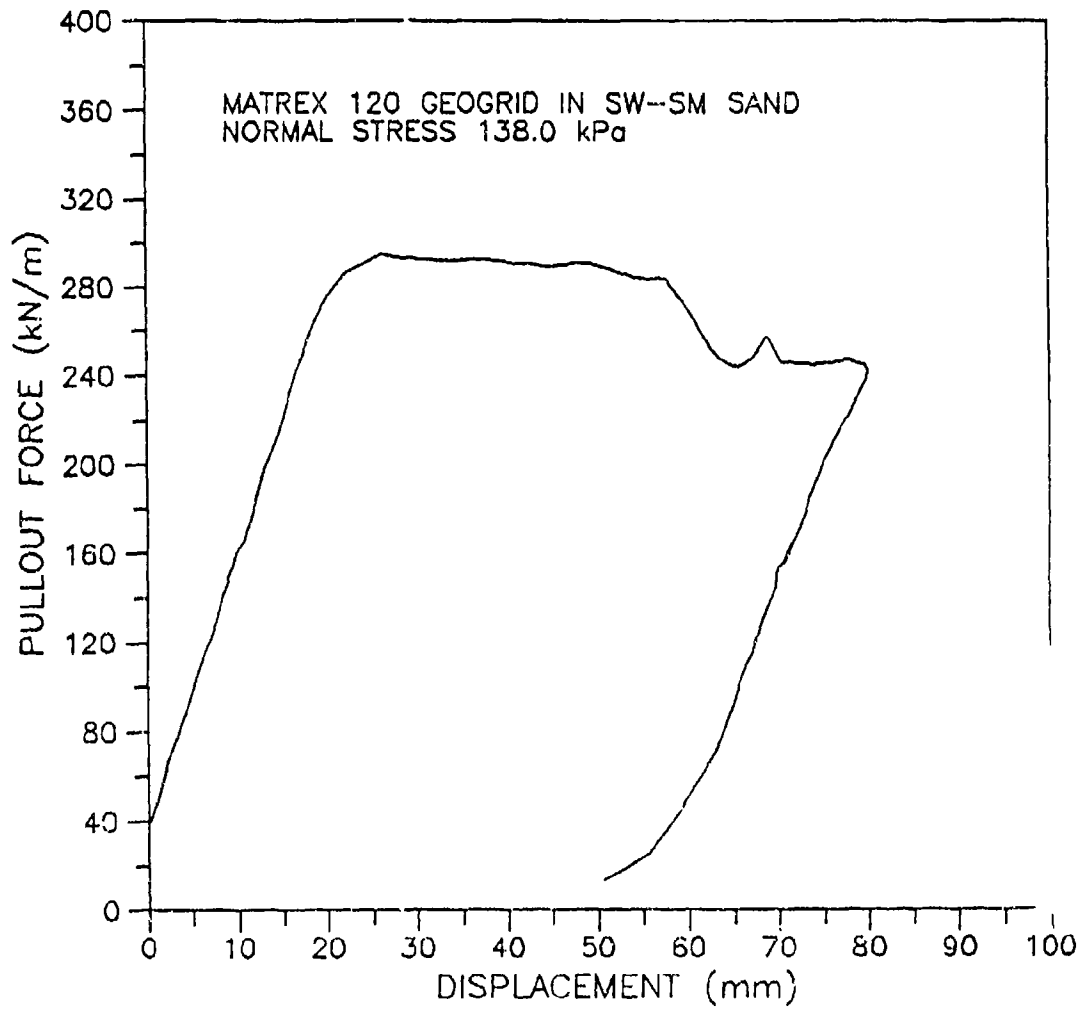


Figure 53. Impact Pullout Response of Matrex 120 Geogrid in SW-SM Sand at High Confining Pressure.

SECTION V

NUMERICAL MODELING AND PARAMETRIC STUDY RESULTS

A. GOALS AND ORGANIZATION

The goals of the numerical analysis task of this project are: (1) to develop a finite-element model for analysis of reinforced soil structures subjected to blast loading; (2) to conduct a parametric study of the influence of critical factors on the behavior of a reinforced soil wall subjected to blast loading; (3) to critically evaluate the finite element model and recommend ways to improve it. This section describes the work conducted to achieve these goals.

Section V is organized as follows:

- a description of the numerical model, including details of the finite element mesh, material properties, boundary conditions and loading is presented in Section V-B;
- details of the parametric study, including the test matrix, the data used for comparison, and the results of the study are presented in Section V-C; and
- conclusions of the study, a critical evaluation of the numerical model, and suggestions for further refinement of the model are presented in Section V-D.

B. DESCRIPTION OF THE NUMERICAL MODEL

The objectives of the parametric study require the use of more than one finite-element mesh, a range of material properties and the simulation of several different weapon sizes and locations. To simplify the description of the numerical model, a "standard" finite-element mesh, material properties and blast loading are described below. The numerical model was developed using these standard parameters. Modifications to the standard mesh, material properties and blast parameters are presented in Section V-C.

1. Background

The numerical model developed in this study is based on the use of the DYNA3D computer code (reference 71). DYNA3D is a nonlinear, explicit, three-dimensional finite-element code developed by LLNL for use in the analysis of dynamic solid and structural mechanics problems. A description of the DYNA3D code and the rationale for its use have been presented in Section II. While it is recognized that the DYNA3D code has many of the capabilities needed to model the response of reinforced soil systems to blast loading, there are shortcomings to the code which limit its accuracy. These are pointed out in the description of the numerical model and are discussed further in Section V-D.

2. Finite-Element Mesh

To develop a useful numerical model, a simple prototype that includes the main attributes of a reinforced soil structure should be modeled. For this study, a geogrid reinforced wall was chosen. The wall is 4.5 meters (14.8 feet) high and contains six layers of Tensar UX1600 geogrid, 4.5 meters (14.8 feet) long. Each layer of geogrid is attached to the center of a concrete facing panel 0.75 meter (2.46 feet) high and 0.15 meter (0.48 foot) thick. The prototype soil used for the wall and the foundation is a clean sand with a friction angle of 35 degrees.

The analysis of the response of such a structure to the detonation of a conventional weapon in the backfill behind the wall is a three-dimensional problem. The DYNA3D code is capable of, and indeed designed for, 3-D analysis; however, because of the complexity of a true 3-D analysis and the large amount of computer time needed for 3-D solutions, it was decided that a two-dimensional, plane-strain model should be developed first. This was accomplished by making the finite-element mesh one element thick and preventing any displacement in the horizontal direction parallel to the wall face.

The standard finite element mesh used in the parametric study is shown in Figure 54, along with the coordinate axis system used to describe the nodal coordinates. All the elements are six-sided, eight node continuum elements with a thickness in the y-direction of 100 mm (3.9 inches). The mesh was generated using the pre-processor code INGRID (Reference 72), which was also used to input all but a few portions of the DYNA3D input file. An example INGRID file and the

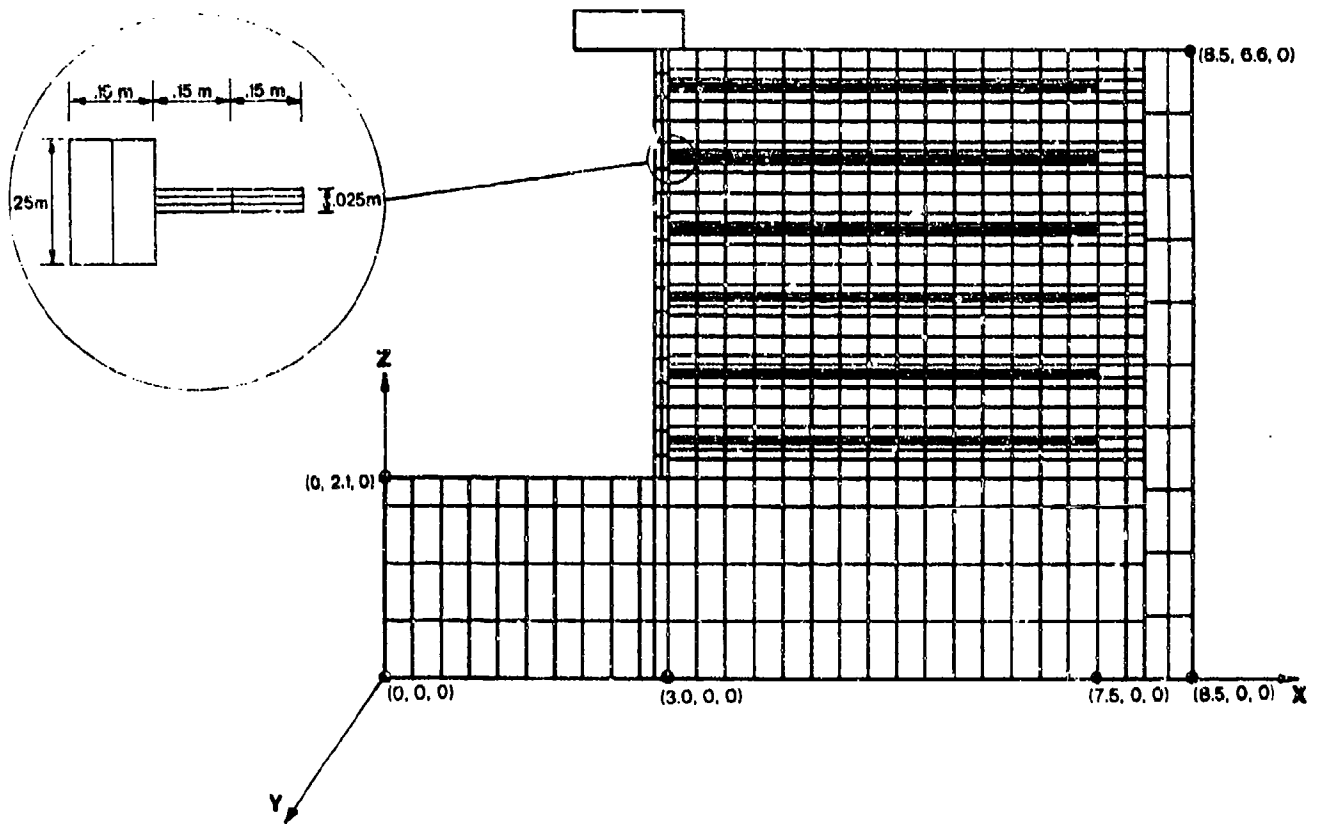


Figure 54. Standard Finite-Element Mesh.

DYNA3D input file it produces are shown in Volume 2, Appendix B. The mesh was generated in seven distinct parts, as illustrated in Figure 55, and the tolerancing feature of INGRID was used to eliminate redundant nodal points. The parts of the finite element mesh are:

- Part 1: Base (104 elements)
- Part 2: Soil in Reinforced Zone (540 elements)
- Part 3: Reinforcement (540 elements)
- Part 4: Soil Behind Reinforced Zone (68 elements)
- Part 5: Concrete Facing Panels (54 elements)
- Part 6: Right Side Constraint (20 elements)
- Part 7: Roof (1 element)

The dimensions of all elements are governed by P-wave velocity and the rise time of the shock wave propagating through the mesh. The transit time across an element should be approximately equal to or faster than the rise time of the loading. For this mesh and for soil properties used in the analyses, rise times less than 1 ms can be modeled.

Part 2 is divided into seven regions with the gaps between each region filled by reinforcement elements (Part 3). The reinforcement is modeled with three layers of elements because it was found that hourglassing, a numerical instability caused by the use of single-point Gaussian quadrature for element integration, occurs when only one or two layers are used. The elements of Part 5 are divided into six concrete facing panels. Each facing panel is independent of the others; sliding and/or separation across facing panels are permitted. This is accomplished by the use of a sliding interface between panels, as described below. Each panel is connected at mid-height to a layer of reinforcement. Part 6 is used to provide lateral support for the soil on the right hand side of the mesh, before the blast load is applied. Relative movement and/or separation are permitted between the soil elements in Part 4 and Part 6. Part 7 is used to model a roof bearing on the top facing panel. Relative movement and/or separation are permitted between the roof and the top facing panel.

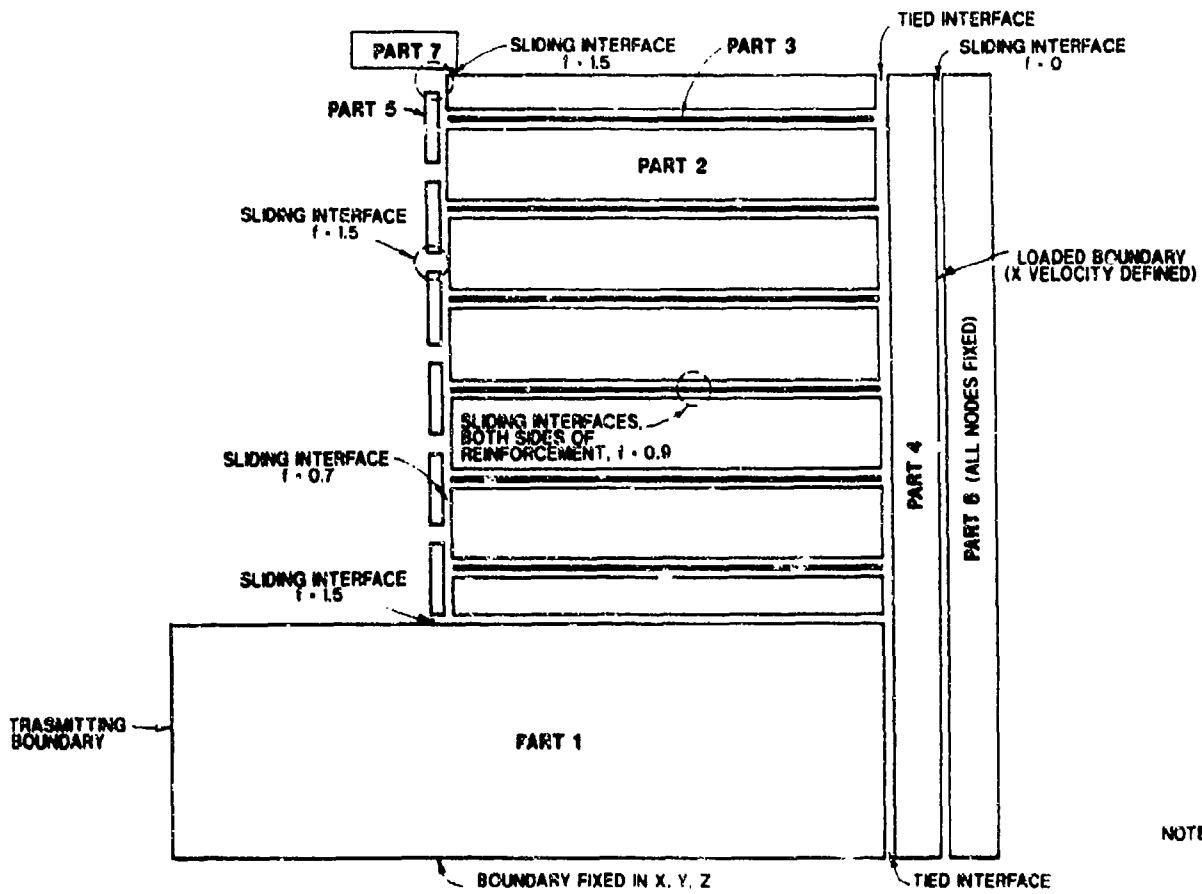


Figure 55. Standard Finite-Element Mesh Showing Boundary Conditions and Interfaces.

The boundary conditions used in the plane-strain analyses are shown in Figure 55. To achieve plane-strain conditions, all nodes are constrained in the Y-direction. The base of the mesh, except for the leftmost nodes at the $x = 0$ plane, is also constrained in the X- and Z-directions. A transmitting boundary is used at the left side of the soil base to minimize reflections. The nodes of the elements used to model the roof and the right hand restraint are fixed in all directions. All boundary conditions are generated by the INGRID code.

A feature of the DYNA3D code which is essential for the analysis of reinforced soil is the ability to model interfaces between parts. Two types of interfaces are used in this study: (1) tied; and (2) sliding with friction and separation. Tied interfaces, shown in Figure 55, are used to connect parts consisting of the same material and to connect the reinforcement to the facing. Neither sliding nor separation is permitted at tied interfaces. Therefore, the connection between the facing panels and the reinforcement cannot be broken. Sliding interfaces, shown in Figure 55, allow relative movement to occur along the interface and also allow gaps to open up between the material on either side of the interface. All sliding interfaces are frictional in nature. A static friction coefficient is defined for each interface and sliding occurs when the shear stress at the interface exceeds the normal stress multiplied by the friction coefficient. The capability of the program to define a lower dynamic friction coefficient was not used. The friction coefficients used for each interface are listed in Figure 55.

3. Material Properties

Three different material constitutive models were used. These are:

- Elastic
 - DYNA3D material Type 1 used for facing, right hand constraint and roof (Parts 5, 6, and 7)
- Kinematic/Isotropic Elastic - Plastic
 - DYNA3D material Type 3 used for reinforcement (Part 3)
- Extended Two-Invariant Geologic Cap Model
 - DYNA3D material Type 25 used for all soil elements (Parts 1, 2, and 4)

The material properties for each of the models are shown in Table 10.

TABLE 10. STANDARD MATERIAL PROPERTIES.

Material Type	Parameter	Symbol	Value
1	Young's Modulus	E	2.07×10^{10} Pa
1	Poisson's Ratio	V	0.25
1	Density	P	2720 kg/m^3
3	Young's Modulus	E	3.7×10^7 Pa
3	Poisson's Ratio	V	0.40
3	Yield Stress	σ_0	3.6×10^6 Pa
3	Tangent Modulus	E_T	3.7×10^5 Pa
3	Hardening Parameter	β	0
3	Density	ρ	1000 kg/m^3
25	Bulk Modulus	K	4.6×10^8 Pa
25	Initial Shear Modulus	G	2.758×10^8 Pa
25	Failure Envelope Parameter	α	8.0×10^3 Pa
25	Failure Envelope Linear Coefficient	θ	.263
25	Failure Envelope Exponential Coefficient	γ	0
25	Failure Envelope Exponent	β	9.719×10^{-8}
25	Cap Surface Axis Ratio	R	2.5
25	Hardening Law Exponent	D	$9.718 \times 10^{-8} \text{ Pa}^{-1}$
25	Hardening Law Coefficient	W	0.066
25	Hardening Law Parameter	χ_0	1.3×10^6 Pa
25	Kinematic Hardening Coefficient	\bar{C}	0
25	Kinematic Hardening Parameter	N	0
25	Tension Cutoff	T	-6.895×10^3 Pa
25	Density	ρ	2000 kg/m^3

The elastic properties used for the facing are approximately that of concrete with an unconfined compressive strength of 3,000 psi (2.04 MPa). This simple material model can not accurately predict the behavior of the facing panels. For example, panel cracking can not occur with an elastic material; however, the stresses generated in the elastic elements will indicate if cracking is likely, and more sophisticated methods of modeling the facing can easily be added at a later time.

The properties used with material type 3 to model the reinforcement are approximately those of Tensar UX1600 geogrid. The use of an elastic-plastic model allows the non-linear stress-strain behavior of geogrid to be approximated, along with the large strains that can be generated before failure.

The cap model parameters were taken from Katona [Reference 66] and describe a sand with a Mohr-Coulomb friction angle of approximately 35 degrees. A small cohesion of 8 kPa (1 psi) is required for numerical stability. Without this cohesion, the state of stress is always on the yield surface and continuous deformations occur under gravity loading.

4. Loading Conditions

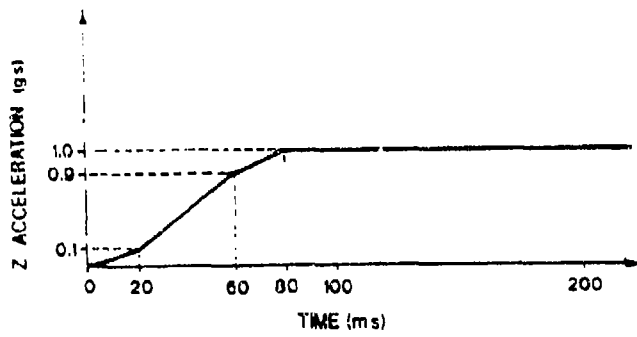
a. Gravity

The stability of a reinforced soil mass requires the presence of normal stress at the reinforcement-soil interface so that friction can be developed between the soil and the reinforcement. This leads to tensile stresses in the reinforcement and overall stability of the system. Under static conditions, the normal stress arises from the self-weight of the soil. Additional normal stress is generated by a blast wave as it propagates through the reinforced soil mass. For a nearby explosion of a conventional weapon, these additional normal stresses typically are several orders of magnitude greater than the gravity-induced normal stresses. Therefore, for analysis of transient behavior only, the exclusion of gravity stresses usually will not significantly alter the results. However, the displacements of the system produced by the blast loading will reduce the static stability of the system. Without the inclusion of gravity stresses in an analysis, the system can cease moving after the dissipation of the dynamic loading even if it comes to rest in a condition

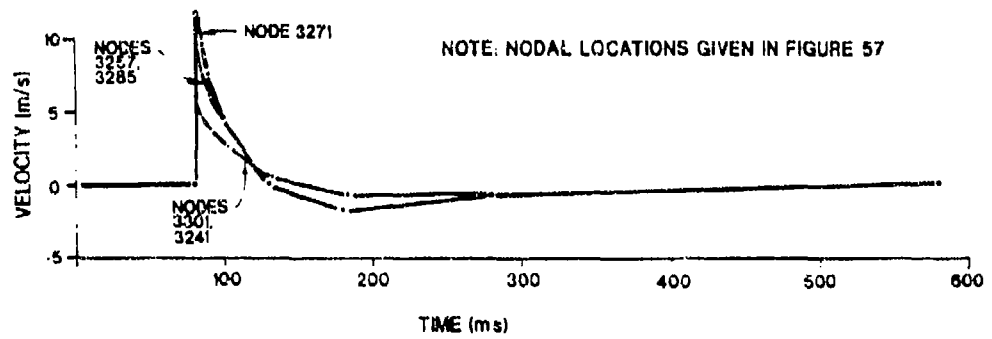
which is unstable under static conditions. To evaluate the stability of the deformed system, the inclusion of gravity is necessary. To accomplish this, each analysis begins with the initialization of gravity stresses by introducing an acceleration of 9.81 m/s^2 (32.2 feet/s^2) in the positive z-direction over an 80 ms time period as shown in Figure 56. The 1-g acceleration remains for the duration of the analysis. This loading time history was found by trial and error to minimize the time required to achieve the desired distribution of vertical stress throughout the system. Transient stresses from the gravity initialization still exist when the blast loading begins at 80 ms; however, their effect is dominated by the transient blast stresses. By the time the blast wave has passed, the gravity-induced stresses have stabilized.

b. Blast

The loading resulting from the detonation of a weapon in the backfill behind the reinforced soil mass is modeled by describing a velocity time history for the nodes along the right hand edge of Part 4 (the $x = 8.0$ plane). Equations V-5, V-6, V-15 and V-16 from the Air Force Design Manual (Reference 2) are used to calculate the horizontal component of soil velocity as a function of radial distance from the center of mass of a spherical explosive containing 89.4 kg (197 pounds) of TNT. The x and z coordinates of the center of the explosive are (11.056, 4.35). This location is 3 meters (10 feet) from the right hand edge of Part 4, 2.25 meters (7.38 feet) below the ground surface. The explosive is assumed to be fully coupled with the ground. The arrival time, peak velocity, rise time, and decay behavior are calculated for each node along the prescribed boundary. The velocity time histories for several selected nodes are shown in Figure 56. The time history of vertical velocity was not included in the modeling of the blast wave. It was felt that reflections from the rigid base of the finite element mesh caused by the vertical component of motion would introduce spurious motions in the system, especially near the facing. The exclusion of the vertical component of input velocity does not of course, preclude vertical motions or stresses in the system.



a) GRAVITY LOADING



b) INPUT FOR VELOCITY TIME HISTORIES OF SELECTED NODES

Figure 56. Input Time Histories.

5. Discussion

The "stick-slip" model used for the interface between soil and wall and between soil and reinforcement is a simplification of the actual behavior of such interfaces; shear displacement occurs even at very low shear stress as illustrated in Figure 35. At present, DYNA3D does not have the capability to model arbitrary shear stress-shear strain behavior; however, incorporation of a relatively simple constitutive model is a possible future refinement to the model.

The time step in the numerical analyses performed for this study is governed by the thickness of the reinforcement elements. This is because the transit time of a P-wave across the thickness of a reinforcement element is shorter than across any other type of element. A significant reduction in the solution time for an analysis could be accomplished by using an orthotropic material constitutive model for the reinforcement and assigning a very low stiffness in the vertical direction, thereby reducing the wave speed in that direction. Unfortunately, the only way to accomplish this using the DYNA3D code results in a linear elastic behavior in the longitudinal direction. This may be acceptable when modeling metal strip reinforcement; however, geosynthetics such as geogrid are highly non-linear. The reduction in accuracy of the material modeling is felt to be too great a price to pay for increased computational speed. A better method of improving computational speed may be to modify the code to allow frictional interfaces between shell and continuum elements so that the reinforcement can be modeled with shell elements. This would negate the necessity of using three layers of reinforcement elements for hourglass control and result in considerable reduction in solution time.

A mass-proportional damping term, α , is used in all analyses to minimize spurious high frequency vibrations. The permanent deformations of the system are, however, sensitive to the value of α . The selection of an appropriate value of α is complicated and involves testing beyond the scope of this project. Therefore, a relatively low value (10) was used in the parametric study and further work is recommended to investigate the selection and influence of this parameter.

C. PARAMETRIC STUDY

To aid in the evaluation of the numerical model described above and to determine the influence of several key parameters on the performance of a reinforced soil structure, a parametric study has been conducted. The study concentrates on the influence of the reinforcement (stiffness and length), the weapon (size and location), and the soil (stiffness and strength) on the behavior of the reinforced soil wall.

The description of the parametric study is presented as follows:

- description of the test matrix;
- basis for comparisons;
- behavior of the standard wall;
- effect of reinforcement stiffness;
- effect of reinforcement length;
- effect of roof panel;
- effect of weapon size;
- effect of weapon location;
- effect of soil/reinforcement friction coefficient;
- effort of soil stiffness;
- effect of soil strength;
- effect of gravity initialization; and
- summary of results.

1. Test Matrix

As discussed in Section V-B, a standard wall and loading environment were used for the development of the numerical model. In the parametric study, one aspect of this standard is varied in each analysis. The test matrix for the parametric study is presented in Table 11.

The analyses conducted are:

- PS1 Standard Analysis
- PS2 Stiffness of Reinforcement Decreased by Two Orders of Magnitude
- PS3 Stiffness of Reinforcement Increased by Two Orders of Magnitude
- PS4 Length of Reinforcement Reduced
- PS5 Standard Analysis Without Roof
- PS6 Standard Weapon Located 6.1 meters (20 feet) from Boundary
- PS7 Large Weapon [227 kg (500 pounds)] Located 3.05 meters (10 feet) from Boundary
- PS8 Large Weapon Located 6.1 meters (20 feet) from Boundary
- PS9 Large Weapon Located 12.2 meters (40 feet) from Boundary
- PS1B Standard Weapon Located at Full Depth of Wall
- PS1S Standard Analysis with Soil/Reinforcement Interface Friction Coefficient Reduced from 0.9 to 0.7
- PS1W Standard Analysis with Soil Stiffness Decreased by a Factor of 10

TABLE 11. TEST MATRIX FOR PARAMETRIC STUDY.

Analysis	Gravity Initialization	Reinforcement				Weapon			Roof	Soil/Reinf Fric Coeff	Soil ϕ	Soil ^a Stiffness	
		Strength		Length		Size	Location						
		U=1600 ÷ 100	U=1600 x 100	4.5 m	3.3 m		mid-height	base					
PS1 ^b	•	•		•		•		•		•	•	34°	H
PS2	•		•		•			•		•		34°	H
PS3	•			•		•				•		34°	H
PS4	•	•				•	•			•		34°	H
PS5	•	•		•		•				•		34°	H
PS6	•	•		•		•				•		34°	H
PS7	•	•		•		•		•		•		34°	H
PS8	•	•		•		•		•		•		34°	H
PS9	•	•		•		•		•		•		34°	H
PS1B	•	•		•		•				•	•	34°	H
PS1S	•	•		•		•				•		34°	H
PS1W	•	•		•		•				•		34°	L
PIP1H	•	•		•		•				•		40°	H
PS1N	•	•		•		•				•		34°	H

• Standard Analysis

^b H: $K = 4.6 \times 10^6$ Pa; $G = 2.758 \times 10^8$ Pa

L: $K = 4.6 \times 10^7$ Pa; $G = 2.758 \times 10^7$ Pa

- P1PHI Standard Analysis with Soil Strength (Friction Angle) Increased from 35 degrees to 40 degrees
- PS1N Standard Analysis Without Gravity Initialization

2. Basis for Comparisons

The computer code TAURUS (Reference 73) was used for post-processing of the data. The primary information obtained from each analysis was: (1) the final deformed shape of the mesh; (2) the maximum displacements, velocities, and accelerations of the top and bottom of each facing panel; (3) the peak horizontal stresses in the soil elements adjacent to facing panel No. 3; (4) the peak compressive and tensile stresses in the reinforcement elements closest to each facing panel; and (5) the peak horizontal stresses in the row of soil elements between the middle two facing panels. Of the data collected, the maximum displacements of the facing panels are considered the most important. The other data are used to help understand the effects of each of the parameters.

For each analysis, data are collected by the use of two different types of data collection, herein referred to as data dumps. The first is a state plot data dump in which information on all nodes and elements is recorded at specific time intervals. The data from a state plot data dump are used to plot the deformed shape of the mesh, as well as contours of stress and strain throughout the mesh. Because of the large disk storage requirements for state plot data dumps, they are made every 40 ms during gravity initialization, every 10 ms during the first 30 ms of blast loading, and every 50 ms thereafter.

The second type of data dump is a time history dump. Information on selected nodes and elements is dumped at frequent intervals so that time history plots of stress, strain, displacement, velocity and acceleration can be produced. Time history data dumps are made at 2.0 ms intervals during an analysis except for the first 30 ms of blast loading when the interval is 0.2 ms. The nodes and elements selected for time history data dumps are shown in Figure 57.

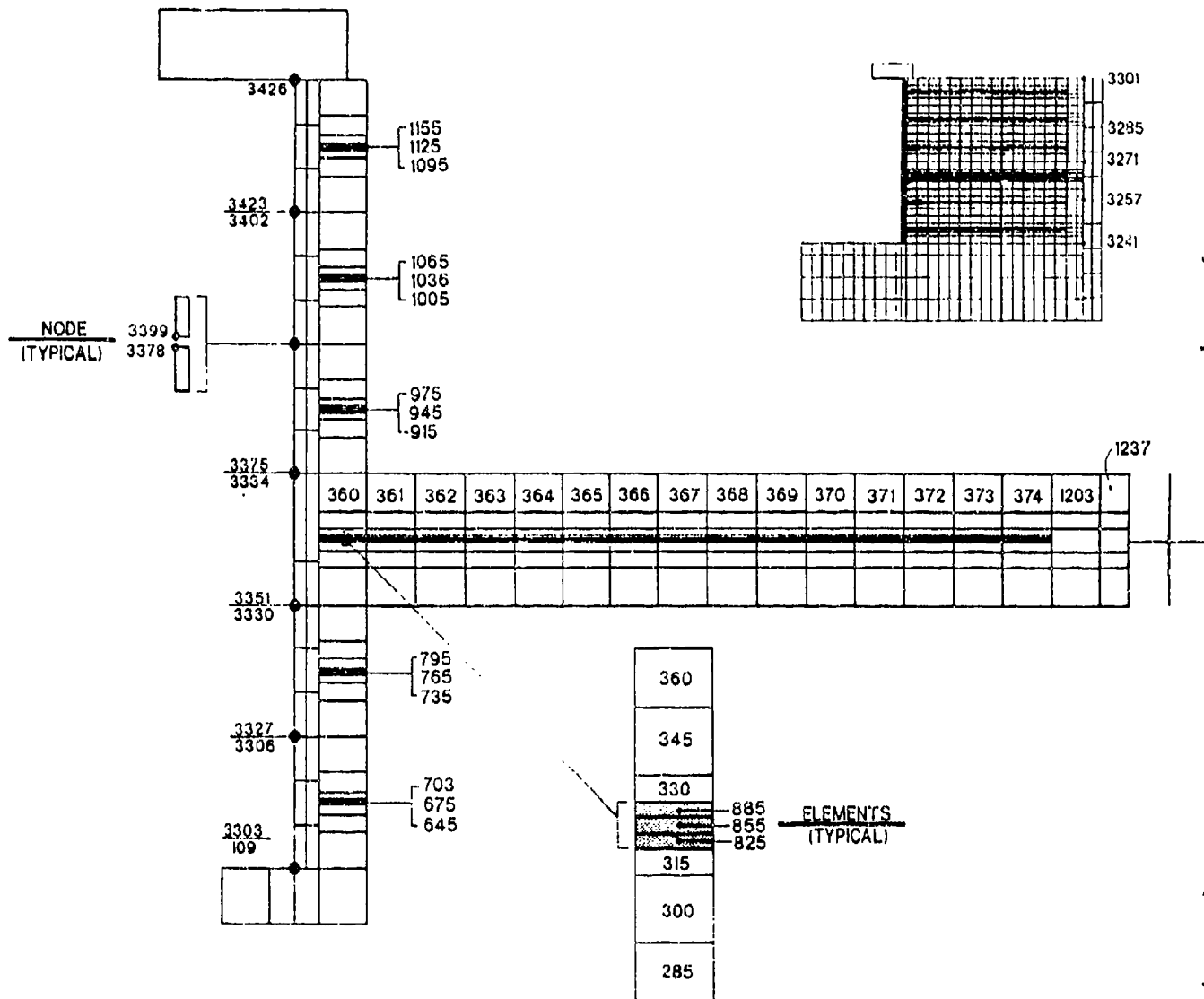


Figure 57. Nodes and Elements Selected for Time History Data Jumps.

3. Behavior of the Standard Wall

The results of the parametric study are described in the following manner. First, the behavior of the standard wall, analysis PSI, is discussed. The deformed shape of the mesh is shown, as well as the peak displacement, velocity, and acceleration of each facing panel, the peak stresses in the reinforcement at the interface with the facing panels, and the peak stresses in selected soil elements. Then, the effects of each parameter, i.e., reinforcement stiffness, reinforcement length, charge size and charge location are presented.

The results of analysis PSI show:

- The standard wall shown in Figure 54 is able to sustain the explosive loading without collapsing. The deformed shape of the finite-element mesh 330 ms after the beginning of the blast loading is shown in Figure 58. At this time the facing panels have negligible horizontal velocity and the system appears stable. (The deformed mesh shapes for all other analyses are presented in Volume 2, Appendix B.)
- The maximum horizontal displacement of the facing is 40.39 cm (15.9 inches) and the average displacement is 24.84 cm (9.78 inch). The maximum horizontal displacements of the top and bottom of each facing element are presented in Table 12.
- The peak velocity of the facing is 6.14 m/s (20.14 feet/sec). The peak velocities of the upper and lower outward corners of each facing panel are presented in Table 13. Figure 59 shows time histories of velocity for the top of facing No. 2 and the top of facing No. 4 (nodes 3330 and 3378, respectively).
- The peak acceleration of the facing is 300 g/s. The peak accelerations of the upper and lower outward corners of each facing panel are presented in Table 14. Figure 60 shows time histories of acceleration for the top of facing panel No. 2 and the top of facing panel No. 4 (nodes 3330 and 3378, respectively).

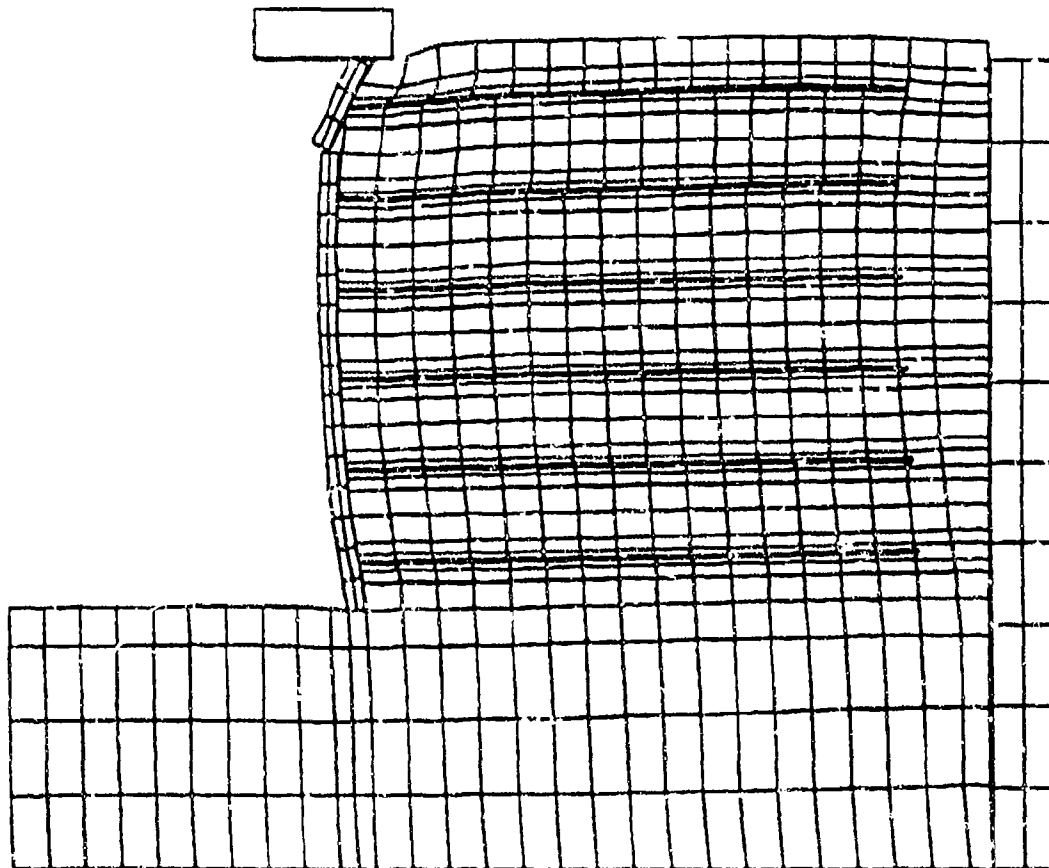


Figure 58. Deformed Shape of Wall at
 $t = 410 \text{ ms}$ - Analysis PS1.

Table 12

TABLE 12: MAXIMUM DISPLACEMENT OF FACING PANELS.

Facing Panel	Node No. (Short)	Node No. (Long)	Maximum Displacement (cm)													PSIM Low Soil Stiffness	PIPHI $\phi = 40^\circ$
			PS1 Standard	PS2 Weak	PS3 Strong	PS4 Short	PS5 No Roof	PS6 197# $\phi 20'$	PS7 500# $\phi 10'$	PS8 500# $\phi 20'$	PS9 500# $\phi 10'$	PS1B Expl. ϕ Base	PS1K No Gravity	PS1S $f = 0.7$			
6	2946	3426	3.00	3.24	0.49	3.37	41.79	0.06	failed	0.06	0.05	0.56	1.65	0.65	2.83	0.05	
	2943	3423	40.39	46.59	37.02	40.81	44.19	12.04	failed	38.61	10.52	23.03	43.16	29.16	45.65	38.57	
5	2922	3402	29.62	42.39	27.92	29.59	46.31	11.40	102.20	32.71	9.41	21.40	36.40	29.40	34.41	26.51	
	2919	3399	32.11	45.17	25.74	32.27	48.83	10.87	83.67	32.45	9.23	27.14	34.79	34.79	41.95	27.04	
4	2898	3378	31.93	45.23	25.71	32.11	48.93	10.96	84.33	32.48	9.23	26.82	33.56	33.56	41.34	26.96	
	2895	3375	30.72	42.50	23.66	30.46	45.05	10.28	81.27	29.85	8.20	28.56	30.80	32.80	40.74	26.36	
3	2874	3354	30.65	42.43	23.74	30.40	44.35	10.19	80.33	29.63	6.48	28.49	30.75	32.75	40.53	26.25	
	2871	3351	26.52	39.63	21.05	25.37	40.04	8.74	71.29	26.94	7.59	26.51	26.64	28.64	34.61	25.2	
2	2850	3330	26.57	39.36	21.07	26.40	41.03	8.74	70.47	26.93	7.81	26.58	26.60	28.60	34.25	23.47	
	2847	3327	19.79	33.82	17.52	19.53	26.75	6.98	53.05	24.36	6.05	19.74	19.87	22.87	25.35	18.69	
1	2826	3306	19.97	32.89	17.52	19.71	29.86	7.17	58.26	24.48	6.50	20.11	20.10	20.10	25.37	18.77	
	2823	3303	6.81	5.42	7.39	6.92	6.73	4.41	15.36	12.79	3.83	10.26	6.96	6.96	8.12	6.18	
Soil	109	109	6.85	5.43	7.15	6.91	6.75	4.44	15.56	12.85	4.01	10.29	6.95	6.95	8.15	6.18	
Average*			24.84	34.89	20.74	24.83	38.65	8.49	70.02**	25.96	7.24	21.61	25.44	25.44	31.26	21.85	

* panel displacement only

** excluding panel No. 6

Table 13

TABLE 13: MAXIMUM VELOCITY OF FACING PANELS.

Facing Panel	Node No. (Short)	Node No. (Long)	Maximum Velocity (m/s)													PSIM low Soil Stiffness	PIPHI $\phi = 40^\circ$
			PS1 Standard	PS2 Weak	PS3 Strong	PS4 Short	PS5 No Roof	PS6 197# Ø20'	PS7 500# Ø10'	PS8 500# Ø20'	PS9 500# Ø40'	PSIB Expl. ØBase	PSIN No Gravity	PSIS $t = 0.7$			
6	2946	3426	0.55	1.00	0.28	0.71	3.46	0.05	110.00	0.03	3.18	0.40	0.34	7.65	7.77	0.03	
	2943	3423	6.05	4.50	5.04	6.53	4.92	1.94	90.20	3.63	1.25	2.89	6.13	6.09	6.66	6.25	
5	2922	3402	6.14	4.31	4.99	6.68	4.58	1.84	16.50	3.49	1.16	2.95	6.33	6.09	6.93	5.90	
	2919	3399	5.66	4.45	5.53	5.72	5.65	2.00	13.40	3.66	1.16	4.18	5.67	5.73	6.43	6.10	
4	2898	3378	5.67	4.47	5.49	5.72	5.17	2.02	13.60	3.69	1.16	4.20	5.69	5.74	6.46	6.14	
	2895	3375	5.64	4.22	5.30	5.65	5.53	1.76	13.70	3.62	1.01	4.82	5.56	5.74	6.09	6.19	
3	2874	3354	5.44	4.23	5.36	5.48	5.42	1.78	13.60	3.64	1.02	4.81	5.58	5.57	6.09	5.96	
	2871	3351	5.21	4.25	5.16	5.18	5.15	1.71	13.40	3.40	0.89	5.36	5.27	5.52	6.02	5.59	
2	2850	3330	5.44	4.22	5.11	5.35	5.47	1.72	13.80	3.40	0.89	5.33	5.38	5.42	6.03	5.69	
	2847	3327	4.76	4.12	4.64	4.79	5.07	1.61	12.80	3.46	0.82	5.60	4.59	5.05	5.89	5.25	
1 Bottom	2826	3306	4.76	4.11	4.69	4.76	5.09	1.62	13.40	3.46	0.85	5.65	4.58	5.05	5.90	5.22	
	2823	3303	2.11	1.57	2.05	2.14	2.07	0.82	5.66	1.90	0.42	4.24	2.02	2.03	3.25	1.95	
Soil	109	109	2.12	1.55	2.09	2.14	2.07	0.82	5.75	1.91	0.44	4.28	2.04	2.06	3.25	1.98	
Average*			4.79	3.79	4.47	4.89	4.80	1.57	27.50	3.11	1.15	4.20	4.76	5.47	5.71	5.62	

* panel velocity only

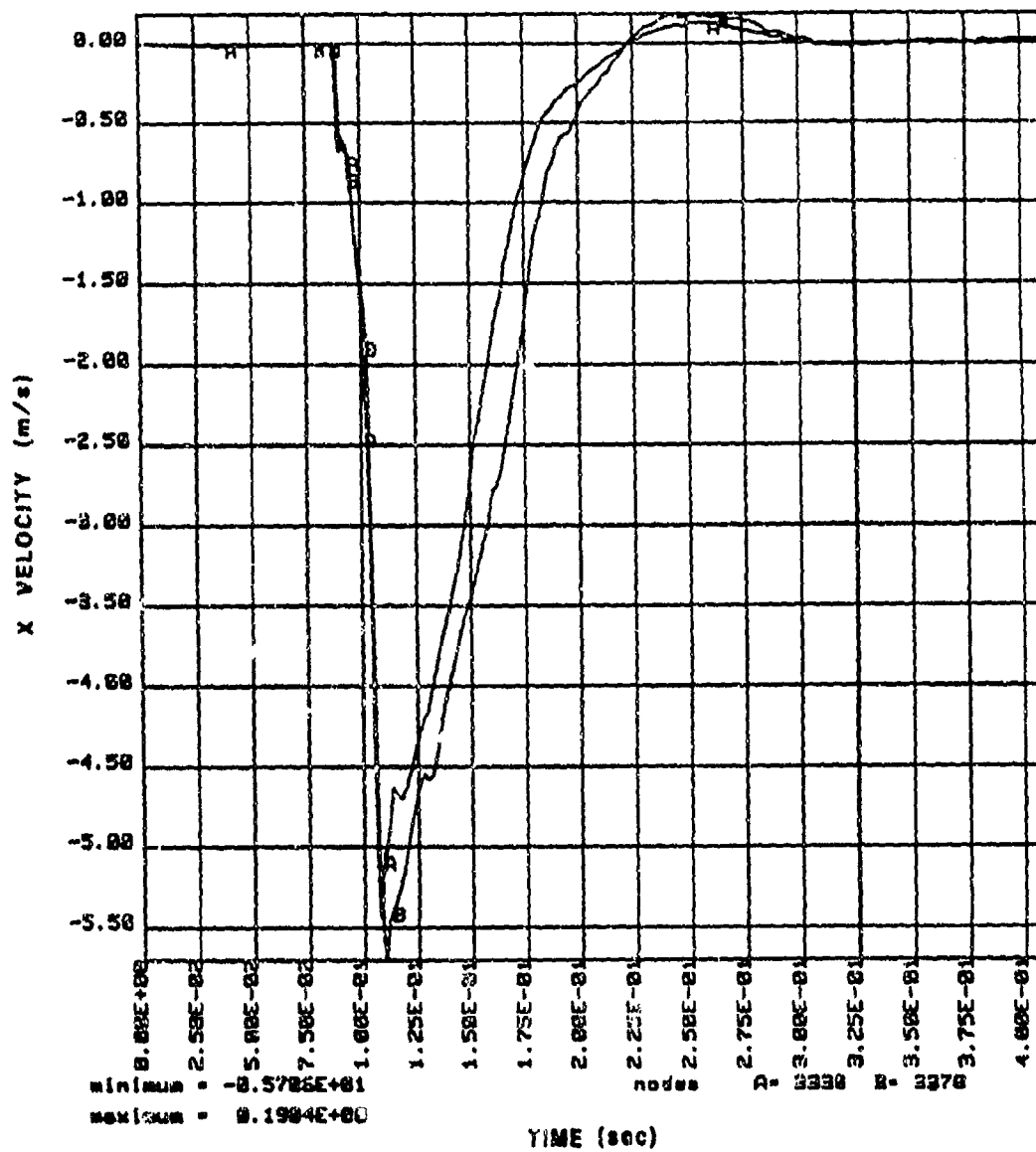


Figure 59. Time Histories of Velocity for Nodes 3330 and 3378 - Analysis PS1.

TABLE 14. MAXIMUM ACCELERATION OF FACING PANELS.

Facing Panel	Node No. (Short)	Node No. (Long)	Maximum Acceleration (g)														
			PS1 Standard	PS2 Weak	PS3 Strong	PS4 Short	PS5 No Roof	PS6 1/2# @20'	PS7 3/4# @10'	PS8 1/2# @20'	PS9 500# @40'	PS10 Expt. Base	PS11 Gravity	PS12 1/2# @10'	PS13 1/2# @10'	PS14 1/2# @10'	PS15 1/2# @10'
6	2946	3426	45	430	263	72	56	63	-83,760	34	49	57	41	61	563	92	
	2943	3423	237	212	-203	-140	-273	93	117,800	137	95	-106	89	-289	252	-274	
5	2922	3402	-300	-114	-125	-161	-139	108	-557	97	-86	-112	76	-266	150	-259	
	2919	3399	-159	-135	181	-112	-202	125	-535	123	-171	106	93	214	163	-169	
4	2898	3378	-183	-93	-177	-98	-147	-107	476	90	87	-74	75	-184	125	168	
	2895	3375	185	-106	-218	+120	-249	98	-486	-100	-123	121	92	173	-156	156	
3	2874	3354	137	110	-234	-92	-194	-80	-503	104	-127	-144	-90	145	95	-108	
	2871	3351	88	70	-176	86	95	63	450	87	-73	81	82	102	93	-100	
2	2859	3330	87	-71	-150	-98	-89	-70	-451	71	-74	-83	-92	-111	-70	-108	
	2847	3327	94	-45	-153	147	82	-90	-349	80	-88	101	90	117	89	97	
1	2826	3306	-110	-48	267	-131	-84	104	355	94	101	108	65	113	70	215	
	2823	3303	-39	17	270	111	37	73	180	28	28	160	37	76	77	134	
Sum	109	109	-32	-25	-62	-38	-32	24	-188	25	-54	-87	29	33	-34	34	
Average			139	121	201	115	137	85	435	91	92	104	79	156	147	157	

* absolute value, panel acceleration only

† excluding panel No. 6

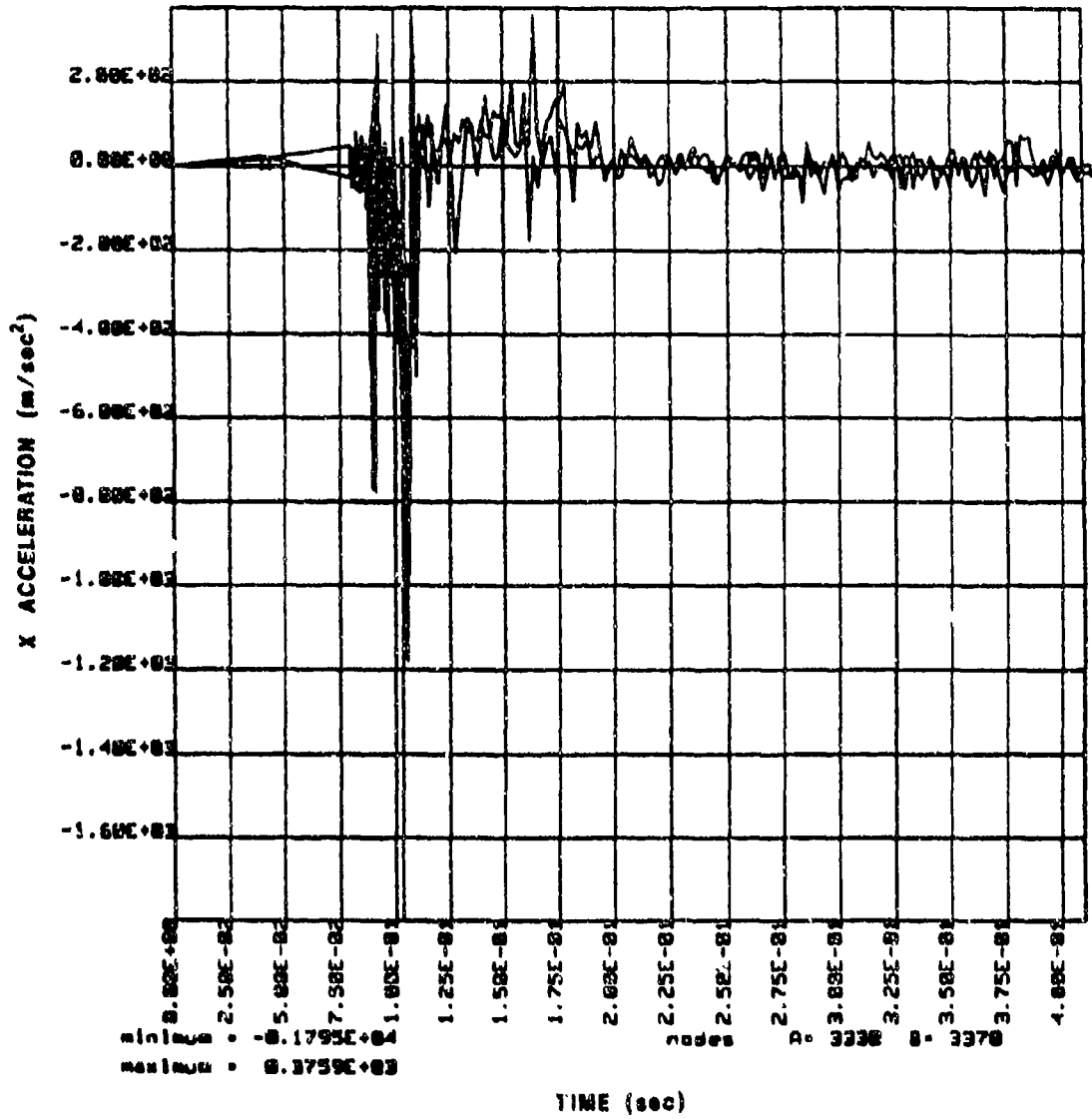


Figure 60. Time Histories of Acceleration for Nodes 3330 and 3378 - Analysis PS1.

- The average peak horizontal stress acting on panel No. 3 is 653 kPa (94.7 psi), as shown in Table 15. This stress causes an approximate peak force of 473 kN per meter of wall length (16.2 tons/feet) on the panel.
- The peak axial tensile and compressive stresses in the reinforcement elements attached to panel No. 3 are 4.68 MPa (244 psi) and 277 kPa (40 psi), respectively. The peak stresses in the other layers of reinforcement are tabulated in Table 16.
- The peak value of σ_v in the row of soil elements from 360 to 1278 varies from 7.58 MPa (1,100 psi) at the loaded boundary (element 1278) to 979 kPa (142 psi) at element No. 360 adjacent to facing panel No. 3. The decay in the peak amplitude of the compression wave as it travels through the soil is shown in Table 17.

The influence of the top and bottom interfaces with the roof and soil base, respectively, are clearly shown, both in Figure 57 and in the recorded displacements of the top and bottom facing panels. Although sliding between the roof and the upper facing panel does occur, the roof clearly inhibits the movement of the panel and causes a significant rotation to occur. The bottom facing panel also rotates, although not as much as the top panel. This difference is apparently due to the outward displacement of the soil base, resulting in very little slippage between the bottom panel and the soil base, but considerable displacement of the panel. The displacement of the other four panels is mainly translational. Significant rotation is restricted to panel No. 2. The average and maximum displacements of the wall, 24.92 and 40.39 cm (9.8 and 15.9 inches), respectively, range from 5.5 to 9.0 percent of the wall height. This is approximately an order of magnitude greater than typical static displacement from gravity loading, but is well within tolerable limits for stability.

The weighted average peak horizontal stress on facing panel No. 3 shown in Table 15 is obtained by weighing the maximum horizontal stress for each of the six elements in contact with the facing panel by that element's cross-sectional area. The time difference between peak horizontal stress in each of these elements varies by less than 1 ms; therefore, the error involved in directly adding peak stresses is considered to be a small overestimate.

TABLE 15. PEAK HORIZONTAL STRESSES IN ELEMENTS ADJACENT TO FACING PANEL NO. 3.

Element (Short)	Element (Long)	Peak Stress (Pa)													
		PS1 Standard	PS2 Weak	PS3 Strong	PS4 Short	PS5 No Roof	PS6 197# Ø20"	PS7 500# Ø10"	PS8 500# Ø20"	PS9 500# Ø40"	PS1B Expl. ØBase	PS1M No Gravity	PS1S f = 0.7	PS1W Low Soil Stiffness	PIP1H φ = 40"
276	360	6.85E+05	5.69E+05	4.59E+05	6.85E+05	6.93E+05	2.26E+05	3.45E+06	2.41E+05	2.25E+05	2.09E+05	6.92E+05	7.23E+05	4.79E+05	8.09E+05
285	345	6.73E+05	4.58E+05	2.78E+05	7.09E+05	7.07E+05	9.24E+04	3.45E+06	1.85E+05	7.13E+04	2.18E+05	7.07E+05	7.14E+05	4.99E+05	8.32E+05
254	330	7.20E+05	4.71E+05	4.12E+05	7.23E+05	7.11E+05	3.12E+05	3.50E+06	3.58E+05	3.05E+05	3.98E+05	3.72E+05	7.26E+05	5.40E+05	8.56E+05
243	315	6.70E+05	4.67E+05	6.56E+05	4.11E+05	6.52E+05	3.83E+05	3.44E+06	4.45E+05	3.71E+05	4.72E+05	6.52E+05	7.18E+05	4.66E+05	8.04E+05
232	300	4.02E+05	4.87E+05	6.16E+05	6.52E+05	3.90E+05	5.95E+04	2.96E+06	1.43E+05	5.45E+04	3.71E+05	6.51E+05	6.04E+05	5.06E+05	5.02E+05
221	265	6.81E+05	3.50E+05	5.41E+05	6.26E+05	6.67E+05	3.31E+05	3.28E+06	4.80E+05	3.11E+05	4.80E+05	5.94E+05	6.55E+05	5.02E+05	8.70E+05
Weighted Average		6.53E+05	4.71E+05	4.97E+05	6.50E+05	6.55E+05	2.35E+05	3.38E+06	3.16E+05	2.24E+05	3.48E+05	6.41E+05	6.85E+05	4.96E+05	7.92E+05

TABLE 16. PEAK REINFORCEMENT STRESSES.

Reel Layer	Elem No. (Short)	Elem No. (Long)	PS1 Standard	PS2 Weak	PS3 Strong	PS4 Short	PSS No. 301	PSS 1977 @ 20'	PSS 50CF @ 10'	PSS 50CF @ 20'	PSS 50CF @ 40'	PSB Expt. @ 40'	PSIM No Gravity	PSIS f = 0.7	PSIW Low Soil Stiffness	PIPR $\phi = 40^\circ$
6	859	1155	-1.65e+06	-1.97e+04	-5.95e+06	-1.54e+06	-5.33e+05	-1.48e+06	4.17e+06	-2.27e+06	9.98e+05	-2.04e+06	-1.44e+06	-1.79e+06	-1.65e+06	-2.14e+06
	837	1175	-1.34e+06	-2.14e+05	-5.02e+06	-1.31e+06	-5.50e+05	-5.16e+05	3.90e+06	-1.27e+06	5.76e+05	-1.23e+06	-1.11e+06	-1.25e+06	-1.05e+06	-1.30e+06
	815	1085	-1.20e+06	-2.06e+05	-4.64e+06	-1.14e+06	-2.57e+05	-3.97e+05	3.57e+06	-8.44e+05	2.70e+05	-2.37e+05	-8.11e+05	-1.14e+06	-8.18e+05	-1.18e+06
	AVERAGE															
5	793	1065	4.93e+05	-9.09e+03	4.43e+06	-6.55e+05	-9.07e+05	5.50e+04	-2.40e+06	-1.29e+05	4.80e+04	2.11e+05	3.95e+05	-5.73e+05	-6.17e+05	-5.29e+05
	771	1035	3.87e+05	-1.06e+04	-3.35e+06	-5.91e+05	-8.35e+05	6.61e+04	2.42e+06	-7.66e+04	4.55e+04	1.11e+05	-2.63e+05	-4.84e+05	-5.71e+05	-4.73e+05
	749	1025	2.85e+05	-2.00e+04	-4.37e+06	-5.47e+05	-8.93e+04	2.29e+06	-5.70e+04	5.87e+04	5.87e+04	8.91e+04	-1.76e+05	-4.13e+05	-5.31e+05	-3.73e+05
	AVERAGE															
4	727	975	4.77e+05	-1.65e+04	4.96e+06	4.04e+06	7.80e+05	9.75e+03	-2.80e+06	-1.19e+05	1.03e+04	1.51e+05	2.79e+05	-4.90e+05	-4.22e+05	-4.05e+05
	705	945	4.84e+05	-1.19e+04	4.04e+06	3.86e+05	7.95e+05	-1.39e+03	-2.82e+06	-1.09e+05	0.00	-1.07e+05	-5.53e+05	-5.25e+05	-4.79e+05	-3.98e+05
	683	915	4.72e+05	-1.82e+04	4.19e+06	-3.87e+05	8.36e+05	3.24e+03	-2.55e+06	-8.17e+04	2.11e+03	6.72e+04	-2.50e+05	-4.95e+05	-4.45e+05	-4.04e+05
	AVERAGE															
3	661	885	2.91e+05	-1.55e+04	4.40e+06	3.93e+05	7.0e+05	4.73e+03	-2.80e+06	-1.83e+05	4.14e+03	1.66e+05	2.53e+05	-5.19e+05	-4.52e+05	-4.04e+05
	639	855	2.66e+05	-1.63e+04	4.71e+06	2.75e+05	3.95e+05	1.12e+04	-2.47e+06	-6.74e+04	-1.52e+04	1.84e+05	-3.31e+05	-2.47e+05	-3.81e+05	-3.91e+05
	617	825	2.74e+05	-2.06e+04	4.30e+06	2.78e+05	3.85e+05	-1.82e+04	-2.47e+06	-6.24e+04	9.22e+03	4.00e+05	-2.73e+05	-2.76e+05	-4.21e+05	-3.75e+05
	AVERAGE															
2	595	795	2.82e+05	-3.63e+04	4.02e+06	2.35e+05	2.77e+05	-6.22e+04	-2.26e+06	-1.06e+05	6.85e+04	3.31e+05	2.47e+05	-3.63e+05	-2.96e+05	-4.47e+05
	573	765	3.00e+05	-3.15e+04	3.29e+06	2.00e+05	2.93e+05	-6.22e+04	-1.12e+05	6.80e+04	6.80e+04	3.27e+05	1.82e+05	-3.21e+05	-3.27e+05	-4.35e+05
	551	735	2.95e+05	-3.47e+04	4.35e+06	2.25e+05	5.58e+05	7.45e+04	-2.15e+06	-1.16e+05	9.09e+04	-3.38e+05	-1.85e+05	-2.93e+05	-3.52e+05	-3.88e+05
	AVERAGE															
1	529	705	3.62e+05	-2.74e+04	4.64e+06	4.53e+05	3.75e+05	-8.26e+04	-1.63e+06	-2.19e+05	-1.22e+05	5.88e+05	3.85e+05	-4.81e+05	-3.35e+05	-4.09e+05
	507	675	4.58e+05	-2.06e+04	4.48e+06	5.56e+05	5.03e+05	2.35e+04	-1.63e+06	-5.35e+05	-1.05e+05	6.13e+05	-4.34e+05	-6.19e+05	-4.76e+05	-5.27e+05
	485	645	5.52e+05	-1.75e+04	4.92e+06	6.23e+05	1.38e+06	-9.05e+04	-1.66e+06	-8.95e+05	-6.72e+05	-5.93e+05	-5.66e+05	-8.78e+05	-5.63e+05	-7.35e+05
	AVERAGE															
	AVERAGE OF ALL		5.43e+05	-4.18e+04	4.41e+06	3.80e+05	6.23e+05	-1.96e+06	-4.01e+05	-1.70e+05	-1.54e+05	4.54e+05	2.87e+05	-6.05e+05	-5.70e+05	-6.27e+05

TABLE 16. (CONCLUDED).

Beam No. (Shield)	Beam No. (Length)	PEAK TENSILE STRESSES (Psi)													PSIW Last Sec Stiffness	PIPHI φ - 40°
		PS1 Standard	PS2 Weld	PS3 String	PS4 Start	PS5 No. 20	PS6 1977 @ 20'	PS7 500' @ 10'	PS8 500' @ 20'	PS9 500' @ 40'	PS10 Base	PS11 No Gravity	PS12 f = 0.7			
6	659	2.01e+06	2.57e+05	2.71e+06	2.30e+06	7.90e+05	4.76e+04	7.27e+06	2.06e+06	4.72e+04	4.72e+04	2.92e+06	4.33e+04	7.35e+04	2.74e+06	
	837	2.15e+06	2.31e+05	4.48e+06	2.25e+06	6.29e+05	3.89e+04	6.69e+06	2.17e+06	8.19e+04	1.03e+06	2.56e+06	1.94e+06	1.79e+06	2.92e+06	
	815	2.15e+06	1.00e+04	6.29e+06	2.22e+06	1.08e+06	6.52e+05	6.10e+06	2.45e+06	9.25e+05	2.21e+06	2.49e+06	3.25e+06	2.75e+06	2.91e+06	
	AVERAGE	2.12e+06	1.62e+05	4.51e+06	2.25e+06	8.39e+05	2.47e+05	6.69e+06	2.24e+06	3.52e+05	1.10e+06	2.66e+06	1.74e+06	1.54e+06	2.86e+06	
5	783	2.48e+06	1.21e+05	5.17e+06	2.70e+06	1.02e+06	1.17e+06	4.32e+06	1.63e+06	6.03e+05	1.89e+06	2.55e+06	2.34e+06	1.32e+06	1.90e+06	
	771	2.27e+06	1.24e+05	4.82e+06	2.40e+06	1.25e+06	1.13e+06	4.31e+06	1.45e+06	8.12e+05	2.19e+06	2.34e+06	2.10e+06	1.31e+06	1.84e+06	
	749	2.04e+06	1.17e+05	4.89e+06	2.10e+06	1.53e+06	1.09e+06	4.41e+06	1.30e+06	8.81e+05	2.52e+06	2.11e+06	1.85e+06	1.40e+06	1.77e+06	
	AVERAGE	2.27e+06	1.21e+05	4.83e+06	2.40e+06	1.25e+06	1.13e+06	4.36e+06	1.45e+06	8.99e+05	2.20e+06	2.23e+06	2.10e+06	1.34e+06	1.84e+06	
4	727	1.66e+06	1.02e+05	5.40e+06	1.86e+06	9.82e+05	6.17e+05	2.95e+06	1.07e+06	2.45e+05	2.11e+06	1.79e+06	1.42e+06	1.44e+06	1.43e+06	
	705	1.50e+06	1.02e+05	4.29e+06	1.61e+06	1.02e+06	5.86e+05	3.22e+06	9.02e+05	2.90e+05	2.17e+06	1.58e+06	1.21e+06	1.02e+06	1.33e+06	
	683	1.31e+06	9.51e+04	4.14e+06	1.26e+06	1.08e+06	5.63e+05	3.59e+06	6.99e+05	2.06e+05	2.24e+06	1.41e+06	9.92e+05	6.53e+05	1.22e+06	
	AVERAGE	1.50e+06	1.00e+05	4.61e+06	1.62e+06	1.02e+06	5.92e+05	3.26e+06	8.50e+05	2.47e+05	2.17e+06	1.58e+06	1.21e+06	1.04e+06	1.33e+06	
3	661	1.97e+06	9.72e+04	4.47e+06	1.97e+06	7.44e+05	5.78e+05	3.22e+06	7.71e+05	3.62e+05	1.97e+06	1.62e+06	1.50e+06	2.25e+06	1.75e+06	
	639	1.69e+06	9.76e+04	4.37e+06	1.72e+06	6.12e+05	5.72e+05	3.18e+06	7.41e+05	4.09e+05	1.76e+06	1.66e+06	1.36e+06	1.81e+06	1.56e+06	
	617	1.37e+06	9.50e+04	4.10e+06	1.40e+06	4.71e+05	5.25e+05	3.20e+06	6.85e+05	4.55e+05	1.70e+06	1.52e+06	1.20e+06	1.35e+06	1.28e+06	
	AVERAGE	1.66e+06	9.66e+04	4.31e+06	1.70e+06	6.09e+05	5.52e+05	3.22e+06	7.32e+05	4.09e+05	1.76e+06	1.67e+06	1.35e+06	1.87e+06	1.53e+06	
2	595	2.50e+06	1.02e+05	5.07e+06	2.49e+06	1.66e+06	2.95e+05	3.35e+06	1.50e+06	4.54e+05	1.62e+06	2.09e+06	2.38e+06	2.32e+06	2.65e+06	
	573	2.31e+06	1.02e+05	5.02e+06	2.22e+06	1.62e+06	3.42e+05	3.41e+06	1.57e+06	5.21e+05	1.58e+06	1.94e+06	2.25e+06	2.14e+06	2.33e+06	
	551	2.08e+06	1.02e+05	3.33e+06	1.97e+06	1.59e+06	3.66e+05	3.40e+06	1.79e+06	5.53e+05	1.56e+06	1.82e+06	2.12e+06	1.98e+06	1.87e+06	
	AVERAGE	2.30e+06	1.02e+05	4.48e+06	2.23e+06	1.62e+06	3.36e+05	3.36e+06	1.62e+06	5.09e+05	1.56e+06	1.94e+06	2.25e+06	2.15e+06	2.32e+06	
1	523	2.44e+06	2.86e+05	5.74e+06	2.37e+06	2.29e+06	1.62e+06	4.09e+06	7.15e+04	6.00e+04	9.54e+05	2.26e+06	2.22e+06	3.07e+06	1.26e+06	
	507	1.82e+06	1.98e+05	4.90e+06	1.72e+06	1.41e+06	1.84e+06	4.04e+06	2.74e+04	9.44e+04	5.64e+05	1.64e+06	1.08e+06	2.31e+06	4.14e+05	
	485	1.02e+06	1.52e+05	3.25e+06	8.04e+03	5.82e+05	1.72e+06	4.12e+06	2.40e+04	7.87e+04	2.00e+05	9.58e+05	5.27e+04	1.41e+06	3.00e+04	
	AVERAGE	1.78e+06	2.12e+05	4.84e+06	1.96e+06	1.42e+06	1.73e+06	4.00e+06	4.43e+04	7.77e+04	5.72e+05	1.63e+06	1.12e+06	2.26e+06	5.69e+05	
	AVERAGE OF ALL	1.94e+06	1.32e+05	4.57e+06	2.02e+06	1.15e+06	5.05e+05	4.17e+06	1.18e+06	4.12e+05	1.57e+06	1.97e+06	1.62e+06	1.69e+06	1.74e+06	

TABLE 17. PEAK HORIZONTAL STRESS VS. DISTANCE FROM EXPLOSIVE.

Element (Short)	Element (Long)	Distance (m)	Peak Horizontal Stress (Pa)													
			PS1 Standard	PS2 Weak	PS3 Strong	PS4 Short	PS5 No Roof	PS6 197# @20'	PS7 500# @10'	PS8 500# @20'	PS9 500# @40'	PS10 Expl. @Bass	PS11 No Gravity	PS12 f = 0.7	PS13 Low Soil Stiffness	PS14 PIPHI φ = 40°
1069	1237	3.148	7.55e+06	7.41e+06	7.42e+06	7.63e+06	7.56e+06	1.20e+06	2.89e+07	2.40e+06	7.62e+05	3.00e+06	7.72e+06	7.49e+06	4.15e+06	7.88e+06
975	1203	3.398	5.91e+06	5.71e+06	5.76e+06	6.02e+06	5.91e+06	1.03e+06	3.09e+07	1.99e+06	5.96e+05	2.61e+06	6.00e+06	5.86e+06	4.04e+06	6.02e+06
974	374	3.698	5.15e+06	4.80e+06	5.04e+06	5.38e+06	5.13e+06	1.00e+06	2.44e+07	1.94e+06	6.07e+05	2.40e+06	5.38e+06	5.14e+06	3.58e+06	5.25e+06
973	373	3.898	4.93e+06	3.92e+06	4.47e+06	4.85e+06	4.93e+06	1.06e+06	2.05e+07	1.93e+06	6.93e+05	2.34e+06	4.78e+06	4.94e+06	3.23e+06	5.08e+06
972	372	4.298	4.25e+06	3.11e+06	3.82e+06	4.27e+06	4.24e+06	9.54e+05	1.59e+07	1.78e+06	5.80e+05	2.13e+06	4.26e+06	4.25e+06	2.93e+06	4.39e+06
971	371	4.598	4.00e+06	2.71e+06	3.54e+06	3.90e+06	4.00e+06	9.35e+05	1.39e+07	1.74e+06	5.69e+05	2.01e+06	3.87e+06	3.97e+06	2.67e+06	4.12e+06
286	370	4.858	3.58e+06	2.61e+06	3.21e+06	3.51e+06	3.57e+06	8.91e+05	1.22e+07	1.65e+06	5.59e+05	1.89e+06	3.51e+06	3.59e+06	2.47e+06	3.73e+06
285	369	5.198	3.31e+06	2.27e+06	3.03e+06	3.24e+06	3.31e+06	8.49e+05	1.16e+07	1.58e+06	5.43e+05	1.74e+06	3.20e+06	3.30e+06	2.27e+06	3.51e+06
284	368	5.498	3.01e+06	2.11e+06	2.75e+06	2.85e+06	3.01e+06	7.85e+05	1.05e+07	1.46e+06	5.11e+05	1.60e+06	2.97e+06	3.04e+06	2.10e+06	3.23e+06
283	367	5.798	2.72e+06	1.89e+06	2.40e+06	2.64e+06	2.72e+06	7.03e+05	9.17e+06	1.32e+06	4.93e+05	1.45e+06	2.58e+06	2.78e+06	1.94e+06	2.94e+06
282	366	6.098	2.49e+06	1.71e+06	2.18e+06	2.35e+06	2.43e+06	6.51e+05	8.06e+06	1.27e+06	4.64e+05	1.32e+06	2.37e+06	2.44e+06	1.79e+06	2.66e+06
281	365	6.398	2.26e+06	1.52e+06	2.04e+06	2.17e+06	2.25e+06	5.80e+05	7.22e+06	1.17e+06	4.37e+05	1.18e+06	2.27e+06	2.25e+06	1.65e+06	2.54e+06
280	364	6.698	2.07e+06	1.36e+06	1.78e+06	1.93e+06	2.06e+06	4.82e+05	6.41e+06	1.06e+06	4.01e+05	1.05e+06	2.01e+06	2.17e+06	1.52e+06	2.34e+06
279	363	6.998	1.83e+06	1.26e+06	1.62e+06	1.73e+06	1.82e+06	3.92e+05	5.73e+06	9.16e+05	3.87e+05	8.73e+05	1.80e+06	1.86e+06	1.29e+06	2.09e+06
278	362	7.298	1.53e+06	9.63e+05	1.26e+06	1.51e+06	1.50e+06	2.89e+05	5.02e+06	6.97e+05	2.65e+05	6.59e+05	1.55e+06	1.60e+06	9.87e+05	1.77e+06
277	361	7.598	1.20e+06	8.10e+05	9.45e+05	1.27e+06	1.15e+06	1.13e+05	4.45e+06	3.54e+05	1.10e+05	3.69e+05	1.25e+06	1.40e+06	8.46e+05	1.55e+06
276	360	7.898	8.85e+05	5.69e+05	4.59e+05	6.85e+05	6.83e+05	2.26e+05	3.43e+06	2.41e+05	2.25e+05	2.09e+05	6.92e+05	6.55e+06	4.78e+06	8.09e+05

The peak compressive stress in the reinforcement occurs at the same time as the peak compressive stress in the soil elements adjacent to the panels. This can be seen in Figure 61, which shows time histories of σ_x for the reinforcement (element 885) and the adjacent soil (element 330). It is only after the compressive wave passes in the soil that significant tensile stress occurs at the interface with the facing panel. It takes approximately 75 ms for the axial stress in the reinforcement to go from its peak compressive value to its peak tensile value. This clearly shows that the reinforcement does not initially act to restrain the panel, but rather moves with the soil and actually exerts compressive force on the panel at the same time that the soil pressures on the panel are a maximum. Also, when the reinforcement does go into tension, the rise time for the tensile loading is quite long compared to the rise time for the blast wave in the soil.

4. Effect of Reinforcement Stiffness

The effects of reinforcement stiffness on wall behavior are investigated with analyses PS2 and PS3. Both are identical to PS1 with the exception of the value used for the elastic and plastic stiffnesses of the reinforcement. In PS2, a reduction in stiffness of two orders of magnitude to 370 and 3.7 kPa (54 and 0.54 psi), respectively, is used; in PS3 an increase of two orders of magnitude to 3.7 GPa and 37 MPa (540,000 and 5400 psi), respectively, is used. These changes have the following effects:

- The use of stiff reinforcement results in an 8 percent reduction in peak displacement of the facing and a 17 percent reduction in average displacement.
- The use of flexible reinforcement results in a 15 percent increase in peak displacement of the facing and a 40 percent increase in average displacement of the facing.
- The pattern of displacement is not significantly affected by reinforcement stiffness.
- Average peak velocities and accelerations are reduced by 21 percent and 13 percent, respectively, when flexible reinforcement is used.

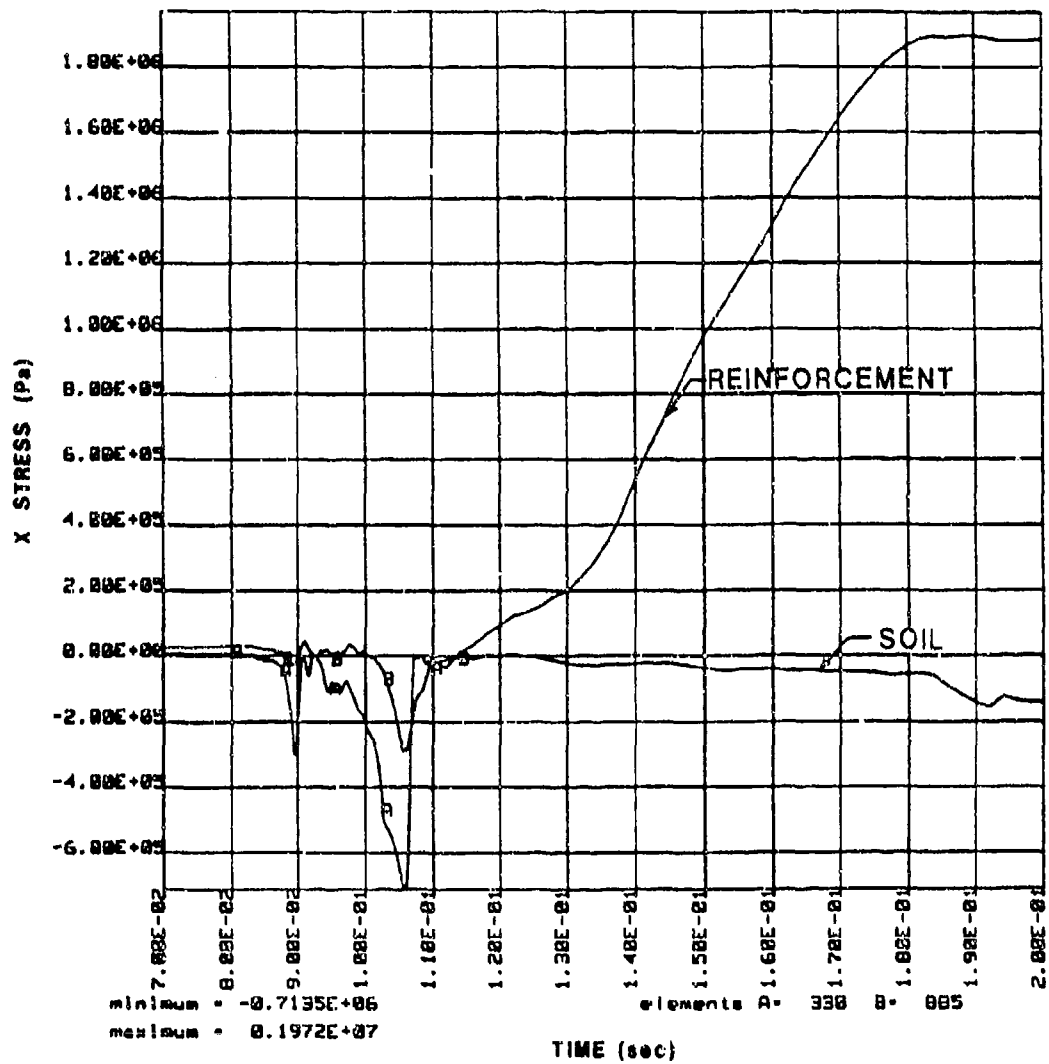


Figure 61. Time Histories of σ_x for Elements 330 and 885 - Analysis PSI.

- Average peak velocity is decreased by 7 percent and average peak acceleration is increased by 45 percent when stiff reinforcement is used.
- Peak horizontal stress on facing panel No. 3 is lower by 28 percent and 24 percent for the flexible and stiff reinforcement, respectively.
- The peak compressive and tensile stresses in the reinforcement at the interface with the facing are strongly influenced by the reinforcement stiffness. Peak compressive and tensile stresses are 92 percent and 93 percent lower, respectively, with flexible reinforcement and 712 percent and 135 percent higher, respectively, with stiff reinforcement.
- The decay in peak horizontal stress in the soil between the middle two layers of reinforcement, as a function of distance from the explosive, is faster for both the flexible and stiff reinforcement compared to the standard reinforcement.

Reinforcement stiffness significantly affects the behavior of the reinforced soil system under study; however, the effects are complex. Peak displacements and accelerations of the facing panels are directly related to reinforcement stiffness, but in a highly nonlinear, and opposite, manner. An increase in stiffness of four orders of magnitude results in a 40 percent decrease in average peak outward displacement of the facing but a 66 percent increase in average peak acceleration. Peak velocities of the facing vary by less than 20 percent between the stiff (PS3) and the flexible (PS2) reinforcement; however, the average peak velocity for the standard wall is larger than for either the stiff or the flexible wall, indicating a more complex relationship between reinforcement stiffness and facing velocity.

Peak stresses in the reinforcement at the interface with the facing are much more strongly influenced by reinforcement stiffness. An increase of four orders of magnitude in stiffness results in 1.3 - 2 orders of magnitude increase in peak tensile and compressive stress, respectively. The relationship between stiffness and tensile stress appears reasonable. The peak displacements of the system decrease with increasing stiffness, leading to smaller strains in the reinforcement. The lower strains partially offset the effect of increased

stiffness on tensile stress generated in the reinforcement. It is less likely that the compressive stresses predicted by the model are realistic because the constitutive model for the reinforcement does not allow a difference between tensile and compressive strength. This point is discussed further in Section V-D.

Reinforcement stiffness affects stress wave propagation through the soil and peak horizontal stress on the facing, but not in a straightforward manner. The peak amplitude in σ_v as the blast wave propagates between the middle two layers of reinforcement toward the facing decreases most slowly in the standard analysis and most quickly in PS2, with the most flexible reinforcement. Peak horizontal stress on facing panel No. 3 follows the same pattern.

5. Effect of Reinforcement Length

The effects of reinforcement length on wall behavior are investigated with analysis PS4. This analysis is identical to PS1, with the exception that the length of the reinforcement is 3.3 meters (10.8 feet), rather than 4.5 meters (14.8 feet). This necessitates an increase in the size of Part 4; however, the overall dimensions of the mesh are not changed. A comparison of the results of PS1 and PS4 lead to the following conclusions:

- There is virtually no difference between the average peak displacement for PS1 and PS4. [24.84 cm vs. 24.83 cm (9.78 in vs 9.78 in), respectively].
- There is less than 2 percent difference between the average peak velocity for PS1 and PS4. [4.79 m/s vs. 4.89 m/s (16.04 fps vs 16.04 fps), respectively].
- The average peak acceleration is approximately 17 percent lower in analysis PS4 compared to PS1 (115 g vs. 139 g). However, peak accelerations are higher in the lower two facing panels in analysis PS4.
- Peak horizontal stresses on facing panel No. 3 are slightly lower (less than 1 percent) in analysis PS4.

- Peak tensile stresses in the reinforcement are very similar in the two analyses; however, peak compressive stresses are significantly lower (approximately 34 percent) when short reinforcement is used.
- There is very little difference in wave propagation through the soil between the middle layers of reinforcement

The effects of reinforcement length on the behavior of the reinforced soil system appear to be much less significant than the effects of reinforcement stiffness. Except for a small difference in the acceleration of the facing, only the difference in peak compressive stress in the reinforcement distinguishes the two analyses. As we have seen in the discussion of the standard wall, the reinforcement is subjected to compressive stress as the blast wave passes through the system. The magnitude of the compressive stress developed in the reinforcement is a function of its length, the normal stress acting on it and the frictional coefficient between the reinforcement and the soil. Taking into account the difference in reinforcement length, the reduction in peak compressive stress can be accounted for.

6. Effect of the Roof

To investigate the difference in behavior between the standard wall which has a roof that provides vertical constraint and lateral friction on the facing, and a free-standing wall, analysis PS5 was conducted. PS5 is identical to PS1, with the exception that there is no roof in PS5 and the top of facing panel No. 6 is free to move in both X and Z directions. The effects of removing the roof are:

- The average displacement of the facing panels is 56 percent higher when no roof is present. The most obvious difference is the reduction in rotation of the upper facing panel when the roof is not present. However, when the displacement of the top of panel No. 6 is excluded, the difference in average displacement is only reduced to 43 percent.
- There are virtually no differences in average peak velocity and acceleration of the facing, and average peak pressure on facing element No. 3. Decay in peak blast wave magnitude is also nearly identical in the two analyses.

- The average peak compressive stress in the reinforcement is approximately 15 percent higher without a roof; the average peak tensile stress is approximately 41 percent lower.

The intention of analysis PS1 is not to accurately model the complex interaction that occurs between the facing panels and a roof structure; that is beyond the scope of this investigation. The vertical constraint imposed by the roof in the analysis is intended to be a lower bound to the actual restriction in the vertical plane. This allows an evaluation of the maximum effect a roof might have. Based on the comparison between PS1 and PS5, the beneficial effects of vertical constraint and lateral friction provided by the roof are clear, the wall suffers significantly less outward displacement.

7. Effect of Weapon Size

Analyses PS1 and PS7 are used to obtain information on weapon size effects. PS7 is identical to the standard analysis except that the velocity time history used to simulate the blast loading is generated by assuming the weapon contains 227 kg (500 pounds) of TNT, rather than 89.4 kg (197 pounds). The effects of this increase in weapon size are:

- The reinforcement at the connection with facing panel No. 6 ruptures, thereby causing a breaching of the wall.
- The average peak displacement and acceleration of the other facing panels are approximately three times greater than with the standard weapon, and the average peak velocity is approximately six times greater.
- The average peak horizontal stress on facing panel No. 3 is approximately five times greater than with the standard weapon.
- Average peak compressive stress in the reinforcement at the interface with the facing is approximately five times higher and average peak tensile stress is approximately twice as high.
- Tensile yielding occurs in half of the reinforcement layers.

- Peak compressive stress in the soil between the third and fourth reinforcement layer averages approximately 3.5 times higher than with the standard weapon.

After 400 ms. the numerical model predicts that facing No. 6 has displaced several meters. This displacement is accompanied by minimal slippage between the reinforcement and the soil. However, predicted axial strain over 2000 percent in the reinforcement elements tied to the facing is predicted. This amount of strain is much greater than that required to cause rupture, indicating that a rupture mode of failure, rather than a slippage mode has occurred.

The greater increase in compressive stress in the reinforcement compared to tensile stress increase is due, at least partly, to the difference in the actual magnitude of the stresses. The reinforcement yields in three of the reinforcement layers, thereby limiting the increase in tensile stress that can be developed. The peak compressive stresses generated by the larger weapon all fall below the compressive yield strength of the material.

This comparison indicates that a wall designed for static loading using conventional design methods may fail by reinforcement rupture, rather than pull-out. If further work verifies this, design of reinforced soil structures may differ little from static design. To prevent rupture, the strength and/or thickness of the reinforcement would have to be increased either over its whole length or perhaps only near the connection with the facing panels.

8. Effect of Weapon Location

The evaluation of weapon location effects involves three comparisons: a) PS1 and PS6; b) PS7, PS8 and PS9; and, c) PS1 and PS1B. The first comparison is between the standard analysis and one in which the weapon is located 3.05 meters (10 feet) farther away from the facing [11.1 meters (36.4 feet) vs. 8.05 meters (26.4 feet)]. The second comparison includes three analyses in which a 227 kg (500 pounds) weapon is located a 8.05 meters (26.4 feet), 11.1 meters (36.4 feet) and 17.2 meters (56.4 feet) from the facing. The last comparison is between the standard analysis and one in which the weapon is placed 4.5 meters (14.8 feet) below the ground surface, at the top elevation of the soil base. These comparisons lead to the following conclusions:

- The overall pattern of displacement of the facing is not significantly affected by the horizontal distance to the explosive, although peak displacement and velocity decrease in a highly non-linear fashion with weapon distance.
- Peak reinforcement stresses decrease with weapon distance in approximately the same ratio as peak displacement and velocity.
- A 227 kg (500 pounds) explosive at 11.1 meters (36.4 feet) produces slightly larger (<5 percent) average peak displacement in the facing compared to an 89.4 kg (197 pounds) explosive located 8.05 meters (26.4 feet) from the facing. Peak velocities and accelerations in the facing are smaller with the larger explosive, as is peak pressure on facing panel No. 3 and peak stresses in the reinforcement.
- Average peak displacement, velocity and acceleration decrease when the weapon is located 4.5 meters (14.8 feet) below the ground surface, compared to 2.25 meters (7.4 feet) below. The pattern of displacement differs also. The peak displacement of the facing occurs at mid-height rather than at the upper portion of the wall.

The pattern of displacement of the facing is affected more by depth of the weapon than by horizontal distance from the reinforced mass. The deeper location of the weapon in analysis PS1B causes the lower facing panels to deflect more than the upper ones. The top facing panel still rotates significantly, but not as much as it does when the weapon is located at mid-height of the reinforced soil mass. The average displacement of the panels is reduced 13 percent by locating the weapon at the base; however, this is a negligible reduction compared to that achieved by moving the weapon horizontally away from the wall.

The effects of horizontal distance of the weapon from the wall are straight forward with the reduction in peak displacement accompanied by similar reductions in soil and reinforcement stresses.

9. Effect of Soil-Reinforcement Interface Friction

The effects of the interface friction coefficient between the soil and the reinforcement are investigated with analysis PS1S. In this analysis, the

interface friction coefficient is reduced from 0.9 to 0.7. All other model parameters are identical to those used in PS1. The effects of the reduction in interface friction are:

- the average peak displacement of the facing increases by 2 percent;
- the average peak velocity of the facing increases by 14 percent;
- the average peak acceleration of the facing increases by 12 percent;
- the average peak horizontal stresses on the elements adjacent to facing panel No. 3 increase by 5 percent;
- average peak reinforcement stresses at the interface with the facing are higher in compression by 11 percent, but lower in tension by 16 percent; and
- the soil/reinforcement friction coefficient has no significant effect on the attenuation of the compression wave in the soil between the middle two layers of reinforcement.

The small increases in panel displacements, velocities and accelerations (≤ 12 percent) compared to the 22 percent reduction in soil/reinforcement friction coefficient imply that the full frictional capacity of the soil/reinforcement interface is not being utilized in the standard analysis. Additional reduction in interface friction should produce more significant increases in panel movement leading to failure, as the friction coefficient approaches that necessary for static stability. The analysis also implies that increases in interface friction are likely to result in disproportionately smaller reductions in panel movement and may not be a cost-effective way of reducing panel displacement.

10. Effect of Soil Stiffness

The effects of soil stiffness are investigated with analysis PS1W. In this analysis, the bulk modulus (K) and the initial shear modulus (G) of the soil are both reduced by a factor of ten from the standard analysis. All other parameters are identical to those used in PS1. These changes have the following effects:

- the average peak displacement of the facing increases by 26 percent;
- the average peak velocity of the facing increases by 19 percent;
- the average peak acceleration of the facing increases by 13 percent;
- average peak horizontal stresses in the elements adjacent to facing panel No. 3 decrease by 24 percent;
- average peak reinforcement stresses at the connection with the facing are higher in compression by 5 percent; but lower in tension by 13 percent; and
- the peak amplitude of the compression wave in the soil between the middle two layers of reinforcement attenuates faster.

As expected, the reduction in bulk and shear moduli of the soil leads to higher panel displacements, velocities and accelerations. The increase in average peak panel displacement is 26 percent, compared to a 40 percent increase caused by a two orders of magnitude reduction in reinforcement stiffness. The reduction in the average peak horizontal stresses in the elements adjacent to panel No. 3 is the result of increased attenuation of peak stresses as the blast wave travels through the soil. However, this reduction in peak stress is accompanied by a longer-duration pulse which produces the large displacements observed. As a relatively soft structural system, the reinforced soil wall is influenced more by the full shape of the blast wave, rather than the absolute peak.

This analysis points out the importance of the placement density of the soil in a reinforced soil system. As the main factor controlling stiffness, it is important to achieve the desired soil density when constructing a reinforced soil system. Also, when conducting model or field tests, comparisons between tests will be difficult to interpret if consistent densities are not achieved.

11. Effect of Soil Strength

The effects of soil strength (i.e., friction angle) on behavior of the reinforced soil system are investigated with analysis PIPSI. In this analysis, the friction angle of the soil is increased from 34 degrees to 40 degrees. All

other soil parameters are the same as those used in analysis PS1. The effects of this increase in strength are:

- the average peak displacement of the facing decreases by 12 percent;
- the average peak velocity of the facing increases by 5 percent;
- the average peak acceleration of the facing increases by 13 percent;
- the average peak horizontal stresses in the elements adjacent to facing panel No. 3 increase by 21 percent;
- average peak reinforcement stresses at the interface with the facing are higher in compression by 15 percent but lower in tension by 10 percent; and
- the peak amplitude of the compression wave through the soil between the middle two layers of reinforcement is about 10 percent higher than in the stronger soil.

The increase in soil friction angle from 34 degrees to 40 degrees results in a 24 percent increase in the friction coefficient, $\tan \phi$. This change produces increases in average velocity and acceleration of the panel of 5 percent and 13 percent, respectively. However, the average displacement of the facing decreases by 12 percent. This is further evidence that wall displacement is not determined by peak acceleration or peak velocity. Changes in soil strength influence panel motions and pressures acting against the panels in the same manner as do changes in soil stiffness, i.e., increases in strength and stiffness lead to lower displacements and higher pressures. The combined effect of strength and stiffness make placement soil density the most important design consideration for a given threat environment.

12. Effect of Gravity Initialization

Analyses PS1 and PS1N are used to investigate the effects of gravity initialization on the standard analysis. The comparison of these analyses leads to the following conclusions:

- The average peak displacement of the facing is slightly higher (2 percent) without gravity initialization. The difference in the upper three panels is greater than in the lower three where the no gravity analysis predicts slightly less displacement.
- There is virtually no difference in average peak velocity; however, the upper three panels have higher peak velocities without gravity and the lower three have higher peak velocities with gravity.
- Average peak acceleration of the facing is approximately 43 percent lower without gravity. The difference is greatest in the upper three panels.
- Average peak compressive stress in the reinforcement is approximately 51 percent lower without gravity, but there is virtually no difference in average peak tensile stress.
- Average peak horizontal stresses on facing panel No. 3 are slightly lower (2 percent) without gravity.
- The pattern of decay in the amplitude of the stress wave vs. distance from the weapon differs between the two analyses. Initially, the amplitude is higher near the weapon in the analysis without gravity. As the wave propagates through the reinforced zone, the amplitude in the analysis without gravity becomes smaller compared to the value with gravity. In the soil element adjacent to the facing, however, the amplitude is higher in the analysis without gravity.

Although gravity stresses do not significantly affect the displacement of the reinforced system for the parameters chosen in PS1, other components of the solution are affected. The differences in peak acceleration are quite large, although they do not lead to significant velocity or displacement differences. The decrease in peak compressive stress in the reinforcement is also significant.

An objective evaluation of this comparison between analyses with and without gravity stresses would indicate that gravity stresses do not significantly influence the overall behavior of the reinforced soil system. However, it should be kept in mind that the standard analysis predicts wall

displacements which do not lead to instability. Under conditions where displacements are large enough to cause an unstable geometry to develop, the inclusion of gravity stresses may be required to properly predict the collapse of the system.

D. CONCLUSIONS OF PARAMETRIC STUDY

The results of the parametric study shed some light on the possible behavior of reinforced soil systems:

- Reinforcement stiffness significantly affects the displacements induced by blast loading. Displacement decreases with increasing reinforcement stiffness in a nonlinear fashion. An increase of four orders of magnitude in reinforcement stiffness leads to approximately a 40 percent decrease in average peak displacement of the wall facing.
- Within the range investigated, reinforcement length has little effect on the behavior of the reinforced soil system, provided the length meets static design criteria.
- The reinforcement is subjected to very high compressive stresses as the blast wave passes through the system. Dynamic tensile stresses do not develop until after the blast wave has reached the facing.
- Dynamic tensile stresses develop relatively slowly in the reinforcement. Rise times of tens of milliseconds are predicted by the numerical code.
- Reinforcement rupture and excessive deflection were the only observed failure mechanisms. Very little relative movement between the reinforcement and the soil (pull-out) was observed.
- Weapon size and distance are critical parameters which influenced wall behavior much more than any other parameters.
- For a constant soil friction angle, soil/reinforcement interface friction coefficient has a relatively small influence over system behavior for the range of values utilized (0.7 - 0.9).

- Soil strength and stiffness are very important parameters governing system behavior. Wall panel motions decrease as soil strength and stiffness increase. This effects appears to be more important than reinforcement stiffness.
- For a given soil, the behavior of a reinforced soil system is very sensitive to placement soil density because of the close relationship between soil density and soil strength and stiffness. Increasing the relative compaction of the soil will lead to enhanced performance.
- To obtain useful results from field and centrifuge tests, it will be necessary to achieve uniform soil density throughout the reinforced soil mass. Meaningful comparisons between tests will require the use of the same soil uniformly compacted to the same relative compaction in each test.

E. RECOMMENDATIONS FOR FURTHER MODEL DEVELOPMENT

The numerical model described in this report is an initial attempt to predict the behavior of a very complicated structure subjected to complex dynamic loading. A state-of-the-art computer code and soil constitutive model are being used in a manner they were not explicitly designed for. A numerical model such as this will require continual modification and improvement over a long period of time before confidence in its ability to accurately predict behavior is achieved. As the next step in the improvement of the model, the following modifications are recommended:

- The constitutive model for the reinforcement should be improved. A non-linear stress-strain relationship with a realistic compressive yield strength and a tensile rupture stress (or strain) is needed.
- A constitutive model for the soil-reinforcement and soil-wall frictional interfaces should be developed. The current model, which prevents any relative movement until the shear strength of the interface is reached, does not match actual behavior of such interfaces.
- A more realistic constitutive model for the facing panels should be used. A model which is capable of predicting concrete cracking is desirable.

- The cap model should be modified so that a cohesionless material can be simulated.
- Cap model parameters should be evaluated for the soil used in the centrifuge tests and/or soil to be used in future field tests. Validation of the numerical model will require comparison of numerical predictions with centrifuge and/or field test results. This will require laboratory data for the soil constitutive model.
- The effect of the mass proportional damping factor should be investigated and a method should be developed to calculate a value based on soil properties.
- Further work on the effects of gravity stresses should be conducted to determine under what circumstances, if any, the inclusion of gravity stresses is necessary. If gravity stresses are deemed necessary, a method of including them as an initial condition in the analysis should be developed.
- A more accurate method of modeling the blast load is needed, especially if the simulation of weapon detonation in the reinforced soil zone is desired. The use of exploding elements may be appropriate.
- The modeling of the reinforcement/facing panel connection should be modified to allow the rupture of this connection. Interface model No. 8 in the DYNA3D code (nodes spotwelded to a surface) may offer the means to accomplish this.
- A true three-dimensional analysis should be developed after the improvements listed above are accomplished.

Further development of the numerical model can be divided into: (1) refinements in the constitutive models used for materials and interfaces; (2) generation of laboratory data to obtain parameters for constitutive models and mass proportional damping; (3) refinements in the simulation of gravity and blast loading; and (4) extension to true three-dimensional analysis.

The use of constitutive models for the reinforcement and facing which permit fracture and cracking, respectively, will more closely simulate actual field

behavior of a reinforced soil wall. Perhaps more important, though, is the inclusion of an interface model that permits shear displacement to occur at shear stresses below the shear strength of the interface. The current stick-slip model leads to underestimates of the relative movements of the reinforcement and the soil. This likely leads to an underestimate of system movement.

If gravity stresses are to be included, the cap model should be modified so that a true cohesionless soil can be modeled without the continuous deformations under gravity loading that now occur. A method of determining an appropriate value of mass proportional damping is essential. This term significantly affects predicted displacement, perhaps more than any other parameter. The analysis of laboratory dynamic tests, such as Split-Hopkinson Bar data, may provide the means of selecting this parameter.

To validate the numerical code, comparisons of code predictions to physical tests will be necessary. This will require laboratory testing to evaluate the cap parameters of the soil used in the centrifuge or field tests. Laboratory testing of the reinforcement may also be required if the data are not already available.

The current method of blast simulation, defining a horizontal velocity time history for boundary nodes, can be significantly improved. The addition of the vertical component of velocity may be sufficient for simulation of weapons behind the reinforced soil mass. However, for simulation of detonations within the reinforced soil mass, exploding elements which simulate the explosive process itself may be required. This would increase the solution time very significantly because of the much shorter time step required and the need for rezoning during the analysis. A comparison between this method of analysis and simpler methods should be performed to determine if the (probable) increased accuracy justifies the added complexity of the analysis.

The eventual goal of this research should be the three-dimensional modeling of the problem. By using the DYNA3D code in a plane strain mode and refining the analysis as recommended above, the extension to three dimensions should be relatively easy, involving mainly geometry changes.

SECTION VI

PHYSICAL MODELING OF REINFORCED SOIL WALL SYSTEMS

A. GOALS AND ORGANIZATION

Physical modeling of two types of reinforced soil wall systems was conducted at Tyndall Air Force Base (AFB), Florida. Reinforcing systems modeled were steel strips and geogrid. The wall systems were subjected to blast loading from explosive charges buried in the backfill material. All tests were performed on the Tyndall AFB centrifuge utilizing small-scale reinforced soil wall models. The modeling was conducted to accomplish the following: (1) to investigate and compare the responses of reinforced soil wall systems subjected to dynamic loading; (2) to obtain data which can be compared to results gathered from numerical modeling methods and full-scale testing; (3) to provide guidance in the selection of wall components to be used in full-scale walls; and (4) to validate the use of the centrifuge as a viable means of studying dynamically loaded geotechnical structures. Section VI of this report is organized as follows:

- Section B describes the types of physical models used in science and engineering.
- Section C describes centrifuge modeling. It includes: (1) a discussion on model similitude and scaling relationships; (2) a description of the Tyndall centrifuge utilized for testing; and (3) a description of the model reinforced soil wall.
- Section D presents a list of the materials utilized to prepare a complete model reinforced soil wall including all wall and reinforcing components, instrumentation and explosives.
- Section E presents the procedures utilized for the construction, instrumentation, detonation, data collection, disassembly and data reduction process of a model reinforced soil wall.
- Section F presents the results of preliminary centrifuge tests. It includes a description of all improvements and/or modifications made to both wall components and construction techniques, based on the preliminary test wall responses.

- Section G presents the results of all production tests. It includes a presentation of the test matrix for all production tests, a discussion of test results, and a comparison of centrifuge modeling results to those predicted from computer programs, full-scale test results, and numerical modeling results.
- Section H summarizes conclusions and recommendations.

B. TYPES OF PHYSICAL MODELS

A physical model is the physical reproduction of a structure, problem, or event (known as the prototype) in which prototype geometry, behavior, or response is simulated by the model. Physical modeling is utilized for the following purposes: (1) to verify or disprove the results of a mathematical analysis of a problem; and (2) to simulate a physical situation or event that, due to any number of reasons (e.g. problem complexity, safety hazards, time constraints, cost considerations, etc.), can not be studied in its true form. The following types of physical models are commonly used in science and engineering:

- Analog Models: An analog model behaves mathematically the same as the prototype problem. Many different physical problems are mathematically similar. For example, both the flow of electricity through a conducting medium and the flow of fluid through a porous medium are governed by the same differential equation:

$$k_x \partial^2 V / \partial x^2 + k_y \partial^2 V / \partial y^2 = 0 \quad (1)$$

where k_x and k_y represent both permittivity and soil permeability (in x and y directions, respectively), and V represents both voltage loss and head loss in electrical and seepage problems, respectively. Therefore, an electrical analog model can be constructed to simulate, for example, the seepage beneath a sheet pile wall. The measured voltage loss in the electrically conductive medium of the model is directly related to total head loss in the prototype structure.

- Scale Models: A scale model is a physical replicate of the prototype structure. It is composed of the same or similar materials as the prototype structure and can be constructed at full scale or at some smaller scale such that there exists similitude between model and

prototype. These models are widely used in all branches of civil engineering (e.g., wind tunnels, hydraulic flumes, small-scale structures, etc.).

Scale models were utilized in the study of reinforced soil walls subjected to dynamic loading. However, for a physical model to accurately simulate the behavior of the prototype structure, there must be both dynamic and geometric similitude between the two. In this study of dynamically loaded geotechnical structures, precise simulation of in-situ soil stresses and explosive energy was crucial to the development of an accurate model. It was for this reason that a centrifuge was utilized to account for these and other gravity-induced effects.

C. CENTRIFUGE MODELING

1. Similitude and Centrifuge Scaling Relations

Soil strength is derived from insitu self-weight stresses which increase with depth in a soil deposit. Soil stresses in a small-scale geotechnical structure will, therefore, be much less than those in the prototype structure, resulting in a lack of similitude. A centrifuge is utilized to simulate prototype soil stresses in the model. The centripetal acceleration of a centrifuge subjects the model to a high level of artificially-induced gravity which essentially increases the model's self weight and, therefore, increases the stress levels in the model to equal those in the prototype structure. For example, the vertical stress at depth "z" in a soil deposit is equal to γz or $\rho g z$, where γ is the unit weight of the soil, ρ is the mass density of the soil and g is the acceleration of gravity. This stress can be simulated in the centrifuge (where $z_{model} < z_{prototype}$) by subjecting it to the appropriate g-level "n" so that $n \rho g z_{model} = \rho g z_{prototype}$. It can then be said that the linear dimension of a centrifuge model accelerated to $n g$'s scales as $1/n$ with the prototype structure.

Many other physical parameters must also be considered for accurate modeling of soil behavior. Table 10 presents the centrifuge scaling relations of several pertinent soil characteristics.

Of particular interest to this study of dynamically loaded reinforced soil walls is the scaling of explosive energy. The most important wall response to be modeled in this study was wall deformation and it was believed that modeling explosive energy would most accurately simulate prototype wall displacement. A

complete discussion of the explosive modeling and design of the detonators used for testing is presented in Section D-4.

TABLE 18. SCALING RELATIONS (REFERENCE 74).

Quantity	Full Scale (prototype)	Model (at ng's)
Linear dimension	1	$1/n$
Area	1	$1/n^2$
Volume	1	$1/n^3$
Time		
dynamic events	1	$1/n$
hydrodynamic events	1	$1/n^2$
viscous flow	1	1
Velocity	1	1
Acceleration	1	n
Mass	1	$1/n^3$
Force	1	$1/n^2$
Energy	1	$1/n^2$
Stress	1	1
Strain	1	1
Density	1	1
Frequency	1	n

2. Centrifuge Description

All centrifuge modeling was conducted utilizing the Air Force Civil Engineering Support Agency (AFCEA) centrifuge at Tyndall AFB, Florida. The Genisco Model E-185 centrifuge is a hydraulically driven rotary accelerator with a payload capacity of up to 2.2 kN (500 pounds) and maximum g-level of up to 100 g's. Payload and g-level must be selected so as not to exceed the maximum in-flight capacity of 133.5 g-kN (15 g-ton) at the sample mounting platform. Therefore, a payload of 2.2 kN (500 pounds), for example, can not be accelerated to the full 100 g's, but is limited to a maximum g-level of 60. The mounting platforms are located at the ends of two 1.83 meters (6 feet) cantilever arms and are free to rotate from a horizontal to vertical position so that the vertical axis of the model is parallel to the resultant acceleration vector at all times during operation (Reference 75).

The centrifuge is housed in a 0.23-meters (0.75-feet) thick reinforced concrete structure with a height of 2.1 meters (6.9 feet) and a diameter of 4.9 meters (16 feet). It is operated via remote control console. Additional features include an on-board 16-channel Pacific Instruments Model 5700 TDR (Transient Data Recorder) data acquisition system, shuttered video camera and 10,000 picture-per-second high-speed camera.

3. Model Description

The centrifuge models prepared for this project were 1:30 (nominal) scale. Each wall was constructed of (29) 5.1 cm x 5.1 cm (2 inches x 2 inches) interlocking panels and two, 2.5 cm x 5.1 cm (1 inch x 2 inches) interlocking panels. The panels were arranged in three rows in a staggered fashion as shown in Figure 62. A constructed model reinforced soil wall was 50.8 cm (20 inches) long and 15.2 cm (6 inches) high. Steel strip reinforcing was modeled with steel shim stock and geogrid reinforcing with woven nylon netting. The reinforcing lengths varied from test to test. In most models a restraint was attached along the top edge of the wall to simulate a roof slab. In most models a berm was excavated behind the wall to simulate the sloping backfill of a soil covered structure. Beach sand found locally at Tyndall AFB was utilized for base and backfill material. The mass of explosive material used in the models was equivalent to 3.42 grams (0.0075 pounds) of TNT.

The above model was accelerated in the centrifuge to simulate a prototype structure 4.5 meters (15 feet) high by 15.2 meters (50 feet) long composed of 29 1.5 meters by 1.5 meters (5 feet by 5 feet) interlocking panels and two 0.8 meter x 1.5 meters (2.5 feet by 2.5 feet) interlocking panels (see Figure 62). When a flight, the explosive event in the centrifuge simulated the detonation of a buried 227 kg (500 pounds) general purpose bomb containing 89.4 kg (197 pounds) of TNT.

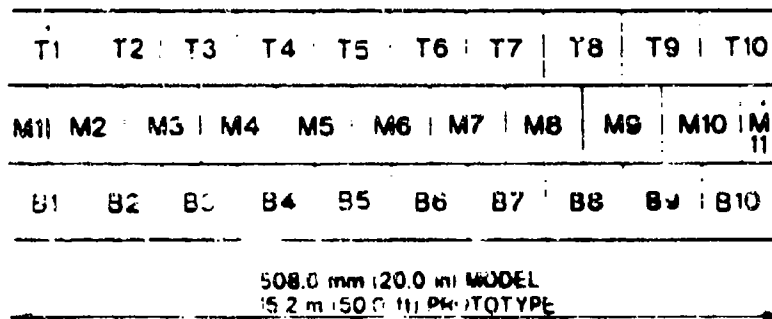
Table 19 presents all pertinent dimensions and measurements of the model and prototype. The selection of model wall component materials and explosives is further discussed in Section VI-D.

D. MODEL MATERIALS

A complete model reinforced soil wall consisted of several components: (1) the wall system itself (facing panels, reinforcing, etc.); (2) backfill material; (3) instrumentation for data collection, (4) detonators; and (5) a containment

50.8 mm x 50.8 mm (2.0 in x 2.0 in) MODEL
 1.5 m x 1.5 m (5.0 ft x 5.0 ft) PROTOTYPE

50.8 mm x 25.4 mm (2.0 in x 1.0 in) MODEL
 1.5 m x 0.75 m (5.0 ft x 2.5 ft) PROTOTYPE



152.4 mm (6.0 in) MODEL
 5.0 m (15.0 ft) PROTOTYPE

Figure 62. Wall Geometry (Model and Prototype).

bucket to house the model. These components are described in detail in the following paragraphs.

1. Wall Components

- Facing Panels: Laboratory testing of several candidate materials was conducted to find a suitable model for concrete facing panels. Gypsum panels were selected, and a plaster-water ratio of 1.72:1 was used. It was desired to scale panel mass in the centrifuge. Because panel length and height were already designed to scale linear dimensions, panel thickness was calculated so that the model panel mass accelerated to 30 g was equal to the prototype panel mass. This thickness was 9.5 mm (0.38 inch) and all panels were constructed at this thickness. Model and prototype facing panel masses are listed in Table 20.

TABLE 19. MODEL/PROTOTYPE DIMENSIONS.

Model Component	Model Dimension	Prototype Dimension
Wall		
length	508 mm (20 inches)	15.2 m (50 feet)
width	13.2 mm (0.5 inches)	396 mm (1 foot)
height	152.4 mm (6 inches)	4.6 m (15 feet)
facing elements	50.8 mm x 50.8 mm (2 inches x 2 inches)	1.5 m x 1.5 m (5 feet x 5 feet)
reinforcing:		
length	152.4 mm (6 inches)	4.6 m (15 feet)
width:		
steel	varies	varies
geogrid	25.4 mm (1 inch)	762 mm (30 inches)
spacing	varies	varies
Backfill		
soil type	Tyndall AFB Sand	Tyndall AFB Sand
depth of base below wall	152.4 mm (6 inches)	4.6 m (15 feet)
Charge		
depth	varies	varies
dist. behind back face of wall	varies	varies
dist. from ends of wall	254 mm (10 inches)	7.6 m (25 feet)
size	3.42 gm (0.008 lb) RDX	39.4 kg (197 lbs) TNT

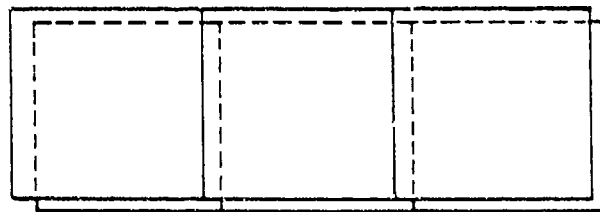
TABLE 20. STRENGTH PROPERTIES OF REINFORCED SOIL WALL COMPONENTS.

Wall Component	Property Modeled	Model Material	Prototype Material
Facing Panel Model = gypsum Prototype = concrete	panel mass	31.5 gr (0.07 lb)	450.5 kg (1.073 lb)
Steel Reinforcement Model = steel Prototype = steel	Modulus (E)	1,399 MPa (19,900 ksi)	1,399 MPa (19,900 ksi)
Geogrid Reinforcement Model = nylon mesh Prototype = commercial HDPE geogrid	Modulus (E)	20.3 kN/m 115 lb/inches	640 kN/m 3,653 lb/in

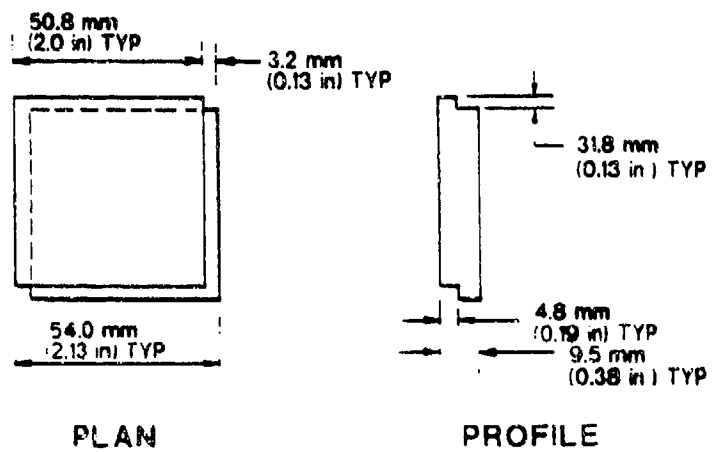
The gypsum mixture was cast in shallow stainless steel baking pans and covered with a smooth piece of high density polyethylene (HDPE) to insure smoothness on all sides, and cured. A table saw was utilized to cut the gypsum into 54 mm x 54 mm (2.13 inches x 2.13 inches) panels. A 3.2 mm (0.13 inch) wide dado was cut along two adjacent panel edges of one face and then on the opposing two edges of the opposite face. These cuts allowed the panels to interlock in much the same way prototype facing panels interlock (see Figure 63). Final panel dimensions when interlocked were 51 mm x 51 mm (2 inches x 2 inches). Two 1.59 mm (0.0625 inch) diameter holes were drilled along the centerline of each element 29.5 mm (1.16 inches) apart for purposes of attaching reinforcement.

A 51 mm x 51 mm (2 inches x 2 inches) HDPE backing plate was cut for each panel. Two 1.59 mm (0.0625 inch) diameter holes were also drilled through the panel and backing plate 29.4 mm (1.16 inches) apart. Reinforcing was then placed between the panel and backing plate and bolted in place.

- Reinforcing: Laboratory testing of several candidate materials was conducted to find suitable material to model prototype reinforcement modulus. The materials selected were: (1) Strips: The material selected to model steel reinforcing strips was steel shim stock.



INTERLOCKING STRUCTURE



PLAN

PROFILE

Figure 63. Interlocking Panel Structure.

The shim stock was cut into 4 mm and 8 mm wide strips of varying length. (2) Geogrid: The material selected to model a geogrid was a woven nylon netting. This material was cut into 51 mm (2 inches) wide strips of varying lengths. The moduli of both model and prototype reinforcing materials are shown in Table 20. Photographs of completed panels used in all centrifuge tests are presented in Figures 64 and 65.

- Connection: For all steel reinforced panels, glue was applied to both the HDPE backing and the gypsum panels. Two segments of steel reinforcing were sandwiched between the facing element and the backing, 25 mm (1 inch) apart on center, such that equal lengths of reinforcing projected both above and below the backing. The assembly was bolted to complete the wall panel. The strips were then trimmed to the desired test length. No glue was utilized for geogrid walls and only one strip of reinforcing was required per panel. The geogrid was bolted and trimmed as described above for the steel reinforcement.
- Leveling Pad and Top Restraint: The reinforced soil walls were constructed on a 13 mm x 508 mm (0.5 inch x 20 inches) wood strip which served as a leveling pad. A 510 mm (20 inches) length of 76 mm (3 inches) wide aluminum stock was selected as a model restraint for the top edge of the wall. A 90 degree bend was introduced along the length of the aluminum stock as shown in Figure 66. Aluminum side panels were welded to both sides of the restraint and a hole was drilled in each for bolting the restraint in place.

2. Soil

All tests were prepared with local beach sand collected at Tyndall AFB. The Tyndall AFB sand was a uniform, subrounded, fine grained quartz sand with $D_{50} = 0.020$ mm (0.00079 inch). The grain size distribution curve is shown in Figure 67 (Reference 76). Dry sand was utilized for all tests and was pluviated in lifts to a unit weight of $16.6 \pm .08$ kN/m³ (105.5 \pm 0.5 pcf).

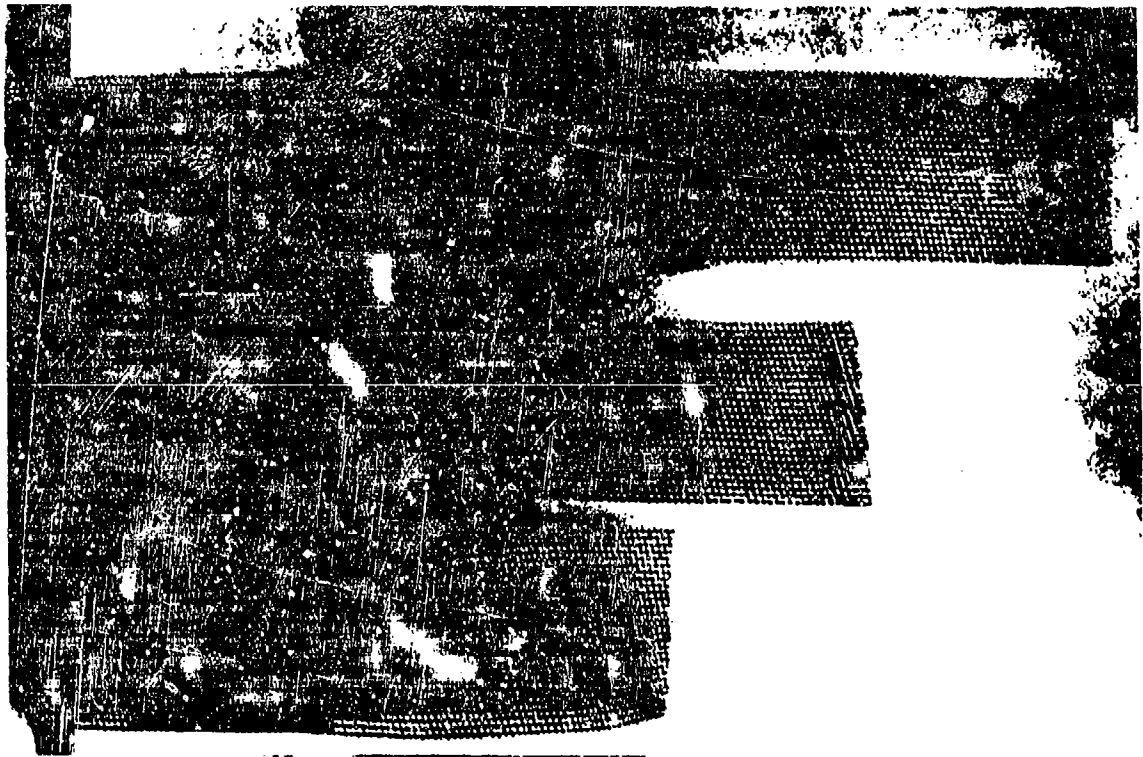


Figure 64. Geogrid Reinforced Panels.

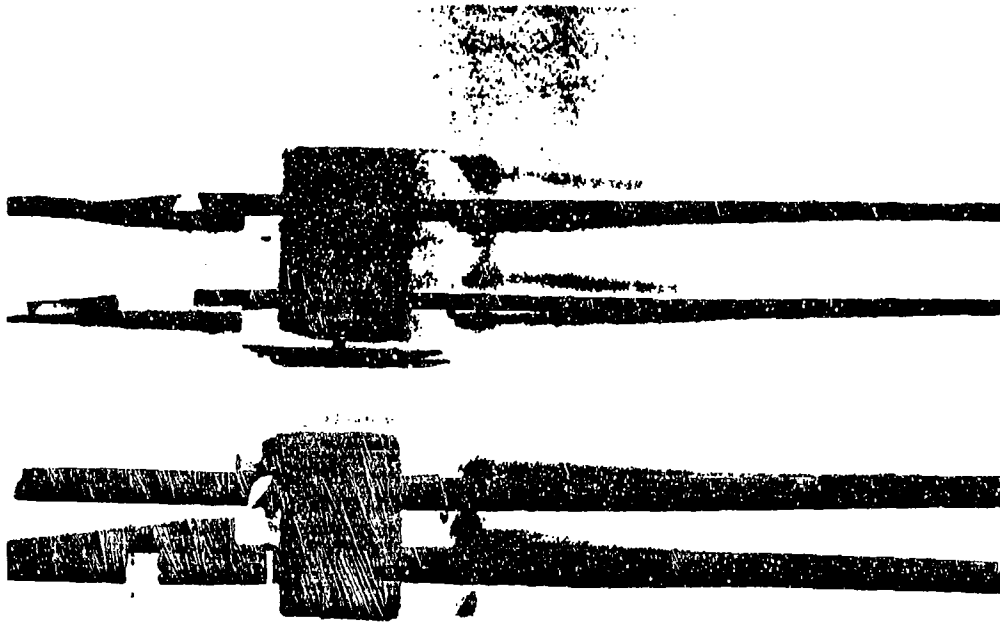


Figure 65. Steel Reinforced Panels.

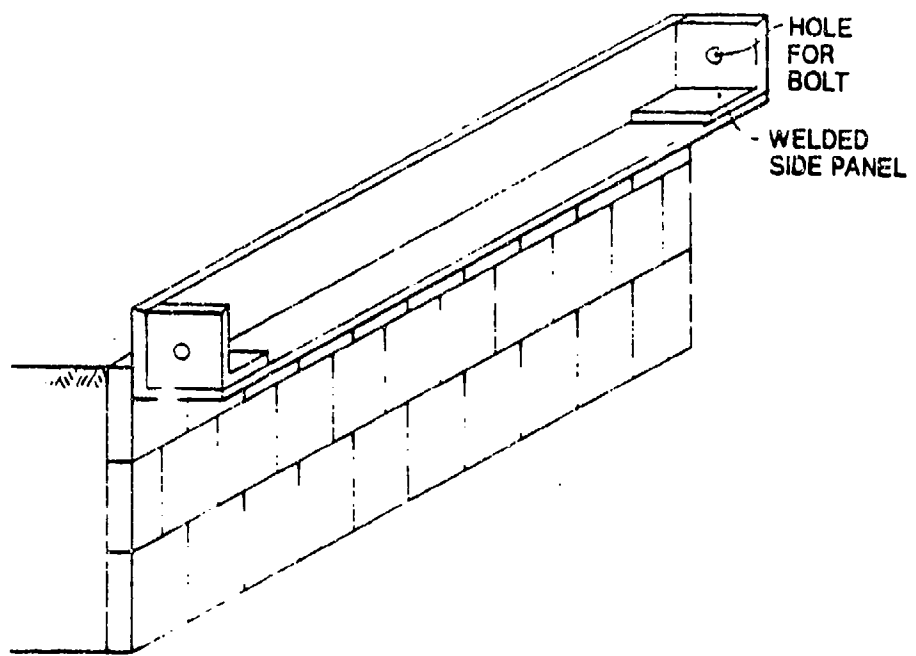


Figure 66. Top Restraint.

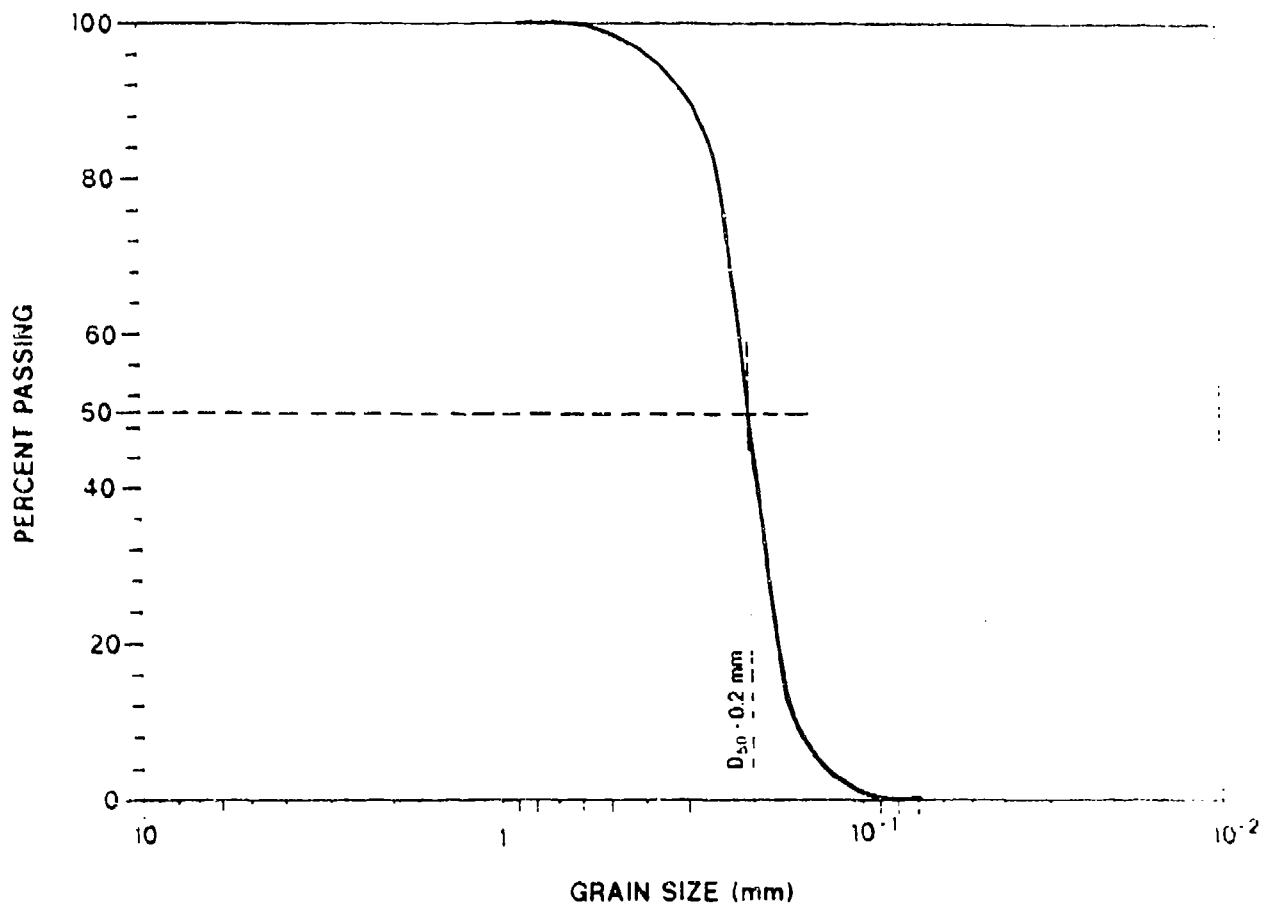


Figure 67. Grain Size Distribution,
Tydall AFB Sand (Reference 76).

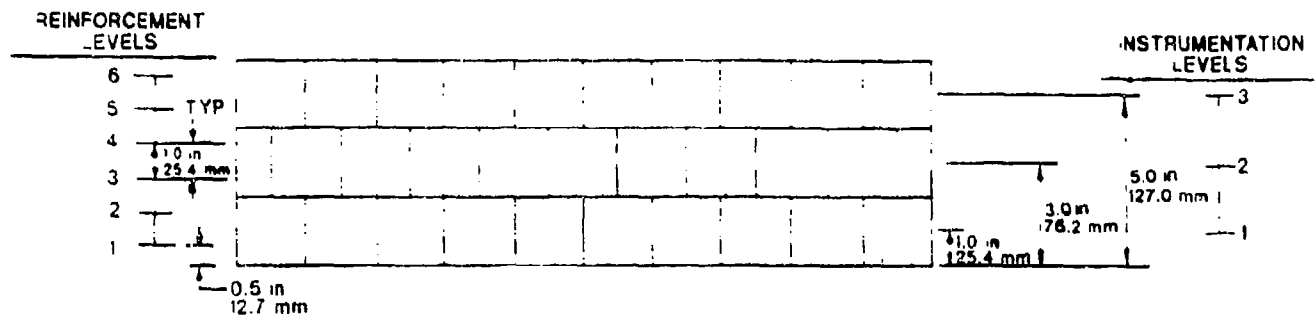
3. Instrumentation

Instrumentation of the model reinforced soil walls included the following:

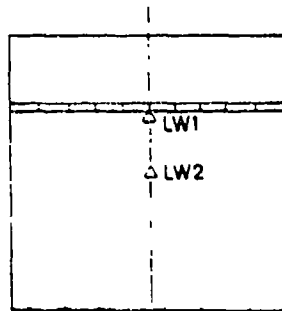
- Resistors: Allen-Bradley industrial grade 1/4-watt 1000 ohm carbon resistors (style RC07 with +/- 5 percent tolerance) were originally used to determine peak stresses and blast wave velocities. Ten resistors were placed at several locations in each model as shown in Table 21 and Figure 68. Voltage time histories obtained from these resistors proved to be of poor quality. A replicate test was conducted using Allen-Bradley Industrial grade 1/8-watt 1,000-ohm carbon resistors (style RC05 with +/- 5 percent tolerance). The quality of the voltage-time histories was greatly improved with these resistors.
- Accelerometers: Endevco series 7270A piezoresistive accelerometers (model 7270A-20K with a range of 20,000 g) were used to measure accelerations at the wall face. Three were used for each model. The accelerometers were glued to the front face of the top center (T6), middle center (M6), and bottom center (B6) facing panels (see Figure 69 and Table 21).

4. Detonator Assembly

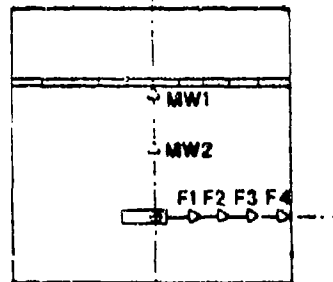
For this study, it was believed that the most important dynamic response to be accurately modeled was wall deflection. This is best accomplished by modeling explosive energy. The heat of detonation of 1 gram (0.0022 pounds) of cyclotrimethylenetrinitramine (RDX) is equal to the heat of detonation of 1.14 gram (0.0025 pounds) of TNT (Reference 77). It was originally intended to accelerate all models to 30 g and to calculate and utilize the mass of RDX required to model the prototype explosive mass. However, the calculated mass of RDX required to accomplish this was not readily available in preassembled detonators. In lieu of manufacturing special detonators for the study, it was decided to utilize in-house detonators, each containing 1 gram (0.0022 pounds) RDX, and to calculate the appropriate g-level required to model the prototype explosive mass. This g-level was calculated as described below.



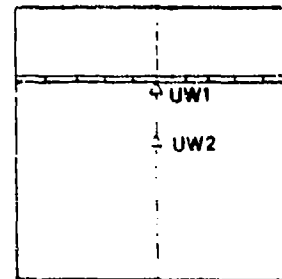
INSTRUMENTATION LEVEL 1
PLAN



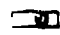
INSTRUMENTATION LEVEL 2
PLAN



INSTRUMENTATION LEVEL 3
PLAN



LEGEND

- Δ RESISTOR
-  DETONATOR ASSEMBLY

NOTE: GAGES F1 - F4 ARE PLACED ALONG THE LONGITUDINAL AXIS OF THE DETONATOR ASSEMBLY.

Figure 68. Resistor Placement.

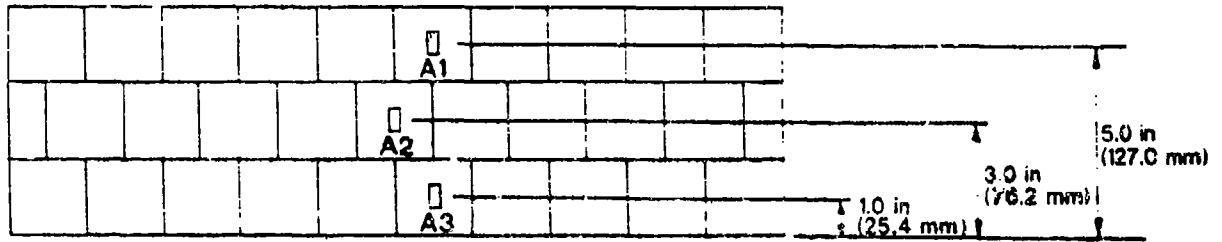


Figure 69. Accelerometer Placement.

TABLE 21. GAGE PLACEMENT

Gage	Horizontal Distance from Detonation Center of Mass to Gage- mm (inch) for Test #:								
	1	2	3	4	5	6	7	8	9
A1	226.1 (8.9)	226.1 (8.9)	226.1 (8.9)	226.1 (8.9)	226.1 (8.9)	226.1 (8.9)	279.4 (11.0)	279.4 (11.0)	162.6 (6.4)
A2	226.1 (8.9)	226.1 (8.9)	226.1 (8.9)	226.1 (8.9)	226.1 (8.9)	226.1 (8.9)	279.4 (11.0)	279.4 (11.0)	162.6 (6.4)
A3	226.1 (8.9)	226.1 (8.9)	226.1 (8.9)	226.1 (8.9)	226.1 (8.9)	226.1 (8.9)	279.4 (11.0)	279.4 (11.0)	162.6 (6.4)
LW1	201.7 (7.9)	206.4 (8.1)	204.7 (8.1)	206.4 (8.1)	204.8 (8.1)	204.8 (8.1)	256.5 (10.1)	259.7 (10.2)	141.3 (5.6)
LW2	63.5 (2.5)	63.5 (2.5)	63.5 (2.5)	63.5 (2.5)	109.2 (4.3)	12.7 (0.5)	116.8 (4.6)	116.8 (4.6)	--- ---
MW1	204.8 (8.1)	204.8 (8.1)	209.6 (8.3)	204.3 (8.1)	204.8 (8.1)	204.8 (8.1)	258.1 (10.2)	258.1 (10.2)	141.3 (5.6)
MW2	63.5 (2.5)	63.5 (2.5)	63.5 (2.5)	63.5 (2.5)	109.2 (4.3)	12.7 (0.5)	116.8 (4.6)	116.8 (4.6)	--- ---
UW1	203.2 (8.0)	208.0 (8.2)	206.4 (8.1)	206.4 (8.1)	208.0 (8.2)	206.4 (8.1)	256.5 (10.1)	258.1 (10.2)	144.5 (5.7)
UW2	63.5 (2.5)	63.5 (2.5)	63.5 (2.5)	63.5 (2.5)	109.2 (4.3)	12.7 (0.5)	116.8 (4.6)	116.8 (4.6)	0.0 (0.0)
F1	76.2 (3.0)	76.2 (3.0)	76.2 (3.0)	76.2 (3.0)	76.2 (3.0)	76.2 (3.0)	76.2 (3.0)	76.2 (3.0)	76.2 (3.0)
F2	127.0 (5.0)	127.0 (5.0)	127.0 (5.0)	127.0 (5.0)	127.0 (5.0)	127.0 (5.0)	127.0 (5.0)	127.0 (5.0)	127.0 (5.0)
F3	177.8 (7.0)	177.8 (7.0)	177.8 (7.0)	177.8 (7.0)	177.8 (7.0)	177.8 (7.0)	177.8 (7.0)	177.8 (7.0)	177.8 (7.0)
F4	228.6 (9.0)	228.6 (9.0)	228.6 (9.0)	228.6 (9.0)	228.6 (9.0)	228.6 (9.0)	228.6 (9.0)	228.6 (9.0)	228.6 (9.0)

For each model, three RISI model RP-83 EBW detonators were used to simulate the prototype explosive event. Each detonator contained 1 gram (0.0022 pounds) RDX. The total mass of explosive for the three detonators was therefore 3 gram (0.0066 pounds) RDX which, in terms of explosive energy, was equal to 3.42 gram (0.0075 pounds) TNT. From the principal of cube root scaling, the relationship between explosive mass of the model and explosive mass of the prototype is defined as follows:

$$\frac{m_p}{n^3} = m_m \quad (2)$$

where m_p = prototype explosive mass, m_m = model explosive mass, n = g-level. Inserting the prototype TNT mass and the model equivalent TNT mass into the above equation resulted in a required g-level of 29.7. This g-level was used in all centrifuge model tests. The dimensions of the model reinforced soil wall were sized for 1:30 scaling. Accelerating the model wall to 29.7 g instead of 30 g resulted in prototype wall dimensions that were 1 percent smaller than intended, a negligible difference.

The detonators were wired together and bundled for placement into the backfill. The lead wires were attached to a Reynolds Firing System FS-17 and were electronically detonated from the control room.

5. Containment Bucket and Bracing Block

A 508 mm (20 inches) long by 508 mm (20 inches) wide by 406 mm (16 inches) deep by 9.5 mm (0.34 in) thick aluminum bucket was utilized to contain the model reinforced soil wall. The bucket mass was 36.3 kg (81 pounds). The reinforced soil wall was constructed against a wood bracing block which insured a uniform airspace between the bucket wall and the face of the reinforced soil wall. This block consisted of a 508 mm (20 inches) length of four by four with a 508 mm (20 inches) length of plywood, 140 mm (5.5 inches) tall by 9.5 mm (0.38 inch) thick, attached (see Figure 70). This block was placed into the sample bucket so that the facing panels of the reinforced soil wall rested against it during construction. Slots were cut into the plywood in the appropriate locations to allow for the thickness of the three accelerometers. The block was removed after fabrication of the wall.

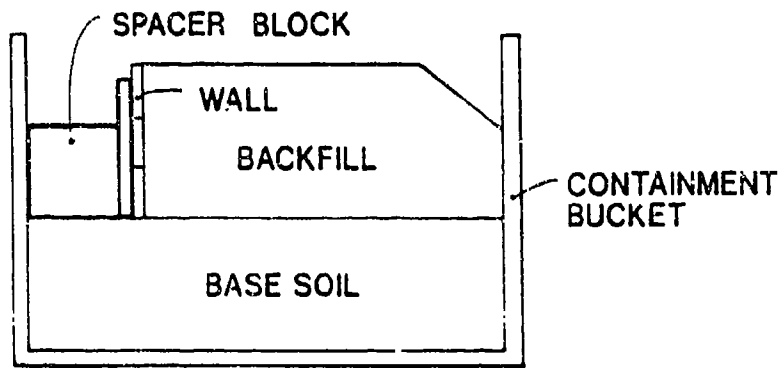
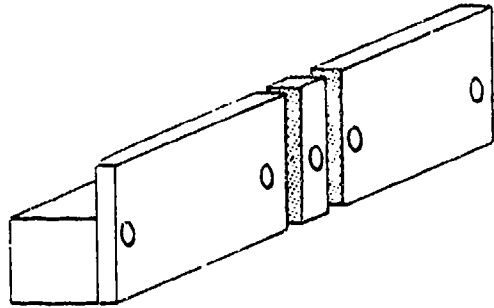


Figure 70. Bracing Block.

E. TEST PROCEDURE

The complete test procedure for each model included four main phases: (1) construction of the model; (2) centrifugation and detonation; (3) data collection and model disassembly; and (4) data reduction. Each phase is described in detail below.

1. Model Construction

For all models, the reinforced soil walls were prepared as follow:

- A 152 mm (6 inch) base of Tyndall AFB sand was pluviated into the containment bucket. The bracing block assembly was placed on the surface of the base against the front wall of the bucket. The levelling pad was set on the surface against the bracing block and gently tapped into the soil with a small mallet until the pad's surface was flush with the surface of the base course.
- The first course of ten facing panels were set on the levelling pad against the bracing block. The reinforcing was temporarily lifted and taped against the bracing block so as not to interfere with the pluviation of the next lift.
- 13 mm (0.5 inch) of sand was pluviated to bring the backfill to the first level of reinforcement. For each panel, the lower level of reinforcement was extended back along the pluviated surface perpendicular to the length of the wall. A small amount of sand was spread over the ends to hold the reinforcing in place. After placement of the entire level of reinforcement, the area was gently hand tamped to densify the soil covering the ends of the reinforcement.
- 13 mm (0.5 inch) of sand was pluviated to bring the backfill to the first level of instrumentation. The appropriate carbon gages were set in place (Table 21, Figure 68). A small amount of sand was spread over the gage wires to hold the resistors in place. The wires were directed out the side of the containment bucket and secured to the outside wall of the bucket with masking tape.

- 13 mm (0.5 inch) of sand was pluviated to bring the backfill to the second level of reinforcement. The second level of reinforcement was placed in the same manner as the first.
- 13 mm (0.5 inch) of sand was pluviated to bring the backfill to the top of the first course of panels. The second course of panels was then ready to be constructed.
- Courses two and three were constructed in the same manner as course one and gages were placed accordingly (Table 21, Figure 68). The detonator assembly was placed at the location of the second level of reinforcing [76 mm (3 inches) above the bottom of the wall], at varying distances from the back face of the wall. The detonator assembly was placed so that the longitudinal axis of the assembly was parallel to the length of the wall and the center of mass of the detonators was a distance of 250 mm (10 inches) from either side of the containment bucket (Figure 68). Sand was poured over the detonator assembly and hand tamped to densify the soil and hold the assembly in place.
- After construction of all courses, the spacer block was carefully removed from the bucket. The calipers and micrometer were utilized to measure the initial airspace (distance between the inside face of the containment bucket and the face of the model wall). This measurement was necessary for later calculation of wall displacements.
- The top restraint was utilized in most models to simulate a roof slab over the structure. The aluminum restraint was placed against the top course of facing panels so that it covered approximately 13 mm (0.5 inch) of the front face of the course. Approximately 25 mm (1 inch) of the restraint extended above the top of the completed wall. This allowed for the pluviation of an additional 25 mm (1 inch) of sand above the wall to act as overburden. The restraint was bolted to the sides of the containment bucket to hold it in place.

- A berm was constructed at the back of the model in most samples, as shown in Figure 71. This modeled the sloping backfill that would be placed over a prototype protective structure.

A photographic series of the complete construction of a model reinforced soil wall is included in Volume 2, Appendix C.

2. Centrifugation

The completed sample was weighed and hoisted by crane onto the centrifuge platform and bolted in place. Counterweights were placed on the opposing platform to balance the arm. All instrumentation was wired to the on-board transient data recorder (TDR) and the buried detonator assembly was wired to the firing system.

After the centrifuge was evacuated and all hatches were closed and secured, the centrifuge was accelerated to a predetermined g-level. A hand held trigger was used to detonate the explosive in most tests. Four tests utilized the high speed camera to film the event. For these tests the camera was hooked to the FS-17 Firing System and triggering occurred automatically when a pre-established film speed (ie: frames/sec) was achieved. All tests were videotaped. After detonation the centrifuge was decelerated.

3. Data Collection and Model Disassembly

After completion of a test, all resistor and accelerometer data were downloaded from the on-board TDR to a Compaq 386/25 personal computer with twin 40 MB Bernoulli drives. The software program ASYST was utilized for data reduction and manipulation.

While still mounted on the centrifuge platform, the post-flight model was photographed. Calipers and a digital micrometer were used to measure the final air space (distances between inside face of the containment bucket and the deflected panels). These measurements were taken at the four corners ("nodes") of each panel for a total of 124 measurements per wall (31 panels X 4 nodes/panel). These measurements were used to calculate wall displacements.

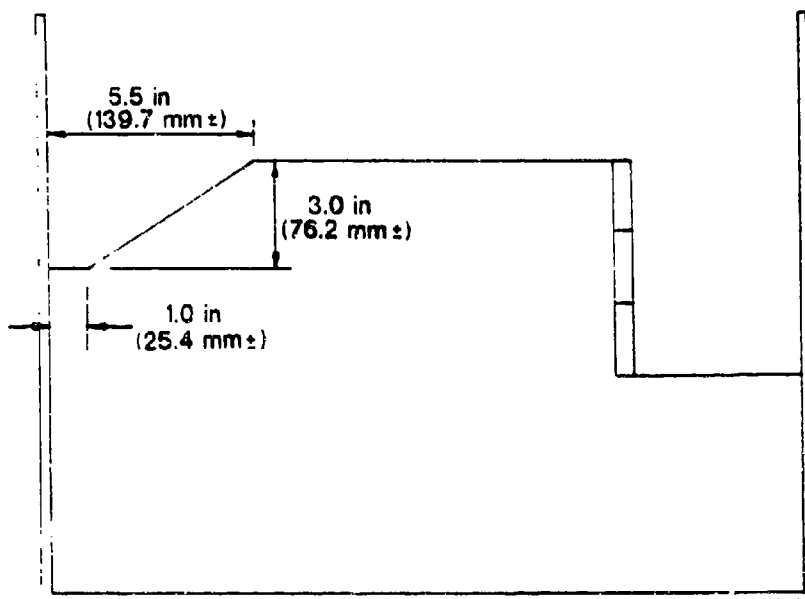


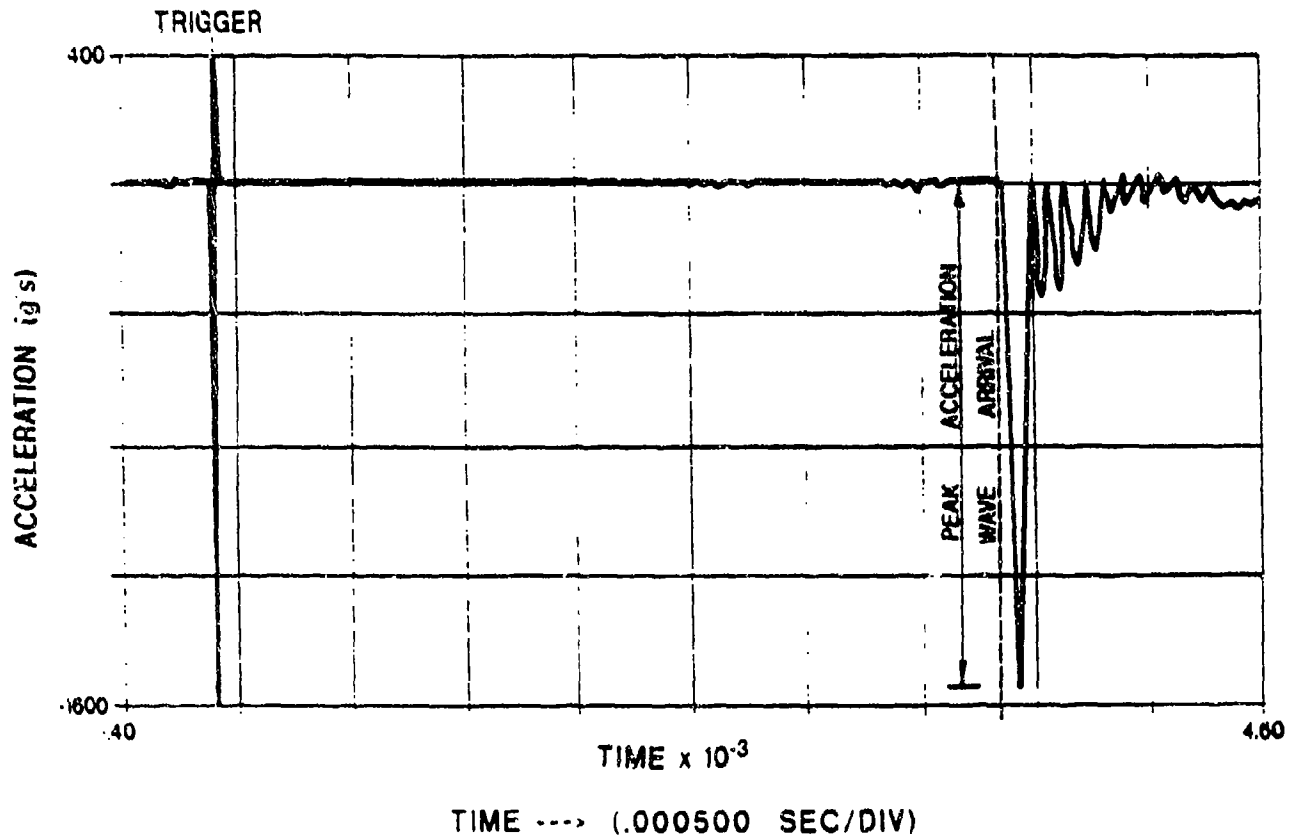
Figure 71. Berm.

After all data were collected, the model was hoisted out of the centrifuge and disassembled. Additional photographs were taken when necessary. Undamaged facing panels and reinforcing were reused in later tests.

4. Data Reduction

Data collected for each centrifuge test conducted consisted of the following: (1) an acceleration-time history for each accelerometer; (2) a voltage-time history for each resistor; and (3) measured deflections for all panel nodes. This information was reduced to obtain estimates of peak facing panel accelerations, peak blast wave pressures, blast wave velocities and wall displacements. The data were reduced as follows:

- Peak acceleration: Peak panel accelerations were taken directly from the acceleration-time histories (see Figure 72).
- Peak pressure: Values of peak voltage were taken directly from the voltage-time histories (see Figure 73). Peak pressures were obtained from the pressure-voltage calibration curve shown in Figure 74 (Reference 78). The curve was prepared by loading several small cylindrical soil specimens, each containing a 1/8 watt resistor, in a load cell. Load and voltage were recorded simultaneously and the loads were divided by cross sectional area of the specimen to obtain pressures. The pressure data obtained from the centrifuge testing are based on the replicate test conducted with 1/8 watt resistors.
- Wave velocity: Stress wave velocities were calculated by dividing the distance traveled (distance between detonator and instrumentation) by the wave arrival time using both voltage-time and acceleration-time histories. Wave velocities calculated with resistor data are based on the replicate test conducted with 1/8 watt resistors.
- Wall displacements: Nodal displacements were calculated by subtracting the final air space (distance from the inner face of the containment bucket to panel node after detonation) from the initial air space (distance from the inner face of the containment bucket to panel node before detonation). Average panel displacements were determined by averaging the displacements of the four nodes.

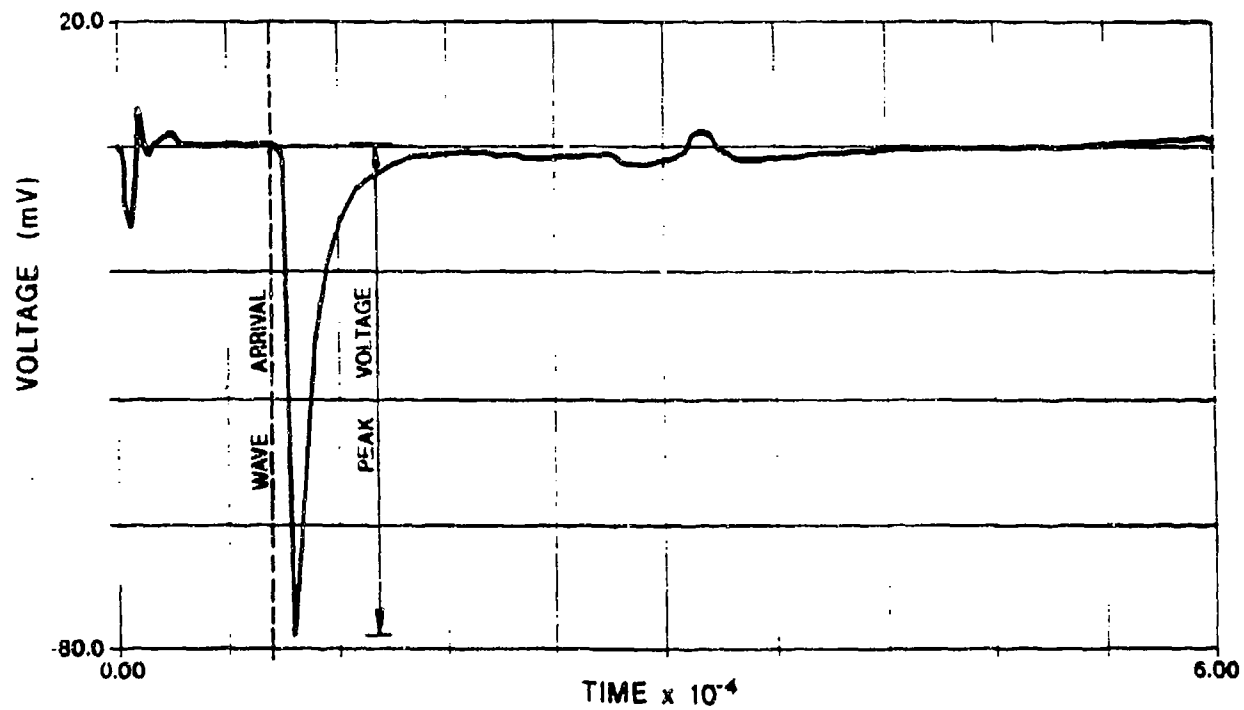


A-2 TRIGGER OCCURRED 14.561820 SECONDS AFTER START

LEGEND:

A-2

Figure 72. Acceleration-Time History



TIME ----> (.0000060 SEC/DIV)

R2 TRIGGER OCCURRED 8.621700 SECONDS AFTER START

LEGEND:

R2

Figure 73. Voltage-Time History.

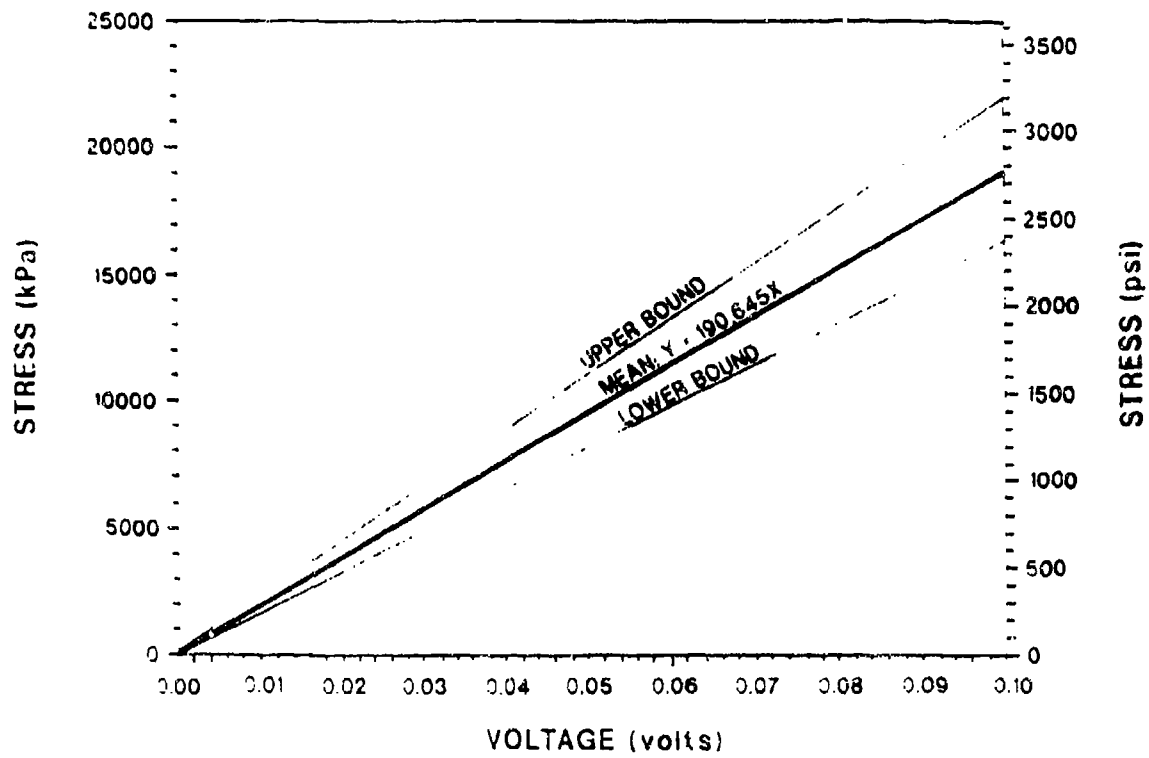


Figure 74. Pressure-Voltage Calibration Curve (Reference 78).

Average total wall displacements (ATWD) were determined by averaging the displacements (ATWD) were determined by averaging the displacements of the 31 panels.

The collected data for all production runs were reduced as described above. A summary of the reduced data is presented in Section VI-G of this report.

F. PRELIMINARY TESTS

Four preliminary tests (PRE1,2,3, and 4) were conducted on model reinforced soil walls containing steel strip reinforcement. For all preliminary tests, steel reinforcing 4 mm (0.016 inch) wide by 152 mm (6.0 inches) long was utilized. All detonators were located at a depth of 76 mm (3 inches) above the bottom of the wall. Variable test parameters are presented in Table 22. The purpose of preliminary testing was to observe the response of the walls to the blast loading and to make any necessary modifications and improvements to the wall components and/or wall construction technique.

TABLE 22. PRELIMINARY TEST PARAMETERS.

Test Parameter:	Preliminary Test #:			
	PRE1	PRE2	PRE3	PRE4
Detonator location (dist. behind wall)	203 mm (8.0 in.)	203 mm (8.0 in.)	216 mm (8.5 in.)	216 mm (8.5 in.)
soil compaction method	hand tamping	hand tamping	Tyndall tamping	Tyndall tamping
interlocking panels	no	no	yes	yes
top restraint	no	no	yes	yes
overburden	no	no	yes	yes
berm	no	no	yes	yes

Tests PRE1 and PRE2 resulted in the breaching of both walls during the blast loading. After careful examination of the failed walls, the following modifications were made for implementation in all subsequent walls in an effort to improve their structural integrity and performance:

- The interlocking panel design was developed for use in all subsequent models.
- Utilization of the top restraint was developed.
- Construction of the berm, which would model the sloping backfill of the prototype structure, was developed.
- The detonator assembly was relocated from 203 mm (8.0 inches) to 216 mm (8.5 inches) behind the back face of the wall.
- Placement of lifts for all subsequent models would be done utilizing the Tyndall pluviator to obtain uniform and reproducible soil densities. A square perforated plate and shutter were constructed for the pluviator to accommodate the shape of the model containment bucket.

The above modifications were implemented in the two remaining preliminary tests (PRE3 and PRE4). Wall response for both showed improvement and neither wall was breached from the blast loading. A method of measuring wall deflection was required and the utilization of calipers and a digital micrometer was proposed for all subsequent tests. The wall design, construction technique, and deflection measurement technique were then rendered satisfactory for commencement of the production tests.

G. PRODUCTION TESTS

A total of nine production tests were conducted on the centrifuge to study the response of model reinforced soil walls to dynamic loading. The production run test matrix is presented in Table 23. Pertinent test data are presented in Section VI-G-1 of this report. These data were used to conduct four comparative studies in which the centrifuge test results were compared to the following:

- Comparison 1: to predicted results
- Comparison 2: to each other
- Comparison 3: to numerical model results
- Comparison 4: to full scale model results

The results of these comparative studies are presented in Section VI-G-2 of this report.

TABLE 23. PRODUCTION RUN TEST MATRIX.

Test #	Wall Type	Rein. Length mm (in.)	Charge Location mm (in.)	Top Restraint	Overburden	Berm
1	Geogrid	152.4 (6.0)	215.9 (8.5)	•	•	•
2	4 mm steel	152.4 (6.0)	215.9 (8.5)	•	•	•
3	Geogrid	152.4 (6.0)	215.9 (8.5)			•
4	8 mm steel	152.4 (6.0)	215.9 (8.5)	•	•	•
5	Geogrid	106.7 (4.2)	215.9 (8.5)	•	•	•
6	Geogrid	203.2 (8.0)	215.9 (8.5)	•	•	•
7	Geogrid	152.4 (6.0)	269.2 (10.6)	•		
8	Geogrid	152.4 (6.0)	269.2 (10.6)	•		
9	Geogrid	152.4 (6.0)	152.4 (6.0)	•		

1. Presentation of Data

Test data utilized in the comparative analyses were:

- peak facing panel accelerations
- peak wave pressures
- wave velocity
- model wall displacements

These data are presented in Tables 24 through 27.

TABLE 24. PEAK PANEL ACCELERATIONS.

Test #	Location	Distance		Peak Panel Acceleration g's	
		Model mm (in.)	Prototype m (ft) ^a	Model	Prototype ^b
1	Top Ctr.	215.9 (8.5)	6.5 (21.3)	2209	74
	Mid. Ctr.	215.9 (8.5)	6.5 (21.3)	1504	50
	Bot. Ctr.	215.9 (8.5)	6.5 (21.3)	2378	79
2	Top Ctr.	215.9 (8.5)	6.5 (21.3)	4405	147
	Mid. Ctr.	215.9 (8.5)	6.5 (21.3)	3371	112
	Bot. Ctr.	215.9 (8.5)	6.5 (21.3)	5451	182
3	Top Ctr.	215.9 (8.5)	6.5 (21.3)	-	-
	Mid. Ctr.	215.9 (8.5)	6.5 (21.3)	1691	56
	Bot. Ctr.	215.9 (8.5)	6.5 (21.3)	3955	132
4	Top Ctr.	215.9 (8.5)	6.5 (21.3)	4392	146
	Mid. Ctr.	215.9 (8.5)	6.5 (21.3)	2888	96
	Bot. Ctr.	215.9 (8.5)	6.5 (21.3)	4485	150
5	Top Ctr.	215.9 (8.5)	6.5 (21.3)	2694	90
	Mid. Ctr.	215.9 (8.5)	6.5 (21.3)	1592	53
	Bot. Ctr.	215.9 (8.5)	6.5 (21.3)	2719	91
6	Top Ctr.	215.9 (8.5)	6.5 (21.3)	2260	75
	Mid. Ctr.	215.9 (8.5)	6.5 (21.3)	1340	45
	Bot. Ctr.	215.9 (8.5)	6.5 (21.3)	3579	119
7	Top Ctr.	269.2 (10.6)	8.2 (26.5)	447	15
	Mid. Ctr.	269.2 (10.6)	8.2 (26.5)	582	19
	Bot. Ctr.	269.2 (10.6)	8.2 (26.5)	1130	38
8	Top Ctr.	269.2 (10.6)	8.2 (26.5)	281	9
	Mid. Ctr.	269.2 (10.6)	8.2 (26.5)	-	-
	Bot. Ctr.	269.2 (10.6)	8.2 (26.5)	836	28
9	Top Ctr.	152.4 (6.0)	4.6 (15.0)	3907	130
	Mid. Ctr.	152.4 (6.0)	4.6 (15.0)	7379	246
	Bot. Ctr.	152.4 (6.0)	4.6 (15.0)	10,877	363

- ^a Centrifuge distances scaled to 1-g
- ^b Centrifuge Accelerations scaled to 1-g

TABLE 25. PEAK WAVE PRESSURES.

Distance		Pressure ^a kPa (psi) (Model and Prototype)
Model - mm (in.)	Prototype ^a - m (ft)	
63.5 (2.5)	1.9 (6.3)	14,786 (2146)
76.2 (3.0)	2.3 (7.5)	13,504 (1960)
101.6 (4.0)	3.0 (10.0)	--
114.3 (4.5)	3.4 (11.3)	4789 (695)
127.0 (5.0)	3.8 (12.5)	3996 (580)
177.8 (7.0)	5.3 (17.5)	1436 (207)
203.2 (8.0)	6.1 (20.0)	713 (103)
215.9 (8.5)	6.5 (21.3)	1068 (155)
228.6 (9.0)	6.9 (22.5)	909 (132)

^a Centrifuge distances scaled to 1-g

^b Model Pressures scale as 1 with prototype pressures

TABLE 26. WAVE VELOCITIES.

Distance		Velocity ^b mps (fps)
Model mm (in.)	Prototype ^b m (ft.)	
63.5 (2.5)	1.9 (6.3)	747 (2451)
76.2 (3.0)	2.3 (7.5)	1088 (3571)
101.6 (4.0)	3.0 (10.1)	668 (2193)
114.3 (4.5)	3.4 (10.3)	762 (2500)
127.0 (5.0)	3.8 (12.5)	847 (2778)
162.6 (6.4)	4.8 (16.0)	613 (2011)
177.8 (7.0)	5.3 (17.5)	651 (2137)
203.2 (8.0)	6.1 (20.0)	549 (1802)
215.9 (8.5)	6.5 (21.3)	590 (1935)
228.1 (8.9)	6.8 (22.3)	500 (1639)
228.6 (9.0)	6.9 (22.5)	534 (1753)
279.4 (11.0)	8.4 (27.5)	425 (1395)
AVG		665 (2180)

^a Centrifuge distances scaled to 1-g

^b Model Pressures scale as 1 with prototype pressures

TABLE 27. MEASURED PANEL DISPLACEMENTS.

Panel	Displacement- mm (in.) for Test #:								
	1	2	3	4	5	6	7	8	9
B1	2.46 (0.10)	4.99 (0.20)	3.61 (0.14)	5.18 (0.20)	4.54 (0.18)	5.39 (0.21)	4.75 (0.19)	4.72 (0.19)	6.82 (0.27)
B2	3.80 (0.15)	6.97 (0.27)	4.51 (0.18)	7.40 (0.29)	5.68 (0.22)	6.20 (0.24)	6.79 (0.27)	4.77 (0.19)	8.66 (0.34)
B3	5.21 (0.21)	8.77 (0.35)	5.26 (0.21)	7.49 (0.30)	6.96 (0.27)	7.33 (0.29)	6.91 (0.27)	6.29 (0.25)	12.40 (0.49)
B4	8.86 (0.35)	16.81 (0.66)	8.66 (0.34)	11.63 (0.46)	9.60 (0.38)	9.45 (0.37)	7.54 (0.30)	7.50 (0.30)	18.05 (0.71)
B5	11.98 (0.47)	22.35 (0.88)	12.09 (0.48)	15.42 (0.61)	12.74 (0.50)	13.46 (0.53)	9.32 (0.37)	8.55 (0.34)	27.41 (1.08)
B6	9.89 (0.39)	26.70 (1.05)	11.52 (0.45)	15.82 (0.62)	13.59 (0.54)	13.31 (0.52)	9.37 (0.37)	8.69 (0.34)	27.33 (1.08)
B7	6.80 (0.27)	20.38 (0.80)	8.78 (0.35)	13.09 (0.52)	9.79 (0.39)	10.45 (0.41)	8.22 (0.32)	7.38 (0.29)	18.35 (0.72)
B8	4.04 (0.16)	13.42 (0.53)	5.40 (0.21)	8.21 (0.32)	7.07 (0.28)	7.27 (0.29)	6.31 (0.25)	5.73 (0.23)	12.19 (0.48)
B9	2.19 (0.09)	9.35 (0.37)	3.66 (0.14)	6.05 (0.24)	6.31 (0.25)	4.84 (0.19)	5.85 (0.23)	4.62 (0.18)	7.26 (0.29)
B10	0.67 (0.03)	3.02 (0.12)	1.23 (0.05)	3.17 (0.12)	3.13 (0.12)	2.71 (0.11)	2.95 (0.12)	1.77 (0.07)	3.15 (0.12)
M1	10.48 (0.41)	5.02 (0.20)	2.88 (0.11)	4.41 (0.17)	5.42 (0.21)	5.43 (0.21)	4.74 (0.19)	4.65 (0.18)	2.51 (0.10)
M2	12.83 (0.51)	8.81 (0.35)	5.61 (0.22)	6.52 (0.26)	7.90 (0.31)	5.52 (0.22)	7.39 (0.29)	6.03 (0.24)	5.80 (0.23)
M3	15.50 (0.61)	13.24 (0.52)	8.37 (0.33)	8.92 (0.35)	9.15 (0.36)	6.92 (0.27)	9.00 (0.35)	7.26 (0.29)	9.35 (0.37)
M4	18.47 (0.73)	18.61 (0.73)	11.75 (0.46)	12.20 (0.48)	11.98 (0.47)	9.12 (0.36)	10.08 (0.40)	9.42 (0.37)	17.48 (0.69)
M5	14.47 (0.57)	28.21 (1.11)	20.20 (0.80)	17.92 (0.71)	15.49 (0.61)	14.01 (0.55)	10.88 (0.43)	11.63 (0.46)	34.24 (1.35)
M6	17.09 (0.67)	33.06 (1.30)	24.76 (0.97)	23.07 (0.91)	18.48 (0.73)	16.43 (0.65)	12.33 (0.49)	12.00 (0.47)	Breach
M7	13.58 (0.53)	28.70 (1.13)	20.47 (0.81)	19.00 (0.75)	16.78 (0.66)	13.72 (0.54)	11.51 (0.45)	10.50 (0.41)	41.47 (1.63)
M8	9.12 (0.36)	21.19 (0.83)	13.04 (0.51)	14.14 (0.56)	12.66 (0.50)	10.18 (0.40)	9.59 (0.38)	8.53 (0.34)	23.30 (0.92)

TABLE 27. MEASURED PANEL DISPLACEMENTS. (CONCLUDED)

Panel	Displacement- mm (in.) for Test #:								
	1	2	3	4	5	6	7	8	9
M9	6.21 (0.24)	13.71 (0.54)	7.26 (0.29)	8.99 (0.35)	8.48 (0.33)	6.51 (0.26)	7.19 (0.28)	6.14 (0.24)	10.09 (0.40)
M10	2.76 (0.11)	7.38 (0.29)	3.12 (0.12)	5.69 (0.22)	6.31 (0.25)	3.99 (0.16)	5.16 (0.20)	3.98 (0.16)	4.09 (0.16)
M11	0.60 (0.02)	2.46 (0.10)	0.41 (0.02)	3.58 (0.14)	3.85 (0.15)	2.41 (0.09)	2.81 (0.11)	1.87 (0.07)	0.91 (0.04)
T1	0.64 (0.03)	4.26 (0.17)	3.81 (0.15)	4.43 (0.17)	4.77 (0.19)	2.53 (0.10)	4.22 (0.17)	3.40 (0.13)	0.15 (0.01)
T2	0.30 (0.01)	4.87 (0.19)	7.33 (0.29)	4.29 (0.17)	5.19 (0.20)	2.29 (0.09)	5.74 (0.23)	4.04 (0.16)	1.47 (0.06)
T3	-1.07 (-0.04)	5.50 (0.22)	13.80 (0.54)	4.83 (0.19)	5.85 (0.23)	2.01 (0.08)	6.48 (0.26)	4.41 (0.17)	2.36 (0.09)
T4	0.99 (0.04)	5.60 (0.22)	25.11 (0.99)	5.42 (0.21)	6.36 (0.25)	2.97 (0.12)	6.26 (0.25)	5.60 (0.22)	Breach
T5	1.61 (0.06)	5.77 (0.23)	Breach	5.81 (0.23)	6.43 (0.25)	2.81 (0.11)	5.30 (0.21)	5.89 (0.23)	Breach
T6	1.68 (0.07)	5.25 (0.21)	Breach	4.69 (0.18)	6.37 (0.25)	2.91 (0.11)	5.21 (0.21)	5.08 (0.20)	Breach
T7	1.01 (0.04)	4.23 (0.17)	20.08 (0.79)	3.52 (0.14)	5.88 (0.23)	2.51 (0.10)	4.00 (0.16)	3.00 (0.12)	Breach
T8	-1.87 (-0.07)	3.08 (0.12)	11.47 (0.45)	1.95 (0.08)	4.45 (0.18)	0.83 (0.03)	2.70 (0.11)	1.86 (0.07)	-1.16 (-0.05)
T9	-2.64 (-0.10)	1.45 (0.06)	4.06 (0.16)	0.60 (0.02)	1.87 (0.07)	-0.13 (-0.00)	2.07 (0.08)	0.91 (0.04)	-3.28 (-0.13)
T10	-3.70 (-0.15)	-0.17 (-0.01)	0.97 (0.04)	0.14 (0.01)	1.63 (0.06)	-1.01 (-0.04)	0.33 (0.01)	-0.61 (-0.02)	-4.60 (-0.18)
ATWD*	5.61 (0.22)	11.39 (0.45)	10.56 (0.42)	8.18 (0.32)	7.89 (0.31)	6.21 (0.24)	6.48 (0.26)	5.66 (0.22)	10.83 (0.43)

* ATWD = Average Total Wall Displacement

A compilation of the collected data, as well as a photographic series of pre- and posttest models are presented in Volume 2, Appendix C.

2. Comparative Studies

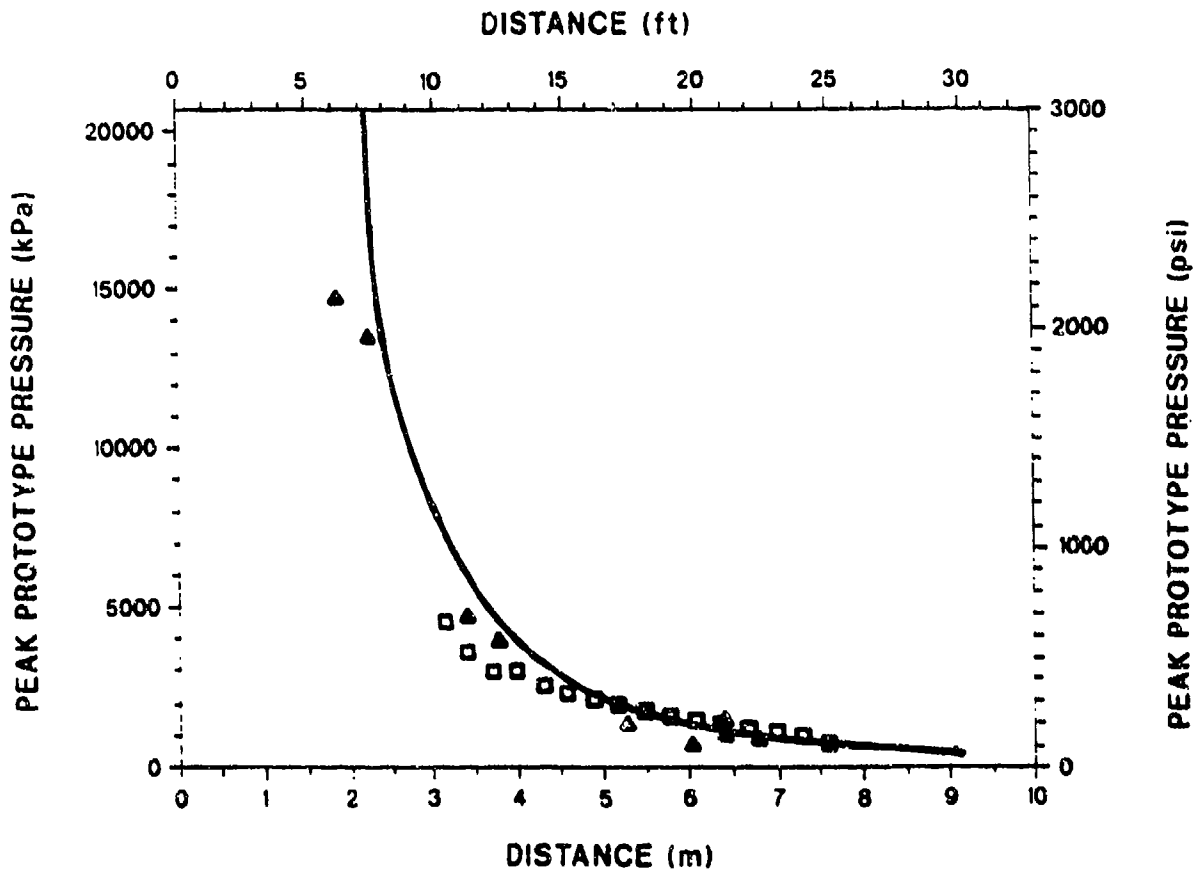
The data from Tables 24 through 27 above were utilized in the preparation of the four comparative studies. The results of these studies are presented below.

a. Comparison 1: Centrifuge Model Results to Expected Values

Peak pressures and accelerations obtained from the centrifuge were compared to those predicted with ConWep, a computer program which calculates the effects of conventional weapons based on the equations and curves of TM 5-855-1, Fundamentals of Protective Design for Conventional Weapons [Reference 79]. The results of the comparison are presented in Figures 75 and 76.

Figure 75 presents a plot of peak pressure versus prototype distance from the detonator. Pressures from numerical modeling results are also shown in the figure and are discussed in Section VI-G-2-c. Centrifuge distances are scaled to their equivalent prototype dimensions ($\text{dist}_{\text{prototype}} = \text{dist}_{\text{model}} \times n$). Peak pressures measured in the centrifuge are also representative of prototype pressures since model pressure scales as 1 with prototype pressure (refer to Table 18). The plot indicates that pressures obtained from centrifuge modeling agree well with the pressures predicted by ConWep, especially at prototype distances greater than 15 feet.

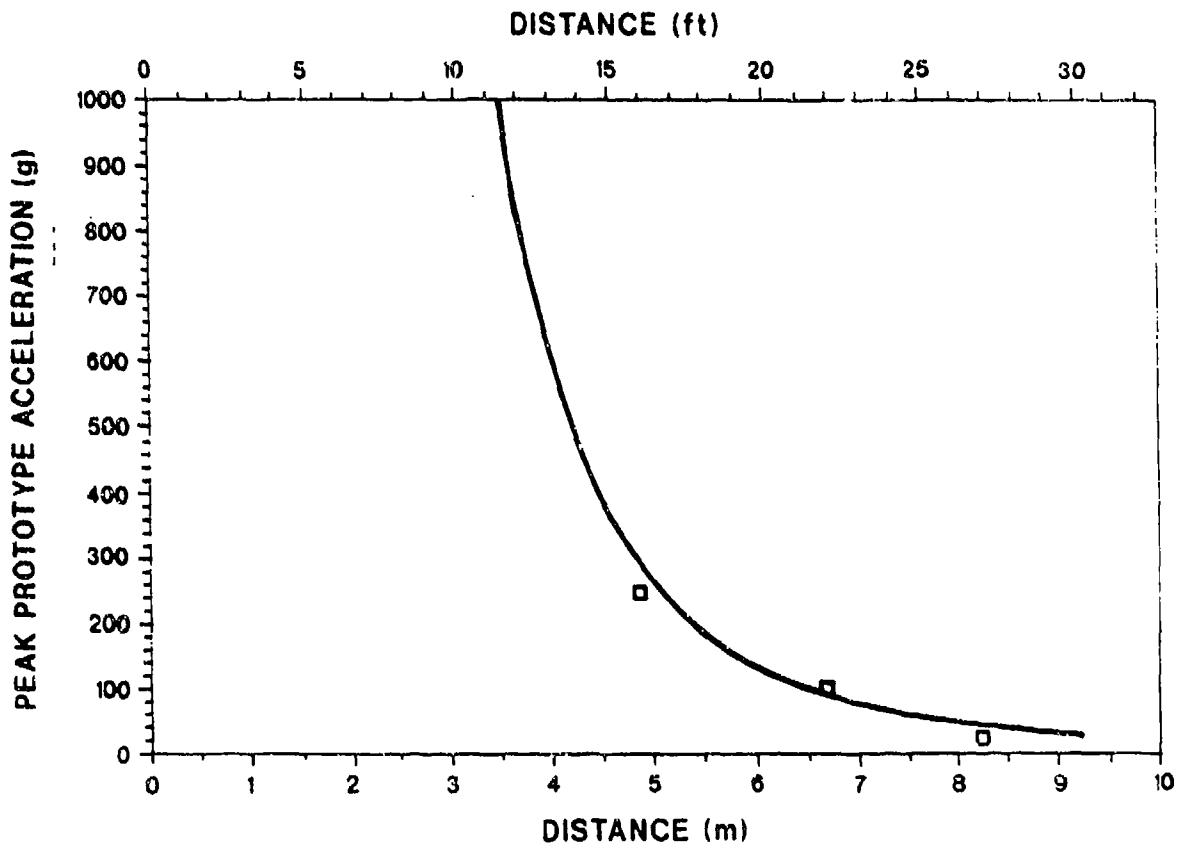
Figure 76 presents a plot of peak panel acceleration versus distance. Again, centrifuge distances are scaled to their equivalent prototype distances. Centrifuge accelerations are also scaled to their equivalent prototype accelerations ($\text{accel}_{\text{prototype}} = \text{accel}_{\text{model}}/n$). Each centrifuge acceleration data point shown on the plot is equal to the average acceleration of the top, middle, and bottom center panels of the model reinforced soil wall at a given distance from the charge. The plot indicates that peak panel acceleration is related to detonator location in much the same way as peak soil accelerations.



LEGEND

- CONWEP DATA
- ▲ CENTRIFUGE DATA (SCALED TO PROTOTYPE DISTANCES)
- NUMERICAL MODELING DATA

Figure 75. Peak Pressure vs. Distance (Prototype).



LEGEND

- CONWEP DATA-PEAK SOIL ACCELERATION
- CENTRIFUGE DATA-PEAK PANEL ACCELERATION (SCALED TO PROTOTYPE)

Figure 76. Peak Acceleration vs. Distance (Prototype).

b. Comparison 2: Centrifuge Model Results to Each Other

The parameters selected for the production run test matrix were chosen so that several studies could be conducted within the centrifuge modeling test program. These studies were:

- reproducibility of test results;
- effects of reinforcement length;
- effects of reinforcement width;
- effects of reinforcement type;
- effects of the top restraint; and
- effects of charge location.

The results of these studies are presented below and are based primarily on measured wall displacements (Table 27) and visual observations of the deformed walls (refer to perspective drawings- Figures 77 - 85).

- Reproducibility of test results:

Tests 7 and 8 were replicate geogrid walls. Test parameters for both are listed in Table 23. Analysis of the test data indicates that the wall response in Tests 8 adequately reproduces the wall response in Test 7 based on ATWD (summarized below from Table 27), average panel displacements (Table 27), and deformed wall geometry (Figures 83, 84).

Test #	ATWD mm (in)
7	6.48 (0.26)
8	5.66 (0.22)

The difference in ATWD between the two tests [0.82 mm (0.04 inch)] is small and is attributed to normal random variation of results (due to subtle variations in sample preparation, human error in measuring displacements, and limited tolerance of measuring device). Additional replicate testing would

be necessary to allow statistical analysis of this random variation. It should be noted that ATWDs of Tests 1 and 6 are also similar to those of Tests 7 and 8; however, the deformed shapes and average panel displacements of these tests are dissimilar. Based on these limited tests results, wall response to dynamic loading appears to be reproducible in the centrifuge.

- Effects of reinforcement length

To study the effects of reinforcement length, three tests were conducted using various lengths of geogrid reinforcement. These were: Tests 1: 152 mm (6 inches) geogrid (1 x wall height), Test 5: 107 mm (4.2 inches) geogrid (0.7 x wall height), and Test 6: 203 mm (8 inches) (1.33 x wall height). All other test parameters were equal. Analyses of the test data indicate that there is significantly more wall displacement when the shortest reinforcing is used than when either of the two longer reinforcing is used.

Test #	Reinforcing Length mm (in.)	ATWD mm (in.)
1	152.4 (6.0)	5.61 (0.22)
5	106.7 (4.2)	7.89 (0.31)
6	203.2 (8.0)	6.21 (0.24)

ATWD for Test 5 is 27 percent to 41 percent larger than those for Tests 6 and 1. The differences in ATWD for Tests 1 and 6 are small and are attributed to natural random variation of results. Replicate testing would be necessary to confirm this. Similar trends were noticed for reinforced soil wall defamations due to static loading (Reference 80) (i.e., there exists a minimum reinforcement length above which there is little change in deformation, and below which deformations increase drastically). The shorter the reinforcement length, the smaller the contact area between soil and reinforcement so that the large ATWD of Test 5 is probably due to inadequate development of interface friction between soil and reinforcing. These limited results indicate that reinforcement length is a factor in wall response to dynamic loading only if the length falls below the minimum length required for static stability. Above this minimum length, there is little change in wall deformation.

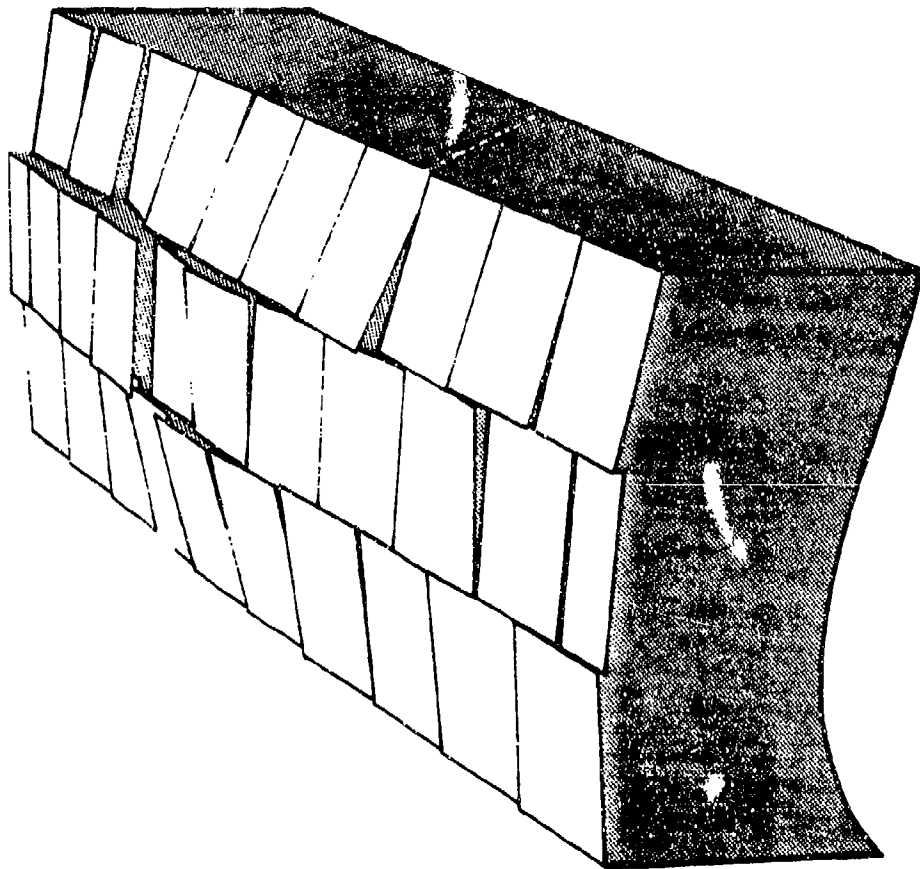


Figure 77. Deformed Wall Geometry: Test 1.

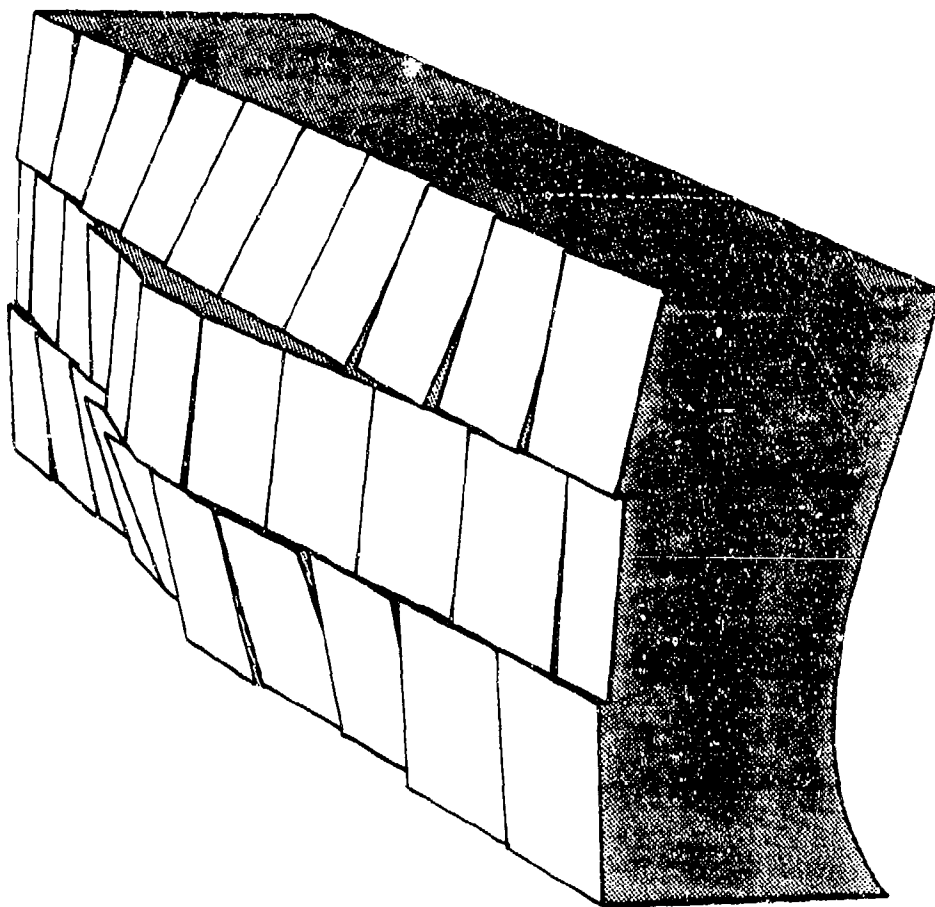


Figure 78. Deformed Wall Geometry: Test 2.

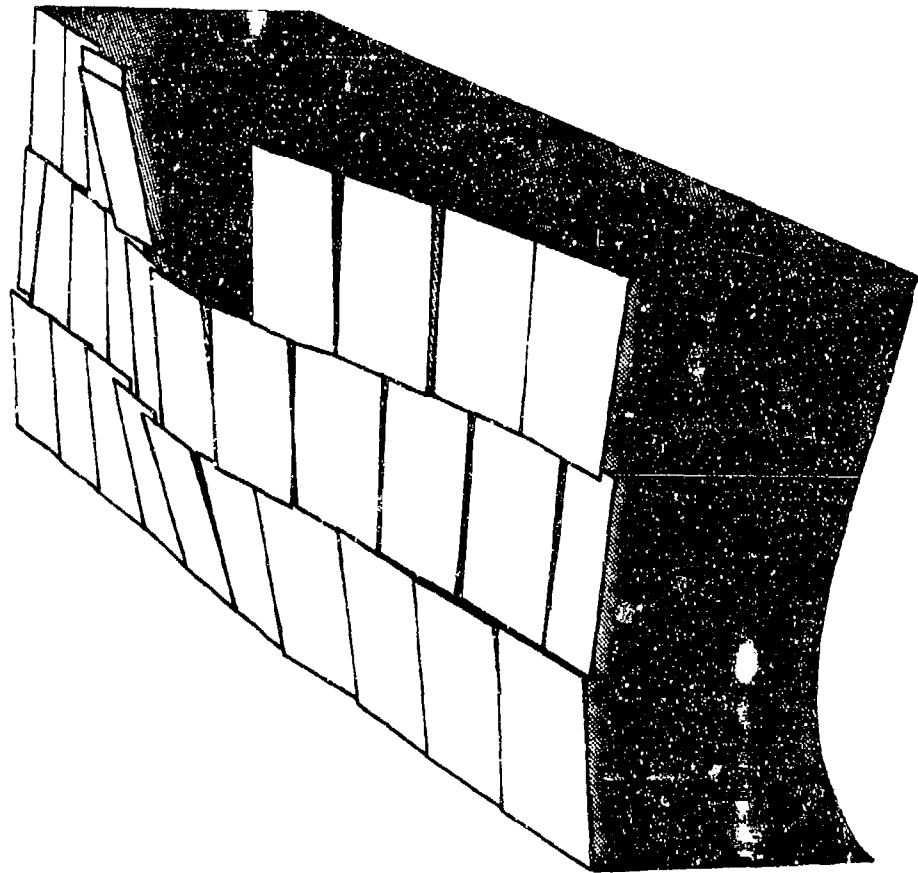


Figure 79. Deformed Wall Geometry: Test 3.

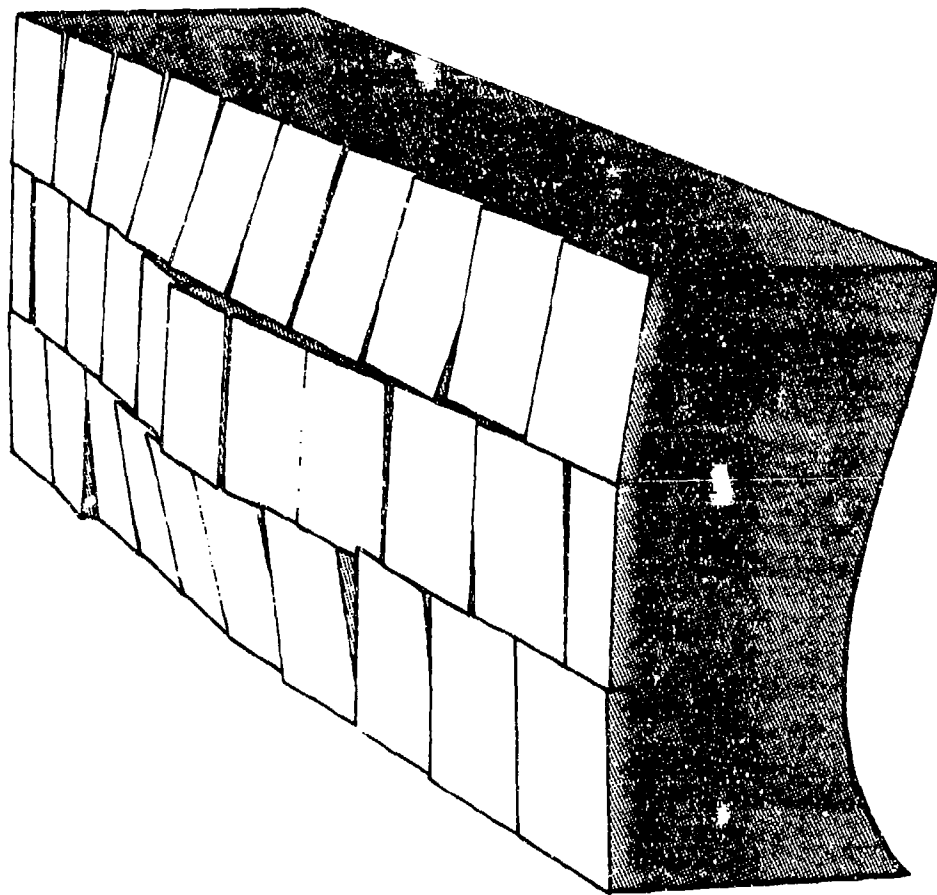


Figure 80. Deformed Wall Geometry: Test 4.

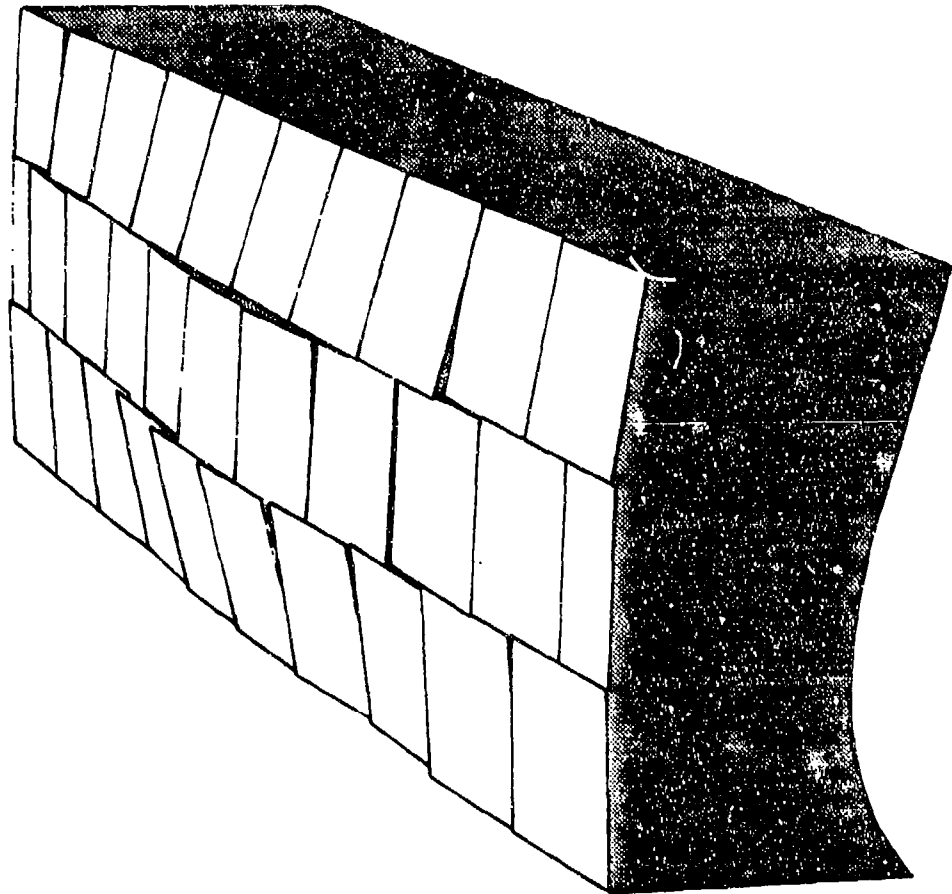


Figure 81. Deformed Wall Geometry: Test 5.

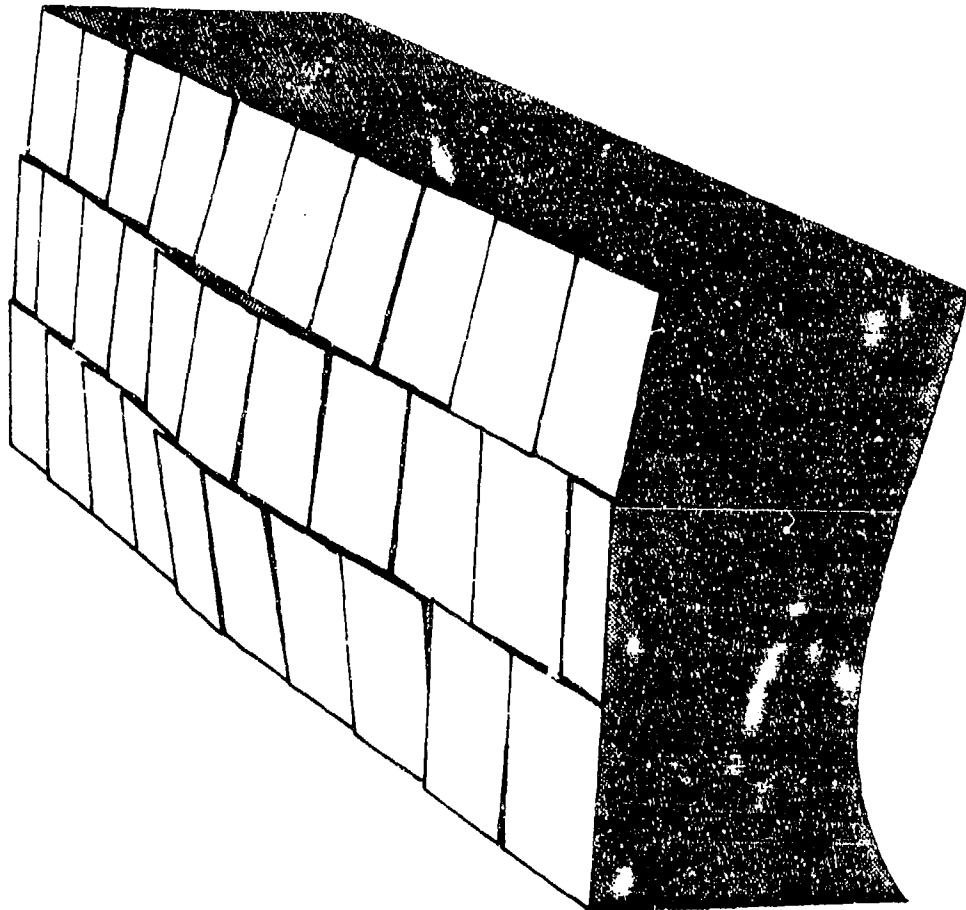


Figure 82. Deformed Wall Geometry: Test 6.

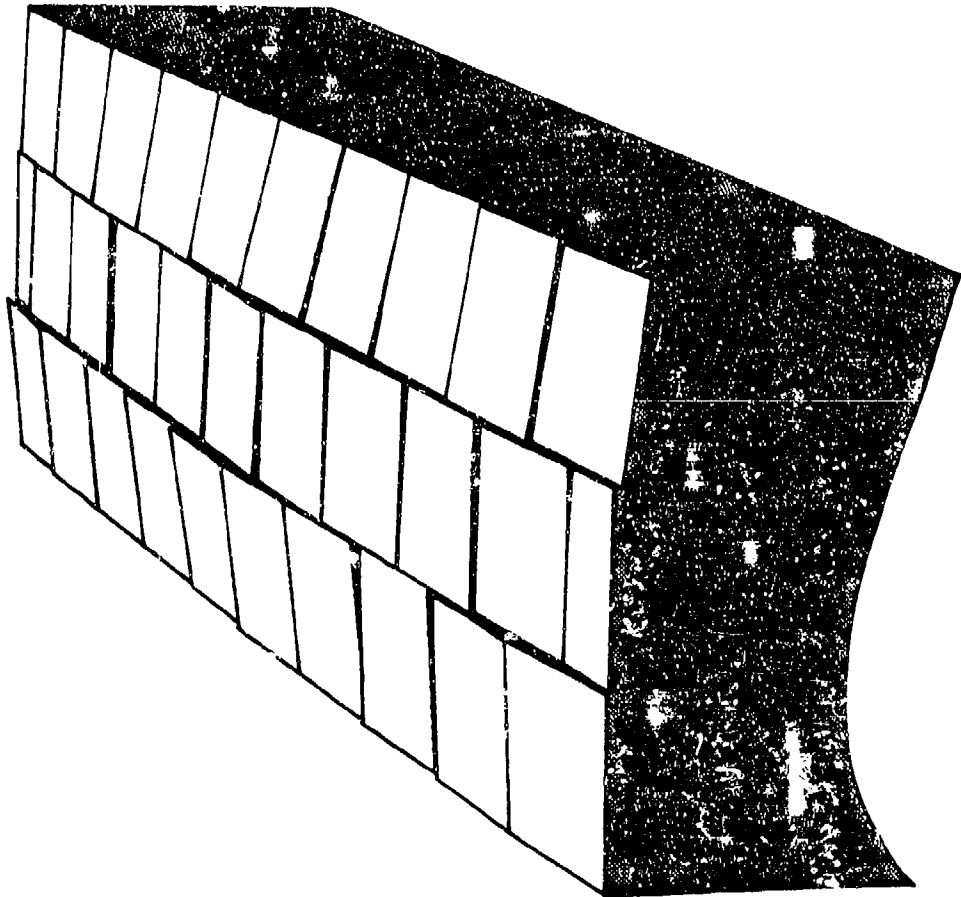


Figure 83. Deformed Wall Geometry: Test 7.

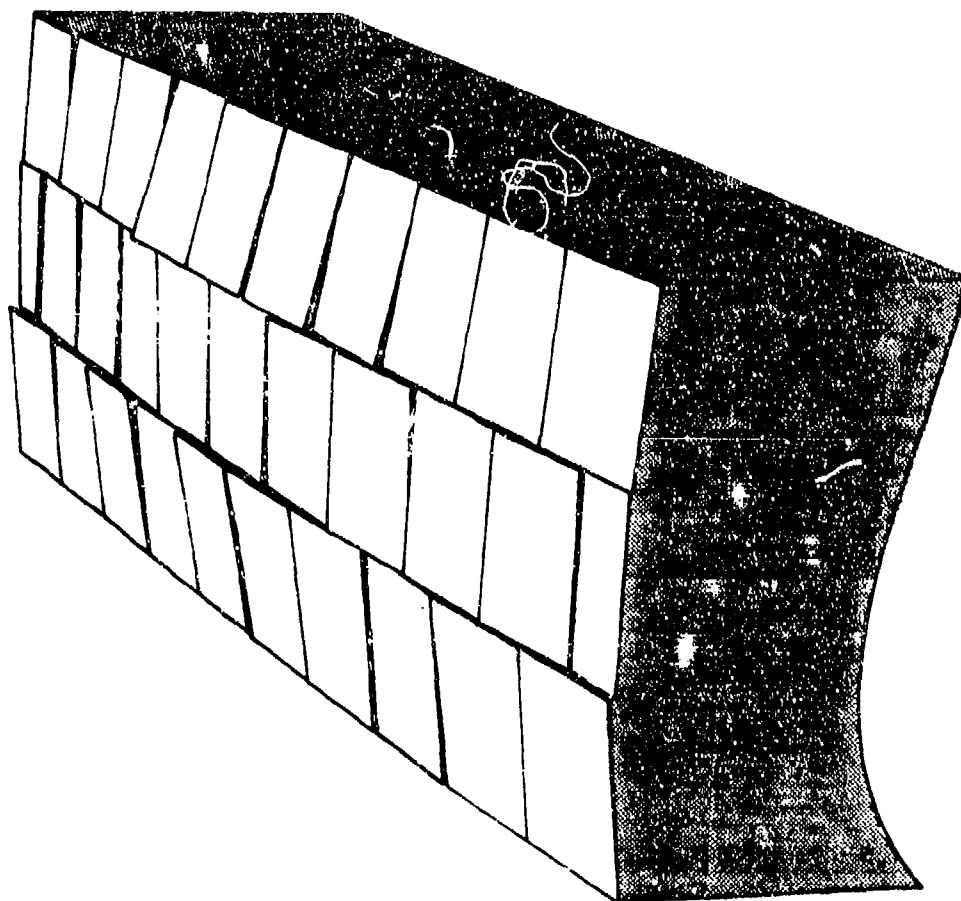


Figure 84: Deformed Wall Geometry: Test 8

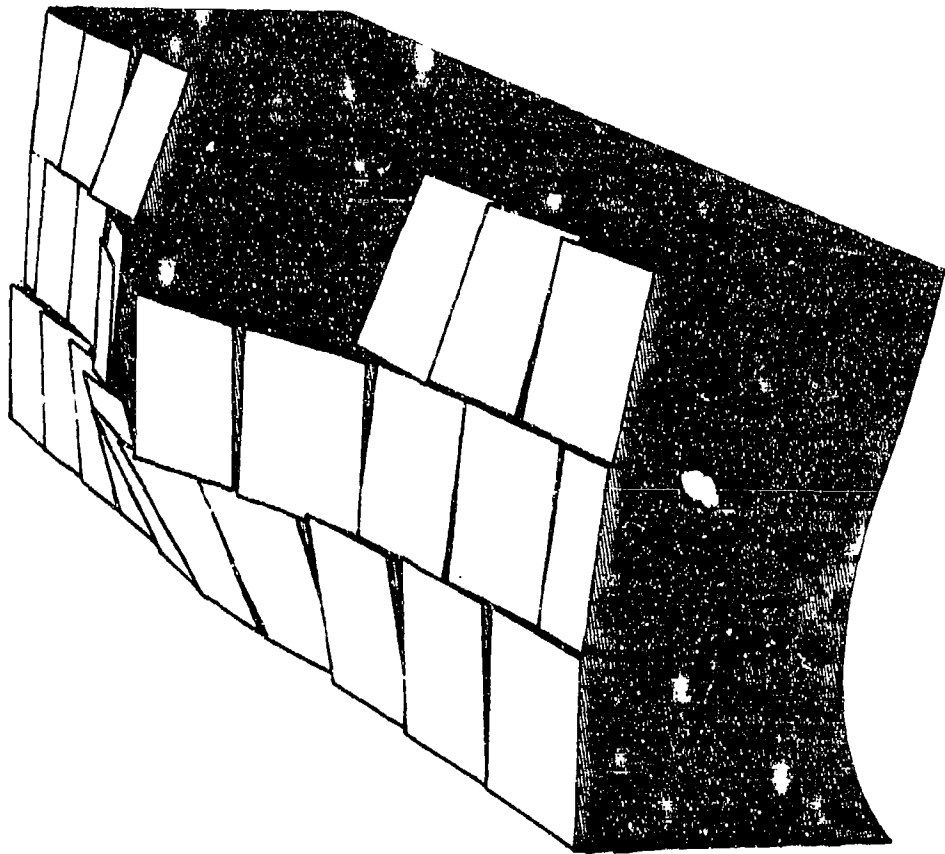


Figure 85. Deformed Wall Geometry: Test 9.

- Effects of reinforcing width

Two tests were conducted to assess the effects of reinforcement width on wall performance. The model wall in Test 2 was reinforced with 4 mm (0.16 inch) wide steel strips and the model wall for Test 4 was reinforced with 8 mm (0.32 inch) wide steel strips. All other test parameters were equal. Analysis the test results indicate that the wall reinforced with narrow reinforcing deformed almost 40 percent more than the wall reinforced with wide reinforcing:

Test No.	Reinforcement Width mm (in.)	ATWD mm (in.)
2	4 (0.16)	11.39 (0.45)
4	8 (0.32)	8.18 (0.32)

The largest differences in panel displacements between the two tests occurred at the center of the wall where average panel displacements for Test 2 were over 50 percent larger than those for Test 4. Smaller variations in panel displacement occurred at the sides and along the base of the wall where average panel displacements for Test 2 were 0 percent to 20 percent larger than those for Test 4. This is noticeable in Figures 78 and 80. These results are to be expected. Because the wide reinforcing covered a larger area, greater interface frictional resistance was developed between the soil and reinforcement for these strips than for the narrow strips. The results of this study indicate that reinforcement width is a factor in wall response to dynamic loading.

- Effects of reinforcement type

Two tests were conducted to compare the performance of steel strip and geogrid reinforcing. The model wall in Test 1 was constructed with steel reinforcing. All other test parameters were equal. Analysis of the test data indicates that the wall reinforced with steel deformed significantly more than the wall reinforced with geogrid:

Test No.	Reinforcement Type	ATWD mm (in.)
1	geogrid	5.61 (0.22)
2	steel	11.39 (0.45)

The ATWD of the steel reinforced wall was over 200 percent larger than the ATWD of the geogrid reinforced wall. The deformed wall shapes are similar (see Figures 77 and 78), but it is apparent that the deformation of the wall center is more pronounced in the steel reinforced wall. An investigation of average panel displacements indicates that all wall panels in Test 2 displaced more than those of Test 1 by amounts ranging from 50 percent to over 400 percent. This large difference is probably due to both a larger interface friction angle and larger area of reinforcement coverage for the geogrid compared to the steel. Also, passive resistance is developed in the soil between the geogrid webbing. The results of this study indicate that reinforcement type is a significant factor in wall response to dynamic loading.

- Effects of top restraint

Two tests were conducted to compare the response of a geogrid reinforced soil wall both with and without a top restraint. The model wall in Test 1 included a top restraint and the model wall in Test 3 did not. All other test parameters were equal. As expected, the ATWD of the wall constructed without a top restraint was over 90 percent larger than the ATWD of the restrained wall. (It should be noted that the ATWD of the unrestrained wall is somewhat underestimated. Two panels were breached on the unrestrained wall (T5 and T6), and for purposes of estimating the ATWD of this wall, average panel displacements of the breached panels were set equal to the average panel displacements of their adjacent intact panels.) Rotation of the top row of panels about the roof restraint was noticed in Test 1. The top row of panels in Test 3 underwent translational motion and two panels were breached. This study illustrates the importance of a top restraint (or roof) in minimizing panel displacement.

- Effects of charge location

Test 9 was conducted to illustrate the effects of charge location on wall response in the centrifuge. For this test, 152 mm (6 inches) long geogrid reinforcing was utilized. The charge was placed 152 mm (6 inches) behind the wall. It is apparent from Figure 85 that damage to the wall for this test is significantly more severe than the damage done to the walls of Tests 7 and 8 [with charge at 269 mm (10.6 inches) and all other parameters equal]. The results of this test indicate that wall response modeled in the centrifuge

follows the expected trend (i.e., wall deformations increase as weapon proximity to wall decreases).

c. Comparison 3: Centrifuge Model Results to Numerical Model Results

Numerical modeling and centrifuge modeling are two very different methods of investigating the behavior of reinforced soil structures. Each provided completely independent predictions of the behavior of specific prototype events, and independent predictions of the influence of individual components of the reinforced soil structures. A comparison of the results of these two investigations can provide much greater confidence in the results of the research program and point out areas where improvement is needed for one or both analysis methods. Two types of comparisons are described below. First, the general results of each method are compared. Second, two specific centrifuge tests are compared to a numerical prediction.

The similarity between the prototype walls and weapons modeled in the centrifuge tests and the numerical parametric study makes a qualitative comparison of the results of both studies possible. However, quantitative comparisons are not meaningful because of the many differences between the two, such as:

- The soil parameters used in the DYNA3D analyses not obtained from tests on the sand used in the centrifuge tests.
- The elastic-plastic constitutive model for the reinforced soil is a simplification of the real behavior of the reinforced soil used in the centrifuge tests.
- The numerical model does not include the details of the facing panels' interlocking geometry.
- The roof in the numerical model prevents upward vertical displacement of the top facing panel, causing high compressive stresses in the panels.
- The weapon location is closer to the wall in most centrifuge tests compared to its location in the numerical model.

- Cratering effects are not modeled in the numerical analyses.
- Most of the centrifuge models have sloping backfills and a soil overburden and the numerical models do not.

Of the differences listed above, the most significant are the constitutive models for the soil and the reinforcement, and the interlocking of the facing panels. The general behavior of the sand used in the centrifuge tests is captured by the numerical model, although the likely differences in actual constitutive property values preclude the accurate modeling of the deformations of the soil. The constitutive model for the reinforcement does not permit rupture, a potential problem pointed out in numerical analysis PS7. However, since reinforcement rupture was not observed in the centrifuge tests, the numerical modeling of the reinforcement is sufficiently accurate to allow quantitative comparisons with the centrifuge tests.

The difference between the geometry of the facing panel used in the centrifuge tests and the numerical model is more likely to affect the comparison of deformation patterns of the wall than average displacement of the wall. The primary purpose of the interlock is to aid in the construction of a "tight" wall; i.e., one with minimal gaps between facing panels. The interlocking panel structure contributes some strength to the wall and inhibits sliding between panels.

Keeping in mind the limitations imposed by these differences, several similarities in the results are meaningful:

- Both models predict high compressive stresses in the reinforcement.
- Reinforcement rupture did not occur in any of the centrifuge tests, or in any numerical analysis where 89.4 kg (197 pounds) of TNT is simulated.
- The general pattern of panel displacement is very similar; i.e., rotation of the top and bottom panels and outward translation of the center panel(s).

- The range of predicted prototype displacements are very similar (16.8 cm to 32.5 cm for all centrifuge tests versus 20.7 cm to 38.7 cm for all numerical analyses utilizing the standard weapon).
- Both methods show significant increases in average panel displacement when the roof is removed.
- Both analyses show that the horizontal distance between the wall and the weapon is a significant parameter.
- Based on very limited data, both analyses indicate that reinforcement stiffness is more important than reinforcement length.

Visual inspection of the steel reinforcement clearly shows the effect of the high compressive stresses in the reinforcement predicted by the numerical analyses. The lack of any reinforcement rupture in the centrifuge tests supports the numerical model, which predicts strain levels inconsistent with the prediction of reinforcement rupture.

The overall pattern of the displacements in the centrifuge tests and the effect of removing the roof agree well with numerical predictions, as does the effect of weapon location. Generally speaking, the deformed wall geometries and magnitudes of wall displacement observed in the centrifuge tests were closely matched by the numerical analyses.

To make more quantitative comparisons between centrifuge and numerical predictions, two centrifuge tests (7 and 8) and one numerical analysis (PS1P2) were performed. It was not possible, due to time constraints, to eliminate all the differences between the centrifuge and numerical models listed above. However, the following adjustments were made:

- The centrifuge tests were conducted without a backfill slope and without overburden soil.
- The location of the explosive in the centrifuge tests was changed to 270 mm (10.6 inches) behind the facing panel at depth

of 76 mm (3 inches) [ie: the additional 2.5 mm (1 inch) overburden layer was not constructed)].

- The interface friction coefficient between the bottom facing panel and the soil was reduced to zero in the numerical model. This was done to negate the effect of the unrealistically high compressive stresses in the numerical model caused by the roof constraint.
- The finite-element grid for the standard numerical analyses (PS1) was modified to have only three facing panels.

The main findings of the comparison between centrifuge tests 7 and 8 and the numerical model analysis PSIP are:

- The magnitudes of the panel displacements are very similar between the two models. Average panel displacement predicted by the numerical model is only about 10 percent higher than the average of the two centrifuge tests, as shown in Table 28.
- The shapes of the deformed walls differ somewhat, with peak wall displacement occurring higher on the wall in the numerical model.
- The displacement of the center panel is almost identical in both analyses.
- Blast wave velocity in the centrifuge model is approximately 15 percent higher than the average measured velocity in the centrifuge tests [575 m/s vs. 665 m/s (1890 fps vs. 2180 fps)].
- The DYNA3D prediction of peak pressure versus distance from the explosive is very close to those predicted from ConWep and estimated from resistor data (Figure 75).
- The peak panel accelerations measured in the centrifuge test, when scaled to prototype values, are lower by approximately one order of magnitude than that predicted by the numerical model.

TABLE 28. COMPARISON OF CENTRIFUGE AND NUMERICAL PREDICTIONS OF PROTOTYPE PANEL DISPLACEMENTS AND ACCELERATIONS.

Centrifuge Facing Panel	Location	Prototype Displacement (cm)				Prototype Acceleration			
		Centrifuge			Numerical	Centrifuge (scaled)			Numerical
		Test 7	Test 8	Average	PS1P2	Test 7	Test 8	Average	PS1P2
T-5; T-6	Top	2.10	-0.79	0.66	2.39				44
	Middle					15	9	12	
	Bottom	29.20	33.53	31.36	45.47				173
M-6	Top	35.85	37.62	36.79	35.00				163
	Middle					20	--	20	
	Bottom	37.51	33.87	35.69	35.76				164
B-5; B-6	Top	40.97	39.28	40.13	47.05				161
	Middle					38	28	33	
	Bottom	14.74	12.07	13.41	7.90				130
Average		25.75	25.93	26.34	28.93	24	19	22	139

The differences in deformed shape are likely the result of the numerical modeling of the panels and the frictional interfaces used in the numerical model. Both top and bottom panels in the numerical model rotate more than they do in either centrifuge test. A possible reason for this may be that the interlocking panel structure of the centrifuge test walls initially prevents the upper and lower panels from displacing outward more than the center panel, thereby limiting their rotation. When sufficient displacement has occurred, the middle panels lose contact with the top and bottom panels and can no longer inhibit their rotation. The purely frictional nature of the interface in the numerical model results in less restraint in the upper and lower panels. The displacement and rotation of the center panel, in comparison, match fairly well between centrifuge and numerical predictions. In the centrifuge tests, the bottom of the middle panel displaces more in Test 7, while the top displaces more in Test 8. The average displacements differ by only approximately 6 percent. A slightly deeper depth of charge burial in Test 7 could account for the difference in direction of rotation for the middle panel. This hypothesis is consistent with the larger displacement of the lower panel and the smaller displacement of the bottom of the top panel in Test 7.

The close match between wave velocity in the numerical analysis and the average measured wave velocity in the centrifuge tests is a good indication that the bulk and shear moduli used in the DYNA3D analyses are appropriate for comparison with the centrifuge tests. Further evidence of the reasonableness of the soil constitutive properties used in DYNA3D is the good agreement between predicted peak pressures vs. distance and measured peak pressures shown in Figure 75. Given the uncertainty in the interpretation of carbon gage data, quantitative comparison is difficult; however, qualitatively the agreement is excellent. The comparison with ConWep predictions is also good. The slower decay in peak pressure predicted by DYNA3D is at least partially due to the plane strain model which prevents geometric damping.

The only major discrepancy between the centrifuge tests and the numerical analyses is the large differences in panel acceleration. Prototype accelerations are predicted to be approximately six times higher by the numerical analysis, compared to the centrifuge tests. It has been seen in Section V that peak panel acceleration is not well correlated with other system responses. This is clearly the case here where panel displacements are very similar. However, an understanding of the reasons for the differences in predicted prototype acceleration is needed for a better understanding of the strengths and weaknesses of the two modeling methods. Possible causes for the differences in acceleration are:

- soil properties used in the numerical analyses are not representative of the sand used in the centrifuge model;
- presence of the HDPE backing on the panels used in the centrifuge test;
- the factor used to scale measured centrifuge acceleration to prototype acceleration; and
- cube root energy scaling.

Differences between the soil constitutive parameters in the numerical analysis and the properties of the soil used in the centrifuge test could cause some but not all of the differences in peak panel acceleration. A more likely cause is the HDPE panel glued to the back of the centrifuge panels. The HDPE is softer than the panel and air gaps are present between the two materials. Both

factors would lead to reduced accelerations of the panels and are considered the most likely reasons for the discrepancy.

To obtain prototype acceleration from the measured centrifuge data, Table 18 indicates that model acceleration should be divided by n , the g -level of the test. While this relationship is well tested at the low accelerations obtained during earthquake simulation, it may not apply to the very high g 's developed during blast loading. A final possibility is the assumption that cube-root energy scaling results in correct scaling for accelerations. This method of scaling leads to good prediction of displacement, which is a function mainly of the total energy input, but may not result in correct simulation of parameters such as peak acceleration, which is more sensitive to the shape of the pressure-time curve than it is to the area under the curve. Because of the differences in explosive type and size, the pressure-time history of the prototype event is not necessarily scaled correctly when total energy is used as the scaling factor.

d. Comparison 4: Centrifuge Model Results to Full Scale Model Results

Security restrictions prohibit the publication of the exact locations of the 227 kg (500 pounds) and 454 kg (1,000 pounds) weapons used in the 1990 full-scale model studies conducted in Israel. Without this information, comparisons of pressures, peak accelerations and wave velocities measured in the centrifuge to those obtained during full-scale testing are meaningless. Only very general comparisons can be made regarding the overall wall responses to blast loading.

Full-scale test results indicate that interior wall damage increased with decreasing weapon proximity to the wall. At best, little or no interior wall damage resulted from the buried blasts. At worst, localized failure of individual panels occurred which did not threaten the overall integrity of the structure (Reference 6). These same trends were observed in the centrifuge models. Wall deformations were larger when the detonator assembly was placed 216 mm (8.5 inches) behind the wall than when the assembly was placed 269 mm (10.6 inches) behind the wall. The structural integrity of the wall was affected when the assembly was placed 152 mm (6 inches) behind the wall, but this was done to intentionally breach the wall. Panel rotation about the roof slab was apparent in both centrifuge and full-scale models.

H. CONCLUSIONS AND RECOMMENDATIONS

Centrifuge modeling of reinforced soil walls subjected to buried blast loading was conducted at Tyndall AFB. Data collected from the test included: (1) peak wave pressures; (2) peak facing panel accelerations; (3) wave velocities; and (4) wall displacements. The results of the testing indicate the following:

- peak pressures measured in the centrifuge agree well with predicted values (based on ConWep analysis);
- based on limited testing, centrifuge tests appear to be reproducible;
- below the minimum length for static stability, reinforcement length is a factor in wall response;
- reinforcement width and reinforcement type are significant factors in wall response;
- wall deformations are smaller when the top restraint is used;
- the effects of detonator location on wall response in the centrifuge are similar to those seen in the full-scale testing;
- peak pressures, wave velocities, panel displacements, and the effects of wall response to detonator location in the centrifuge tests agree well with the numerical modeling results; and
- peak panel accelerations in the centrifuge do not agree well with those predicted in the numerical model.

The results of the centrifuge modeling study are very encouraging. The responses of the model reinforced soil walls show favorable agreement with those of the numerical model and full-scale model. This is a positive indication that centrifuge modeling is an effective means of studying dynamically loaded geotechnical structures.

It is recommended that further centrifuge modeling of reinforced soil walls be undertaken. To enable detailed quantitative analyses of future tests, the following recommendations are offered:

- Tests of a single set of model parameters should be reproduced several times to obtain the data necessary to conduct statistical analyses of the results.
- Pressure gages should be implemented for direct measurement of blast wave pressures.
- Because wall displacements were relatively small (up to approximately 25 mm (1 inch)), a displacement measuring technique with a correspondingly small tolerance (0.0254 mm (0.001 inch)) is needed to improve the accuracy of displacement measurements.
- The portion of the containment bucket surrounding the air space between bucket and model wall should be detachable so that post-test wall deformations can easily be observed and photographed.
- Tests should be conducted at two or more scaling factors (eg: 1:20, 1:30, and 1:40 scale) to verify the scaling relationships used, especially for panel acceleration.
- Improvements to gage and detonator placement techniques are necessary to reduce soil disturbance and improve uniformity of soil density at these locations.
- For comparisons to numerical modeling results, laboratory testing of the sand used for the centrifuge tests should be conducted to obtain the constitutive model properties required for a DYNA3D analysis using DYNA3D's cap model.
- After the improvements to the DYNA3D code recommended in Section V are accomplished, Class A predictions of centrifuge test results should be made.

SECTION VII

SUMMARY AND CONCLUSIONS

A. SUMMARY

Recent full-scale tests have demonstrated the potential advantages of using reinforced soil systems for aircraft shelters and other blast-resistant structures. For example, compared to reinforced concrete structures, reinforced soil structures can be constructed more quickly and easily with less need for skilled labor, specialized equipment, and supplies. However, very little is known about the response of reinforced soil to blast loading and the influence of system parameters on the behavior of reinforced soil structures.

The objectives of this study were to investigate the behavior of reinforced soil systems subjected to blast loading, and to assess the feasibility of using reinforced soil to provide blast resistance. This has been accomplished by conducting: (1) a literature review, (2) a laboratory testing program; (3) a numerical modeling program; and (4) a physical modeling testing program. A brief summary of each is discussed below.

The literature review presents a summary of the current knowledge and practices in the following areas of reinforced soil response under blast loading: (1) the use of soil berms in blast protection design; (2) soil response to dynamic loading; (3) response of micro- and macro- reinforced soil systems to impulse loading; (4) constitutive modeling of dynamically loaded soil; and (5) implementation of constitutive models in numerical modeling techniques.

A laboratory testing program was carried out to evaluate the influence of microreinforcement on the static properties of cohesionless soil and to evaluate dynamic pullout behavior of geogrid reinforcement in cohesionless soil. Triaxial tests were performed on a uniform sand reinforced with up to 2 percent (by mass) monofilament or fibrillated fiber. These tests are used to establish the influence of fiber type and concentration on: (1) strength; (2) stiffness; (3) stress-strain behavior; and (4) volumetric behavior. Static and dynamic pullout tests were performed to determine dynamic interface behavior. Rise times for the dynamic pullout load are in the tens of milliseconds, matching the predicted rise time from the numerical model.

A dynamic, plane strain, finite element numerical model was developed using the computer code DYNA3D. The reinforcing, facing and soil were represented by continuum elements with sliding interfaces between the soil and the reinforcement, and between the soil and the facing. The reinforcement, facing and soil were modeled by elastic-plastic, elastic and 2-invariant cap constitutive models, respectively. Blast loading was simulated by defining a time history of velocity for nodes on the side of the finite element mesh near the explosive.

For the numerical modeling study, a parametric analysis was performed to determine the response of a 4.5-meters (15-feet) high geogrid reinforced soil wall subjected to fully-coupled blast loads in the backfill behind the reinforced mass. The parametric study evaluated the effect on wall performance of: (1) reinforcement stiffness and length; (2) soil stiffness and strength; (3) weapon size and location; (4) soil/reinforcement interface friction; and (5) the exclusion of gravity-induced body forces.

Nine 1:30 scale physical model tests were conducted at the Tyndall AFB geotechnical centrifuge facility. Model walls were constructed of Tyndall Beach sand, gypsum facing panels and six layers of either steel shim stock or woven nylon netting reinforcement. The explosive was modeled with 3 grams of RDX placed at various locations in the backfill behind the reinforced soil mass. Instrumentation included accelerometers placed on selected facing panels and carbon resistance gages placed within the soil mass. Video and high-speed cameras were used to document the tests. The centrifuge tests were used to evaluate the influence on wall displacement of: (1) reinforcement type, length, and stiffness; (2) weapon location; and (3) top facing restraint. Two of the centrifuge tests were conducted to provide a comparison with numerical predictions.

B. CONCLUSIONS

In this section, a brief summary of the most significant conclusions of each task are presented followed by conclusions based on an integration of all the work performed for this project. Detailed conclusions from the laboratory testing are found in Section IV-H; from the numerical modeling in Section V-D; and from the physical modeling in Section VI-H.

Laboratory Testing: The laboratory testing has shown that dynamic pullout behavior of geogrid in sand, when measured in terms of load vs. displacement, is very similar under constant normal stress to that observed with standard pullout rates used for static design. The dynamic pullout tests subjected the geogrid to a stress path similar to that caused by blast loading.

Numerical Modeling: The numerical model has shown that soil stiffness and friction angle and the presence of a roof significantly affect wall performance, as does reinforcement stiffness. Reinforcement length and soil/reinforcement interface friction coefficient are relatively less important parameters, provided they are kept within normal ranges for static stability.

Physical Modeling: The physical modeling tests provide evidence that reinforcement type and stiffness play a significant role in wall behavior. The importance of a horizontal constraint at the top facing panel has also been demonstrated. Reproducibility of test results and the close agreement between centrifuge test results and numerical predictions provide evidence of the appropriateness of the centrifuge modeling technique for this problem.

The objectives of this work included answering specific questions regarding blast response of reinforced soil structures. The following conclusions are presented in response to those questions:

- Reinforced soil walls, in general, offer significant resistance to blast loading. Evidence from physical and numerical modeling tests indicate that geogrid reinforced soil walls offer more resistance to blast loading than steel strip or geotextile reinforced walls.
- Static design procedures appear sufficient for blast loading conditions.
- Strength and deformation properties of both unreinforced and reinforced cohesionless soil are relatively unaffected by loading rate, provided they are not saturated. Static and dynamic pullout behavior of geogrid in cohesionless soil is very similar.
- Small-scale centrifuge models of reinforced soil walls provide data on wall deformation consistent with full-scale tests and numerical model studies when cube-root energy scaling is used.

- A numerical model using the DYNA3D code provides predictions of reinforced soil wall behavior which are consistent with full-scale test results. Parametric numerical analyses provide logical and testable conclusions regarding the influence of system parameters on wall performance.
- Reinforced soil appears to move as a single mass with little relative movement between the soil and the reinforcement. Failure modes observed are excessive displacement and reinforcement rupture.
- The numerical model can be extended from the analysis of a reinforced soil wall to the analysis of a complete reinforced soil protective structure, provided the recommendations for model improvement made in Section V are carried out.

Additional conclusions are:

- The reinforcement is subjected to significant compressive loading as the blast wave passes through the reinforced soil mass.
- After the blast wave reaches the facing panels, reinforcement stresses change from compressive to tensile with a rise time from peak compressive to peak tensile load of several tens of milliseconds.
- The horizontal constraint provided by a roof significantly reduces deflection of a reinforced soil wall.
- Reinforcement length has relatively little effect on wall displacement, provided the minimum requirements for static stability are maintained.
- For a given reinforcement type, stiffness is a significant factor in wall deflection.
- Standard pullout tests used for static design appear adequate for evaluation of geogrid/soil interface behavior under pullout rates similar to that encountered in blast loading of reinforced soil walls.

SECTION VIII

RECOMMENDATIONS

A. GOALS AND ORGANIZATION

The purpose of this section is to present overall recommendations for future research on use of reinforced soil systems in blast resistant structures. These recommendations are based on an integration of all results obtained from this study and are presented in Section B below. More detailed recommendations related to numerical modeling are found in Section V-D; and centrifuge modeling in Section VI-H.

B. RECOMMENDATIONS

The results of this study of dynamically loaded reinforced soil structures are very encouraging. Laboratory, centrifuge modeling, and numerical modeling test results indicate that statically designed reinforced soil structures perform well as blast protection structures. Because construction of reinforced soil systems is relatively easy and requires only moderately skilled labor, their use is particularly appealing to an application where rapid construction of protective structures is crucial.

It is recommended that the Air Force pursue a more comprehensive study of the use of reinforced soil structures for blast protection with the ultimate goal of developing design procedures and drawings for such structures for inclusion in the Protective Construction Design Manual (Reference 2). In order to achieve this ultimate goal, the following recommendations are made:

- Four full-scale tests are to be conducted in 1993. The authors recommend the following test parameters be used to provide data which can be compared to the results of this study:
 - Investigation of Reinforcement Stiffness: Two tests should be conducted in which the only variable is the stiffness of the reinforcement. Two types of geogrid which have approximately the same ultimate tensile strength but different stiffness should be used. If feasible, weapon size and location, wall dimensions and

soil type should match those used in the centrifuge and numerical models of this study so that direct comparisons can be made.

- Investigation of Blast Location: One test should be conducted with the charge located closer to the reinforced soil wall. All other parameters should be equal to either one of the first two full-scale tests (geogrid reinforcing is recommended) so that direct comparison between them is possible.
- Investigation of Reinforcement Length: One test should be conducted using either a shorter or a longer reinforcement length. Geogrid reinforcing is recommended. All other parameters should be the same as those in Tests 1 and 2.

Because soil stiffness and strength were found to be significant parameters in wall response, all field testing should utilize the same soil. Tyndall AFB beach sand is preferable to enable comparisons of field tests with centrifuge tests. A major effort should be made to compact the soil the same way and to the same density in each test. Alternatively, one test could be conducted with significantly lower (or higher) soil density to investigate the influence of this parameter.

All laboratory tests should be conducted to determine the cap parameters for the soil used in the field tests. Care should be taken to conduct these tests on soil specimens compacted to the same density as that achieved in the field.

Gage placement for the full-scale tests should include accelerometers at the outside center wall panels and located at the top, middle, and bottom of the wall; and pressure gages at both ends of the center reinforcing and located at the top, center, and bottom of the wall. This will provide pressure and acceleration data that can be compared directly to those obtained from numerical and centrifuge models.

Panel displacements of the full-scale tests should be carefully measured for comparisons to those measured in both the centrifuge and numerical models.

- A comprehensive series of centrifuge tests should be carried out. These tests should include:

- Modeling of the full-scale tests, if there are significant differences between the full-scale tests and the prototype centrifuge walls used for this study. These tests should be accomplished before full-scale testing begins.
- An investigation of random variation in the test results. A specific centrifuge test should be repeated enough times to allow statistically valid data on mean and standard deviation of significant parameters such as wall deflection. Only with this information can valid predictions of the effects of various system parameters be made.
- A modeling-of-models study to validate the cube-root energy scaling used in the initial centrifuge tests. Suggested scales are 1:20, 1:30, and 1:40.
- Modifications to the numerical model described in Section V-E should be accomplished. Incorporation of a constitutive model for the sliding interface, development of a method to evaluate an appropriate mass damping factor, a more realistic modeling of the reinforcement material and connection, and a true three dimensional analysis are particularly important to achieve.
- After modifications are made to the DYNA3D code, validation of the code should be accomplished by Class A predictions of the centrifuge tests, followed by Class A predictions of the full-scale tests.
- In the future, studies should be developed that investigate other weapons effects on reinforced soil structures such as airblasts and projectile penetration.

REFERENCES

1. Sues, R.H., Murphy, C.E., Dass, W.C. and Twisdale, L.A., "Expedient Hardening Methods for Structures Subjected to the Effects of Nonnuclear Munitions," Proceedings of the Fourth International Symposium on the Interaction of Nonnuclear Munitions with Structures, Panama City Beach, Florida, Vol. 2, pp. 19-23, April 17-21, 1989.
2. Drake, J.L. et al., Protective Construction Design Manual, Report FSL-ER-87-57, Air Force Engineering and Services Center, Tyndall AFB, FL, Nov. 1989.
3. Colthorp, D.R., Kiger, S.A. and Vitayaudom, K.P., "Blast Response Tests of Reinforced Concrete Box Structures: Methods for Reducing Spall," Proceedings of the Second International Symposium on the Interaction of Nonnuclear Munitions with Structures, Panama City Beach, Florida, pp. 95-100, April 15-18, 1985.
4. Hyde, D.W., "Expedient Methods of Protection to Mitigate Structural Damage and Spall," Fourth International Symposium on the Interaction of Nonnuclear Munitions with Structures, Panama City Beach, Florida, Vol. 2, pp. 65-70, April 17-21, 1989.
5. Majka, R.J. and Buchholtz, W.C., "Protective Construction Design Validation," Proceedings of the Fourth International Symposium on the Interaction of Nonnuclear Munitions with Structures, Panama City Beach, Florida, Vol. 2, pp. 71-75, April 17-21, 1989.
6. Reid, R.A., "Full-Scale Blast Test of a Reinforced Soil Bunker," Proceedings of the Fifth International Symposium on the Interaction of Nonnuclear Munitions with Structures, Mannheim, Germany, pp. 12-16, April 22-26, 1991.
7. Whitman, R.V., The Response of Soils to Dynamic Loadings; Report 3, First Interim Report on Soil Tests, report for U.S. Army Engineer Waterways Experiment Station by Soil Engineering Division, Massachusetts Institute of Technology, Cambridge Massachusetts, Publication 104, 1959.

8. Whitman, R.V., The Response of Soils to Dynamic Loading, Report No. 17, Stress-Strain-Time Behavior of Soils in One Dimensional Compression, Contract Report No. 3-26, U.S. Army Engineers, Waterways Experiment Station, Vicksburg, MS, May 1963.
9. Farr, J.V. and Woods, R.D., "A Device for Evaluating One-Dimensional Compressive Loading Rate Effects," Geotechnical Testing Journal, Vol. 11, No. 4, pp. 269-275, June 1988.
10. Felice, C.W., Gaffney, E.S., Brown, J.A., and Olsen, J.M., "Dynamic High Stress Experiments on Soil," Geotechnical Testing Journal, Vol. 10, No. 4, pp. 192-202, Dec 1987.
11. Seaman, L., One-Dimensional Stress Wave Propagation in Soils, report for Defense Atomic Support Agency by Stanford Research Institute, Menlo Park, California, 1966.
12. Calhoun, D.E., Kraft, D.C., An Investigation of the Dynamic Behavior of a Partially Saturated Silt with applications to Shock-Wave Propagation, report by Eric H. Wang Civil Engineering Research Facility for Air Force Weapons Laboratory, Kirtland Air Force Base, New Mexico, AFWL-TR-65-176, 1966.
13. Schindler, L., A New Device for Testing Soils in One-Dimensional Compression, U.S. Army Engineer Waterways Experiment Station Technical Report, 1967.
14. Whitman, R.V., The Response of Soils to Dynamic Loadings, Contract Report 3-26, U.S. Army Engineer Waterways Experiment Station, Vicksburg, MS, May, 1970.
15. Jackson, J.G., Jr., Ehr Gott, J.Q., and Rohoni, B., Loading Rate Effects on Compressibility of Sand, Miscellaneous Paper SL-79-24, U.S. Army Waterways Experiment Station, Vicksburg, MS, Nov 1979.
16. Farr, J.V., "One-Dimensional Loading-Rate Effects," Journal of Geotechnical Engineering, ASCE, Vol 116, No. 1, pp. 119-135, 1990.

17. Schimming, B.B. and Saxe, H.C., "Inertial Effects and Soil Strength Criteria," Proceedings of the Symposium on Soil-Structure Interaction, University of Arizona, Tucson, AZ, pp. 118-128, Sept 1964.
18. Cassagrande, A. and Shannon, W.C., "Strength of Soils Under Dynamic Loads," Transactions of ASCE, pp. 755-772, 1949.
19. Seed, H.B. and Lundgren, R., "Investigation of the Effect of Transient Loads on Strength and Deformation Characteristics of Saturated Sand," Journal of the Soil Mechanics and Foundation Engineering Division, Vol. 88, No. SM2, pp. 99-132, 1962.
20. Whitman, R.V. and Healy, K.A., "Shear Strength of Sand During Rapid Loadings," Journal of the Soil Mechanics and Foundation Engineering Division, ASCE, Vol. 88, No. SM2, pp. 95-132, April 1962.
21. Carroll, W.F., Vertical Displacements of Spread Footings on Clay: Static and Impulsive Loadings; Report 5. Dynamic Bearing Capacity of Soils, Technical Report 3-599, U.S. Army Engineer Waterways Experiment Station, Vicksburg, MS, Dec. 1963.
22. Carroll, W.F., Fast Triaxial Shear Device Evaluation, Technical Report SL-88-2, U.S. Army Engineer Waterways Experiment Station, Vicksburg, MS Sept 1988.
23. Carroll, F.W., "A Fast Triaxial Shear Device," Geotechnical Testing Journal, ASTM, Vol. 11, No. 4, pp. 276-280, Dec 1988.
24. Carroll, W.F., Rate Effects in Shear for CARES-Dry Soil, Technical Report SL-88-9, U.S. Army Engineer Waterways Experiment Station, Vicksburg, MS, Feb, 1988.
25. Mitchell, J.K. and W.B. Villet, Reinforcement of Earth Slopes and Embankments, National Cooperative Highway Research Program Report 290, Transportation Research Board, Washington, D.C., 1987.
26. Schlosser, F. and N.C. Long, "La Terre Armee dans l'Echangeur de Sete," Revue Generale des Rates et des Areodromes, No. 430, 1972.

27. Yang, Z., "Strength and Deformation Characteristics of Reinforced Sand," Ph.D. Dissertation, University of California at Los Angeles, 1972.
28. Mercer, F.B., Andrawes, K.Z., McGown, A. and Hytivist, N., "A New Method of Soil Stabilization," Proceedings, Polymer Grid Reinforcement, pp. 244-249, Thomas Telford Limited, London, 1985.
29. Farrag, K., Pullout Testing Facility for Geosynthetics, Report FHWA/LA-91/240, Louisiana Transportation Research Center, Baton Rouge, LA, 1991.
30. McGown, A., Andrawes, K.Z., and Kabir, M.H., "Load-Extension Testing of Geotextiles Confined In-Soil," Proceedings of the 2nd International Conference on Geotextiles, Las Vegas, NV, Vol. 3, pp. 793-798, 1982.
31. Siel, B.D., Tzong, W.H., and Chou, N.N., "In-Soil Stress-Strain Behavior of Geotextiles," Proceedings, Geosynthetics Conference, New Orleans, LA, Vol. 1, pp. 260-265, 1987.
32. Rowe, R.K. and Ho, S.K., "Determination of Geotextile Stress-Strain Characteristics Using a Wide Strip Test," Proceedings of the 3rd International Conference on Geotextiles, Vienna, Vol. 3, pp. 885-890, 1986.
33. Myles, B., "Assessment of Soil Fabric Friction by Means of Shear," Proceedings of the 2nd International Conference on Geotextiles, Las Vegas, NV, Vol. 3, pp. 787-791, 1982.
34. Kaul, R.N., "The Influence of Roots on Certain Mechanical Properties of an Uncompacted Soil," Ph.D. dissertation, North Carolina State Univ., 1965.
35. Endo, T. and Tsuruta, T., Effects of Tree's Roots upon the Shearing Strength of Soils, Ann. Report of the Hokkaido Branch Gov. Forest Exp. Station, Tokyo, pp. 167-179. In Japanese with English summary, 1986.
36. Maher, M.H., "Static and Dynamic Response of Sands Reinforced with Discrete, Randomly Distributed Fibers," Ph.D. Dissertation, Univ. of Michigan, 1988.

37. Hoare, D.I., "Laboratory Study of Granular Soils Reinforced with Randomly Oriented Discreet Fibres," Proceedings, International Conference on Soil Reinforcement, Vol. 1., pp. 47-54, Paris, 1979.
38. Gray, D.H. and Al-Referi, T., "Behavior of Fabric- versus Fiber- Reinforced Sand," Journal of Geotechnical Engineering, ASCE, Vol 112, No. 8, pp. 804-820, Aug 1986.
39. Maher, M.H. and Woods, R.D., "Dynamic Response of Sand Reinforced with Randomly Distributed Fibers," Journal of Geotechnical Engineering, ASCE, Vol. 116, No. 7, pp. 1116-1131, Jul 1990.
40. Saada, A., "A Brief Review of Constitutive Models," Constitutive Equations for Granular Non-Cohesive Soils, Balkema, pp. 7-10, 1988.
41. Kondner, R.L. and Zelasko, J.S., "A Hyperbolic Stress-Strain Formulation for Sands," Proceedings of Second Pan-Am Conference on Soil Mechanics, Brazil, pp. 289-394, 1963.
42. Duncan, J.M. and Chang, C.Y., "Non-linear Analysis of Stress and Strain in Soils," Journal of the Soil Mechanics and Foundations Division, ASCE, Vol. 96, pp. 1629-1653, 1970.
43. Seed, R.B., Collins, J.G., and Mitchell, J.K., "FEM Analysis of Compacted Reinforced Soil Walls," Proc. Second International Conference on Numerical Models in Geomechanics, pp. 553-562, Ghent, Belgium, 1986.
44. Adib, M., Mitchell, J.K., and Christopher, B.R., "Finite Element Modeling of Reinforced Soil Walls and Embankments," Proceedings, ASCE Specialty Conference on Design and Performance of Earth Retaining Structures, Ithaca, NY, pp. 409-423, Jun 1990.
45. Jaber, M., Mitchell, J.K., Christopher, B.R., and Kutter, B.L., "Large Centrifugal Modeling of Full-Scale Reinforced Soil Walls," Proceedings, ASCE Specialty Conference on Design and Performance of Earth Retaining Structures, Ithaca, NY, pp. 379-393, Jun 1990.
46. Finn, J.H., "A Simple Plasticity Theory for Frictional Cohesionless Soils," Soil Dynamics and Earthquake Engineering, Vol. 4, No. 1, pp. 9-17, 1985.

47. Truesdell, C., "Hypoelasticity," J. Rational Mech. Analysis, Vol. 4, pp. 83-133, 1955.
48. Mroz, Z., "On the Description of Anisotropic Work Hardening," J. Mech. Phy. Solids, Vol. 15, pp. 163-175, 1967.
49. Desai, C.S., "A General Model for Yield, Failure and Potential Function in Plasticity," International Journal for Numerical and Analytical Methods in Geomechanics, pp. 361-375, 1980.
50. Biot, M.A., "Theory of Stress-Strain Relations in Anisotropic Viscoelasticity and Relaxation Phenomena," Journal of Applied Physics, pp. 1385-1391, 1954.
51. Bazant, Z.P. and Krizek, R.J., "Endochronic Constitutive Law for Liquefaction of Sand," Journal of the Engineering Mechanics Division, ASCE, pp. 225-238, 1976.
52. Bazant, Z.P., Ansal, A.M., and Krizek, R.J., "Constitutive Relation for Isotropically Consolidated Clays," Report 77-12/-643/1, Department of Civil Engineering, Northwestern University, Evanston, Illinois, 1977.
53. Bazant Z.P., Ansal, A.M., and Krizek, R.J., "Visco-Plasticity of Transversely Isotropic Clays," Journal of the Engineering Mechanics Division, ASCE, pp. 549-565, 1979.
54. Lanier, J., "Etude d'une Loi de Comportement pour des Materiaux non Visqueux," Journal de Mecanique, 1979.
55. Drucker, D.C., Gibson, R.E., Henkel, D.J., "Soil Mechanics and Work-Hardening Theories of Plasticity," Transactions, ASCE, pp. 338-346, 1957.
56. Roscoe, K.H., Schofield, A.N., and Wroth, C.P., "On the Yielding of Soils," Geotechnique, Vol. 8, No. 1, pp. 22-63, 1958.
57. Roscoe, K.H. and Burland, J.B., "On the Generalized Stress-Strain Behaviour of Wet Clay," Engineering Plasticity, Cambridge University Press, p. 535-609, 1968.

58. Lade, P.V. and Duncan, J.M., "Elastoplastic Stress-Strain Theory for Cohesionless Soil," Journal of the Soil Mechanics and Foundation Engineering Division, ASCE, Vol. 101, pp. 1037-1053, 1975.
59. Prevost, J.H., "Mathematical Modelling of Monotonic and Cyclic Undrained Clay Behaviour," Int. Jnl. Num. Anal. Methods in Geomechanics, pp. 195-216, 1977.
60. DiMaggio, F.L. and Sandler, I.S., "Material Model for Granular Soil," Journal of the Engineering Mechanics Division, ASCE, pp. 935-950, 1971.
61. Baron, M.I., Nelson, I. and Sandler, I.S., "Influence of Constitutive Model of Ground Motion Predictions," Journal of the Engineering Mechanics Division, ASCE, Vol. 99, pp. 1181-1200, 1973.
62. Sandler, Y.S., DiMaggio, F.L., and Baladi, G.Y., "Generalized Cap Model for Geological Materials," Journal of the Geotechnical Engineering Division, ASCE, Vol. 102, p. 683-699, 1976.
63. Nelson, I., Baron, M.L., and Sandler, I.S., "Mathematical Models for Geologic Materials for Wave Propagation Studies," Shock Waves and the Mechanical Properties of Solids, Syracuse University, Syracuse, New York, 1971.
64. Sandler, F.S. and Rubin, A.D., "Adaption of a Simple Cap Model," Constitutive Equations for Granular Non-Cohesive Soils, Balkema, Rotterdam, pp. 615-621, 1988.
65. Sandler, I.S. and Baron, M.L., "Recent Developments in the Constitutive Modelling of Geological Materials," 3rd Int. Conf. on Numerical Methods in Geomechanics, Aachen, 1979.
66. Katona, M.G., "Evaluation of Viscoplastic Cap Model," Journal of Geotechnical Engineering, ASCE, Vol. 110., No. 8, pp. 1106-1125, 1984.
67. Simo, J.C., Ju, J.W., Pister, K.S., and Taylor, R.L., "An Assessment of the Cap Model: Consistent Return Algorithms and Rate-Dependent Extension," Report UCB/SESM-85/5, Department of Civil Engineering, U.C. Berkeley, Berkeley, California, 1985.

68. Perzyna, P., "Fundamental Problems on Viscoplasticity," Advances in Applied Mechanics, Vol. 9, pp. 244-368, 1966.
69. Geotechnical Fabrics Report, Industrial Fabrics Association International, St. Paul, MN, pp. 119-120, December 1990.
70. Solomone, W.G., Boutrup, E., Holtz, R.D., Kovacs, W.D., Sutton, C.D., "Fabric Reinforcement Designed Against Pullout," The Use of Geotextiles for Soil Improvement, ASCE National Convention, Portland, OR, pp. 75-88, April 1980.
71. Whirley, R.G. and Hallquist, J.O., DYNA3D A Nonlinear Explicit, Three-Dimensional Finite Element Code For Solid and Structural Mechanics - User Code, Report UCRL-MA-107254, Lawrence Livermore National Laboratory, California, May, 1991.
72. Stillman, D.W. and Hallquist, J.O., INGRID: A Three-Dimensional Mesh Generator for Modeling Nonlinear Systems, Report UCID-20506, Lawrence Livermore National Laboratory, California, December, 1981, Revised, July, 1985.
73. Spelce, T. and Hallquist, J.O., TAURUS: An Interactive Post-Processor for the Analysis of Codes NIKE3D, DYNA3D, and TOPAZ3D, Report UCRL-MA-105401, Lawrence Livermore National Laboratory, CA, May 1991.
74. Scott, R.F. and Morgan, N.R., Feasibility and Desirability of Constructing a Very Large Centrifuge for Geotechnical Studies, Report 760-170, National Science Foundation, Washington, DC, 1977.
75. Thompson, P.Y. and Kim Y.S., "The Development of a Geotechnical Centrifuge Facility at Tyndall Air Force Base", Proceeding of the International Conference on Geotechnical Centrifuge Modeling (Centrifuge '88), pp. 67-72, 25 - 27 April 1988.
76. Taylor, T., Use of a Centrifuge in Investigation of Dynamic Phenomena in Partially Saturated Sands, Final Report, USAF-TDL Summer Faculty Research Program, sponsored by AFOSR, September, 1991.

77. Baker, W.E., et. al., "A Manual for the Prediction of Blast and Fragment Loading on Structures," Southwest research Institute, San Antonio, TX, 738 pp., November 1980.
78. Walsh, A., "Centrifuge Modeling of Explosive-Induced Stress Waves in Unsaturated Sand," M.S. thesis, Colorado State University, Fort Collins, Colorado, 1992.
79. Hyde, D.W., ConWep (Conventional Weapons Effects), computer programs, USAEWES, 17 February 1988.
80. Chew, S.H. and Schmertmann, G.R., "Reinforced Soil Wall Deformations by Finite Element Method," Performance of Reinforced Soil Structures, Proceedings of the International Reinforced Soil Conference, pp. 35-40, Sept. 10-12, 1990.